FAST, ADAPTIVE ALGORITHMS FOR FLOW PROBLEMS

by

Michael Edward McLaughlin

B.S. in Mathematics, Ohio University, 2014

M.A. in Mathematics, University of Pittsburgh, 2018

Submitted to the Graduate Faculty of

the Dietrich School of Arts and Sciences in partial fulfillment

of the requirements for the degree of

Doctor of Philosophy

University of Pittsburgh

2020

UNIVERSITY OF PITTSBURGH

DIETRICH SCHOOL OF ARTS AND SCIENCES

This dissertation was presented

by

Michael Edward McLaughlin

It was defended on

March 30th, 2020

and approved by

William Layton, Professor of Mathematics, University of Pittsburgh

Michael Neilan, Associate Professor of Mathematics, University of Pittsburgh

Catalin Trenchea, Associate Professor of Mathematics, University of Pittsburgh

Peyman Givi, Distinguished Professor of Mechanical Engineering, University of Pittsburgh

Dissertation Director: William Layton, Professor of Mathematics, University of Pittsburgh

FAST, ADAPTIVE ALGORITHMS FOR FLOW PROBLEMS

Michael Edward McLaughlin, PhD

University of Pittsburgh, 2020

Time-accurate simulations of physical phenomena (e.g., ocean dynamics, weather, and combustion) are essential to economic development and the well-being of humanity. For example, the economic toll hurricanes wrought on the United States in 2017 exceeded $200 billon dollars. To mitigate the damage, the accurate and timely forecasting of hurricane paths are essential. Ensemble simulations, used to calculate mean paths via multiple realizations, are an invaluable tool in estimating uncertainty, understanding rare events, and improving forecasting. The main challenge in the simulation of fluid flow is the complexity (runtime, memory requirements, and efficiency) of each realization. This work confronts each of these challenges with several novel ensemble algorithms that allow for the fast, efficient computation of flow problems, all while reducing memory requirements. The schemes in question exploit the saddle-point structure of the incompressible Navier-Stokes (NSE) and Boussinesq equations by relaxing incompressibility appropriately via artificial compressibility (AC), yielding algorithms that require far fewer resources to solve while retaining time-accuracy. Paired with an implicit-explicit (IMEX) ensemble method that employs a shared coefficient matrix, we develop, analyze, and validate novel schemes that reduce runtime and memory requirements. Using these methods as building blocks, we then consider schemes that are time-adaptive, i.e., schemes that utilize varying timestep sizes.

The consideration of time-adaptive artficial compressibility methods, used in the algorithms mentioned above, also leads to the study of a new slightly-compressible fluid flow continuum model. This work demonstrates stability and weak convergence of the model to the incompressible NSE, and examines two associated time-adaptive AC methods. We show that these methods are unconditionally, nonlinearly, long-time stable and demonstrate numerically their accuracy and efficiency.

The methods described above are designed for laminar flow; turbulent flow is addressed with the introduction of a novel one-equation unsteady Reynolds-averaged Navier-Stokes

(URANS) model with multiple improvements over the original model of Prandtl. This work demonstrates analytically and numerically the advantages of the model over the original.

TABLE OF CONTENTS

LIST OF TABLES

LIST OF FIGURES

1.0 INTRODUCTION

Simulations of physical phenomena, such as combustion, weather, and climate, have been and are integral to economic development and human well-being. In particular, the increased likelihood of extreme weather impacting human settlements and valuable natural resources due to climate change makes accurate simulations of the weather and climate of the utmost importance. The Navier-Stokes equations (NSE), a system of equations describing conservation laws for linear momentum and mass applied to a fluid parcel, form the core of numerical weather prediction (NWP) and climate codes, in one way or another. The construction of numerical methods for this system suffer from two main challenges:

1. The prognostic variables u (velocity) and p (pressure) are coupled due to the incompressibility constraint;
2. The convective term contains a nonlinearity.

The first issue, velocity/pressure coupling, arises due to the saddle-point structure of the incompressible NSE and requires the satisfaction of an inf-sup condition. Furthermore, if left coupled, the linear solves needed to solve the velocity and pressure concurrently can overwhelm even the most advanced computer systems. For decades, numerical methods that are used to appoximate flow problems have attempted to exploit the incompressibility constraint in various ways to improve speed. One, the artificial compressibility (AC) method, relaxes incompressibility appropriately, allowing for the velocity and pressure to be decoupled and advanced in time explicitly. The method is fast and efficient at low-temporal orders and allows for the rapid computation of the velocity and pressure.

However, one drawback of the method is its resistance to adapting in time in an efficient manner. For long-time simulations, an algorithm allowing for the efficient use of time adaptivity can save orders of magnitude of runtime. A main contribution of this dissertation is to tackle this challenge: We present mutiple AC methods that are able to adapt in time. We first consider a new, slightly compressible continuum model and show that, under some conditions, the model converges weakly to the NSE. Then, we construct, analyze, and validate

two unconditionally stable time-adaptive AC methods.

The second challenge, nonlinearity of the convective term, complicates the construction of unconditionally stable and efficient methods. For example, the nonlinearity in a Backward Euler solve can be treated implicitly (requiring the use of Newton's method), explicitly (requiring the satisfaction of a Courant-Friedrichs-Lewy (CFL) condition), or linearly implicitly (equivalent to solving an Oseen problem at every timestep). The first treatment is accurate but computationally expensive. The second allows for the movement of the nonlinear term to the right-hand-side at the cost of unconditional stability. The third, wherein one term in the nonlinearity is lagged while the other remains implicit, yields unconditionally stable methods. However, the linear system that arises from the final treatment ceases to be symmetric positive-definite (SPD), disallowing the use of efficient Krylov solvers, e.g., Conjugate Gradient. The presence of an implicit term also requires the update of the linear system at every timestep. Thus, treating the nonlinearity with a linearly implicit approach yields stability, but also tethers the nonlinearity to the solution of each realization. This fact becomes crucial when considering ensemble methods.

In the 1960s, Lorenz [87, 88, 86] showed that even miniscule perturbations in initial conditions yield flow simulations that output wildly different results. This fact, that minor differences in initial conditions (or parameters, etc.) yield simulations that vary wildly, imposes on the approximation of atmospheric flow a *predictability horizon* of about two weeks. It was then understood, notably by Toth and Kalnay [133], that any meaningful model that could reach this predictability horizon would have to incorporate ensemble averaging in order to find the most likely forecasts. These ensemble models, used by NWP models around the world and which are generated by considering multiple realizations of a flow with different initial conditions and parameters, have been wildly successful in generating accurate forecasts and extending the (reachable) predictability horizon.

The increased accuracy of ensemble methods comes at a cost: Due to their construction, every realization needs to be solved on each time interval, limiting the number of ensembles that can realistically be used, the underlying spatial accuracy of each realization, or both. Furthermore, *each realization* needs to store a separate stiffness matrix when considering ensemble flow problems that are at least semi-implicit in the nonlinearity, again limiting the

number of accurate realizations that can be realistically considered and therefore limiting the predictability horizon.

The second main contribution of this dissertation is to resolve these challenges. Using an implicit-explicit (IMEX) technique on the nonlinear term introduced by Layton and Jiang [65], we construct a time-adaptive artificial compressibility ensemble method for the Boussinesq equations that utilizes a *shared* coefficient matrix for each realization, increasing speed, efficiency, and decreasing memory requirements, thus extending the predictability horizon.

Ensemble schemes of this nature must satisfy a CFL-like condition that is inversely dependent on the kinematic viscosity; hence, the results listed above are for laminar flow. This CFL-like condition can be improved with the addition of an eddy-viscosity model; this is not the focus of this work. We do however consider turbulence in the final contribution of this dissertation: We develop, analyze, and test numerically a novel one-equation URANS model of turbulence that shows multiple improvements over the original model by Prandtl [100]. Specifically, we demonstrate that using a *kinematic*, as opposed to static, mixing length offers many advantages over the original. We also consider an AC one-equation model in the same framework, offering analysis and numerical tests. We believe this model can be extended to the context of ensemble simulations; however, this is for a future work.

We consider notation and preliminaries in Chapter 2. In Chapter 3, we present a brief overview of AC methods and demonstrate our results on time-adaptive AC methods. Then, in Chapter 4, we construct constant and variable timestep artificial compressibility ensemble schemes for the Boussinesq equations. We consider our kinematic one-equation model in Chapter 5. Finally, conclusions and open problems are given in Chapter 6.

2.0 THE EQUATIONS OF FLUID FLOW AND THEIR APPROXIMATION

We begin our preliminary chapter on a brief derivation of the incompressible Navier-Stokes equations. Then, using the Boussinesq assumption, give the system describing buoyancy-driven flow, otherwise known as the natural convection problem or the Boussinesq equations. In Section 2.2, we provide common notation, function spaces, and results to be used throughout the dissertation.

2.1 THE NAVIER-STOKES AND BOUSSINESQ EQUATIONS

The derivation of the Navier-Stokes equations has been covered in breathtaking detail and much more effectively in works other than this one. We would refer the reader to [75, 67] for a more comprehensive treatment. The derivations herein are themselves derived from these works.

2.1.1 THE INCOMPRESSIBLE NAVIER-STOKES EQUATIONS

Let Ω^* be an open domain in $\mathbb{R}^3$ representing a small parcel of fluid with boundary $\partial\Omega^*$. We denote by $\mathbf{x}$ the spatial variable, t the temporal variable, $\rho(\mathbf{x};t)$ the density of the fluid, and ρu be the flux of mass, where u is the velocity field of the flow. We let then the mass of the fluid equal

$$m(t) = \int_{\Omega^*} \rho d\mathbf{x}.$$

If mass is to be *conserved*, then the change of mass of the fluid in Ω^* must equal the flux of the mass across $\partial\Omega^*$. Thus, by the Divergence Theorem,

$$\begin{aligned} \frac{d}{dt}\int_{\Omega^*} \rho d\mathbf{x} = \frac{dm}{dt} &= -\int_{\partial\Omega^*} (\rho u)\cdot \mathbf{n} dS \\ &= -\int_{\Omega^*} \nabla\cdot(\rho u) d\mathbf{x}. \end{aligned}$$

Pulling the temporal derivative on the left-hand-side into the integral and rewriting yields

$$\int_{\Omega^*} (\partial_t \rho + \nabla \cdot (\rho u))\, d\mathbf{x} = 0.$$

We chose Ω^* to be an arbitrary domain in $\mathbb{R}^3$, so shrinking Ω^* to a point yields

$$\partial_t \rho + \nabla \cdot (\rho u) = 0.$$

If the flow is *incompressible*, the density $\rho(\mathbf{x}; t) \equiv \rho$ a constant; thus,

$$\nabla \cdot u = 0. \tag{2.1}$$

We call (2.1) the *continuity* equation, or refer to it as the incompressibility constraint. Unless otherwise noted, we shall assume that all flows are incompressible.

Next, we shall consider the conservation of linear momentum. Let the linear momentum $\mathbf{p} = \int_{\Omega^*} \rho u d\mathbf{x}$, where ρ and u are constant density and velocity as before. Using Newton's Second Law ($\mathbf{F} = m\mathbf{a}$), the conseration of momentum states that the rate of change in linear momentum in a fluid is equal to all forces acting upon the fluid. Let $\mathbf{F}$ be the net force vector (both internal and external) acting on the fluid and ρuu be the momentum flux. Thus, by the Divergence Theorem,

$$\begin{aligned} \frac{d}{dt}\int_{\Omega^*} \rho u d\mathbf{x} = \frac{d\mathbf{p}}{dt} &= \int_{\Omega^*} \mathbf{F} d\mathbf{x} - \int_{\partial\Omega^*} (\rho u)(u \cdot \mathbf{n}) dS \\ &= \int_{\Omega^*} \mathbf{F} d\mathbf{x} - \int_{\Omega^*} \nabla \cdot (\rho uu) d\mathbf{x}. \end{aligned}$$

Note that the density is constant in an incompressible fluid; therefore, by (2.1) we can write the divergence of momentum flux as

$$\begin{aligned} \nabla \cdot (\rho uu) = \rho \nabla \cdot (uu) &= \rho \left((\nabla \cdot u)u + (u \cdot \nabla)u \right) \\ &= \rho (u \cdot \nabla)u. \end{aligned}$$

Pulling the temporal derivative inside the integral on the left-hand-side of the momentum equation gives

$$\int_{\Omega^*} \rho \left(\partial_t u + (u \cdot \nabla)u \right) d\mathbf{x} = \int_{\Omega^*} \mathbf{F} d\mathbf{x}.$$

Let now $\mathbf{f}$ be all external forces acting on the fluid, e.g., buoyancy. We wish now to model all *internal* forces acting on the surface of a fluid, i.e., contact forces. To that end, we let $\mathbf{s}$ be the Cauchy stress vector. It was shown by Cauchy that if the conservation of linear momentum holds, then $\mathbf{s}$ is linear with respect to the normal vector $\mathbf{n}$. A rigorous derivation of this fact can be found in [67]. Hence, we write $\mathbf{s} = \mathbf{n} \cdot \mathbb{T}$, where $\mathbb{T}$ is called the Cauchy stress tensor. It can also be shown that, under the conservation of angular momentum, $\mathbb{T}$ is symmetric. We therefore write the momentum equation as, again by the Divergence Theorem,

$$\int_{\Omega^*} \left[\rho \left(\partial_t u + (u \cdot \nabla)u\right) - \nabla \cdot \mathbb{T}\right] d\mathbf{x} = \int_{\Omega^*} \mathbf{f} d\mathbf{x}.$$

Shrinking Ω^* to a point yields

$$\rho \left(\partial_t u + (u \cdot \nabla)u\right) - \nabla \cdot \mathbb{T} = \mathbf{f}.$$

We now consider the components of $\mathbb{T}$. The first is pressure, the force acting normal to the surface of a fluid. We define the pressure to be $P = \frac{1}{3}\text{tr}\mathbb{T}$, the average of the diagonal of the Cauchy stress tensor. The pressure force we then define as $-P\mathbb{I}\mathbf{n}$, where $\mathbb{I}$ is the identity tensor. We then write the nonpressure terms of the Cauchy stress tensor as $\mathbb{V} = \mathbb{T} + P\mathbb{I}$, also called the tangential, or *viscous*, forces. For these, we assume the fluid is *Newtonian*, that is, assume that there is a linear relation between stress and the deformation tensor $\mathbb{D} = \frac{1}{2}(\nabla u + \nabla u^T)$. For incompressible flows, the relation is given by

$$\mathbb{V} = 2\mu\mathbb{D},$$

where we say that μ is the dynamic viscosity. Hence, we write $\mathbb{T} = 2\mu\mathbb{D} - P\mathbb{I}$, and the momentum equation becomes

$$\rho \left(\partial_t u + (u \cdot \nabla)u\right) - \nabla \cdot (2\mu\mathbb{D} - P\mathbb{I}) = \mathbf{f}.$$

We notice that $\nabla \cdot P\mathbb{I} = \nabla P$ and $\nabla \cdot (2\mu\mathbb{D}) = \mu\Delta u$ by incompressibility. Thus, after dividing by ρ, we obtain the momentum equation

$$\partial_t u + (u \cdot \nabla)u - \frac{\mu}{\rho}\Delta u + \nabla\left(\frac{P}{\rho}\right) = \frac{1}{\rho}\mathbf{f}.$$

After defining the pressure to be $p = \frac{P}{\rho}$, the kinematic viscosity to be $\nu = \frac{\mu}{\rho}$, and $f = \frac{1}{\rho}\mathbf{f}$, we define the *incompressible Navier-Stokes equations (NSE)* to be

$$\partial_t u + (u \cdot \nabla)u - \nu\Delta u + \nabla p = f, \tag{2.2}$$

$$\nabla \cdot u = 0. \tag{2.3}$$

The system (2.2)–(2.3) characterizes the conservation of mass and linear momentum for a Newtonian fluid subjected to an external body force f. Here, f is an arbitrary force, and generally represents another physical action (e.g., temperature) acting on the fluid. The system forms the core of the next system we will consider, the Boussinesq equations.

Remark 1. *The incompressible NSE can be nondimensionalized in various ways by rescaling the variables by characteristic values. A common (but not the only) way yields the nondimensionalized system*

$$\partial_t u + (u \cdot \nabla)u - Re^{-1}\Delta u + \nabla p = f,$$

$$\nabla \cdot u = 0,$$

where, if U and L are a characteristic velocity and length, respectively, then $Re = \frac{UL}{\nu}$ the Reynolds number. We refer to [75, 67] for more details.

Remark 2. *Taking an inner product of* (2.2) *with u and integrating over Ω^* yields*

$$\int_{\Omega^*} \left(\frac{1}{2}\frac{d}{dt}|u|^2 + \nu\Delta u \cdot u + \nabla p \cdot u \right) d\mathbf{x} = \int_{\Omega^*} f \cdot u d\mathbf{x}.$$

Then, by 2.3 and integration by parts, we have the kinetic energy *evolution over a volume*

$$\int_{\Omega^*} \left(\frac{1}{2}\frac{d}{dt}\|u\|^2 + \nu|\nabla u| \right) d\mathbf{x} = \int_{\Omega^*} f \cdot u d\mathbf{x}.$$

By using the definition of the dual norm and Young's inequality, we arrive at the kinetic energy inequality

$$\int_{\Omega^*} \frac{1}{2} \left(\frac{d}{dt}\|u\|^2 + \nu|\nabla u| \right) d\mathbf{x} \leq \int_{\Omega^*} f^2 d\mathbf{x}.$$

2.1.2 THE BOUSSINESQ EQUATIONS

For flows with a nearly constant density, we can write $\rho = \rho_0 + \rho'$, a constant and fluctuation term where $\rho' \ll 1$. The *Boussinesq approximation* states that the fluctuation in density is proportional to the difference between observed and reference temperature values, i.e., $\rho' = \rho_0\beta(T - T_0)$. We say that β is the coefficient of thermal expansion. Furthermore, in our model we ignore all density variations that are not present in any buoyancy forces. We let $\mathbf{f}_g = \frac{\rho-\rho_0}{\rho_0}\widetilde{g}\xi$ be the force due to buoyancy, where $\widetilde{g}$ is acceleration due to gravity and ξ is the unit vector pointing in the upward direction. Then, we write $f \Leftarrow f + \mathbf{f}_g = f + (\rho - \rho_0)\widetilde{g}\xi$. Noting that $\rho - \rho_0 = \rho_0\beta(T - T_0)$, we have by (2.2)

$$\partial_t u + (u \cdot \nabla)u - \nu\Delta u + \nabla p = f + \widetilde{g}\beta(T - T_0)\xi.$$

This gives the momentum equation from the Boussinesq system. Since we are assuming there are no density variations in terms other than buoyancy, the continuity equation (2.3) remains the same.

Finally, we consider the conservation of energy [97, 11]. We let ρE be the total energy density in a fluid volume. Let $c_V T$ be the thermodynamic energy and $\frac{1}{2}\|u\|^2$ the kinetic energy, where c_V is the specific heat of a fluid at a constant volume. We let $\rho E = \rho(c_V T + \frac{1}{2}\|u\|^2)$ and consider potential energy density elsewhere (in the terms of a forcing function). The conservation of energy states that the rate of change of energy in the system equals the rate at which the system receives transfers of heat and work, i.e.,

$$\begin{aligned}\frac{d}{dt}\int_{\Omega^*} \rho(c_V T + \frac{1}{2}\|u\|^2)d\mathbf{x} &= \frac{d}{dt}\int_{\Omega^*} \rho E d\mathbf{x} \\ &= -\int_{\partial\Omega^*} \mathbb{Q} \cdot \mathbf{n} dS + \int_{\Omega^*} \rho(u \cdot f + \mathbf{g})d\mathbf{x} + \int_{\partial\Omega^*} (\mathbb{T} \cdot u) \cdot \mathbf{n} dS \\ &\quad - \int_{\partial\Omega^*} \rho(u(c_V T + \frac{1}{2}\|u\|^2)) \cdot \mathbf{n} dS,\end{aligned}$$

where $\mathbb{Q} = -k\nabla T$ is the heat flux, k the (constant) thermal conductivity, and $\mathbf{g}$ a heat source. By Remark 2, moving the temporal derivative in, and the Divergence Theorem, we have

$$\begin{aligned}\int_{\Omega^*} \rho(c_V\partial_t T - \nu\Delta u \cdot u + \nabla p \cdot u + f \cdot u)d\mathbf{x} &= \int_{\Omega^*} (k\Delta T + \rho(u \cdot f + \mathbf{g}) + \nabla \cdot (\mathbb{T} \cdot u) \\ &\quad - \rho\nabla \cdot (u(c_V T + \frac{1}{2}\|u\|^2)))d\mathbf{x}.\end{aligned}$$

Now, we note that for incompressible flow, $\mathbb{T} = \mu\nabla u - P\mathbb{I}$. Since $\rho\nu = \mu$, we have, by cancellation

$$\int_{\Omega^*} \rho(c_V \partial_t T + \nabla \cdot (u(c_V T + \frac{1}{2}\|u\|^2))) - k\Delta T d\mathbf{x} = \int_{\Omega^*} \rho \mathbf{g} d\mathbf{x}.$$

We also have that $\nabla \cdot (u(c_V T + \frac{1}{2}\|u\|^2)) = c_V((u \cdot \nabla)T + (\nabla \cdot u)T) + \frac{1}{2}\|u\|^2(\nabla \cdot u) = (u \cdot \nabla)T$ by incompressibility. Thus,

$$\int_{\Omega^*} \rho c_V(\partial_t T + (u \cdot \nabla)T) - k\Delta T d\mathbf{x} = \int_{\Omega^*} \rho \mathbf{g} d\mathbf{x}.$$

Divide the equation by ρc_V and define $\kappa = \frac{k}{\rho c_V}$ the thermal diffusivity and $g = \frac{1}{c_V}\mathbf{g}$ the scaled heat source. Shrinking then Ω^* to a point yields the temperature equation

$$\partial_t T + (u \cdot \nabla)T - \kappa\Delta T = g.$$

Combining the momentum equation with buoyancy, the continuity equation (2.3), and the temperature equation yields the *Boussinesq equations*

$$\partial_t u + (u \cdot \nabla)u - \nu\Delta u + \nabla p = f + \widetilde{g}\beta(T - T_0)\xi, \tag{2.4}$$

$$\nabla \cdot u = 0, \tag{2.5}$$

$$\partial_t T + (u \cdot \nabla)T - \kappa\Delta T = g. \tag{2.6}$$

Remark 3. *The Boussinesq equations can also be nondimensionalized in various ways by rescaling the variables [39]. We will present two ways, including the formulation which will be used in analyses later in this dissertation. One way is*

$$\partial_t u + (u \cdot \nabla)u - Pr\Delta u + \nabla p = f + PrRaT\xi, \tag{2.7}$$

$$\nabla \cdot u = 0, \tag{2.8}$$

$$\partial_t T + (u \cdot \nabla)T - \Delta T = g, \tag{2.9}$$

where $Pr = \frac{\nu}{\kappa}$ *is the Prandtl number and* $Ra = \frac{\rho\beta(T-T_0)L^3\widetilde{g}}{\nu\kappa}$ *the Rayleigh number. Another nondimensionalization, which will be used in numerical tests, is given by*

$$\partial_t u + (u \cdot \nabla)u - \frac{1}{Re}\Delta u + \nabla p = f + RiT\xi, \tag{2.10}$$

$$\nabla \cdot u = 0, \tag{2.11}$$

$$\partial_t T + (u \cdot \nabla)T - \frac{1}{ReRi}\Delta T = g, \tag{2.12}$$

2.1.3 BOUNDARY AND INITIAL CONDITIONS

Different boundary conditions for the velocity and temperature can be used in the NSE/Boussinesq systems. Our primary focus will be the so-called *noslip* boundary condition for the velocity, i.e., $u = 0$ on the boundary of our domain. Other boundary conditions for the velocity, e.g., inhomogeneous Dirichlet, Neumann, etc., can be used; for a summary of different velocity boundary conditions see [67]. The temperature boundary condition is more varied depending on the context. We use domains that are perfectly insulated, i.e., $T = 0$ on the boundary and boundaries that are adiabatic, i.e., $\mathbf{n} \cdot \nabla T = 0$. This is done to simplify the analysis; inhomogeneous Dirichlet boundary conditions add technical details to the proofs contained herein but no more difficulty. An example of using inhomogeneous Dirichlet boundary conditions for the temperature lies in the so-called double-pane problem, which is considered in our numerical tests. A full analysis of this problem in the context of ensemble methods can be found in the works of Fiordilino [39].

For regularity purposes, the presence of temporal derivatives in the momentum and temperature equations necessitates initial conditions for the velocity and temperature. We typically write $u(\mathbf{x}; 0) = u_0$ and $T(\mathbf{x}; 0) = T_0$.

2.2 SPATIAL AND TEMPORAL PRELIMINARIES

In this section, we define Ω to be an open domain in $\mathbb{R}^d$ for $d = 2, 3$ with boundary $\partial\Omega$. We will primarily use as function spaces $W^{k,p}(\Omega)$, the Sobolev space of functions in L^p whose weak derivatives of order up to and including k are in L^p. An important class of Sobolev space that we will consider is denoted $H^k(\Omega) := W^{k,2}(\Omega)$.

2.2.1 CONTINUOUS PRELIMINARIES

We define the Hilbert spaces $X^{k,d} := \left(H^k(\Omega)\right)^d$ with associated inner products and norms (irrespective of dimension) $(\cdot, \cdot)_k$ and $\| \cdot \|_k$, respectively. In particular, we will consider $X^{0,d} = \left(L^2(\Omega)\right)^d$, $X^{1,d} = \left(H^1(\Omega)\right)^d$, the notation for the L^2 inner product and norm being

changed to $(\cdot,\cdot)$ and $\|\cdot\|$, respectively. For all other L^p spaces, we let norms be given by $\|\cdot\|_{L^p}$. Let the velocity and pressure spaces be defined by

$$X := \left(H_0^1(\Omega)\right)^d = \{v \in X^{1,d} : v|_{\partial\Omega} = 0\},\ Q := L_0^2(\Omega) = \{q \in X^{0,1} : (1,q) = 0\},$$
$$V := \{v \in X : (q, \nabla \cdot v) = 0\ \forall q \in Q\}$$

and the temperature spaces (for the Boussinesq problem) be

$$W := H^1(\Omega) = X^{1,1},\ W_{\Gamma_D} := \{S \in W : S|_{\Gamma_D} = 0\}.$$

The dual norm $\|\cdot\|_{-1}$ is understood to correspond to either X or W_{Γ_D}, e.g.,

$$\|u\|_{-1} = \sup_{v \in X} \frac{(u,v)}{\|\nabla v\|}.$$

We describe the following inf-sup condition for the velocity and pressure spaces (also called the Ladyzhenskaya-Babuška-Brezzi (LBB) condition): For any $v \in X$, $q \in Q$, there is a constant $\beta_{\text{LBB}} > 0$ such that

$$\inf_{q \in Q} \sup_{v \in X} \frac{(q, \nabla \cdot v)}{\|q\|\|\nabla v\|} \geq \beta_{\text{LBB}} > 0. \tag{2.13}$$

Letting $u \in X,\ v, w \in X^{1,m}$ for $m \in \{1, \ldots, d\}$, we let the explicitly skew-symmetric trilinear form be given as

$$b^m(u,v,w) := \frac{1}{2}(u \cdot \nabla v, w) - \frac{1}{2}(u \cdot \nabla w, v).$$

It is easily shown (e.g., Lemma 1 from [41]) that

$$b^m(u,v,w) = (u \cdot \nabla v, w) + \frac{1}{2}\left((\nabla \cdot u)\, v, w\right).$$

Using the techniques in Lemma 1 from [41], the following lemma can be proven and will be used to bound the nonlinear terms:

Lemma 1. *There exist constants C_1, C_2, C_3 such that for all $u \in X$, $v, w \in X^{1,m}$,*

$$b^m(u,v,w) \leq C_1 \|\nabla u\|\|\nabla v\|\|\nabla w\|,$$
$$b^m(u,v,w) \leq C_2 \sqrt{\|u\|\|\nabla u\|}\|\nabla v\|\|\nabla w\|,$$
$$b^m(u,v,w) \leq C_3 \|\nabla u\|\|\nabla v\|\sqrt{\|w\|\|\nabla w\|}.$$

Herein we consider the nonlinear terms for the momentum and temperature equations, given by

$$b_u(u,v,w) := b^d(u,v,w),\ b_T(u,T,S) := b^1(u,T,S),$$

and where the constants from Lemma 1 are indexed $C_{i,u},\ C_{i,T}$ $(i=1,2,3)$ for the velocity and temperature, respectively.

A result (e.g., [37]) that will be used in our analyses is the Poincaré-Friedrichs inequality: For $v \in X, S \in W_{\Gamma_D}$, there exist constants $C_{\text{pf},1} > 0$ and $C_{\text{pf},2} > 0$, independent of Ω, such that $\|v\|^2 \leq C_{\text{pf},1}\|\nabla u\|^2$ and $\|S\|^2 \leq C_{\text{pf},2}\|\nabla S\|^2$.

We also require the definition of the temporally continuous norms

$$\|v\|_{L_t^p L_{\mathbf{x}}^q} = \left(\int_0^{t^*} \|v\|_{L^q}^p dt\right)^{\frac{1}{p}}, \|v\|_{L_t^\infty L_{\mathbf{x}}^q} = \sup_{t\in[0,t^*]} \|v\|_{L^q}.$$

Analogous definitions hold when the spatial $L^q(\Omega)$ is replaced with the spatial $H^k(\Omega)$, or the more general Sobolev spaces $W^{k,p}(\Omega)$.

2.2.2 DISCRETE PRELIMINARIES

First, let $X_h \subset X$, $Q_h \subset Q$, $\widehat{W}_h = (W_h, W_{\Gamma_D,h}) \subset (W, W_{\Gamma_D}) = \widehat{W}$ be conforming finite element spaces on a regular, quasi-uniform discretization of Ω (with maximal mesh width h) consisting of piecewise-continuous polynomials of degrees j, l, and j, respectively. We assume that they satisfy the following approximation properties for any $1 \leq j,\ l \leq k, m$:

$$\inf_{v_h\in X_h}\left\{\|u-v_h\| + h\|\nabla(u-v_h)\|\right\} \leq Ch^{k+1}|u|_{k+1}, \tag{2.14}$$

$$\inf_{q_h\in Q_h}\|p-q_h\| \leq Ch^m|p|_m, \tag{2.15}$$

$$\inf_{S_h\in \hat{W}_h}\left\{\|T-S_h\| + h\|\nabla(T-S_h)\|\right\} \leq Ch^{k+1}|T|_{k+1}, \tag{2.16}$$

for all $u \in X \cap X^{k+1,d}$, $p \in Q \cap X^{m,1}$, and $T \in \widehat{W} \cap X^{k+1,1}$. We further only consider spaces for which the discrete inf-sup/LBB condition is satisfied,

$$\inf_{q_h\in Q_h}\sup_{v_h\in X_h}\frac{(q_h, \nabla\cdot v_h)}{\|q_h\|\|\nabla v_h\|} \geq \beta_{\text{LBB},h} > 0, \tag{2.17}$$

where $\beta_{\text{LBB},h}$ is independent of h. We define the discrete dual norms in a similar way to the continuous dual norms, i.e.,

$$\|u_h\|_{-1} = \sup_{v_h \in X_h} \frac{(u_h, v_h)}{\|\nabla v_h\|}.$$

We will also assume that the finite element spaces satisfy the standard inverse inequality [36]:

$$\|\nabla \phi_{1,2}\| \leq C_{\text{inv},1,2} h^{-1} \|\phi_{1,2}\| \quad \forall \phi_1 \in X_h, \ \forall \phi_2 \in W_{\Gamma_D,h},$$

where $C_{\text{inv},1,2}$ depend on the minimum angle α_{min} in the triangulation.

The Cauchy-Schwarz-Young (CSY) inequality $(u, v) \leq \frac{\epsilon}{2}\|u\|^2 + \frac{1}{2\epsilon}\|v\|^2$ will be used extensively, as well the polarization identity $2(u, v) = \|u\|^2 + \|v\|^2 - \|u - v\|^2$. The discrete time analysis will utilize the following norms $\forall \ -1 \leq k < \infty$:

$$|||v|||_{\infty,k} := \max_{1 \leq n \leq N} \|v^n\|_k, \ |||v|||_{p,k} := \Big(\Delta t \sum_{n=1}^{N} \|v^n\|_k^p\Big)^{1/p}.$$

The Stokes projection will be vital in the upcoming error analyses. Let $I_h^{Stokes} : V \times Q \to X_h \times Q_h$ via $I_h^{Stokes}(u, p) = (U, P)$ satisfy the discrete Stokes problem

$$\begin{aligned} \Pr(\nabla(U - u), \nabla v_h) - (P - p, \nabla \cdot v_h) &= 0 \ \forall \ v_h \in X_h, \\ (\nabla \cdot (U - u), q_h) &= 0 \ \forall \ q_h \in Q_h. \end{aligned}$$

There holds the following approximation error result.

Lemma 2. *Assume the approximation properties 2.14-2.15 and associated regularity hold. Then, there exists $C > 0$ such that*

$$h^{-1}\|u - U\| + \|\nabla(u - U)\| + \|p - P\| \leq C\Big\{ \inf_{v_h \in X_h} \|\nabla(u - v_h)\| + \inf_{q_h \in Q_h} \|p - q_h\| \Big\}.$$

Proof. See Theorem 13 of [75] and apply the Aubin-Nitsche technique. □

We will also require a Discrete Gronwall inequality, given below:

Lemma 3. *(Discrete Gronwall Lemma). Let Δt, H, a_n, b_n, c_n, and d_n be finite nonnegative numbers for $n \geq 0$ such that for $N \geq 1$*

$$a_N + \Delta t \sum_0^N b_n \leq \Delta t \sum_0^{N-1} d_n a_n + \Delta t \sum_0^N c_n + H,$$

then for all $\Delta t > 0$ and $N \geq 1$

$$a_N + \Delta t \sum_0^N b_n \leq \exp\Big(\Delta t \sum_0^{N-1} d_n\Big)\Big(\Delta t \sum_0^N c_n + H\Big).$$

Proof. See Lemma 5.1 on p. 369 of [56]. □

3.0 TIME-ADAPTIVE ARTIFICIAL COMPRESSIBILITY METHODS

The coupling of velocity and pressure in flow problems creates inefficiencies and challenges when attempting to approximate the solutions numerically. Artificial compressibility methods, like penalty and projection schemes, attempt to decouple the velocity and pressure to make a numerical approximation feasible. These methods are most efficient when used in low temporal order schemes and are extremely fast. However, they are not amenable to time-adaptive stepping methods. This chapter develops, analyzes, and demonstrates multiple time-adaptive AC methods. Section 3.1 gives a brief overview of AC methods. Next, a slightly compressible continuum model is developed and explored in Section 3.2. Numerical methods derived from this model, as well as another time-adaptive AC method are analyzed and tested in Section 3.3. Concluding remarks are given in Section 3.4.

3.1 AN OVERVIEW OF ARTIFICIAL COMPRESSIBILITY METHODS

The numerical approximation of the incompressible NSE is made more difficult by the coupling of the velocity and pressure variables. This challenge was identified early on in the history of computational fluid dynamics, and in the late 1960s several new methods were developed to tackle this difficulty. Temam, in 1968 [131], introduced the well-known *penalty* method, which perturbs (2.3) by a weighted pressure term, replacing (2.2)–(2.3) by the system

$$\partial_t u^\varepsilon + (u^\varepsilon \cdot \nabla) u^\varepsilon - \nu \Delta u^\varepsilon + \nabla p^\varepsilon = f,$$
$$\varepsilon p^\varepsilon + \nabla \cdot u^\varepsilon = 0.$$

One decouples the variables by noting that $p^\varepsilon = -\frac{1}{\varepsilon} \nabla \cdot u^\varepsilon$, so that one may solve the momentum equation for the velocity and then update the pressure. This method decouples the variables, and is first-order in time for $\varepsilon = \mathcal{O}(\Delta t)$. However, the condition number of the discrete viscous term, $-\nu\Delta$ is approximately $\mathcal{O}(\nu \Delta t h^{-2})$. The new term arising from

the variable separation, $-\frac{1}{\varepsilon}\nabla\nabla\cdot u$, has condition number $\mathcal{O}(h^{-2})$ if the method is first-order convergent. If the timestepping method is of order $k \geq 2$, the condition number acts like $\mathcal{O}(\Delta t^{1-k}h^{-2})$, implying the condition number of the stiffness matrix blows up as $\Delta t \to 0$.

Later, Chorin [14, 15], Oskolkov [95] and Temam [127, 128] developed *artificial compressibility* (or artificial compression) methods to alleviate this issue. These methods use a weighted stabilization to the continuity equation involving the temporal derivative of pressure, i.e.,

$$\begin{aligned} \partial_t u^\varepsilon + (u^\varepsilon\cdot\nabla)u^\varepsilon - \nu\Delta u^\varepsilon + \nabla p^\varepsilon &= f, \\ \varepsilon\partial_t p^\varepsilon + \nabla\cdot u^\varepsilon &= 0. \end{aligned} \tag{3.1}$$

The method decouples the velocity and pressure, eliminating the need for a mixed formulation and linear solve. Indeed, the main solve is just for velocity (the pressure is an update), and if a backward Euler time-discretization is used, then $p^{n+1} = p^n - \frac{\Delta t}{\varepsilon}\nabla\cdot u^{n+1}$, implying the condition number of the resulting matrix $-\frac{\Delta t}{\varepsilon}\nabla\nabla\cdot u$ is like the viscous term, $\mathcal{O}(h^{-2})$.

Remark 4. *The term $\varepsilon\partial_t p^\varepsilon$ implies a pseudo-density $\rho^\varepsilon = \varepsilon p^\varepsilon$ from the compressible NSE with wave speed $c = \frac{1}{\sqrt{\varepsilon}}$.*

Remark 5. *Convergence of the AC approximation* (3.1) *to a weak solution of the NSE* (2.2)–(2.3) *as $\varepsilon \to 0$ has been proven for bounded $\Omega \subset \mathbb{R}^2$ by Temam [127, 128, 130] (using the method of fractional derivatives of Lions [83]). Donatelli-Marcati [32, 33] extended $\varepsilon \to 0$ convergence to the case of $\mathbb{R}^3$ and exterior domains and in [32] by using the dispersive structure of the acoustic pressure equation. There is also a growing literature establishing convergence of discretizations of AC models to NSE solutions including [48], [49], [68], [74], and [108].*

Clearly, serious advantages exist for AC methods. They are stable, time accurate, and fast at low temporal orders. Furthermore, they do not require that velocity and pressure spaces satisfy the discrete LBB condition (2.17). However, they begin to suffer from condition number issues at higher orders (similarly to penalty methods). When using a conservative timestepping method, nonphysical acoustics in the pressure appear due to the lack of numerical dissipation (see [25, 26]). They also suffer from a so-called *order barrier* in the pressure,

identified by Shen [106] and overcome by Guermond and Minev [48]. AC methods also suffer from difficulties when using a variable timestep.

3.2 A NEW COMPRESSIBLE CONTINUUM MODEL

3.2.1 INTRODUCTION

Of the many methods for predicting incompressible flow, artificial compressibility (AC) methods, based on replacing $\nabla \cdot u = 0$ by $\varepsilon \partial_t p + \nabla \cdot u = 0$ $(0 < \varepsilon \ll 1)$ and advancing the pressure explicitly in time, are among the most efficient. These methods also have a reputation for low time accuracy. Herein we study one source of low accuracy, propose a resolution, give analytical support for the corrected method and show some numerical comparisons of a common AC method and its proposed correction. Consider the incompressible NSE (2.2)–(2.3) in a $3d$ domain Ω, here either a bounded open set or $\mathbb{R}^3$,

$$\partial_t u + (u \cdot \nabla)u + \nabla p - \nu \Delta u = f(t, x)$$
$$\nabla \cdot u = 0,$$

where $(t, x) \in [0, t^*] \times \Omega$, $u \in \mathbb{R}^3$ is the velocity, $p \in \mathbb{R}$ the pressure, ν the kinematic viscosity, and $f \in \mathbb{R}^3$ the external force.

AC methods, e.g., [46], [101], [25], are based on approximating the solution of the slightly compressible equations

$$\partial_t u^\varepsilon + (u^\varepsilon \cdot \nabla)u^\varepsilon + \frac{1}{2}(\nabla \cdot u^\varepsilon)u^\varepsilon + \nabla p^\varepsilon - \nu \Delta u^\varepsilon = f$$
$$\varepsilon \partial_t p^\varepsilon + \nabla \cdot u^\varepsilon = 0,$$

where $0 < \varepsilon$ is small. Here, u^ε is the approximate velocity, p^ε is the approximate pressure and the nonlinearity has been explicitly skew-symmetrized. (This is a common formulation but not the only one, see Section 3.2.1.2). Time accuracy is obtained by either using explicit time discretization methods and small time steps for short time simulations, using high order methods with moderate timesteps for longer time simulations or by adding time adaptivity

to a low or high order implicit method. The first is not considered herein. The second leads to highly ill-conditioned linear systems (Shen [107] also suggests that an accuracy barrier exists in AC methods). The third, considered herein, has the possibility to both increase efficiency and provide time accuracy. To our knowledge, the defect correction based scheme of Guermond and Minev [47] is the only previous work in this direction.

Remark 6. *The separate issue of pressure initialization, not addressed here, also exists. We do note that for internal flows pressure data is often more reliable than velocity data.*

Remark 7. *For a 4th order time discretization, $\varepsilon = \mathcal{O}(\Delta t^4)$ is necessary to retain accuracy. This leads to a viscous term $-\nu\Delta u^\varepsilon_{n+1} - \Delta t^{-3}\nabla\nabla\cdot u^\varepsilon_{n+1}$ and a linear system to be solved at each timestep with condition number $\mathcal{O}(\Delta t^{-2}h^{-2})$.*

To fix ideas, suppress the space discretization and consider a commonly used fully-implicit time discretization

$$\begin{aligned}\frac{u^\varepsilon_{n+1}-u^\varepsilon_n}{\Delta t} + (u^\varepsilon_{n+1}\cdot\nabla)u^\varepsilon_{n+1} + \frac{1}{2}(\nabla\cdot u^\varepsilon_{n+1})u^\varepsilon_{n+1} + \nabla p^\varepsilon_{n+1}\\ -\nu\Delta u^\varepsilon_{n+1} = f(t_{n+1}),\\ \varepsilon\frac{p^\varepsilon_{n+1}-p^\varepsilon_n}{\Delta t} + \nabla\cdot u^\varepsilon_{n+1} = 0.\end{aligned}$$

For other time discretizations see, e.g., [69], [94], [25], [145]. Here Δt is the timestep, $t_n = n\Delta t$, u^ε_n, p^ε_n are approximations to the velocity and pressure at $t = t_n$. Since $\nabla p^\varepsilon_{n+1} = \nabla p^\varepsilon_n - (\Delta t/\varepsilon)\nabla\nabla\cdot u^\varepsilon_{n+1}$, this uncouples into

$$\begin{aligned}\frac{u^\varepsilon_{n+1}-u^\varepsilon_n}{\Delta t} + (u^\varepsilon_{n+1}\cdot\nabla)u^\varepsilon_{n+1} + \frac{1}{2}(\nabla\cdot u^\varepsilon_{n+1})u^\varepsilon_{n+1} + \nabla p^\varepsilon_n - \frac{\Delta t}{\varepsilon}\nabla\nabla\cdot u^\varepsilon_{n+1}\\ -\nu\Delta u^\varepsilon_{n+1} = -\nabla p^\varepsilon_n + f_{n+1},\\ \text{then given } u^\varepsilon_{n+1}\text{:}\quad p^\varepsilon_{n+1} = p^\varepsilon_n - (\Delta t/\varepsilon)\nabla\cdot u^\varepsilon_{n+1}.\end{aligned} \tag{3.2}$$

This method is unconditionally, nonlinearly, long-time stable, e.g., [46], [48]. It has consistency error $\mathcal{O}(\Delta t + \varepsilon)$ and thus determines ε balancing errors by $\varepsilon = \Delta t$. Time adaptivity means decreasing or increasing the time step according to solution activity, [45]. Given the $\mathcal{O}(\Delta t + \varepsilon)$ consistency error, this means varying both $\Delta t = \Delta t_n$ and $\varepsilon = \varepsilon_n$. To our knowledge, no long-time stability analysis of this method with variable $\Delta t = \Delta t_n$ and $\varepsilon = \varepsilon_n$

is known or even possible at present, see Section 3.2.2. Peculiar solution behavior seen in an adaptive simulation thus cannot be ascribed to either a flow phenomenon or to an anomaly created by the numerical method. This is the problem we address herein for the time discretized AC method (with $\varepsilon = \varepsilon_n$) and for the associated continuum AC model (with $\varepsilon = \varepsilon(t)$).

In Section 3.2.2 we first show that the standard AC method, (3.2) above, is 0-stable for variable $\varepsilon, \Delta t$ provided $\varepsilon, \Delta t$ are slowly varying (0-stability allows non-catastrophic exponential growth). Thus, (3.2) suffices for short time simulations with nearly constant timesteps. The long time stability of (3.2) with variable-ε, k is analyzed in Section 3.2.2 as well. Some preliminary conclusions are presented but then complete resolution of instability or stability is an open problem for the standard method.

Section 3.2.2 presents a stable extension of AC methods to variable $\varepsilon, \Delta t$, one central contribution of this dissertation. The proposed method is

$$\begin{aligned} &\frac{u^{\varepsilon}_{n+1} - u^{\varepsilon}_{n}}{\Delta t_{n+1}} + \nabla p^{\varepsilon}_{n+1} - \nu \Delta u^{\varepsilon}_{n+1} + (u^{\varepsilon}_{n+1} \cdot \nabla) u^{\varepsilon}_{n+1} \\ &\qquad + \frac{1}{2}(\nabla \cdot u^{\varepsilon}_{n+1}) u^{\varepsilon}_{n+1} = f_{n+1}, \\ &\frac{1}{2}\frac{\varepsilon_{n+1} p^{\varepsilon}_{n+1} - \varepsilon_n p^{\varepsilon}_{n}}{\Delta t_{n+1}} + \frac{\varepsilon_n}{2}\frac{p^{\varepsilon}_{n+1} - p^{\varepsilon}_{n}}{\Delta t_{n+1}} + \nabla \cdot u^{\varepsilon}_{n+1} = 0. \end{aligned} \tag{3.3}$$

This method reduces to the standard AC method (3.2) for constant $\varepsilon, \Delta t$. Section 3.2.2 shows that the new method (3.3) is unconditionally, nonlinearly, long time stable without assumptions on $\varepsilon_n, \Delta t_n$, Theorem 2. In numerical tests of (3.3), for problems on bounded domains, in Section 3.2.5, the new method works well (as expected) when $\Delta t_{n+1} = \varepsilon_{n+1}$ is picked self adaptively to ensure $||\nabla \cdot u||$ is below a present tolerance. It also performs well in tests where $\Delta t_n = \varepsilon_n$ is pre-chosen to try to break the method's stability or physical fidelity by increasing or fluctuating ε or Δt.

In support, we give an analysis of the physical fidelity of the non-autonomous continuum model associated with (3.3):

$$\begin{aligned} \partial_t u^{\varepsilon} + (u^{\varepsilon} \cdot \nabla) u^{\varepsilon} + \tfrac{1}{2}(\nabla \cdot u^{\varepsilon}) u^{\varepsilon} + \nabla p^{\varepsilon} - \nu \Delta u^{\varepsilon} = f, \\ \partial_t(\varepsilon(t) p^{\varepsilon}) - \tfrac{1}{2}\partial_t \varepsilon(t) p^{\varepsilon} + \nabla \cdot u^{\varepsilon} = 0. \end{aligned} \tag{3.4}$$

Sections 3.2.3 and 3.2.4 address the question: *Under what conditions on $\varepsilon(t)$ do solutions to the new AC model (1.3) converge to weak solutions of the incompressible NSE as $\varepsilon \to 0$?* Convergence (modulo a subsequence) is proven for the pure Cauchy problem under the assumption on the fluctuation $\varepsilon_t(t)$ that

$$\varepsilon(t) \leq C\epsilon \to 0, \quad \left|\frac{\varepsilon_t(t)}{\varepsilon(t)}\right| \leq C, \quad \text{for } t \in [0, t^*]. \tag{3.5}$$

This extension of model convergence to the non-autonomous system is a second central contribution herein. In self-adaptive simulations based on (3.3), this condition requires smooth adjustment of timesteps and precludes a common strategy of timestep halving or doubling. A similar smoothness condition on $\varepsilon_t(t)$ recently arose in stability analysis of other variable timestep methods in [115]. Weakening the condition (3.5) on $\varepsilon(t)$ (which we conjecture is possible) is an important open problem.

3.2.1.1 ANALYTICAL DIFFICULTIES OF THE $\varepsilon(t) \to 0$ LIMIT For $\Omega = \mathbb{R}^3$, one difficulty in establishing convergence is the estimate for acoustic pressure waves. From the acoustic pressure wave equation (3.25) for the new model (3.4), the pressure wave speed is $\mathcal{O}(1/\varepsilon)$, suggesting only weak convergence of the velocity u^ε. Strong convergence of u^ε thus hinges upon the dispersive behavior of these waves at infinity. In the case when ε is constant, the classical Strichartz type estimates [43, 71, 120] together with a refined bilinear estimate [72, 116] of the three-dimensional inhomogeneous wave equations can be directly applied to infer (after some technical difficulties) sufficient control of the pressure waves. However, when $\varepsilon = \varepsilon(t)$, the resulting acoustic equation is *non-autonomous*. There are still results on the space-time Strichartz estimates for variable-coefficient wave equations at our disposal; see, e.g., [125]. However the refined bilinear estimates do not seem to be immediately available, since these estimates are based on the explicit structure of the Kirchhoff's formula for the classical wave operator. To overcome this difficulty, we further introduce a scale change in the time variable so that the resulting pressure wave equation becomes the classical wave operator. This allows us to obtain the refined bilinear estimates, and therefore establish the desired dispersive estimates for the pressure. Please refer to Section 3.2.3.3 for more details.

3.2.1.2 OTHER AC FORMULATIONS Generally AC methods skew-symmetrize the nonlinearity and include a term $\varepsilon\partial_t p$ that uncouples pressure and velocity and lets the pressure be explicitly advanced in time. There are several choices for the first and several for the second. A few alternate possibilities are described next and combinations of these are certainly possible.

Motivated by the equations of hyposonic flow [146], the material derivative can be used for the artificial compressibility term, e.g., [95],

$$\partial_t u^\varepsilon + (u^\varepsilon \cdot \nabla)u^\varepsilon + \frac{1}{2}(\nabla \cdot u^\varepsilon)u^\varepsilon + \nabla p^\varepsilon - \nu\Delta u^\varepsilon = f,$$
$$\varepsilon\left(\partial_t p^\varepsilon + u^\varepsilon \cdot \nabla p^\varepsilon\right) + \nabla \cdot u^\varepsilon = 0.$$

Numerical dissipation can be incorporated into the pressure equation, e.g. [74], as in

$$\partial_t u^\varepsilon + (u^\varepsilon \cdot \nabla)u^\varepsilon + \frac{1}{2}(\nabla \cdot u^\varepsilon)u^\varepsilon + \nabla p^\varepsilon - \nu\Delta u^\varepsilon = f$$
$$\varepsilon\left(\partial_t p^\varepsilon + p^\varepsilon\right) + \nabla \cdot u^\varepsilon = 0.$$

A dispersive regularization has been included in the momentum equation in [25],

$$\partial_t\left(u^\varepsilon - \frac{1}{\varepsilon}\nabla\nabla \cdot u^\varepsilon\right) + (u^\varepsilon \cdot \nabla)u^\varepsilon + \frac{1}{2}(\nabla \cdot u^\varepsilon)u^\varepsilon + \nabla p^\varepsilon - \nu\Delta u^\varepsilon = f,$$
$$\varepsilon\partial_t p^\varepsilon + \nabla \cdot u^\varepsilon = 0.$$

The nonlinearity can be skew symmetrized in various ways, replacing $(u \cdot \nabla)u$ in the NSE by one of the following

$$\begin{array}{rcc} \text{Standard skew-symmetrization} & : & (u^\varepsilon \cdot \nabla)u^\varepsilon + \frac{1}{2}(\nabla \cdot u^\varepsilon)u^\varepsilon \\ \text{Rotational form} & : & (\nabla \times u^\varepsilon) \times u^\varepsilon \\ \text{EMA form [12]} & : & (\nabla u^\varepsilon + (\nabla u^\varepsilon)^T)u^\varepsilon + (\nabla \cdot u^\varepsilon)u^\varepsilon \end{array}$$

The penalty model (not studied herein) where $\nabla \cdot u = 0$ is replaced by $\nabla \cdot u^\varepsilon = -\varepsilon p^\varepsilon$, is sometimes also viewed as an artificial compressibility model, [101]. Other artificial (or pseudo) compressibility schemes have been constructed of varying orders, each with strengths and weaknesses. We refer to Shen [112] for more details.

3.2.2 STABILITY OF VARIABLE-ε AC METHODS

We begin by considering variable ε stability of the standard method under noslip boundary conditions (here, we change notation so that $(u^n, p^n) = (u_n^\varepsilon, p_n^\varepsilon)$)

$$\begin{aligned}\frac{u^{n+1}-u^n}{\Delta t_{n+1}} + \nabla p^{n+1} - \nu\Delta u^{n+1} + (u^{n+1}\cdot\nabla)u^{n+1} \\ +\frac{1}{2}(\nabla\cdot u^{n+1})u^{n+1} = f^{n+1}, \\ \varepsilon_{n+1}\frac{p^{n+1}-p^n}{\Delta t_{n+1}} + \nabla\cdot u^{n+1} = 0,\end{aligned} \tag{3.6}$$

subject to initial and boundary conditions:

$$u^0(x) = u_0, \quad p^0(x) = p_0, \text{ in } \Omega\ ,$$

$$u^n = 0 \text{ on } \partial\Omega \text{ for } t > 0.$$

We first prove 0-stability, namely that u^n can grow no faster than exponential, when ε_n is slowly varying. The case when $f \equiv 0$ is clearest since then any energy growth is then incorrect.

Theorem 1. *For the standard method (3.6), let $f_n = 0$ for all n and suppose*

$$\frac{\varepsilon_{n+1}-\varepsilon_n}{\Delta t_n} \le \beta\varepsilon_n \text{ for some } \beta \text{ for all } n.$$

Then

$$\begin{aligned}\|u^n\|^2 + \varepsilon_n\|p^n\|^2 &\le \left(\Pi_{j=1}^{n-1}(1+\beta\Delta t_j)\right)\left(\|u^0\|^2 + \varepsilon_0\|p^0\|^2\right) \\ &\le e^{\beta t_n}\left(\|u^0\|^2 + \varepsilon_0\|p^0\|^2\right).\end{aligned}$$

Proof. Take an inner product of the first equation with $2\Delta t_{n+1}u^{n+1}$, the second with $2\Delta t_{n+1}p^{n+1}$, integrate over Ω, integrate by parts, use skew-symmetry and add. This yields, by the polarization identity,

$$\begin{aligned}\|u^{n+1}\|^2 - \|u^n\|^2 + \|u^{n+1}-u^n\|^2 + 2\Delta t_{n+1}\nu\|\nabla u^{n+1}\|^2 \\ +\varepsilon_{n+1}\|p^{n+1}\|^2 - \varepsilon_{n+1}\|p^n\|^2 + \varepsilon_{n+1}\|p^{n+1}-p^n\|^2 = 0.\end{aligned}$$

The pressure terms do not collapse into a telescoping sum upon adding due to the variability of ε. Thus we correct for this effect, rearrange and adjust appropriately to yield

$$\left(\|u^{n+1}\|^2 + \varepsilon_{n+1}\|p^{n+1}\|^2\right) - \left(\|u^n\|^2 + \varepsilon_n\|p^n\|^2\right) + \|u^{n+1} - u^n\|^2 + \varepsilon_{n+1}\|p^{n+1} - p^n\|^2$$
$$+2\Delta t_{n+1}\nu\|\nabla u^{n+1}\|^2 = (\varepsilon_{n+1} - \varepsilon_n)\,\|p^n\|^2.$$

Note that $(\varepsilon_{n+1} - \varepsilon_n)\,\|p^n\|^2 \leq \Delta t_n \beta \varepsilon_n \|p^n\|^2$. Dropping the (non-negative) dissipation terms we have

$$E_{n+1} - E_n \leq \beta \Delta t_n E_n \text{ where } E_n := \|u^n\|^2 + \varepsilon_n\|p^n\|^2,$$

from which the first result follows immediately. For the second inequality, note that since $1 + \beta\Delta t_j \leq e^{\beta \Delta t_j}$ we have

$$\Pi_{j=1}^{n-1}(1 + \beta\Delta t_j) \leq \Pi_{j=1}^{n-1} e^{\beta\Delta t_j} = e^{\beta\left[\sum_{j=1}^{n-1}\Delta t_j\right]} = e^{\beta t_n}$$

□

Since β (by assumption) is independent of the timestep Δt, this implies 0-stability. For short time simulations, 0-stability suffices, but is insufficient for simulations over longer time intervals. The assumption that ε (and thus also the timestep) is slowly varying:

$$\frac{\varepsilon_{n+1} - \varepsilon_n}{\Delta t_n} \leq \beta \varepsilon_n$$

precludes the common adaptive strategy of timestep halving and doubling. For example, suppose

$$\begin{aligned} \varepsilon_{n+1} &= 2\varepsilon_n \text{ and } \Delta t_{n+1} = 2\Delta t_n \text{ then} \\ \frac{\varepsilon_{n+1} - \varepsilon_n}{\Delta t_n \varepsilon_n} &= \frac{2\varepsilon_n - \varepsilon_n}{\Delta t_n \varepsilon_n} = \frac{1}{\Delta t_n} \to \infty \text{ as } \Delta t \to 0. \end{aligned}$$

3.2.2.1 THE CORRECTED, VARIABLE-ε AC METHOD The above proof indicates that the problem arises from the fact that the discrete $\varepsilon\partial_t p$ term is not a time difference when multiplied by p. Under noslip boundary conditions, the standard method obeys the discrete energy law

$$\left(\|u^{n+1}\|^2 + \varepsilon_{n+1}\|p^{n+1}\|^2\right) - \left(\|u^n\|^2 + \varepsilon_n\|p^n\|^2\right) + \|u^{n+1} - u^n\|^2 + \varepsilon_{n+1}\|p^{n+1} - p^n\|^2 \quad (3.7)$$
$$+2\Delta t_{n+1}\nu\|\nabla u^{n+1}\|^2 = (\varepsilon_{n+1} - \varepsilon_n)\,\|p^n\|^2.$$

Since the variable-ε term $(\varepsilon_{n+1} - \varepsilon_n)\,\|p^n\|^2$ has two signs, depending only on whether the timestep is increasing or decreasing, it can either dissipate energy or input energy. The sign of the right-hand-side shows that if:

- Δt_n is decreasing the effect of changing the timestep is *dissipative*, while if
- Δt_n is increasing the effect of changing the timestep *inputs energy* into the approximate solution.

In the second case, if the term $(\varepsilon_{n+1} - \varepsilon_n)\,\|p^n\|^2$ dominates in the aggregate the other dissipative terms non-physical energy growth may be possible. However, we stress that we have neither a proof of long time stability of the variable-ε standard method nor a convincing example of instability. Resolving this is an open problem discussed in the next sub-section.

The practical question is how to adapt the AC method to variable-ε so as to ensure long time stability. After testing a few natural alternatives we propose the new AC method

$$\begin{aligned}
&\frac{u^{n+1} - u^n}{\Delta t_{n+1}} + (u^{n+1}\cdot\nabla)u^{n+1} + \frac{1}{2}(\nabla\cdot u^{n+1})u^{n+1} \\
&\qquad -\nu\Delta u^{n+1} + \nabla p^{n+1} = f^{n+1}, \\
&\frac{1}{2}\frac{\varepsilon_{n+1}p^{n+1} - \varepsilon_n p^n}{\Delta t_{n+1}} + \frac{\varepsilon_n}{2}\frac{p^{n+1} - p^n}{\Delta t_{n+1}} + \nabla\cdot u^{n+1} = 0.
\end{aligned} \quad (3.8)$$

When ε is constant the new method (3.8) reduces to the standard method (3.2).

Remark 8 (Higher Order Methods)**.** *If a higher order time discretization such as BDF2 is desired, the modification required is to use the higher order discretization for the momentum equation, the same modification of the continuity equation and select* $\varepsilon_n = \Delta t_n^{\text{method order}}$ *to preserve higher order consistency error. For example, for variable step BDF2, let* $\tau = \Delta t_{n+1}/\Delta t_n$*. Then we have*

$$\begin{aligned}
&\frac{\frac{2\tau+1}{\tau+1}u^{n+1} - (\tau+1)u^n + \frac{\tau^2}{\tau+1}u^{n-1}}{\Delta t_{n+1}} + (u^{n+1}\cdot\nabla)u^{n+1} + \frac{1}{2}(\nabla\cdot u^{n+1})u^{n+1} \\
&\qquad +\nabla p^{n+1} - \nu\Delta u^{n+1} = f(t_{n+1}), \\
&\frac{1}{2}\frac{\varepsilon_{n+1}p^{n+1} - \varepsilon_n p^n}{\Delta t_{n+1}} + \frac{\varepsilon_n}{2}\frac{p^{n+1}-p^n}{\Delta t_{n+1}} + \nabla\cdot u^{n+1} = 0 \text{ with } \varepsilon_{n+1} = \Delta t_{n+1}^2.
\end{aligned}$$

This is easily proven A-stable for constant timesteps. Since BDF2 is not A-stable for increasing timesteps, the above would also not be expected to be more than 0-stable for increasing timesteps.

Theorem 2. *The variable-*$\varepsilon, \Delta t$ *method (3.8) under noslip boundary conditions is unconditionally, long time stable. For any* $N > 0$ *the energy equality holds:*

$$\begin{aligned}
&\|u^N\|^2 + \varepsilon_N\|p^N\|^2 + \sum_{n=0}^{N-1}\left(\|u^{n+1}-u^n\|^2 + \varepsilon_n\|p^{n+1}-p^n\|^2 + 2\Delta t_{n+1}\nu\|\nabla u^{n+1}\|^2\right) \\
&\qquad = \|u^0\|^2 + \varepsilon_0\|p^0\|^2 + \sum_{n=0}^{N-1} 2\Delta t_{n+1}(f^{n+1}, u^{n+1})
\end{aligned}$$

and the stability bound holds:

$$\begin{aligned}
&\|u^N\|^2 + \varepsilon_N\|p^N\|^2 + \sum_{n=0}^{N-1}\left(\|u^{n+1}-u^n\|^2 + \varepsilon_n\|p^{n+1}-p^n\|^2 + \Delta t_{n+1}\nu\|\nabla u^{n+1}\|^2\right) \\
&\qquad = \|u^0\|^2 + \varepsilon_0\|p^0\|^2 + \sum_{n=0}^{N-1}\frac{\Delta t_{n+1}}{\nu}\|f^{n+1}\|_{-1}^2
\end{aligned}$$

Proof. We follow the stability analysis in the last proof. Take an inner product of the first equation with $2\Delta t_{n+1}u^{n+1}$, the second with $2\Delta t_{n+1}p^{n+1}$, integrate over the flow domain,

integrate by parts, use skew-symmetry, use the polarization identity twice, and add. This yields

$$\begin{aligned}\|u^{n+1}\|^2 - \|u^n\|^2 + \|u^{n+1} - u^n\|^2 + 2\Delta t_{n+1}\nu\|\nabla u^{n+1}\|^2 \\ +\varepsilon_{n+1}\|p^{n+1}\|^2 - 2\varepsilon_n(p^n, p^{n+1}) + \varepsilon_n\|p^{n+1}\|^2 \\ = 2\Delta t_{n+1}(f^{n+1}, u^{n+1}).\end{aligned}$$

From the polarization identity on the pressure inner product, the energy equality becomes

$$\begin{aligned}\left(\|u^{n+1}\|^2 + \varepsilon_{n+1}\|p^{n+1}\|^2\right) - \left(\|u^n\|^2 + \varepsilon_n\|p^n\|^2\right) \\ 2\Delta t_{n+1}\nu\|\nabla u^{n+1}\|^2 + \|u^{n+1} - u^n\|^2 + \varepsilon_n\|p^{n+1} - p^n\|^2 \\ = 2\Delta t_{n+1}(f^{n+1}, u^{n+1}).\end{aligned}$$

Upon summation the first two terms telescope, completing the proof of the energy equality. The stability estimate follows from the energy equality, the definition of the dual norm, and the Cauchy-Schwarz-Young inequality. □

3.2.2.2 INSIGHT INTO A POSSIBLE VARIABLE-ε INSTABILITY The difficulty in ensuring long time stability when simply solving (3.6) for variable ε can be understood at the level of the continuum model. When $f = 0$ the NSE kinetic energy is monotonically decreasing so any growth in model energy represents an instability. Dropping the superscript ε for this sub-section, consider the kinetic energy evolution of

$$\begin{aligned}\partial_t u + \nabla p = \nu\Delta u - (u\cdot\nabla)u - \frac{1}{2}(\nabla\cdot u)u, \\ \varepsilon(t)\partial_t p + \nabla\cdot u = 0,\end{aligned} \tag{3.9}$$

subject to periodic or noslip boundary conditions. Computing the model's kinetic energy by taking the inner product with, respectively, u and p, integrating and then adding gives the continuum equivalent of the kinetic energy law of the standard AC method (3.7) above:

$$\frac{d}{dt}\left(\|u(t)\|^2 + \varepsilon(t)\|p(t)\|^2\right) + \nu\|\nabla u(t)\|^2 = \varepsilon_t(t)\|p(t)\|^2.$$

The RHS suggests the following:

Decreasing ε ($\varepsilon_t(t) < 0$) acts to decrease the L^2 norm of u and p while increasing ε ($\varepsilon_t(t) > 0$) acts to increase the L^2 norm of u and p.

Thus, it seems like an example of instability would be simple to generate by taking a solution with large pressure, small velocity, small ν and $\partial_t\varepsilon(t) \gg \varepsilon(t)$. However, consider next the equation for pressure fluctuations about a rest state. Beginning with

$$\partial_t u + \nabla p = 0 \text{ and } \varepsilon(t)\partial_t p + \nabla \cdot u = 0, \tag{3.10}$$

eliminate the velocity in the standard manner for deriving the acoustic equation. This yields the induced equation for acoustic pressure oscillations $(\varepsilon(t)\partial_t p)_t - \Delta p = 0$. Oddly, $\varepsilon(t) = t$ (increasing) occurs in [76]. Multiplying by $\partial_t p$ and integrating yields

$$\frac{d}{dt}\left(\varepsilon(t)\|\partial_t p(t)\|^2 + \|\nabla p(t)\|^2\right) = -\varepsilon_t(t)\|\partial_t p(t)\|^2. \tag{3.11}$$

The RHS of (3.11) yields the nearly opposite prediction that

Decreasing ε ($\varepsilon_t(t) < 0$) acts to increase the L^2 norm of $\partial_t p$ and ∇p while increasing ε ($\varepsilon_t(t) > 0$) acts to increase the L^2 norm of $\partial_t p$ and ∇p.

The analytical conclusion is that long time stability of the standard AC method with variable-$\varepsilon, \Delta t$ is a murky open problem.

3.2.3 ANALYSIS OF THE VARIABLE-ε CONTINUUM AC MODEL

The last subsection suggests that insight into the new model may be obtained through analysis of its continuum analog without the assumption of small fluctuations about a rest state. Accordingly, this section considers the pure Cauchy problem, $\Omega = \mathbb{R}^3$, for

$$\begin{aligned}\partial_t u^\varepsilon + \nabla p^\varepsilon &= \nu\Delta u^\varepsilon - (u^\varepsilon \cdot \nabla)u^\varepsilon - \frac{1}{2}(\nabla \cdot u^\varepsilon)u^\varepsilon + f^\varepsilon \\ \partial_t(\varepsilon(t)p^\varepsilon) - \frac{1}{2}\varepsilon_t(t)p^\varepsilon + \nabla \cdot u^\varepsilon &= 0.\end{aligned}$$

To explain the change of the pressure term in the continuity equation from $\varepsilon p_t^\varepsilon$ to $\partial_t(\varepsilon(t)p^\varepsilon) - \frac{1}{2}\varepsilon_t(t)p^\varepsilon$, note that

$$\left(\frac{1}{2}\varepsilon(p^\varepsilon)^2\right)_t = p^\varepsilon\left[(\varepsilon p^\varepsilon)_t - \frac{1}{2}\varepsilon_t p^\varepsilon\right] = p^\varepsilon\left[\varepsilon p_t^\varepsilon + \frac{1}{2}\varepsilon_t p^\varepsilon\right].$$

This can equivalently be formulated as $\frac{1}{2}(\varepsilon p^\varepsilon)_t + \frac{1}{2}\varepsilon p_t^\varepsilon$ since

$$\left(\frac{1}{2}\varepsilon(p^\varepsilon)^2\right)_t = p^\varepsilon \frac{1}{2}\left[(\varepsilon p^\varepsilon)_t + \varepsilon p_t^\varepsilon\right].$$

Recall from (3.5) that our assumptions on the relaxation parameter $\varepsilon(t)$ are

$$\varepsilon(t) \in C^1([0,T]), \quad 0 < c\epsilon \leq \varepsilon(t) \leq C\epsilon, \quad \left|\frac{\varepsilon_t(t)}{\varepsilon(t)}\right| \leq C, \tag{3.12}$$

for $t \in [0,T]$, c and C are some positive constants, and $\epsilon > 0$ is some vanishing constant.

From the assumption (3.12) we may write

$$\varepsilon(t) = \epsilon A(t) \tag{3.13}$$

for some function $A(t)$ satisfying

$$A \in C^1([0,t^*]),\ c \leq A(t) \leq C,\ \left|\frac{A_t(t)}{A(t)}\right| \leq C. \tag{3.14}$$

We will first recall the notion of Leray weak solution of the NS equation, and then derive the basic energy estimate for the new AC system (3.4), which will lead to the appropriate assumptions on initial conditions. We then use the assumption on the variable $\varepsilon(t)$, and perform a dispersive approach to obtain the Strichartz estimate for the pressure.

3.2.3.1 LERAY WEAK SOLUTION FOR THE NSE We analyze the $\varepsilon \to 0$ limit of the continuum AC model (3.4). Since we will be focused on the convergence of the approximated system to a weak solution of the NSE, from now on we will for simplicity take $\nu = 1$ and $f = 0$. The inclusion of a body force and a different value of the kinematic viscosity adds no technical difficulty to the analysis.

Let us recall the notion of a Leray weak solution (see, for e.g. Lions [84] and Temam [130]) of the NSE.

Definition 1. *We say that* $u \in L^\infty([0,t^*];L^2(\mathbb{R}^3)) \cap L^2([0,t^*];\dot{H}^1(\mathbb{R}^3))$ *is a Leray weak solution of the NS equation if it satisfies* (2.2)–(2.3) *in the sense of distribution for all test functions* $\varphi \in C_0^\infty([0,t^*]\times\mathbb{R}^3)$ *with* $\nabla\cdot\varphi = 0$ *and moreover the following energy inequality holds for every* $t \in [0,t^*]$

$$\begin{aligned}&\frac{1}{2}\int_{\mathbb{R}^3}|u(t,x)|^2\,dx + \nu\int_0^t\int_{\mathbb{R}^3}|\nabla u(s,x)|^2\,dxds\\ &\quad\leq \frac{1}{2}\int_{\mathbb{R}^3}|u(0,x)|^2\,dx.\end{aligned} \tag{3.15}$$

3.2.3.2 ENERGY ESTIMATES We can easily verify that system (3.4) obeys the classical energy type estimate.

Theorem 3. *Let $(u^\varepsilon, p^\varepsilon)$ be a strong solution to* (3.4) *on $[0, t^*]$. Then it follows that for all $t \in [0, t^*]$*

$$E(t) + \int_0^t \int_{\mathbb{R}^3} |\nabla u^\varepsilon(s,x)|^2 \, dxds = E(0), \tag{3.16}$$

where

$$E(t) = \frac{1}{2} \int_{\mathbb{R}^3} \left(|u^\varepsilon(t,x)|^2 + \varepsilon(t)|p^\varepsilon(t,x)|^2 \right) dx. \tag{3.17}$$

Since we expect the approximated solution $(u^\varepsilon, p^\varepsilon)$ to converge to the Leray solution, we require the finite energy constraint to be satisfied by $(u^\varepsilon, p^\varepsilon)$. So following [32] we further restrict the initial condition to system (3.4) (or (3.1)) to satisfy

$$\begin{cases} u_0^\varepsilon := u^\varepsilon(0,\cdot) \to u_0 \text{ strongly in } L^2(\mathbb{R}^3) \text{ as } \varepsilon \to 0, \\ \sqrt{\varepsilon(0)} p_0^\varepsilon := \sqrt{\varepsilon(0)} p^\varepsilon(0,\cdot) \to 0 \text{ strongly in } L^2(\mathbb{R}^3) \text{ as } \varepsilon \to 0. \end{cases} \tag{3.18}$$

This way we can obtain the following uniform estimates which are similar to those in [32, Corollary 4.2], except for (3.20), where we can use assumption (3.5) to conclude $\varepsilon_t = \mathcal{O}(\varepsilon)$, and hence we omit the proof.

Corollary 1. *Under the assumptions of Theorem 3, together with* (3.18)*, it follows that*

$$\sqrt{\varepsilon} p^\varepsilon \quad \text{is bounded in } L^\infty([0,t^*]; L^2(\mathbb{R}^3)), \tag{3.19}$$

$$\varepsilon p_t^\varepsilon \quad \text{is relatively compact in } H^{-1}([0,t^*] \times \mathbb{R}^3), \tag{3.20}$$

$$\nabla u^\varepsilon \quad \text{is bounded in } L^2([0,t^*] \times \mathbb{R}^3), \tag{3.21}$$

$$u^\varepsilon \quad \text{is bounded in } L^\infty([0,t^*]; L^2(\mathbb{R}^3)) \cap L^2([0,t^*]; L^6(\mathbb{R}^3)), \tag{3.22}$$

$$(u^\varepsilon \cdot \nabla) u^\varepsilon \quad \text{is bounded in } L^2([0,t^*]; L^1(\mathbb{R}^3)) \cap L^1([0,t^*]; L^{3/2}(\mathbb{R}^3)), \tag{3.23}$$

$$(\nabla \cdot u^\varepsilon) u^\varepsilon \quad \text{is bounded in } L^2([0,t^*]; L^1(\mathbb{R}^3)) \cap L^1([0,t^*]; L^{3/2}(\mathbb{R}^3)). \tag{3.24}$$

3.2.3.3 ACOUSTIC PRESSURE WAVE AND STRICHARTZ ESTIMATES

Note that we can derive from system (3.4) that the pressure p^ε satisfies the following wave equations

$$(\varepsilon p^\varepsilon)_{tt} - \left(\frac{1}{2}\varepsilon_t p^\varepsilon\right)_t - \Delta p^\varepsilon = -\Delta(\nabla\cdot u^\varepsilon) + \nabla\cdot\left[(u^\varepsilon\cdot\nabla)u^\varepsilon + \frac{1}{2}(\nabla\cdot u^\varepsilon)u^\varepsilon\right]. \tag{3.25}$$

Performing the following rescaling

$$\tau = \frac{t}{\sqrt{\epsilon}},\quad \mathring{p}(\tau,x) = p^\varepsilon(\sqrt{\epsilon}\tau,x),\quad \widetilde{u}(\tau,x) = u^\varepsilon(\sqrt{\epsilon}\tau,x),\quad \widetilde{A}(\tau) = A(\sqrt{\epsilon}\tau), \tag{3.26}$$

and plugging into (3.25) we obtain

$$(\widetilde{A}\mathring{p})_{\tau\tau} - \Delta\mathring{p} - \left(\frac{1}{2}\widetilde{A}_\tau\mathring{p}\right)_\tau = -\Delta(\nabla\cdot\widetilde{u}) + \nabla\cdot\left[(\widetilde{u}\cdot\nabla)\widetilde{u} + \frac{1}{2}(\nabla\cdot\widetilde{u})\widetilde{u}\right].$$

Setting

$$\widetilde{p}(\tau) := \sqrt{\widetilde{A}(\tau)}\mathring{p}(\tau),$$

then the above acoustic equation becomes following second order hyperbolic equation

$$(\sqrt{\widetilde{A}}\widetilde{p}_\tau)_\tau - \frac{1}{\sqrt{\widetilde{A}}}\Delta\widetilde{p} = -\Delta(\nabla\cdot\widetilde{u}) + \nabla\cdot\left[(\widetilde{u}\cdot\nabla)\widetilde{u} + \frac{1}{2}(\nabla\cdot\widetilde{u})\widetilde{u}\right]. \tag{3.27}$$

Note that here the wave operator contains time-dependent coefficients. The space-time Strichartz estimates involving variable coefficients were established by Mockenhaupt et al. [91] when the coefficients are smooth. Operators with $C^{1,1}$ coefficients were first considered by Smith [114] using wave packets. An alternative method based on the FBI transform was later employed by Tataru [123, 124, 125] to prove the full range of Strichartz estimates under weaker assumptions. It can be easily checked that the wave operator at the left-hand side of (3.27) does satisfy those assumptions provided that, in addition to (3.14), $A(t)$ enjoys certain extra regularity, for e.g., $A_{tt} \in L^1([0,t^*])$.

However, assuming that A is only C^1, we can further introduce a time-scale change

$$\tau = \beta(s),\quad \bar{p}(s,x) = \widetilde{p}(\beta(s),x),\quad \bar{u}(s,x) = \widetilde{u}(\beta(s),x),\quad a(s) = \widetilde{A}(\beta(s)).$$

From (3.26)–(3.27) we know that $\sqrt{a} = \sqrt{\widetilde{A}(\beta)}$ is Lipschitz in β. From standard ODE theory, we can uniquely solve the following ODE for β:

$$\beta'(s) = \sqrt{a(s)} \geq \sqrt{c} > 0, \quad \beta(0) = 0, \tag{3.28}$$

which allows us to rewrite (3.27) as

$$\bar{p}_{ss} - \Delta\bar{p} = \sqrt{a}\left\{-\Delta(\nabla\cdot\bar{u}) + \nabla\cdot\left[(\bar{u}\cdot\nabla)\bar{u} + \frac{1}{2}(\nabla\cdot\bar{u})\widetilde{u}\right]\right\}, \tag{3.29}$$

which fits well in the classical framework of Strichartz estimates for wave equations, as given in the following theorem.

Theorem 4. ***(see, e.g., [71])***. *Let w be a (weak) solution of the following wave equations in $[0,t^*]\times\mathbb{R}^n$*

$$\begin{cases} w_{tt} - \Delta w = F(t,x), \\ w(0,\cdot) = w_0, \quad w_t(0,\cdot) = w_1. \end{cases} \tag{3.30}$$

Then the following Strichartz estimates hold

$$\|w\|_{L_t^q L_x^r} + \|w_t\|_{L_t^q W_x^{-1,r}} \lesssim \|w_0\|_{\dot{H}_x^\gamma} + \|w_1\|_{\dot{H}_x^{\gamma-1}} + \|F\|_{L_t^{\tilde{q}'} L_x^{\tilde{r}'}}, \tag{3.31}$$

where (q,r,γ) and $(\tilde{q}',\tilde{r}')$ satisfy

$$\begin{cases} 2 \leq q, r \leq \infty, \\ (q,r,\gamma), (\tilde{q}',\tilde{r}',\gamma) \neq (2,\infty,1), \ \textit{when } n = 3, \\ \dfrac{1}{q} + \dfrac{n}{r} = \dfrac{n}{2} - \gamma = \dfrac{1}{\tilde{q}'} + \dfrac{n}{\tilde{r}'} - 2, \\ \dfrac{2}{q} + \dfrac{n-1}{r} \leq \dfrac{n-1}{2}, \quad \dfrac{2}{\tilde{q}} + \dfrac{n-1}{\tilde{r}} \leq \dfrac{n-1}{2}. \end{cases} \tag{3.32}$$

For our purpose, $n = 3$, and we will take $(q, r) = (4, 4)$, $(\tilde{q}', \tilde{r}') = (1, 3/2)$, and $\gamma = 1/2$. This way the above Strichartz estimate becomes

$$\|w\|_{L^4_{t,x}} + \|w_t\|_{L^4_t W^{-1,4}_x} \lesssim \|w_0\|_{\dot{H}^{\frac{1}{2}}_x} + \|w_1\|_{\dot{H}^{-\frac{1}{2}}_x} + \|F\|_{L^1_t L^{\frac{3}{2}}_x}. \tag{3.33}$$

Moreover, in the case when $n = 3$, taking advantage of the explicit structure of the Kirchhoff's formula for the classical wave operator, one may perform a refined bilinear estimates as in [72, Theorem 2.2] in the weak solution setting to obtain (see also [32, (2.4)])

$$\|w\|_{L^4_{t,x}} + \|w_t\|_{L^4_t W^{-1,4}_x} \lesssim \|w_0\|_{\dot{H}^{\frac{1}{2}}_x} + \|w_1\|_{\dot{H}^{-\frac{1}{2}}_x} + \|F\|_{L^1_t L^2_x}. \tag{3.34}$$

Following [32], we decompose the pressure as $\bar{p} = \bar{p}_1 + \bar{p}_2$ where

$$\begin{cases} \partial_{ss}\bar{p}_1 - \Delta\bar{p}_1 = \sqrt{a}\nabla \cdot \left[(\bar{u} \cdot \nabla)\bar{u} + \frac{1}{2}(\nabla \cdot \bar{u})\bar{u}\right] =: \nabla \cdot \bar{F}, \\ \bar{p}_1(x, 0) = \bar{p}(x, 0), \quad \partial_s\bar{p}_1(x, 0) = \bar{p}_s(x, 0), \end{cases} \tag{3.35}$$

$$\begin{cases} \partial_{ss}\bar{p}_2 - \Delta\bar{p}_2 = -\sqrt{a}\Delta(\nabla \cdot \bar{u}), \\ \bar{p}_2(x, 0) = \partial_s\bar{p}_2(x, 0) = 0. \end{cases} \tag{3.36}$$

Applying Theorem 4 to the above two systems and unraveling the change-of-variables (3.26) we obtain the following estimates.

Theorem 5. *Let $(u^\varepsilon, p^\varepsilon)$ be a strong solution of the Cauchy problem on $[0, t^*]$ to system (3.4) with initial data $(u^\varepsilon_0, p^\varepsilon_0)$ satisfying (3.18). Assume also that $\varepsilon(t)$ satisfies (3.5). Then for ϵ small enough the following estimate holds.*

$$\begin{aligned} \epsilon^{\frac{3}{8}}\|p^\varepsilon\|_{L^4_t W^{-2,4}_x} + \epsilon^{\frac{7}{8}}\|p^\varepsilon_t\|_{L^4_t W^{-3,4}_x} \lesssim\ & \sqrt{\epsilon}\|p^\varepsilon_0\|_{L^2_x} + \|\nabla \cdot u^\varepsilon_0\|_{H^{-1}_x} \\ & + \sqrt{T}\|\nabla \cdot u^\varepsilon\|_{L^2_{t,x}} + \left\|(u^\varepsilon \cdot \nabla)u^\varepsilon + \frac{1}{2}(\nabla \cdot u^\varepsilon)u^\varepsilon\right\|_{L^1_t L^{\frac{3}{2}}_x}. \end{aligned} \tag{3.37}$$

Proof. We first apply (3.33) with $w = \Delta^{-1/2}\bar{p}_1$ to obtain

$$\begin{aligned}\|\bar{p}_1\|_{L^4_s W^{-1,4}_x} + \|\partial_s \bar{p}_1\|_{L^4_s W^{-2,4}_x} &\lesssim \|\bar{p}(x,0)\|_{\dot{H}^{-\frac{1}{2}}_x} \\ &+ \|\bar{p}_s(x,0)\|_{\dot{H}^{-\frac{3}{2}}_x} + \|\bar{F}\|_{L^1_s L^{\frac{3}{2}}_x}. \end{aligned} \tag{3.38}$$

Then we apply (3.34) to $w = \Delta \bar{p}_2$ to obtain

$$\|\bar{p}_2\|_{L^4_s W^{-2,4}_x} + \|\partial_s \bar{p}_2\|_{L^4_s W^{-3,4}_x} \lesssim \|\sqrt{a}(\nabla \cdot \bar{u})\|_{L^1_s L^2_x} \lesssim \|(\nabla \cdot \bar{u})\|_{L^1_s L^2_x}. \tag{3.39}$$

Unraveling notation, we have that

$$\begin{aligned}\|\nabla \cdot \bar{u}\|_{L^1_s} = \int_0^{\beta^{-1}(t^*/\sqrt{\epsilon})} |\nabla \cdot \bar{u}(s)|\, ds &\leq \left[\beta^{-1}\left(\frac{t^*}{\sqrt{\epsilon}}\right)\right]^{1/2} \|\nabla \cdot \bar{u}\|_{L^2_s} \\ &\leq \frac{\sqrt{t^*}}{(c\epsilon)^{1/4}} \|\nabla \cdot \bar{u}\|_{L^2_s},\end{aligned}$$

where the last inequality is due to the fact that $(\beta^{-1})' = 1/\sqrt{a} \leq 1/\sqrt{c}$. Moreover,

$$\|\bar{p}\|_{L^r_s} = \epsilon^{-1/2r} \|A^{\frac{r-1}{2r}} p^\varepsilon\|_{L^r_t} \sim \epsilon^{-1/2r} \|p^\varepsilon\|_{L^r_t}, \qquad \bar{p}_s = \sqrt{\epsilon A}(\sqrt{A} p^\varepsilon)_t. \tag{3.40}$$

Putting together (3.38) and (3.39) we have that

$$\begin{aligned}\|\bar{p}\|_{L^4_s W^{-2,4}_x} + \|\bar{p}_s\|_{L^4_s W^{-3,4}_x} &\lesssim \|\bar{p}(x,0)\|_{\dot{H}^{-\frac{1}{2}}_x} + \|\bar{p}_s(x,0)\|_{\dot{H}^{-\frac{3}{2}}_x} \\ &+ \frac{\sqrt{t^*}}{\epsilon^{1/4}} \|\nabla \cdot \bar{u}\|_{L^2_s L^2_x} + \|\bar{F}\|_{L^1_s L^{\frac{3}{2}}_x}.\end{aligned}$$

Note from the second equation in (3.4) and (3.13) that

$$\sqrt{\epsilon A}(\sqrt{A} p^\varepsilon)_t = -\frac{\nabla \cdot u}{\sqrt{\epsilon}}. \tag{3.41}$$

Therefore from (3.40) and (3.41) we can estimate

$$\|\bar{p}_s(x,0)\|_{\dot{H}^{-\frac{3}{2}}_x} \leq \|\bar{p}_s(x,0)\|_{\dot{H}^{-1}_x} \lesssim \epsilon^{-1/2} \|\nabla \cdot u_0^\varepsilon\|_{H^{-1}_x}.$$

Putting all the above together we derive (3.37). □

Given the *á priori* energy estimates Theorem 3 and the pressure estimates Theorem 5, we can now obtain the global existence of weak solutions to system (3.4).

Theorem 6. *Let $\varepsilon(t) > 0$ and $(u_0^\varepsilon, p_0^\varepsilon)$ satisfy condition* (3.18)*. Then for any $t^* > 0$, system* (3.4) *admits a weak solution $(u^\varepsilon, p^\varepsilon)$ with the following properties*

(1) $u^\varepsilon \in L^\infty([0,t^*]; L^2(\mathbb{R}^3)) \cap L^2([0,t^*]; \dot{H}^1(\mathbb{R}^3))$*;*

(2) $\sqrt{\varepsilon} p^\varepsilon \in L^\infty([0,t^*]; L^2(\mathbb{R}^3))$*.*

Proof. We will prove the theorem using the classical Friedrich's method (also called Galerkin method in the periodic case) which consists of approximating the system (3.4) by a cutoff in the frequency space. For this, we define the operator J_n as follows.

$$J_n f := \mathcal{F}^{-1}\left(\mathbf{1}_{B(0,n)}(\xi)\hat{f}(\xi)\right),$$

where $\mathcal{F}$ denotes the Fourier transform in the space variables. Let us consider the approximate system:

$$\begin{aligned} &\partial_t u_n^\varepsilon + J_n\left(J_n u_n^\varepsilon \cdot \nabla J_n u_n^\varepsilon\right) + \tfrac{1}{2} J_n\left[(\nabla \cdot J_n u_n^\varepsilon) J_n u_n^\varepsilon\right] + \nabla J_n p_n^\varepsilon - \Delta J_n u_n^\varepsilon = 0, \\ &\partial_t p_n^\varepsilon + \frac{\varepsilon_t(t)}{2\varepsilon(t)} p_n^\varepsilon + \frac{1}{\varepsilon(t)} \nabla \cdot J_n u_n^\varepsilon = 0 \end{aligned} \tag{3.42}$$

with initial data

$$u_n^\varepsilon(0,\cdot) = J_n u^\varepsilon(0,\cdot), \quad p_n^\varepsilon(0,\cdot) = J_n p^\varepsilon(0,\cdot).$$

The above system appears as a system of ODEs on L^2 in transform space, and hence the standard Cauchy-Lipschitz theorem implies the existence of a strictly positive maximal time $t_n^* > 0$ such that a unique solution exists which is continuous in time with values in L^2. On the other hand, as $J_n^2 = J_n$, we claim that $J_n(u_n^\varepsilon, p_n^\varepsilon)$ is also a solution. Therefore uniqueness implies that $J_n(u_n^\varepsilon, p_n^\varepsilon) = (u_n^\varepsilon, p_n^\varepsilon)$ and hence one can remove all the J_n in front of u_n^ε and p_n^ε in (3.42) keeping only those in front of the nonlinear terms:

$$\begin{aligned} &\partial_t u_n^\varepsilon + J_n\left(u_n^\varepsilon \cdot \nabla u_n^\varepsilon\right) + \tfrac{1}{2} J_n\left[(\nabla \cdot u_n^\varepsilon) u_n^\varepsilon\right] + \nabla p_n^\varepsilon - \Delta u_n^\varepsilon = 0, \\ &\partial_t p_n^\varepsilon + \frac{\varepsilon_t(t)}{2\varepsilon(t)} p_n^\varepsilon + \frac{1}{\varepsilon(t)} \nabla \cdot u_n^\varepsilon = 0 \end{aligned} \tag{3.43}$$

Since J_n is a Fourier multiplier, it commutes with constant coefficient differentiations and hence, the energy estimate (3.16) still holds:

$$\begin{aligned}&\frac{1}{2}\left(\|u_n^\varepsilon\|_{L^2}^2+\varepsilon\|p_n^\varepsilon\|_{L^2}^2\right)(t)+\int_0^t\|\nabla u_n^\varepsilon\|_{L^2}^2\\&=\frac{1}{2}\left(\|J_nu^{\varepsilon_0}\|_{L^2}^2+\varepsilon(0)\|J_np^{\varepsilon_0}\|_{L^2}^2\right)\leq C.\end{aligned}$$

This implies that the L^2 norm of $(u_n^\varepsilon, p_n^\varepsilon)$ is controlled and thus $t_n^*=+\infty$.

Moreover we also have that for any $t^*>0$, there exists some constant C_{t^*} such that

$$\|\partial_t u_n^\varepsilon\|_{L^2(0,T;H^{-1})}\leq C_{t^*}.$$

Therefore, extracting a subsequence, standard compactness arguments allow us to pass to the limit in (3.43), proving the theorem. □

3.2.4 CONVERGENCE TO THE NSE

The goal of this section is to establish the convergence of the AC system (3.4) to the NS system, cf. Theorem 7. The key step is to show the strong convergence of the gradient part and the divergence-free part of the velocity field. For this, let us denote $\mathbb{P}$ the Leray projection defined by

$$\mathbb{P}=I-\mathbb{Q},\qquad\text{where}\qquad\mathbb{Q}=\nabla(\Delta^{-1}\nabla\cdot). \tag{3.44}$$

Note that $\mathbb{P}$ and $\mathbb{Q}$ are both bounded linear operators on $W^{k,q}(\mathbb{R}^3)$ for any k and $q\in(1,\infty)$. See, e.g., [119].

From Corollary 1 and Theorem 5 we easily obtain the following result.

Proposition 1. *Let the assumptions in Theorem 5 hold. Then as $\varepsilon\to 0$ it follows that*

$$\varepsilon p^\varepsilon\to 0\qquad\textit{strongly in } L^\infty([0,t^*];L^2(\mathbb{R}^3))\cap L^4([0,t^*];W^{-2,4}(\mathbb{R}^3)), \tag{3.45}$$

$$\nabla\cdot u^\varepsilon\to 0\qquad\textit{strongly in } W^{-1,\infty}([0,t^*];L^2(\mathbb{R}^3))\cap L^4([0,t^*];W^{-3,4}(\mathbb{R}^3)). \tag{3.46}$$

Proof. It is easily seen that (3.45) follows from (3.19), (3.37). Further, (3.46) follows from (3.37) and the second equation of (3.4). □

3.2.4.1 STRONG CONVERGENCE OF $\mathbb{Q}u^\varepsilon$ We will first prove that $\mathbb{Q}u^\varepsilon$ goes to zero in some strong sense as $\varepsilon \to 0$.

Lemma 4. *Let $(u^\varepsilon, p^\varepsilon)$ be the solution of the Cauchy problem to system (3.4) with initial data $(u_0^\varepsilon, p_0^\varepsilon)$ satisfying (3.18). Assume also that $\varepsilon(t)$ satisfies (3.12). Then for any $4 \le p < 6$,*

$$\mathbb{Q}u^\varepsilon \to 0 \quad \text{in} \quad L^2([0,t^*];L^p), \quad \text{as} \ \ \varepsilon \to 0. \tag{3.47}$$

Proof. We follow the idea from [32, Proposition 5.3]. Consider the standard mollifier

$$\eta \in C_0^\infty(\mathbb{R}^3),\ \eta \ge 0,\ \int_{\mathbb{R}^3} \eta\, dx = 1; \qquad \eta_\alpha(x) := \alpha^{-3}\eta(x/\alpha),\ 0<\alpha<1.$$

Set $f_\alpha := f * \eta_\alpha$. Then for any $f \in \dot{H}^1(\mathbb{R}^3)$ it holds

$$\|f - f_\alpha\|_{L^p} \le C\alpha^{1-3\left(\frac{1}{2}-\frac{1}{p}\right)}\|\nabla f\|_{L^2}, \quad \|f_\alpha\|_{L^r} \le C\alpha^{-s-3\left(\frac{1}{q}-\frac{1}{r}\right)}\|f\|_{W^{-s,q}} \tag{3.48}$$

where $p \in [2,6]$, $1 \le q \le r \le \infty$, $s \ge 0$.

With the above, we decompose $\mathbb{Q}u^\varepsilon$ as

$$\|\mathbb{Q}u^\varepsilon\|_{L_t^2L_x^p} \le \|\mathbb{Q}u^\varepsilon - (\mathbb{Q}u^\varepsilon)_\alpha\|_{L_t^2L_x^p} + \|(\mathbb{Q}u^\varepsilon)_\alpha\|_{L_t^2L_x^p} =: J_1 + J_2.$$

Applying (3.48) to J_1 we have

$$J_1 \le C\alpha^{1-3\left(\frac{1}{2}-\frac{1}{p}\right)}\left(\int_0^T \|\nabla\mathbb{Q}u^\varepsilon\|_{L_x^2}^2\, dt\right)^{1/2} \le C\alpha^{1-3\left(\frac{1}{2}-\frac{1}{p}\right)}\|\nabla u^\varepsilon\|_{L_t^2L_x^2}.$$

As for J_2, from (3.41) we see that

$$\mathbb{Q}u^\varepsilon = \nabla\Delta^{-1}(\nabla\cdot u^\varepsilon) = -\epsilon\nabla\Delta^{-1}\left(Ap_t^\varepsilon + \frac{1}{2}A_tp^\varepsilon\right).$$

Thus from (3.48) we have

$$\begin{aligned} J_2 &= \epsilon\left\|\nabla\Delta^{-1}\left(Ap_t^\varepsilon + \frac{1}{2}A_tp^\varepsilon\right) * \psi_\alpha\right\|_{L_t^2L_x^p} \\ &\lesssim \epsilon\alpha^{-\frac{3}{2}-3\left(\frac{1}{4}-\frac{1}{p}\right)}\|Ap_t^\varepsilon\|_{L_t^2W_x^{-3,4}} + \epsilon\alpha^{-\frac{1}{2}-3\left(\frac{1}{4}-\frac{1}{p}\right)}\|A_tp^\varepsilon\|_{L_t^2W_x^{-2,4}} \\ &\lesssim T^{\frac{1}{4}}\epsilon^{\frac{1}{8}}\alpha^{-\frac{3}{2}-3\left(\frac{1}{4}-\frac{1}{p}\right)}\|\epsilon^{\frac{7}{8}}p_t^\varepsilon\|_{L_t^4W_x^{-3,4}} + T^{\frac{1}{4}}\epsilon^{\frac{5}{8}}\alpha^{-\frac{1}{2}-3\left(\frac{1}{4}-\frac{1}{p}\right)}\|\epsilon^{\frac{3}{8}}p^\varepsilon\|_{L_t^4W_x^{-2,4}}. \end{aligned}$$

Now summing up the estimates for J_1 and J_2 and using Corollary 1 and Theorem 5 we find that for any $4 \le p < 6$,

$$\|\mathbb{Q}u^\varepsilon\|_{L_t^2 L_x^p} \lesssim \alpha^{1-3\left(\frac{1}{2}-\frac{1}{p}\right)} + \epsilon^{\frac{1}{8}}\alpha^{-\frac{3}{2}-3\left(\frac{1}{4}-\frac{1}{p}\right)} + \epsilon^{\frac{5}{8}}\alpha^{-\frac{1}{2}-3\left(\frac{1}{4}-\frac{1}{p}\right)}.$$

Therefore when choosing, e.g.,

$$\alpha = \epsilon^{\frac{1}{14}},$$

the above estimate becomes

$$\|\mathbb{Q}u^\varepsilon\|_{L_t^2 L_x^p} \lesssim \epsilon^{\frac{6-p}{28p}} + \epsilon^{\frac{6+15p}{28p}} \lesssim \epsilon^{\frac{6-p}{28p}}, \quad \text{for any } \ 4 \le p < 6,$$

which implies (3.47). □

3.2.4.2 STRONG CONVERGENCE OF $\mathbb{P}u^\varepsilon$ Let us first recall the celebrated Aubin-Lions lemma [4, 82].

Lemma 5. *Let X_0, X and X_1 be Banach spaces with $X_0 \subset X \subset X_1$. Suppose that X_0 is compactly embedded in X and that X is continuously embedded in X_1. Suppose also that X_0 and X_1 are reflexive. For $1 < p, q < \infty$, let*

$$W := \left\{ u \in L^q([0,t^*]; X_0) : \ \frac{du}{dt} \in L^q([0,T]; X_1) \right\}.$$

Then the embedding of W into $L^p([0,t^*]; X)$ is compact.

Next we will apply the above lemma to establish the strong compactness of $\mathbb{P}u^\varepsilon$, the divergence-free part of the velocity field.

Lemma 6. *Let $(u^\varepsilon, p^\varepsilon)$ be the solution of the Cauchy problem to system (3.4) with initial data $(u_0^\varepsilon, p_0^\varepsilon)$ satisfying (3.18). Assume also that $\varepsilon(t)$ satisfies (3.14). Then $\mathbb{P}u^\varepsilon$ is pre-compact in $L^2([0,t^*]; L^2_{loc}(\mathbb{R}^3))$.*

Proof. We follow the standard idea in treating the NS equation to show that

$$\mathbb{P}u_t^\varepsilon \text{ is uniformly bounded in } L^{\frac{4}{3}}([0,t^*];H^{-1}(\mathbb{R}^3)). \tag{3.49}$$

To this end, we apply $\mathbb{P}$ to the first equation in (3.4) to obtain

$$\mathbb{P}u_t^\varepsilon = \Delta(\mathbb{P}u^\varepsilon) - \mathbb{P}\left[(u^\varepsilon\cdot\nabla)u^\varepsilon\right] - \mathbb{P}\left[\frac{1}{2}(\nabla\cdot u^\varepsilon)u^\varepsilon\right].$$

From Theorem 3 we know that u^ε is uniformly bounded in $L^2([0,t^*];H^1(\mathbb{R}^3))$, and hence $\Delta(\mathbb{P}u^\varepsilon)$ is uniformly bounded in $L^2([0,t^*];H^{-1}(\mathbb{R}^3))$. The estimates for the second and the third terms on the right-hand side of the above equation are quite similar. So we only consider the second term. From [129, Lemma 2.1] we know that

$$\|(u^\varepsilon\cdot\nabla)u^\varepsilon\|_{H^{-1}} \le \|u^\varepsilon\|_{L^2}^{\frac{1}{2}}\|u^\varepsilon\|_{H^1}^{\frac{3}{2}}.$$

Therefore

$$\|(u^\varepsilon\cdot\nabla)u^\varepsilon\|_{L_t^{\frac{4}{3}}H_x^{-1}} \le \|u^\varepsilon\|_{L_t^\infty L_x^2}^{\frac{1}{2}}\|u^\varepsilon\|_{L_t^2H_x^1}^{\frac{3}{2}},$$

which implies (3.49), and hence proves the lemma. □

3.2.4.3 CONVERGENCE THEOREM We are now in a position to state and prove the main theorem of this section.

Theorem 7. *Let $(u^\varepsilon,p^\varepsilon)$ be the solution of the Cauchy problem to system (3.4) with initial data $(u_0^\varepsilon,p_0^\varepsilon)$ satisfying (3.18). Assume also that $\varepsilon(t)$ satisfies (3.12). Then it holds that*

(1) there exists $u\in L^\infty([0,t^*];L^2(\mathbb{R}^3))\cap L^2([0,t^*];\dot{H}^1(\mathbb{R}^3))$ such that

$$u^\varepsilon \rightharpoonup u \quad \text{weakly in } L^2([0,t^*];\dot{H}^1(\mathbb{R}^3)).$$

(2) the divergence-free part and the gradient part of u^ε satisfy

$$\mathbb{P}u^\varepsilon \to \mathbb{P}u = u \quad \text{strongly in } L^2([0,t^*];L^2_{loc}(\mathbb{R}^3));$$
$$\mathbb{Q}u^\varepsilon \to 0 \quad \text{strongly in } L^2([0,t^*];L^p(\mathbb{R}^3)), \text{ for any } 4\le p<6.$$

(3) the pressure p^ε will converge in the sense of distribution. Indeed,

$$p^\varepsilon \to p = \Delta^{-1}\nabla\cdot[(u\cdot\nabla)u] \quad \text{in } \mathcal{D}'.$$

Moreover, $u = \mathbb{P}u$ is a Leray weak solution to the incompressible NS equation

$$\mathbb{P}\left[u_t - \Delta u + (u \cdot \nabla)u\right] = 0 \quad in \;\; \mathcal{D}',$$

and the energy inequality (3.15) holds.

Proof. It is easily seen that (1) follows from Theorem 3 and Corollary 1, and (2) follows from Lemmas 4 and 6. The proof of (3) and the energy inequality follows the same way as in the proof of [32, Theorem 3.3], so we omit it here. □

3.2.5 NUMERICAL TESTS OF THE NEW MODEL

To test the stability and accuracy of the new model, we perform numerical tests of the variable timestep algorithm for problems on bounded domains under noslip boundary conditions. The tests employ the finite element method to discretize space, with Taylor-Hood ($\mathbb{P}_2/\mathbb{P}_1$) elements, [50]. The meshes used for both tests are generated using a 2d and 3d Delaunay algorithms. Finally, the software package FEniCS is used for both experiments [1].

3.2.5.1 TEST 1: OSCILLATING $\varepsilon(t)$ We first apply the method to a three-dimensional offset cylinder problem. Let $\Omega_1 = \{(x, y, z) : x^2 + y^2 < 1, 0 < z < 2\}$ and $\Omega_2 = \{(x, y, z) : (x - .5)^2 + y^2 \leq .01, 0 \leq z \leq 2\}$ be cylinders of radii 1 and .1 and height 2, respectively. Let then $\Omega = \Omega_1 \setminus \Omega_2$. Both cylinders and the top and bottom surfaces are fixed, so noslip boundary conditions are imposed. A rotational body force f is imposed, where the Reynolds number Re = 1 and

$$f(x; t) := (-4y(1 - x^2 - y^2), 4x(1 - x^2 - y^2), 0)^T.$$

For initial conditions, we let $u(x; 0), p(x; 0)$ be the solutions to a stationary Stokes solve at $t = 0$. This does not yield a fully developed initial condition so damped pressure oscillations

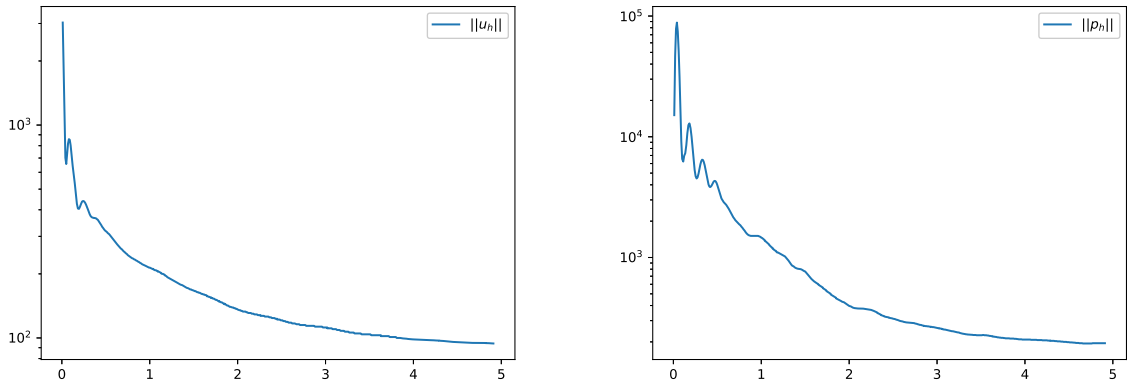

(a) (b)

Figure 3.1: Velocity and pressure norms over time t.

at startup are expected and observed. For this test, we let $\nu = .001$ and the final time $t^* = 5$. We let $\varepsilon_n = \Delta t_n$, where Δt_n changes according the function

$$\varepsilon(t_n) = \Delta t(t_n) := \begin{cases} .01 & 0 \leq n \leq 10 \\ .01 + .002 \sin(10 t_n) & n > 10. \end{cases}$$

The first plots in Figure 3.1 below track the velocity and pressure L^2 norms over the duration of the simulation. After an initial spike (typical of artificial compressibility methods with poorly initialized pressures), the velocity and pressure stabilize. The vertical axes of $||u_h||$ and $||p_h||$ are on a logarithmic scale. The variable ε, velocity, and pressure are all clearly stable.

In Figure 3.2, we give plots of velocity magnitude at times $t = 1, 2, 3, 4$ on Ω at five cross-sections of Ω.

3.2.5.2 TEST 2: ADAPTIVE, VARIABLE $\varepsilon(t)$ The next test investigates self-adaptive variation of ε_n and the resulting accuracy. We now consider a two-dimensional flow

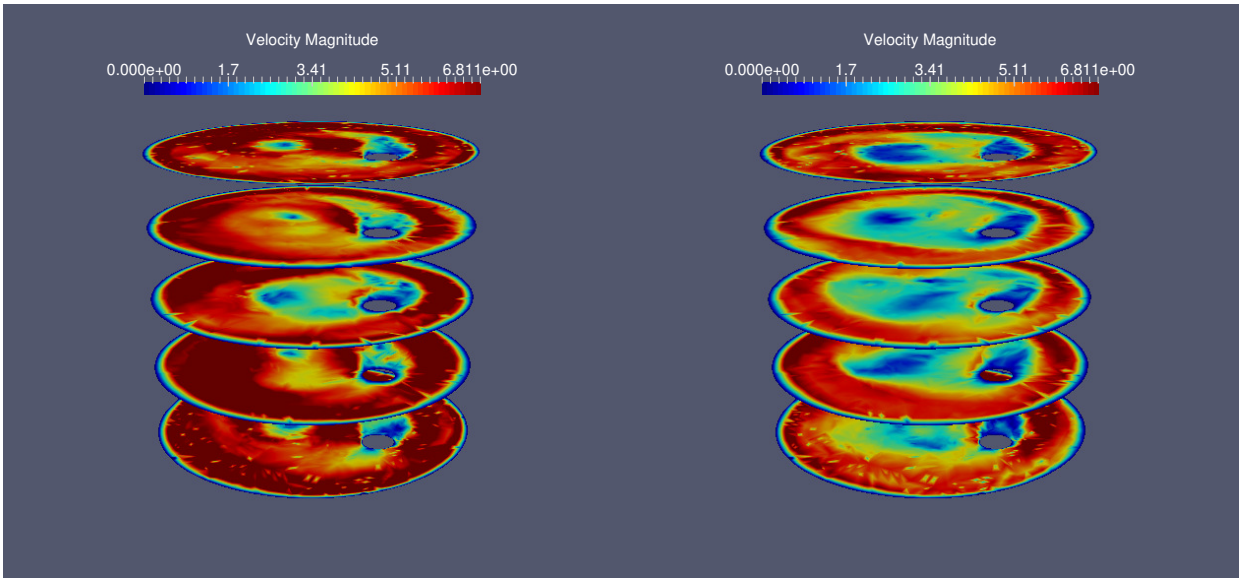

(a) $t = 1$ (b) $t = 2$

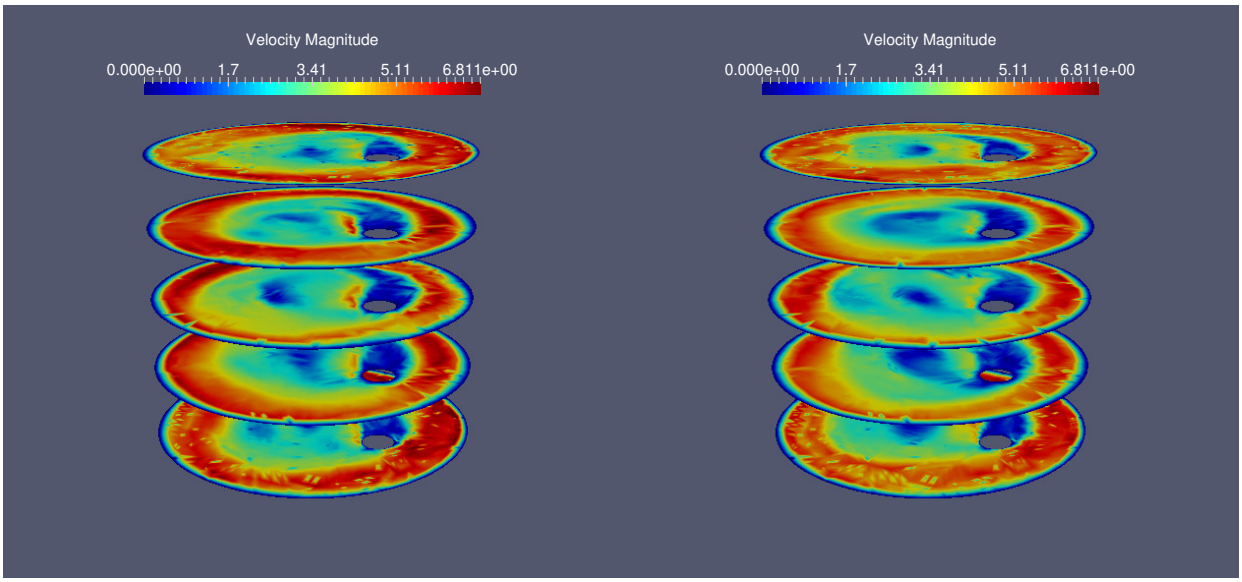

(c) $t = 3$ (d) $t = 4$

Figure 3.2: Velocity magnitude at different t.

over $\Omega = \ ]0,1[^2$ with the exact solution

$$u(x,y;t) := \sin(t)(\sin(2\pi x)\sin^2(2\pi x), \sin(2\pi x)\sin^2(2\pi y))^T,$$
$$p(x,y;t) := \cos(t)\cos(\pi x)\sin(\pi y)$$

and corresponding body force f. We let Re = 1000, the final time $t^* = 1$, $\varepsilon_n = \Delta t_n$, and $\Delta t_0 = .001$. To adapt the timestep (and generate Δt_n), we employ a halving-and-doubling technique using $\|\nabla \cdot u_h\|$ as the estimator. We let the tolerance interval be $(.001, .01)$ (If $\|\nabla \cdot u_h\| < 0.001$, Δt_n and ε_n are doubled, while if $\|\nabla \cdot u_h\| > 0.01$, the two are halved and the step is repeated). This procedure does not control the local truncation error, only the violation of incompressibility.

The plots in Figure 3.3 show the velocity and pressure errors, as well as the fluctuation of Δt_n and $\nabla \cdot u$, over time. We see that the errors of both the velocity and pressure fluctuate with changes in the timestep, as does the divergence.

Figure 3.3a shows that the velocity error is reasonable but does grow (slowly), consistent with separation of trajectories of the Navier-Stokes equations. Figure 3.3d shows $\|\nabla \cdot u_h\|$ is controlled. Figure 3.3b shows the pressure error actually decreases. Figure 3.3c shows that the evolution of Δt_n, and therefore ε_n, is not as smooth as required by condition (3.12). Nevertheless, the simulation produced approximations of reasonable accuracy.

3.2.6 CONCLUSIONS AND FUTURE PROSPECTS

Slightly compressible fluids models provide a basis for challenging numerical simulations. Efficiency and especially time accuracy in such simulations require variable timestep and thus variable $\varepsilon = \varepsilon(t)$. Variable ε is beyond existing mathematical foundations for slightly compressible models. The method and associated continuum model considered herein is modified from the standard one for variable ε, has been proven to be stable and converge to a weak solution of the incompressible Navier-Stokes equations as $\varepsilon(t) \to 0$ and $\varepsilon_t(t) \to 0$, provided $\varepsilon_t(t) \leq C\varepsilon(t)$. The analysis of the long time stability of the standard method and model for variable $\varepsilon = \varepsilon(t)$ is an open problem with no clear entry point for its analysis (Section 2).

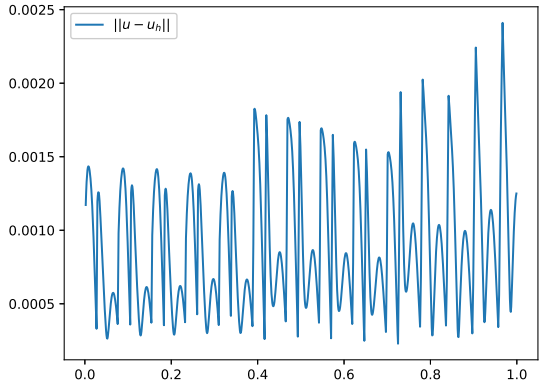

(a) Velocity error

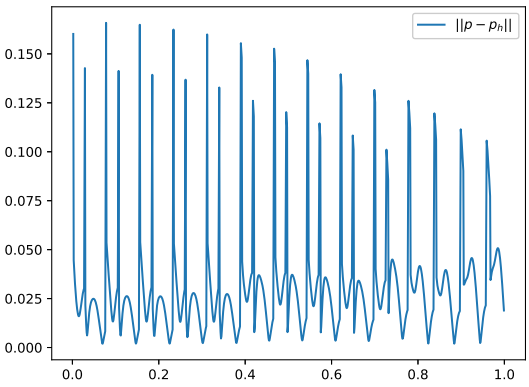

(b) Pressure error

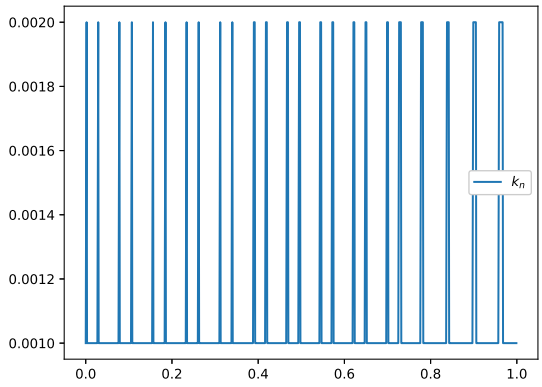

(c) Timestep evolution

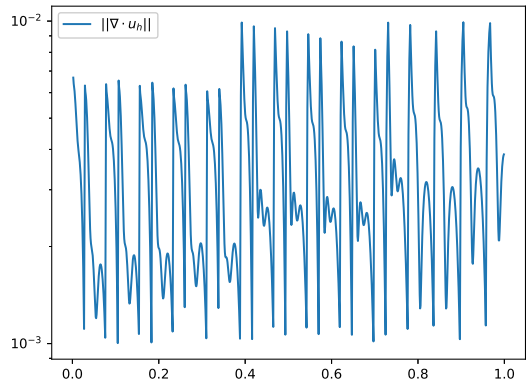

(d) Divergence evolution

Figure 3.3: Accuracy and adaptability results.

Preliminary numerical tests in Section 3.2.5 with halving and doubling indicate a good agreement with the analytical results under the fluctuation condition $\varepsilon_t(t) \leq C\varepsilon(t)$. Other open questions include convergence of flow quantities (e.g., vorticity, lift, drag, energy dissipation rates, Q-criterion values and so on) to their incompressible values as $\varepsilon(t), \varepsilon_t(t), \cdots \to 0$, derivation of the rates of convergence for strong solutions and extension of the analysis herein.

3.3 DOUBLY ADAPTIVE AC SCHEMES

3.3.1 INTRODUCTION

Artificial compressibility (AC) methods are based on replacing $\nabla \cdot u = 0$ by $\varepsilon \partial_t p + \nabla \cdot u = 0$ ($0 < \varepsilon$ small), uncoupling velocity and pressure and advancing the pressure explicitly in time. Their high speed and low storage requirements recommend them for complexity bound fluid flow simulations. Unfortunately, *time-accurate* artificial compressibility approximations have proven elusive. Time accuracy (along with increased efficiency and decreased memory) is obtained by *time-adaptive* algorithms. To our knowledge, the defect correction based scheme of Guermond and Minev [47] and the non-autonomous AC method in [13], presented in Section 3.2, both adapting the timestep with $\varepsilon = \Delta t$ (timestep), are the only previous implicit, time-adaptive AC methods.

This section presents time-adaptive AC algorithms based on an approach of *independently* adapting the AC parameter ε and timestep Δt. The methods proceed as follows: A standard, first-order, implicit method, (1st Order) below, is used to advance the *momentum* equation in the artificial compressibility equations. A second-order *velocity* approximation, (2nd Order) below, is then computed at negligible cost using a time filter adapted from [53]. The difference between the first-order and second-order approximations gives a reliable estimator, $EST(1)$, for the local error in the momentum equation for the first-order method and is used to adapt the time step in Algorithm 2, Section 3.3.8.

Adapting the AC parameter ε is more challenging. Stability of the standard AC discrete

continuity equation ($\varepsilon\partial_t p + \nabla \cdot u = 0$) is unknown for variable ε, see Section 3.2 and [13]. We present two new, variable ε, discrete continuity equations in (3.53) below and prove their unconditional, long-time stability in Theorems 8, 9 and 10. These results show that adaptivity will respond to accuracy constraints rather than try to correct stability problems with small time-steps. In these continuity equations, the size of $||\nabla \cdot u||$ is monitored and used to adapt the choice of the AC parameter ε (e.g., Algorithm 1, Section 3.3.6) whereupon the calculation proceeds to the next time step. The self-adaptive strategy for independently adapting ε also side steps the practical problem of how to pick ε in AC methods and related penalty methods, even for constant time-steps. The new discrete continuity equations reduce to the standard $\varepsilon\partial_t p + \nabla \cdot u = 0$ for constant ε, improve, through greater simplicity, a non-autonomous ($\varepsilon = \varepsilon(t)$) AC formulation in [13] and yield now three proven stable extensions of the discrete AC continuity equation to variable ε. A comparison of the three is presented in Section 3.3.9. Determining if one or some combination of the three, or some other yet undetermined possibility is an important open problem.

The second-order method. To obtain an $\mathcal{O}(\Delta t^2)$ approximation of the momentum equation (with embedded error estimator), Algorithms 2 and 3 incorporate a recent idea of [53] of increasing accuracy and estimating errors by time filters. Theorem 10 of Section 3.3.6 gives a proof of unconditional, long-time stability of the second-order, constant timestep but variable ε method. The resulting embedded structure of Algorithms 2 and 3 suggests low-complexity, variable-order methods may be possible once an adaptive ε strategy is well developed.

The second-order method is a one leg method. Reliable estimators of the local truncation error (LTE) in one leg methods are expensive as detailed in [27]. An inexpensive estimator, $EST(2)$ in Algorithm 3, of the LTE in the method's linear multistep twin, based on a second time filter, is presented. For the one leg method, this estimator is inexpensive but heuristic. The doubly adapted, second-order method in Algorithm 3 is tested in Section 3.3.9. The embedded structure of the first and second-order method suggests that adapting the *method order* in addition to the timestep and AC parameter ε may increase accuracy and efficiency further (see Algorithm 4).

Three stable treatments of the momentum equation (first, second and even variable order)

are possible. Three stable treatments of the variable ε continuity are now possible: two in Section 3.3.2 below and one in Section 3.2 [13]. The results are nine adaptive AC methods with computational complexity comparable to the common first-order method, described herein.

3.3.2 REVIEW OF A COMMON AC METHOD

Denote by u the velocity, p the pressure, ν the kinematic viscosity, and f the external force. Consider the slightly compressible/hyposonic [146] approximation to the incompressible Navier-Stokes equations in a domain Ω in $\mathbb{R}^d, d = 2, 3$

$$\begin{cases} \partial_t u + (u \cdot \nabla)u + \frac{1}{2}(\nabla \cdot u)u + \nabla p - \nu \Delta u = f \\ \varepsilon \partial_t p + \nabla \cdot u = 0, \text{ where } 0 < \varepsilon \text{ is small.} \end{cases} \tag{3.50}$$

This is the most common of several possible formulations reviewed in Section 3.2. To present methods herein we will consistently suppress the secondary spatial discretization.

Remark 9. *All stability results proven herein hold, by the same proof, for standard variational spatial discretizations such as finite element methods with div-stable elements.*

Let u^* denote the standard (second-order) linear extrapolation of u from previous values to t_{n+1}

$$u^* = \left(1 + \frac{\Delta t_{n+1}}{\Delta t_n}\right) u^n - \frac{\Delta t_{n+1}}{\Delta t_n} u^{n-1} \left(= 2u^n - u^{n-1} \text{ for constant timestep}\right).$$

Here, we note that Temperton and Staniforth [132] advocated even higher order extrapolation. To fix ideas, among many possible, e.g., [46, 48, 49, 68, 74, 101, 25, 94, 145], consider a common, constant timestep, semi-implicit time discretization of (3.50):

$$\begin{aligned} \frac{u^{n+1} - u^n}{\Delta t} + (u^* \cdot \nabla)u^{n+1} + \frac{1}{2}(\nabla \cdot u^*)u^{n+1} + \nabla p^{n+1} - \nu \Delta u^{n+1} = f(t_{n+1}), \\ \varepsilon \frac{p^{n+1} - p^n}{\Delta t} + \nabla \cdot u^{n+1} = 0. \end{aligned} \tag{3.51}$$

Here Δt is the timestep, $t_n = n\Delta t$, u^n, p^n are approximations to the velocity and pressure at $t = t_n$. This has consistency error $\mathcal{O}(\Delta t + \varepsilon)$ leading to the most common choice of selecting

$\varepsilon = \Delta t$ to balance errors. Since $\nabla p^{n+1} = \nabla p^n - (\Delta t/\varepsilon)\nabla\nabla\cdot u^{n+1}$, this uncouples into a velocity solve followed by an algebraic pressure update

$$\frac{u^{n+1}-u^n}{\Delta t} + (u^*\cdot\nabla)u^{n+1} + \frac{1}{2}(\nabla\cdot u^*)u^{n+1} - \frac{\Delta t}{\varepsilon}\nabla\nabla\cdot u^{n+1}$$
$$-\nu\Delta u^{n+1} = -\nabla p^n + f^{n+1},$$
$$\text{then given } u^{n+1}: \quad p^{n+1} = p^n - \frac{\Delta t}{\varepsilon}\nabla\cdot u^{n+1}. \tag{3.52}$$

For constant $\varepsilon, \Delta t$, this method is unconditionally, nonlinearly, long-time stable, e.g., [46, 48, 109, 108]. Its long-time stability for *variable* $\varepsilon, \Delta t$ is an open problem, see Section 3.2 and [13].

3.3.3 NEW METHODS FOR VARIABLE $\varepsilon, \Delta t$

Although well motivated, the choice $\varepsilon = \Delta t$ cannot be more than a step to a correct choice. First, observe, for T_* a time scale and L a length scale, that the units of ε scale like T_*^2/L^3 while the units of Δt scale like T_*. Thus, a correct choice of ε should be scaled to be dimensionally consistent and afterwards the constant multiplier optimized. Aside from dimensional inconsistency, the standard choice $\varepsilon = \Delta t$ ignores the different roles of ε and Δt. To leading orders, the consistency error in the *continuity* equation is $\mathcal{O}(\varepsilon)$, independent of Δt, and the consistency error in the *momentum* equation is $\mathcal{O}(\Delta t)$, independent of ε. This observation on the standard method (3.51), (3.52) motivates the development plan for the doubly adaptive algorithms herein:

- *Develop first (Section 3.3.5) and second (Section 3.3.6) order methods stable for variable* $\Delta t, \varepsilon$.
- *Adapt* ε_n *to control the consistency error in the continuity equation by monitoring* $||\nabla\cdot u||$, *Sections 3.3.6, 3.3.8.*
- *Develop inexpensive estimators for momentum equation consistency error and adapt* $\Delta t = \Delta t_n$ *for its control, Section 3.3.8.*
- *Use (Section 3.3.8) and test (Section 3.3.9) the estimators in a doubly adaptive, variable* $\varepsilon, \Delta t$, *algorithm.*

In adaptive methods, *strong stability is necessary*, so $\varepsilon_n, \Delta t_n$ can be adapted for time-accuracy rather than to correct instabilities. One key difficulty, resolved by the two methods (3.53) below, is that useful *stability is unknown* for the common AC method (3.51) with variable ε, see Section 3.2 and [13], and even for the continuum model (3.50) with $\varepsilon = \varepsilon(t)$. A second key difficulty is that (unconditional, nonlinear) G-stability for variable time-steps is uncommon. For example, the popular BDF2 method loses A-stability for increasing time-steps.

Remark 10. *To our knowledge, the only such two-step method is the little explored one of Dahlquist, Liniger, and Nevanlinna [20]. This second issue may be resolvable by a variable (first and second) order implementation since it would include the A-stable, fully implicit method.*

The continuity equation is treated by either a geometric average (GA-Method) or a minimum term (min-Method) as follows. Given $u^n, p^n, \varepsilon_n, \Delta t_n$, select $\varepsilon_{n+1}, \Delta t_{n+1}$, calculate u^{n+1}, then

$$\begin{aligned} &\text{GA-Method:} \quad \tfrac{\varepsilon_{n+1}p^{n+1} - \sqrt{\varepsilon_{n+1}\varepsilon_n}p^n}{\Delta t_{n+1}} + \nabla \cdot u^{n+1} = 0, \text{ or} \\ &\text{min-Method:} \quad \tfrac{\varepsilon_{n+1}p^{n+1} - \min\{\varepsilon_{n+1},\varepsilon_n\}p^n}{\Delta t_{n+1}} + \nabla \cdot u^{n+1} = 0. \end{aligned} \tag{3.53}$$

These methods are proven in Section 3.3.5 to be unconditionally, variable $\varepsilon, \Delta t$ stable. For the discrete momentum equation, recall u^* is an extrapolated approximation to $u(t_{n+1})$. The first-order method's momentum equation is the standard one (3.51) above given by

$$\frac{u^{n+1} - u^n}{\Delta t_{n+1}} + (u^* \cdot \nabla)u^{n+1} + \frac{1}{2}(\nabla \cdot u^*)u^{n+1} + \nabla p^{n+1} - \nu \Delta u^{n+1} = f^{n+1}. \qquad \text{(1st Order)}$$

The (linearly-implicit) treatment of the nonlinear term is inspired by Baker [5]. The second method, adapted from [53], adds a time filter to obtain $\mathcal{O}(\Delta t^2)$ accuracy and automatic error estimation as follows. Let the timestep ratio be denoted $\tau = \Delta t_{n+1}/\Delta t_n$. Call u_1^{n+1} the solution obtained from the first-order method (1st Order) above. The second-order

approximation u^{n+1} is obtained by filtering u_1^{n+1}:

$$\frac{u_1^{n+1}-u^n}{\Delta t_{n+1}}+(u^*\cdot\nabla)u_1^{n+1}+\frac{1}{2}(\nabla\cdot u^*)u_1^{n+1}+\nabla p^{n+1}-\nu\Delta u_1^{n+1}=f^{n+1},$$

$$\text{For } \tau=\frac{\Delta t_{n+1}}{\Delta t_n} \text{ let } \alpha_1=\frac{\tau(1+\tau)}{(1+2\tau)}, \text{ then :} \qquad \text{(2nd Order)}$$

$$u^{n+1}=u_1^{n+1}-\frac{\alpha_1}{2}\left\{\frac{2\Delta t_n}{\Delta t_n+\Delta t_{n+1}}u_1^{n+1}-2u^n+\frac{2\Delta t_{n+1}}{\Delta t_n+\Delta t_{n+1}}u^{n-1}\right\}.$$

Denote by $D_2(n+1)$ the quantity above in braces

$$D_2(n+1):=\frac{2\Delta t_n}{\Delta t_n+\Delta t_{n+1}}u_1^{n+1}-2u^n+\frac{2\Delta t_{n+1}}{\Delta t_n+\Delta t_{n+1}}u^{n-1}.$$

Note that $D_2(n+1)$ is $2\Delta t_n\Delta t_{n+1}\times$(a second divided difference).

A simple estimate of the local error in the first-order approximation u_1^{n+1} is given by a measure (here the L^2 norm) of the difference of the two approximations

$$EST(1)=\|u^{n+1}-u_1^{n+1}\|=\frac{\alpha_1}{2}\|D_2(n+1)\|.$$

3.3.3.1 ESTIMATING THE ERROR IN THE SECOND-ORDER APPROXIMATION Naturally one would like to use the second-order approximation for more than an estimator. It is possible to use $EST(1)$ above as a pessimistic estimator for u^{n+1}. In Section 3.3.6 we show that, eliminating the intermediate step u_1^{n+1}, the second-order method is equivalent to the second-order, one leg method (3.61) below. Estimation of the LTE for this OLM cannot be done by a simple time filter for reasons delineated in [27] and based on classical analysis of the LTE in OLMs of Dahlquist. We test an inexpensive but heuristic estimator that can be calculated by a second time filter. $EST(2)$ below is an LTE estimator for the OLMs linear multi-step twin. To estimate the local error in the second-order approximation we use the third divided difference with multiplier chosen (by a lengthy but elementary Taylor series calculation) to cancel the first term of the LTE of the methods linear multi-step twin

$$EST(2) = \frac{\alpha_2}{6}\left\|\frac{3\Delta t_{n-1}}{\Delta t_{n+1}+\Delta t_n+\Delta t_{n-1}}D_2(n+1)-\frac{3\Delta t_{n-1}}{\Delta t_{n+1}+\Delta t_n+\Delta t_{n-1}}D_2(n)\right\|$$

where

$$\alpha_2 = \frac{\tau_n(\tau_{n+1}\tau_n+\tau_n+1)(4\tau_{n+1}^3+5\tau_{n+1}^2+\tau_{n+1})}{3(\tau_n\tau_{n+1}^2+4\tau_n\tau_{n+1}+2\tau_{n+1}+\tau_n+1)}, \text{ and } \tau_n=\Delta t_n/\Delta t_{n-1}.$$

The resulting adaptive algorithm uncouples like (3.52) into a velocity update with a grad-div term then an algebraic pressure update. More reliable but more expensive estimators are possible. The above inexpensive but heuristic one is tested herein because the motivation for AC methods is often based on the need for faster and reduced memory algorithms in specific applications.

Section 3.3.5 presents the analysis of the two first-order methods, proving long-time, unconditional stability for variable $\varepsilon, \Delta t$. This analysis develops the key treatment of the discrete continuity equation necessary for stability. Section 3.3.6 gives a proof of unconditional, long time stability for the variable ε, constant Δt second-order method. This proof can be extended to decreasing time-steps but not increasing time-steps.

3.3.4 RELATED WORK

Artificial compressibility (AC) methods were introduced in the 1960's by Chorin, Oskolkov and Temam. Their mathematical foundation has been extensively developed by Shen [107, 108, 109, 111] and Prohl [101]. Recent work includes [74, 25, 48, 49, 68, 94, 145]. The GA-method (geometric averaging method) herein is motivated by work in [18] for stably uncoupling atmosphere-ocean problems.

There has been extensive development of adaptive methods for *assured* accuracy in fully coupled, *u-p* discretizations, e.g., [57], and adaptive methods based on estimates of local truncation errors including [54, 70, 136]. In complement, the work herein aims at methods that use less expensive local (rather than global) error estimators, do not provide assured time-accuracy but *emphasize* (consistent with the artificial compressibility methods) low cognitive, computational, and space complexity. Aside from [13] and Guermond and Minev [47], extension of implicit, time-adaptive methods to artificial compressibility discretizations is undeveloped.

Herein accuracy is increased and local errors estimated by time filters. Other approaches are clearly possible. Time filters are an important tool in GFD to correct weak instabilities and extend forecast horizons, [3, 77, 102, 141, 142]. In [53], it was noticed that a time filter can also increase the convergence rate of the Backward Euler method and estimate errors.

G-stability of the resulting (constant timestep) time discretization was recently proven for the *fully-coupled*, velocity-pressure Navier-Stokes equations in [24].

3.3.5 FIRST-ORDER, VARIABLE $\Delta t, \varepsilon$ METHODS

This section establishes unconditional, long-time, nonlinear stability of the two variable $\Delta t, \varepsilon$ first-order methods of Section 3.3.3 in the usual $L^2(\Omega)$ norm. The methods differ in the treatment of the discrete continuity equation and reduce to the standard AC method (3.51) for constant $\varepsilon, \Delta t$. We prove that the first-order implicit discretization of the momentum equation with both new methods (3.54), (3.55) are unconditionally, nonlinearly, long-time stable without assumptions on $\varepsilon_n, \Delta t_n$. We study these new methods in a bounded, regular domain Ω subject to the initial and boundary conditions

$$u^0 = u_0(x) \text{ and } p^0 = p_0(x), \text{ in } \Omega,$$
$$u^n = 0 \text{ on } \partial\Omega \text{ for } t > 0.$$

The two first-order methods are: Given $u^n, p^n, \varepsilon_n, \Delta t_n$, select $\varepsilon_{n+1}, \Delta t_{n+1}$ and

$$\frac{u^{n+1} - u^n}{\Delta t_{n+1}} + (u^* \cdot \nabla)u^{n+1} + \frac{1}{2}(\nabla \cdot u^*)u^{n+1} + \nabla p^{n+1} - \nu \Delta u^{n+1} = f^{n+1},$$
$$\frac{\varepsilon_{n+1} p^{n+1} - \widehat{\varepsilon} p^n}{\Delta t_{n+1}} + \nabla \cdot u^{n+1} = 0, \text{ where}$$
$$\widehat{\varepsilon} = \min\{\varepsilon_{n+1}, \varepsilon_n\} \quad \text{for the min-Method and} \tag{3.54}$$
$$\widehat{\varepsilon} = \sqrt{\varepsilon_{n+1}\varepsilon_n} \quad \text{for the GA-Method} \tag{3.55}$$

For constant ε both methods reduce to the standard method (3.51), (3.52) for which stability is known. Thus, *the interest is stability for variable* ε.

3.3.5.1 STABILITY OF THE MIN-METHOD It is useful to recall that

$$(\varepsilon_{n+1}-\varepsilon_n)^+ = \max\{0,\varepsilon_{n+1}-\varepsilon_n\} = \varepsilon_{n+1} - \min\{0,\varepsilon_{n+1}-\varepsilon_n\}.$$

Theorem 8 (Stability of the min-Method)**.** *The variable $\varepsilon, \Delta t$ min-Method is unconditionally, long-time stable. For any $N > 0$ the energy equality holds:*

$$\begin{aligned}\|u^N\|^2 + \varepsilon_N\|p^N\|^2 + \sum_{n=0}^{N-1}\Big(&\min\{\varepsilon_{n+1},\varepsilon_n\}\|p^{n+1}-p^n\|^2 + (\varepsilon_{n+1}-\varepsilon_n)^+\|p^{n+1}\|^2 \\ &+(\varepsilon_n-\varepsilon_{n+1})^+\|p^n\|^2 + \|u^{n+1}-u^n\|^2 + 2\Delta t_{n+1}\nu\|\nabla u^{n+1}\|^2\Big) \\ &= \|u^0\|^2 + \varepsilon_0\|p^0\|^2 + \sum_{n=0}^{N-1} 2\Delta t_{n+1}(f^{n+1},u^{n+1}).\end{aligned}$$

Consequently, the stability bound holds:

$$\begin{aligned}\|u^N\|^2 + \varepsilon_N\|p^N\|^2 + \sum_{n=0}^{N-1}\Big(&\min\{\varepsilon_{n+1},\varepsilon_n\}\|p^{n+1}-p^n\|^2 + (\varepsilon_{n+1}-\varepsilon_n)^+\|p^{n+1}\|^2 \\ &+(\varepsilon_n-\varepsilon_{n+1})^+\|p^n\|^2 + \|u^{n+1}-u^n\|^2 + \Delta t_{n+1}\nu\|\nabla u^{n+1}\|^2\Big) \\ &\le \|u^0\|^2 + \varepsilon_0\|p^0\|^2 + \sum_{n=0}^{N-1}\frac{\Delta t_{n+1}}{\nu}\|f^{n+1}\|_{-1}^2.\end{aligned}$$

Proof. First we note that using the polarization identity, algebraic rearrangement and considering the cases $\varepsilon_{n+1} > \varepsilon_n$ and $\varepsilon_{n+1} < \varepsilon_n$ we have

$$\begin{aligned}&(\varepsilon_{n+1}p^{n+1} - \min\{\varepsilon_{n+1},\varepsilon_n\}p^n, p^{n+1}) \\ &= \varepsilon_{n+1}\|p^{n+1}\|^2 - \min\{\varepsilon_{n+1},\varepsilon_n\}(p^n,p^{n+1}) \\ &= \varepsilon_{n+1}\|p^{n+1}\|^2 - \min\{\varepsilon_{n+1},\varepsilon_n\}\left\{\frac{1}{2}\|p^n\|^2 + \frac{1}{2}\|p^{n+1}\|^2 - \frac{1}{2}\|p^n-p^{n+1}\|^2\right\} \\ &= \left(\varepsilon_{n+1} - \frac{1}{2}\min\{\varepsilon_{n+1},\varepsilon_n\}\right)\|p^{n+1}\|^2 \\ &\quad -\frac{1}{2}\min\{\varepsilon_{n+1},\varepsilon_n\}\|p^n\|^2 + \frac{1}{2}\min\{\varepsilon_{n+1},\varepsilon_n\}\|p^n-p^{n+1}\|^2 \\ &= \frac{1}{2}\varepsilon_{n+1}\|p^{n+1}\|^2 - \frac{1}{2}\varepsilon_n\|p^n\|^2 + \frac{1}{2}\min\{\varepsilon_{n+1},\varepsilon_n\}\|p^n-p^{n+1}\|^2 \\ &\quad +\frac{1}{2}\left(\varepsilon_{n+1} - \min\{\varepsilon_{n+1},\varepsilon_n\}\right)\|p^{n+1}\|^2 + \frac{1}{2}\left(\varepsilon_n - \min\{\varepsilon_{n+1},\varepsilon_n\}\right)\|p^n\|^2.\end{aligned}$$

We have $\varepsilon_{n+1} - \min\{\varepsilon_{n+1}, \varepsilon_n\} = (\varepsilon_{n+1} - \varepsilon_n)^+$ and $\varepsilon_n - \min\{\varepsilon_{n+1}, \varepsilon_n\} = (\varepsilon_n - \varepsilon_{n+1})^+$. Thus, because $\|p^n - p^{n+1}\|^2 = \|p^{n+1} - p^n\|^2$,

$$
\begin{aligned}
&(\varepsilon_{n+1}p^{n+1} - \min\{\varepsilon_{n+1}, \varepsilon_n\}p^n, p^{n+1}) = \\
&= \frac{1}{2}\varepsilon_{n+1}\|p^{n+1}\|^2 - \frac{1}{2}\varepsilon_n\|p^n\|^2 + \frac{1}{2}\min\{\varepsilon_{n+1}, \varepsilon_n\}\|p^{n+1} - p^n\|^2 \\
&\quad + \frac{1}{2}(\varepsilon_{n+1} - \varepsilon_n)^+\|p^{n+1}\|^2 + \frac{1}{2}(\varepsilon_n - \varepsilon_{n+1})^+\|p^n\|^2.
\end{aligned} \tag{3.56}
$$

With this identity, take the inner product of the first equation with $2\Delta t_{n+1}u^{n+1}$, the second with $2\Delta t_{n+1}p^{n+1}$, integrate over the flow domain, integrate by parts, use skew-symmetry, use the polarization identity twice and add. This yields

$$
\begin{aligned}
&\|u^{n+1}\|^2 - \|u^n\|^2 + \|u^{n+1} - u^n\|^2 + 2\Delta t_{n+1}\nu\|\nabla u^{n+1}\|^2 \\
&(\varepsilon_{n+1}p^{n+1} - \min\{\varepsilon_{n+1}, \varepsilon_n\}p^n, p^{n+1}) = 2\Delta t_{n+1}(f^{n+1}, u^{n+1}).
\end{aligned}
$$

From (3.56) the energy equality becomes

$$
\begin{aligned}
&\left(\|u^{n+1}\|^2 + \varepsilon_{n+1}\|p^{n+1}\|^2\right) - \left(\|u^n\|^2 + \varepsilon_n\|p^n\|^2\right) \\
&+2\Delta t_{n+1}\nu\|\nabla u^{n+1}\|^2 + \|u^{n+1} - u^n\|^2 + \min\{\varepsilon_{n+1}, \varepsilon_n\}\|p^{n+1} - p^n\|^2 \\
&+(\varepsilon_{n+1} - \varepsilon_n)^+\|p^{n+1}\|^2 + (\varepsilon_n - \varepsilon_{n+1})^+\|p^n\|^2 = 2\Delta t_{n+1}(f^{n+1}, u^{n+1}).
\end{aligned}
$$

Upon rearrangements and summation, the first two terms telescope, completing the proof of the energy equality. The stability estimate follows from the energy equality, the definition of the dual norm, and the Cauchy-Schwarz-Young inequality. □

The stability analysis shows that the numerical dissipation $\mathcal{D}_{\min}^{n+1}$ at t_{n+1} in the min-Method is

$$
\begin{aligned}
\mathcal{D}_{\min}^{n+1} &= \|u^{n+1} - u^n\|^2 + \min\{\varepsilon_{n+1}, \varepsilon_n\}\|p^{n+1} - p^n\|^2 \\
&\quad +(\varepsilon_{n+1} - \varepsilon_n)^+\|p^{n+1}\|^2 + (\varepsilon_n - \varepsilon_{n+1})^+\|p^n\|^2.
\end{aligned}
$$

3.3.5.2 STABILITY OF THE GA-METHOD The proof of stability of the GA-method differs from the last proof only in the treatment of the variable ε term, resulting is a different numerical dissipation for the method.

Theorem 9 (Stability of GA-Method)**.** *The variable $\varepsilon, \Delta t$, first-order GA-Method is unconditionally, long-time stable. For any $N > 0$ the energy equality holds:*

$$\begin{aligned}\|u^N\|^2 + \varepsilon_N\|p^N\|^2 + \sum_{n=0}^{N-1}\left(\|u^{n+1}-u^n\|^2 + \|\sqrt{\varepsilon_{n+1}}p^{n+1} - \sqrt{\varepsilon_n}p^n\|^2 + 2\Delta t_{n+1}\nu\|\nabla u^{n+1}\|^2\right)\\ = \|u^0\|^2 + \varepsilon_0\|p^0\|^2 + \sum_{n=0}^{N-1} 2\Delta t_{n+1}(f^{n+1}, u^{n+1}).\end{aligned}$$

and the stability bound holds:

$$\begin{aligned}\|u^N\|^2 + \varepsilon_N\|p^N\|^2 + \sum_{n=0}^{N-1}\left(\|u^{n+1}-u^n\|^2 + \|\sqrt{\varepsilon_{n+1}}p^{n+1} - \sqrt{\varepsilon_n}p^n\|^2 + \Delta t_{n+1}\nu\|\nabla u^{n+1}\|^2\right)\\ \leq \|u^0\|^2 + \varepsilon_0\|p^0\|^2 + \sum_{n=0}^{N-1}\frac{\Delta t_{n+1}}{\nu}\|f^{n+1}\|_{-1}^2.\end{aligned}$$

Proof. First we note that using the polarization identity we have

$$\begin{aligned}(\varepsilon_{n+1}p^{n+1} - \sqrt{\varepsilon_{n+1}\varepsilon_n}p^n, p^{n+1}) =\\ = \varepsilon_{n+1}\|p^{n+1}\|^2 - (\sqrt{\varepsilon_n}p^n, \sqrt{\varepsilon_{n+1}}p^{n+1})\\ = \varepsilon_{n+1}\|p^{n+1}\|^2 - \left\{\frac{1}{2}\varepsilon_n\|p^n\|^2 + \frac{1}{2}\varepsilon_{n+1}\|p^{n+1}\|^2 - \frac{1}{2}\|\sqrt{\varepsilon_n}p^n - \sqrt{\varepsilon_{n+1}}p^{n+1}\|^2\right\}\\ = \frac{1}{2}\varepsilon_{n+1}\|p^{n+1}\|^2 - \frac{1}{2}\varepsilon_n\|p^n\|^2 + \frac{1}{2}\|\sqrt{\varepsilon_{n+1}}p^{n+1} - \sqrt{\varepsilon_n}p^n\|^2.\end{aligned}$$

The remainder of the proof is the same as for the min-Method. □

The stability analysis shows that the numerical dissipation $\mathcal{D}_{\text{GA}}^{n+1}$ at t_{n+1} in the GA-Method is

$$\mathcal{D}_{\text{GA}}^{n+1} = \|u^{n+1}-u^n\|^2 + \|\sqrt{\varepsilon_{n+1}}p^{n+1} - \sqrt{\varepsilon_n}p^n\|^2.$$

There is no obvious way to tell *á priori* which method's numerical dissipation is larger or to be preferred. A numerical comparison is thus presented in Section 5.

Remark 11 (The Continuum Analogues)**.** *It is natural to ask if there is a non-autonomous continuum AC model associated with each method. The momentum equation for each continuum model is the standard*

$$\partial_t u + (u \cdot \nabla)u + \frac{1}{2}(\nabla \cdot u)u - \nu \Delta u + \nabla p = f.$$

The associated continuum continuity equation for the min-Method is

$$\varepsilon(t)\partial_t p + \varepsilon_t^+ p + \nabla \cdot u = 0, \tag{3.57}$$

whereas the continuum continuity equation for the GA-method is

$$\sqrt{\varepsilon}\partial_t(\sqrt{\varepsilon}p) + \nabla \cdot u = 0.$$

Analyzing convergence of (3.57) *to a weak solution of the incompressible NSE as the non-autonomous $\varepsilon(t) \to 0$ is a significant open problem. The convergence of the GA-method can be inferred from the results in Section 3.2.*

3.3.6 SECOND-ORDER, VARIABLE ε METHODS

The first-order methods are now extended to embedded first and second-order methods adapting [53] from ODEs to the NSE. First we review the idea of extension used.

3.3.6.1 REVIEW OF THE ODE ALGORITHM

Consider the initial value problem

$$y'(t) = f(t, y(t)), y(0) = y_0.$$

Recall $\tau = \Delta t_{n+1}/\Delta t_n$ is the timestep ratio. The second-order accurate, variable timestep method of [53] is the standard backward Euler (fully-implicit) method followed by a time filter:

$$\begin{aligned} &\text{Step 1} && \tfrac{y_1^{n+1}-y^n}{\Delta t_{n+1}} = f(t_{n+1}, y_1^{n+1}), \\ & && \text{pick filter parameter } \alpha(1) = \tfrac{\tau(1+\tau)}{(1+2\tau)}, \text{ then} \\ &\text{Step 2} && y^{n+1} = y_1^{n+1} - \tfrac{\alpha_1}{2}\left\{\tfrac{2\Delta t_n}{\Delta t_n+\Delta t_{n+1}} y_1^{n+1} - 2y^n + \tfrac{2\Delta t_{n+1}}{\Delta t_n+\Delta t_{n+1}} y^{n-1}\right\}. \end{aligned} \tag{3.58}$$

The combination is second-order accurate, A-stable for constant or decreasing time-steps and a measure of the pre- and post-filter difference

$$EST(1) = |y^{n+1} - y_1^{n+1}| \tag{3.59}$$

can be used in a standard way as a local error estimator for the lower order approximation y_1^{n+1} or a (pessimistic) estimator for the higher order approximation y^{n+1}.

3.3.6.2 A SIMPLE, ADAPTIVE-ε, SECOND-ORDER AC ALGORITHM

The continuity equation for both methods can be written

$$\frac{\varepsilon_{n+1}p^{n+1} - \widehat{\varepsilon}p^n}{\Delta t_{n+1}} + \nabla \cdot u^{n+1} = 0 \text{ where } \widehat{\varepsilon} = \sqrt{\varepsilon_{n+1}\varepsilon_n} \text{ or } \min\{\varepsilon_{n+1}, \varepsilon_n\}.$$

This can be used to uncouple velocity and pressure using

$$\nabla p^{n+1} = \frac{\widehat{\varepsilon}}{\varepsilon_{n+1}}\nabla p^n - \frac{\Delta t_{n+1}}{\varepsilon_{n+1}}\nabla\nabla \cdot u^{n+1}.$$

The discrete momentum equation for either first-order method is then

$$\begin{aligned} \frac{u_1^{n+1} - u^n}{\Delta t_{n+1}} + (u^* \cdot \nabla)u_1^{n+1} + \frac{1}{2}(\nabla \cdot u^*)u_1^{n+1} - \frac{\Delta t_{n+1}}{\varepsilon_{n+1}}\nabla\nabla \cdot u_1^{n+1} \\ -\nu\Delta u_1^{n+1} = f^{n+1} - \frac{\widehat{\varepsilon}}{\varepsilon_{n+1}}\nabla p^n. \end{aligned}$$

Applying the time filter of (3.58) to the velocity approximation increases the methods accuracy to $\mathcal{O}(\Delta t^2)$. This combination yields a simple, second-order, constant timestep but adaptive ε algorithm. In the algorithm below the change in ε is restricted to be between halving and doubling the previous ε value.

Algorithm 1 (Simple, adaptive ε, constant timestep, second-order AC method)**.** *Given* $u^n, u^{n-1}, p^n, \Delta t, \varepsilon_{n+1}, \varepsilon_n$*, and tolerance* TOL_c*, perform the following steps:*
Step 1: Select $\widehat{\varepsilon} = \sqrt{\varepsilon_{n+1}\varepsilon_n}$ *or* $\widehat{\varepsilon} = \min\{\varepsilon_{n+1}, \varepsilon_n\}$*, set* $u^* = 2u^n - u^{n-1}$*, and solve for* u_1^{n+1} *satisfying*

$$\frac{u_1^{n+1} - u^n}{\Delta t} + (u^* \cdot \nabla)u_1^{n+1} + \frac{1}{2}(\nabla \cdot u^*)u_1^{n+1} - \frac{\Delta t}{\varepsilon_{n+1}}\nabla\nabla \cdot u_1^{n+1}$$
$$-\nu\Delta u_1^{n+1} = f^{n+1} - \frac{\widehat{\varepsilon}}{\varepsilon_{n+1}}\nabla p^n.$$

Step 2: Filter u_1^{n+1} *and compute the estimator* EST_c*:*

$$u^{n+1} = u_1^{n+1} - \frac{1}{3}\left\{u_1^{n+1} - 2u^n + u^{n-1}\right\},$$
$$EST_c = \|\nabla \cdot u^{n+1}\| = \frac{1}{3}\|u_1^{n+1} - 2u^n + u^{n-1}\|.$$

Step 3: Adapt ε *: If* $EST_c > TOL_c$*, then repeat Steps 1 and 2 after resetting* ε_{n+1} *by*

$$\varepsilon_{n+1} = \max\{0.9\varepsilon_{n+1}\frac{TOL_c}{EST_c}, 0.5\varepsilon_{n+1}\}$$

Otherwise, adapt by

$$\varepsilon_{n+2} = \max\{\min\{0.9\varepsilon_{n+1}\frac{TOL_c}{EST_c}, 2\varepsilon_{n+1}\}, .5\varepsilon_{n+1}\}.$$

Step 4: Update the pressure

$$p^{n+1} = \frac{\widehat{\varepsilon}}{\varepsilon_{n+1}}p^n - \frac{\Delta t_{n+1}}{\varepsilon_{n+1}}\nabla \cdot u^{n+1}$$

and proceed to the next time, repeating the steps listed above.

3.3.7 STABILITY OF THE SECOND-ORDER METHOD FOR VARIABLE ε, CONSTANT Δt

This section establishes unconditional, nonlinear, long-time stability of the second-order GA-method for constant timesteps but variable ε. The proof addresses the interaction between the filter step with the continuity equation. It is adapted to the min-Method following ideas in the proof of Theorem 8. For constant time-steps and variable ε the GA-method is as follows. Given $u^n, u^{n-1}, p^n, p^{n-1}, \varepsilon_n$, select ε_{n+1} and $u^* = 2u^n - u^{n-1}$ (since the timestep is here constant). Then,

$$\begin{aligned} &\frac{u_1^{n+1} - u^n}{\Delta t} + (u^* \cdot \nabla)u_1^{n+1} + \frac{1}{2}(\nabla \cdot u^*)u_1^{n+1} + \nabla p^{n+1} - \nu \Delta u_1^{n+1} = f^{n+1}, \\ &\qquad \text{Filter: } u^{n+1} = u_1^{n+1} - \frac{1}{3}\left\{u_1^{n+1} - 2u^n + u^{n-1}\right\} \\ &\text{Find } p^{n+1} : \frac{\varepsilon_{n+1}p^{n+1} - \sqrt{\varepsilon_{n+1}\varepsilon_n}p^n}{\Delta t} + \nabla \cdot u_1^{n+1} = 0 \text{ \& proceed to next step.} \end{aligned} \tag{3.60}$$

We now prove an energy equality for the method which implies stability.

Theorem 10. *The method (3.60) satisfies the following discrete energy equality (from which stability follows). For any $N > 1$*

$$\begin{aligned} &\|u^N\|^2 + \|2u^N - u^{N-1}\|^2 + \|u^N - u^{N-1}\|^2 + 2\varepsilon_N\|p^N\|^2 \\ &\sum_{n=1}^{N-1}\left(3\|u^{n+1} - 2u^n + u^{n-1}\|^2 + 2\|\sqrt{\varepsilon_{n+1}}p^{n+1} - \sqrt{\varepsilon_n}p^n\|^2 + \Delta t\nu\|\nabla(3u^{n+1} - 2u^n + u^{n-1})\|^2\right) \\ &= \|u^1\|^2 + \|2u^1 - u^0\|^2 + \|u^1 - u^0\|^2 + 2\varepsilon_1\|p^1\|^2 + \sum_{n=1}^{N-1} 2\Delta t(f^{n+1}, 3u^{n+1} - 2u^n + u^{n-1}). \end{aligned}$$

Proof. To prove stability, we eliminate the intermediate value u_1^{n+1} in the momentum equation. From the filter step $u^{n+1} = u_1^{n+1} - \frac{1}{3}\left\{u_1^{n+1} - 2u^n + u^{n-1}\right\}$ we have

$$u_1^{n+1} = \frac{3}{2}u^{n+1} - u^n + \frac{1}{2}u^{n-1}.$$

Replacing u_1^{n+1} by $\frac{3}{2}u^{n+1} - u^n + \frac{1}{2}u^{n-1}$ yields the equivalent discrete momentum equation:

$$\begin{aligned} &\frac{3u^{n+1} - 4u^n + u^{n-1}}{2\Delta t} + \frac{1}{2}(u^* \cdot \nabla)(3u^{n+1} - 2u^n + u^{n-1}) \\ &+\frac{1}{4}(\nabla \cdot u^*)(3u^{n+1} - 2u^n + u^{n-1}) + \nabla p^{n+1} - \frac{\nu}{2}\Delta(3u^{n+1} - 2u^n + u^{n-1}) = f^{n+1}. \end{aligned} \tag{3.61}$$

Multiply by the timestep Δt, take the L^2 inner product of the momentum equation (3.61) with $2\Delta t(3u^{n+1} - 2u^n + u^{n-1})$, the L^2 inner product of the discrete continuity equation with $4\Delta t p^{n+1}$ and add. Two pressure terms cancel since $u_1^{n+1} = \frac{1}{2}(3u^{n+1} - 2u^n + u^{n-1})$and the nonlinear terms vanish due to skew-symmetry. Thus, we obtain

$$(3u^{n+1} - 4u^n + u^{n-1}, 3u^{n+1} - 2u^n + u^{n-1}) + (\varepsilon_{n+1}p^{n+1} - \sqrt{\varepsilon_{n+1}\varepsilon_n}p^n, p^{n+1})$$
$$+\Delta t\nu\|\nabla(3u^{n+1} - 2u^n + u^{n-1})\|^2 = \Delta t(f^{n+1}, 3u^{n+1} - 2u^n + u^{n-1}).$$

The key terms are the first two. For the first term, apply the following identity from [24]:

$$\left(\|u^{n+1}\|^2 + \|2u^{n+1} - u^n\|^2 + \|u^{n+1} - u^n\|^2\right) - \left(\|u^n\|^2 + \|2u^n - u^{n-1}\|^2 + \|u^n - u^{n-1}\|^2\right)$$
$$+3\|u^{n+1} - 2u^n + u^{n-1}\|^2 = (3u^{n+1} - 4u^n + u^{n-1}, 3u^{n+1} - 2u^n + u^{n-1}).$$

For the pressure term $(\sqrt{\varepsilon_{n+1}\varepsilon_n}p^n, p^{n+1})$ the polarization identity, suitably applied, yields

$$(\sqrt{\varepsilon_{n+1}\varepsilon_n}p^n, p^{n+1}) = (\sqrt{\varepsilon_n}p^n, \sqrt{\varepsilon_{n+1}}p^{n+1}) =$$
$$= \frac{1}{2}\left(\varepsilon_{n+1}\|p^{n+1}\|^2 + \varepsilon_n\|p^n\|^2 - \|\sqrt{\varepsilon_{n+1}}p^{n+1} - \sqrt{\varepsilon_n}p^n\|^2\right).$$

Thus,

$$(\varepsilon_{n+1}p^{n+1} - \sqrt{\varepsilon_{n+1}\varepsilon_n}p^n, p^{n+1}) = \frac{1}{2}\varepsilon_{n+1}\|p^{n+1}\|^2 - \frac{1}{2}\varepsilon_n\|p^n\|^2 + \frac{1}{2}\|\sqrt{\varepsilon_{n+1}}p^{n+1} - \sqrt{\varepsilon_n}p^n\|^2.$$

Combining the pressure and velocity identities, we have

$$\left(\|u^{n+1}\|^2 + \|2u^{n+1} - u^n\|^2 + \|u^{n+1} - u^n\|^2 + 2\varepsilon_{n+1}\|p^{n+1}\|^2\right)$$
$$-\left(\|u^n\|^2 + \|2u^n - u^{n-1}\|^2 + \|u^n - u^{n-1}\|^2 + 2\varepsilon_n\|p^n\|^2\right)$$
$$+3\|u^{n+1} - 2u^{n-1} + u^{n-1}\|^2 + 2\|\sqrt{\varepsilon_{n+1}}p^{n+1} - \sqrt{\varepsilon_n}p^n\|^2$$
$$+\Delta t\nu\|\nabla(3u^{n+1} - 2u^n + u^{n-1})\|^2 = 2\Delta t(f^{n+1}, 3u^{n+1} - 2u^n + u^{n-1}).$$

Summing from $n = 1$ to N proves unconditional, long-time stability. □

3.3.8 DOUBLY $\Delta t, \varepsilon$ ADAPTIVE ALGORITHMS

We present three doubly adaptive AC algorithms: *first-order*, *second-order*, and a third that *adapts the method order*. The first two are tested in Section 3.3.9. While not tested herein, we include the variable order adaptive algorithm for its clear interest. In the first algorithm, the error is estimated by a time filter and the next timestep and next ε are adapted based on first-order prediction:

$$\Delta t_{new} = \Delta t_{old} \left(\frac{TOL_m}{EST(1)} \right)^{1/2} \text{ and } \varepsilon_{new} = \varepsilon_{old} \frac{TOL_c}{\|\nabla \cdot u^{n+1}\|},$$

where TOL_m and TOL_c are tolerances for the error in the momentum and continuity equations, respectively. In our implementation, a safety factor of 0.9 is used and the maximum change in both is (additionally) restricted to be between 0.5 and 2.0.

Algorithm 2 (Doubly $\Delta t, \varepsilon$ Adaptive, First-Order Method)**.** *Given TOL_m,TOL_c, u^n, u^{n-1}, k_{n+1}, k_n, k_{n-1}, and ε_n, perform the following steps:*

Step 1: Compute $\tau = \frac{\Delta t_{n+1}}{\Delta t_n}$ and $\alpha_1 = \frac{\tau(1.0+\tau)}{1.0+2.0\tau}$, select $\widehat{\varepsilon} = \sqrt{\varepsilon_{n+1}\varepsilon_n}$ or $\widehat{\varepsilon} = \min\{\varepsilon_{n+1}, \varepsilon_n\}$, and set $u^* = (1+\tau)u^n - \tau u^{n-1}$.

Step 2: Find BE approximation u^{n+1} satisfying

$$\frac{u^{n+1}-u^n}{\Delta t_{n+1}} + (u^* \cdot \nabla)u^{n+1} + \frac{1}{2}(\nabla \cdot u^*)u^{n+1} - \frac{\Delta t_{n+1}}{\varepsilon_{n+1}} \nabla \nabla \cdot u^{n+1} - \nu \Delta u^{n+1} = f^{n+1} - \frac{\widehat{\varepsilon}}{\varepsilon_{n+1}} \nabla p^n.$$

Step 3: Compute the difference D_2 and estimators:

$$\begin{aligned} D_2 &= \frac{2\Delta t_n}{\Delta t_n + \Delta t_{n+1}} u^{n+1} - 2u^n + \frac{2\Delta t_{n+1}}{\Delta t_n + \Delta t_{n+1}} u^{n-1} \\ EST(1) &= \frac{\alpha_1}{2} \|D_2\|, \\ EST_c &= \|\nabla \cdot u_1^{n+1}\|. \end{aligned}$$

Step 4: If $EST_c > TOL_c$ or $EST(1) > TOL_m$, then repeat Steps 1–3 after resetting ε_{n+1}, Δt_{n+1} by

$$\begin{aligned} \varepsilon_{n+1} &= \max\{0.9\varepsilon_{n+1} \frac{TOL_c}{EST_c}, 0.5\varepsilon_{n+1}\}, \\ \Delta t_{n+1} &= 0.9 \left(\frac{TOL_m}{EST(1)} \right)^{1/2} \max \left\{ 0.9\Delta t_n \left(\frac{TOL_m}{EST(1)} \right)^{1/2}, 0.5\Delta t_{n+1} \right\}. \end{aligned}$$

Otherwise, predict the best next step for each approximation:

$$\varepsilon_{n+2} = \max\{\min\{0.9\varepsilon_{n+1}\frac{TOL_c}{EST_c}, 2\varepsilon_{n+1}\}, 0.5\varepsilon_{n+1}\},$$
$$\Delta t_{n+2} = \max\left\{\min\left\{0.9\Delta t_{n+1}\left(\frac{TOL_m}{EST(1)}\right)^{1/2}, 2\Delta t_{n+1}\right\}, 0.5\Delta t_{n+1}\right\}.$$

Step 5: Update the pressure

$$p^{n+1} = \frac{\widehat{\varepsilon}}{\varepsilon_{n+1}}p^n - \frac{\Delta t_{n+1}}{\varepsilon_{n+1}}\nabla \cdot u^{n+1}$$

and proceed to the next timestep, repeating the steps listed above.

3.3.8.1 THE SECOND-ORDER, DOUBLY ADAPTIVE ALGORITHM For the second-order, doubly adaptive method, we predict the next ε value in the same way as in the first-order method and predict the next timestep based on the second-order prediction

$$\Delta t_{new} = \Delta t_{old}\left(\frac{TOL_m}{EST(2)}\right)^{1/3}.$$

Next, we calculate $EST(2)$. The second-order method is equivalent, after elimination of the intermediate (first-order) approximation, to a one leg method exactly as in (3.60) in the constant timestep case. The one leg method's linear multistep twin has local error proportionate to $\Delta t^3\partial_t^3 u + \mathcal{O}(\Delta t^4)$. Thus, an estimate of $\partial_t^3 u$ is computed using difference of D_2. Write

$$D_2(n+1) = \frac{2\Delta t_n}{\Delta t_n + \Delta t_{n+1}}u_1^{n+1} - 2u^n + \frac{2\Delta t_{n+1}}{\Delta t_n + \Delta t_{n+1}}u^{n-1}.$$

From differences of $D_2(n+1)$, $D_2(n)$ we obtain the estimator

$$EST(2) = \frac{\alpha_2}{6}\left\|\frac{3\Delta t_{n-1}}{\Delta t_{n+1} + \Delta t_n + \Delta t_{n-1}}D_2(n+1) - \frac{3\Delta t_{n-1}}{\Delta t_{n+1} + \Delta t_n + \Delta t_{n-1}}D_2(n)\right\|,$$

where the coefficient α_2 is determined through a Taylor series calculation to be

$$\alpha_2 = \frac{\tau_n(\tau_{n+1}\tau_n + \tau_n + 1)(4\tau_{n+1}^3 + 5\tau_{n+1}^2 + \tau_{n+1})}{3(\tau_n\tau_{n+1}^2 + 4\tau_n\tau_{n+1} + 2\tau_{n+1} + \tau_n + 1)}$$

Algorithm 3 (Doubly Δt, ε Adaptive, Second-Order Method)**.** *Given TOL_m, TOL_c, u^n, u^{n-1}, u^{n-2}, $D_2(n)$, Δt_{n+1}, Δt_n, Δt_{n-1}, and ε_n, perform the following steps:*

Step 1: Compute

$$\tau_{n+1} = \frac{\Delta t_{n+1}}{\Delta t_n},\ \tau_n = \frac{\Delta t_n}{\Delta t_{n-1}},\ \alpha_1 = \frac{\tau_{n+1}(1.0+\tau_{n+1})}{1.0+2.0\tau_{n+1}},$$
$$\alpha_2 = \frac{\tau_n(\tau_{n+1}\tau_n+\tau_n+1)(4\tau_{n+1}^3+5\tau_{n+1}^2+\tau_{n+1})}{3(\tau_n\tau_{n+1}^2+4\tau_n\tau_{n+1}+2\tau_{n+1}+\tau_n+1)},$$

select $\widehat{\varepsilon} = \sqrt{\varepsilon_{n+1}\varepsilon_n}$ or $\widehat{\varepsilon} = \min\{\varepsilon_{n+1}, \varepsilon_n\}$, and set $u^* = (1+\tau_{n+1})u^n - \tau_{n+1}u^{n-1}$.

Step 2: Find BE approximation u_1^{n+1}

$$\frac{u_1^{n+1}-u^n}{\Delta t_{n+1}} + (u^*\cdot\nabla)u_1^{n+1} + \frac{1}{2}(\nabla\cdot u^*)u_1^{n+1} - \frac{\Delta t_{n+1}}{\varepsilon_{n+1}}\nabla\nabla\cdot u_1^{n+1} - \nu\Delta u_1^{n+1} = f^{n+1} - \frac{\widehat{\varepsilon}}{\varepsilon_{n+1}}\nabla p^n.$$

Step 3: Compute the difference $D_2(n+1)$, update the velocity, and compute the estimators

$$D_2(n+1) = \frac{2\Delta t_n}{\Delta t_n+\Delta t_{n+1}}u_1^{n+1} - 2u^n + \frac{2\Delta t_{n+1}}{\Delta t_n+\Delta t_{n+1}}u^{n-1},\ u^{n+1} = u_1^{n+1} - \frac{\alpha_1}{2}D_2(n+1),$$
$$EST(2) = \frac{\alpha_2}{6}\left\|\frac{3\Delta t_{n-1}}{\Delta t_{n+1}+\Delta t_n+\Delta t_{n-1}}D_2(n+1) - \frac{3\Delta t_{n-1}}{\Delta t_{n+1}+\Delta t_n+\Delta t_{n-1}}D_2(n)\right\|,$$
$$EST_c = \|\nabla\cdot u^{n+1}\|.$$

Step 4: If $EST_c > TOL_c$ or $EST(2) > TOL_m$ then repeat Steps 1–3 after resetting ε_{n+1}, Δt_{n+1} by

$$\varepsilon_{n+1} = \max\{0.9\varepsilon_{n+1}\frac{TOL_c}{EST_c}, 0.5\varepsilon_{n+1}\}$$
$$\Delta t_{n+1} = \max\left\{\min\left\{0.9\Delta t_{n+1}\left(\frac{TOL_m}{EST(2)}\right)^{1/3}, 2\Delta t_{n+1}\right\}, 0.5\Delta t_{n+1}\right\}.$$

Otherwise predict the best next step for each approximation:

$$\varepsilon_{n+2} = \max\{\min\{0.9\varepsilon_{n+1}\frac{TOL_c}{EST_c}, 2\varepsilon_{n+1}\}, 0.5\varepsilon_{n+1}\},$$
$$\Delta t_{n+2} = \max\left\{\min\left\{0.9\Delta t_{n+1}\left(\frac{TOL_m}{EST(2)}\right)^{1/3}, 2\Delta t_{n+1}\right\}, 0.5\Delta t_{n+1}\right\}.$$

Step 5: Update the pressure

$$p^{n+1} = \frac{\widehat{\varepsilon}}{\varepsilon_{n+1}}p^n - \frac{\Delta t_{n+1}}{\varepsilon_{n+1}}\nabla\cdot u^{n+1}.$$

and proceed to next timestep, repeating the steps listed above.

3.3.8.2 THE ADAPTIVE ORDER, TIMESTEP AND ε ALGORITHM To adapt $\varepsilon, \Delta t$, and the method order we use the local truncation error indicators for the momentum and continuity equations, respectively,

$$\begin{aligned} \text{Adapt } \Delta t \text{ for } u_1 \text{ using} &: \quad EST(1) \\ \text{Adapt } \Delta t \text{ for } u \text{ using} &: \quad EST(2) \\ \text{Adapt } \varepsilon \text{ for } p \text{ using} &: \quad EST_c := ||\nabla \cdot u^{n+1}||. \end{aligned}$$

The algorithm computes two velocity approximations. The first, u_1, is first-order and A-stable for all combinations of timestep and ε. The second u is second-order and A-stable for constant (or decreasing) timestep but only $0-$stable for increasing time-steps. Variable (1 or 2) order is introduced as follows. The local error in each approximation is estimated. If both are above the tolerance, the step is repeated. Otherwise, the optimal next timestep is predicted for each method by the following first- and second-order predictions:

$$\Delta t_{n+1} = \Delta t_n \left(\frac{TOL_m}{EST(1)} \right)^{1/2},$$
$$\Delta t_{n+1} = \Delta t_n \left(\frac{TOL_m}{EST(2)} \right)^{1/3}.$$

The actual Δt_{n+1} presented below and in the tests in Section 3.3.9 is restricted to be 0.5 to 2.0 times Δt_n and includes a safety factor of 0.9.

Algorithm 4 (Adaptive order, k, ε Method)**.** *Given TOL_m, TOL_c, u^n, u^{n-1}, u^{n-2}, $D_2(n)$, Δt_{n+1}, Δt_n, Δt_{n-1}, and ε_n, perform the following steps:*

Step 1: Compute

$$\tau_{n+1} = \frac{\Delta t_{n+1}}{\Delta t_n}, \ \tau_n = \frac{\Delta t_n}{\Delta t_{n-1}}, \ \alpha_1 = \frac{\tau_{n+1}(1.0 + \tau_{n+1})}{1.0 + 2.0\tau_{n+1}},$$
$$\alpha_2 = \frac{\tau_n(\tau_{n+1}\tau_n + \tau_n + 1)(4\tau_{n+1}^3 + 5\tau_{n+1}^2 + \tau_{n+1})}{3(\tau_n\tau_{n+1}^2 + 4\tau_n\tau_{n+1} + 2\tau_{n+1} + \tau_n + 1)},$$

select $\widehat{\varepsilon} = \sqrt{\varepsilon_{n+1}\varepsilon_n}$ or $\widehat{\varepsilon} = \min\{\varepsilon_{n+1}, \varepsilon_n\}$, and set $u^* = (1 + \tau_{n+1})u^n - \tau_{n+1}u^{n-1}$.

Step 2: Find BE approximation u_1^{n+1}

$$\frac{u_1^{n+1} - u^n}{\Delta t_{n+1}} + (u^* \cdot \nabla)u_1^{n+1} + \frac{1}{2}(\nabla \cdot u^*)u_1^{n+1} - \frac{\Delta t_{n+1}}{\varepsilon_{n+1}}\nabla\nabla \cdot u_1^{n+1} - \nu\Delta u_1^{n+1} = f^{n+1} - \frac{\widehat{\varepsilon}}{\varepsilon_{n+1}}\nabla p^n.$$

Step 3: Compute the difference $D_2(n+1)$, update the velocity, and compute the estimators

$$D_2(n+1) = \frac{2\Delta t_n}{\Delta t_n + \Delta t_{n+1}} u_1^{n+1} - 2u^n + \frac{2\Delta t_{n+1}}{\Delta t_n + \Delta t_{n+1}} u^{n-1},\ u^{n+1} = u_1^{n+1} - \frac{\alpha_1}{2} D_2(n+1),$$

$$EST(1) = \frac{\alpha_1}{2} \left\| D_2(n+1) \right\|,$$

$$EST(2) = \frac{\alpha_2}{6} \left\| \frac{3\Delta t_{n-1}}{\Delta t_{n+1} + \Delta t_n + \Delta t_{n-1}} D_2(n+1) - \frac{3\Delta t_{n-1}}{\Delta t_{n+1} + \Delta t_n + \Delta t_{n-1}} D_2(n) \right\|,$$

$$EST_c = \|\nabla \cdot u^{n+1}\|.$$

Step 4: If $EST_c > TOL_c$ or $\min\{EST(1), EST(2)\} > TOL_m$, then repeat Steps 1–3, resetting $\varepsilon_{n+1}, \Delta t_{n+1}$ by

$$\varepsilon_{n+1} = \max\{0.9\varepsilon_{n+1} \frac{TOL_c}{EST_c}, 0.5\varepsilon_{n+1}\},$$

$$\Delta t_{BE} = 0.9 \left(\frac{TOL_m}{EST(1)} \right)^{1/2} \max \left\{ 0.9\Delta t_n \left(\frac{TOL_m}{EST(1)} \right)^{1/2}, 0.5\Delta t_{n+1} \right\},$$

$$\Delta t_{Filter} = 0.9 \left(\frac{TOL_m}{EST(2)} \right)^{1/3} \max \left\{ 0.9\Delta t_n \left(\frac{TOL_m}{EST(2)} \right)^{1/3} 0.5\Delta t_{n+1} \right\},$$

$$\Delta t_{n+1} = \max\{\Delta t_{BE}, \Delta t_{Filter}\}.$$

Otherwise predict $\varepsilon, \Delta t$ for each approximation:

$$\varepsilon_{n+2} = \max\{\min\{0.9\varepsilon_{n+1} \frac{TOL_c}{EST_c}, 2\varepsilon_{n+1}\}, 0.5\varepsilon_{n+1}\},$$

$$\Delta t_{BE} = \max \left\{ \min \left\{ 0.9\Delta t_{n+1} \left(\frac{TOL_m}{EST(1)} \right)^{1/2}, 2\Delta t_{n+1} \right\}, 0.5\Delta t_{n+1} \right\},$$

$$\Delta t_{Filter} = \max \left\{ \min \left\{ 0.9\Delta t_{n+1} \left(\frac{TOL_m}{EST(2)} \right)^{1/3}, 2\Delta t_{n+1} \right\}, 0.5\Delta t_{n+1} \right\}.$$

Step 5: Select the method order with larger next timestep, i.e., if $\Delta t_{BE} > \Delta t_{Filter}$, then $\Delta t_{n+2} = \Delta t_{BE}$ and $u^{n+1} = u_1^{n+1}$. Otherwise, $\Delta t_{n+2} = \Delta t_{Filter}$ and $u^{n+1} = u^{n+1}$.

Step 6: Update the pressure

$$p^{n+1} = \frac{\widehat{\varepsilon}}{\varepsilon_{n+1}} p^n - \frac{\Delta t_{n+1}}{\varepsilon_{n+1}} \nabla \cdot u^{n+1}$$

and proceed to next timestep, repeating the steps listed above.

The fixed order methods can, if desired, be implemented by commenting out parts of the variable order Algorithm 4.

3.3.9 THREE NUMERICAL TESTS

The stability and accuracy of the new methods are interrogated in two numerical tests and the three discrete continuity equations are compared in our third test. The tests employ the finite element method to discretize space, with Taylor-Hood ($\mathbb{P}_2/\mathbb{P}_1$) elements, [50]. All the stability results proven herein hold for this spatial discretization by essentially the same proofs. The meshes used for both tests are generated using a Delaunay triangulation. The software package FEniCS is used for both experiments [1].

We begin with comparative tests of the adaptive $\Delta t, \varepsilon$, first and second-order method. Both adapt ε based on $||\nabla \cdot u||$. The first-order method accepts the first-order approximation u_1^{n+1} and adapts the timestep based on $EST(1)$. The second-order method accepts u^{n+1} as the approximation and adapts the time step based on $EST(2)$.

3.3.9.1 TEST 1: FLOW BETWEEN OFFSET CIRCLES To interrogate stability and accuracy of the GA-method, we present the results of two numerical tests. Pick

$$\Omega = \{(x,y) : x^2 + y^2 \leq r_1^2 \text{ and } (x-c_1)^2 + (y-c_2)^2 \geq r_2^2\},$$
$$r_1 = 1.0, r_2 = 0.1, c = (c_1, c_2) = (0.5, 0.0),$$
$$f = \min\{t, 1\}(-4y(1-x^2-y^2), 4x(1-x^2-y^2))^T, \text{ for } 0 \leq t \leq 10.$$

with no-slip boundary conditions on both circles and $\nu = 0.001$. The finite element discretization has a maximal mesh width of $h_{max} = 0.0133$, and the flow was solved using the direct solver UMFPACK [23]. For this test, we use fixed tolerances $TOL_m = TOL_c = 0.001$. The flow (inspired by the extensive work on variants of Couette flow, [34]), driven by a counterclockwise force (with $f \equiv 0$ at the outer circle), rotates about $(0,0)$ and interacts with the immersed circle. This induces a von Kármán vortex street which re-interacts with the immersed circle creating more complex structures. There is also a central (polar) vortex that alternately self-organizes then breaks down. Each of these events includes a significant pressure response.

For both approximations we track the evolution of Δt_n and ε_n, the pressure at the origin, the violation of incompressibility, and the algorithmic energy $\|u_h^{n+1}\|^2 + \varepsilon_{n+1}\|p_h^{n+1}\|^2$.

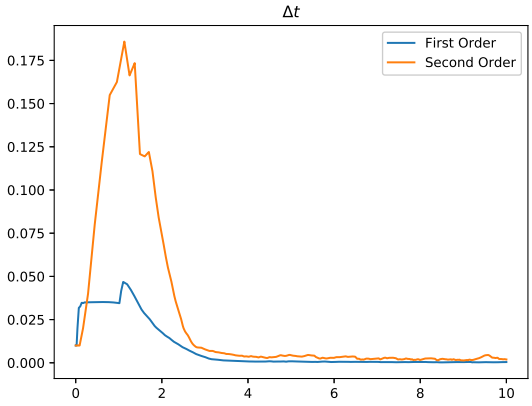

(a) Timestep evolution

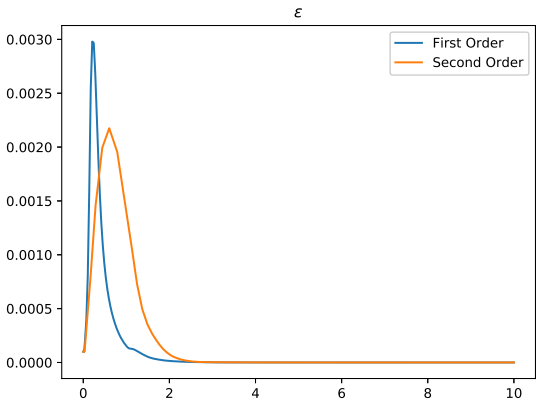

(b) ε evolution

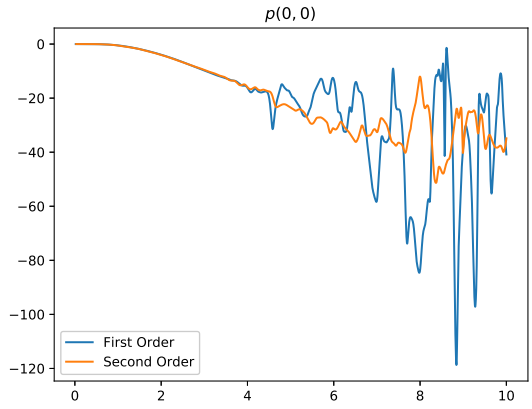

(c) Pressure at the origin

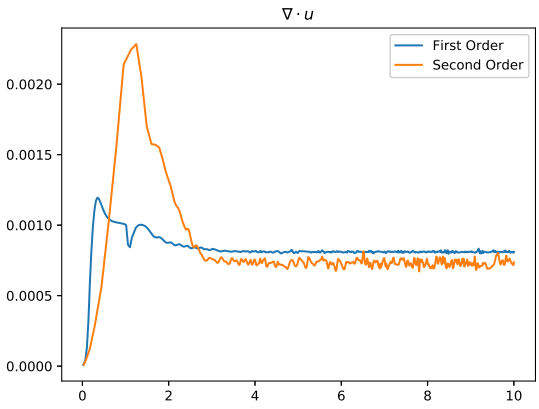

(d) Divergence evolution

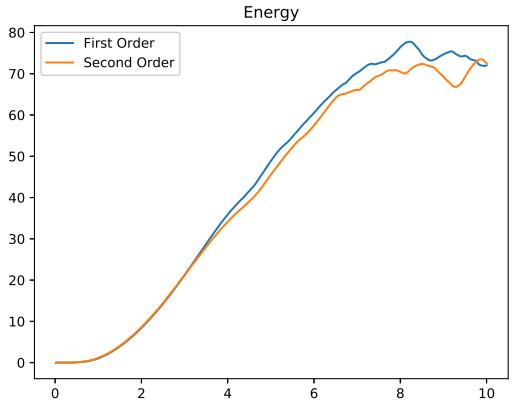

(e) Energy evolution

Figure 3.4: Stability and adaptability results for AC methods.

These are all depicted in Figure 3.4 below. Figure 3.4a shows that the second-order scheme consistently chooses larger time-steps than the first-order method. The evolution of ε, in Figure 3.4b, behaves similarly for both methods once the flow evolves. In testing AC methods pressure initialization often causes irregular, transient spiky behavior near $t = 0$ such as in Figures 3.4a, 3.4b, 3.4d.

The behavior of the pressure at the origin, $p(0, 0; t)$ vs. t, is depicted in Figure 3.4c. To our knowledge, there is no convergence theory for AC methods (or even fully coupled methods) which implies maximum norm convergence for the pressure over significant time intervals and for larger Reynolds numbers. Still, the irregular behavior observed in approximate solutions, while not conforming to a convergence theory, reflects vortex events across the whole domain and is interesting to compare. The profiles of the pressure at the origin are similar for both methods over $0 \leq t \leq 4$. For $t > 4$, $p(0, 0; t)$ for the second-order scheme is less oscillatory. This is surprising because the first-order scheme has more numerical dissipation. The divergence evolution of the schemes also differ in the initial transient of $||\nabla \cdot u(t)||$. After the initial transient, the divergence behavior is similar. It is also possible that the difference in $||\nabla \cdot u||$ transients is due to the strategy of ε-adaptation being sub-optimal. The model energy of both methods is largely comparable. We note that the model energy depends on the choices of ε made. Thus model energy is not expected to coincide exactly. Generally, Figures 3.4d–3.4e behave similarly for both algorithms.

3.3.9.2 TEST 2: CONVERGENCE AND ADAPTIVITY The second numerical test concerns the accuracy and adaptivity of the GA-method. Let $\Omega =]0, 1[^2$, with $\nu = 1$. Consider the exact solution (obtained from [46] and applied to the Navier-Stokes equations)

$$u = \pi \sin t(\sin 2\pi y \sin^2 \pi x, -\sin 2\pi x \sin^2 \pi y)$$

$$p = \cos t \cos \pi x \sin \pi y,$$

and consider a discretization of Ω obtained by 300 nodes on each edge of the square. We proceed by running five experiments, adapting both the first- and second-order schemes using the algorithms above, where the tolerance for the continuity and momentum equations is $10^{-(.25i+3)}$ for $i = 0, 1, 2, 3, 4$. To control the size of the timesteps, we require Δt_n to be chosen

such that $EST(1) \in (TOL_m/10, TOL_m)$. The solutions were obtained in parallel, utilizing the MUMPS direct solver [2]. To examine convergence, we present in Figure 3.5 log-log plots of the errors of the pressure and the velocity against the average timestep taken during the test. We also present semilog plots of the evolution of the pressure error and timestep during the final test below. The plots show that the timestep adaptation is working as expected and reducing the velocity error, Figure 3.5c. Our intuition is that the pressure error is linked to satisfaction of incompressibility; however, Figure 3.5d indicates convergence with respect to the timestep. In our calculations we did observe the following: If $\|\nabla \cdot u\|$ is, e.g., two orders of magnitude smaller then the tolerance, ε is rapidly increased to be even $\mathcal{O}(1)$. At this point the pressure error and violation of incompressibility spike upward and ε is then cut rapidly. This behavior suggests that a band of acceptable ε-values should be imposed in the adaptive algorithm.

To compare the GA-, Min-method and the scheme introduced in Section 3.2 and [13], we use the test problem given above in this section with a known exact solution. The results are given in Figure 3.6 below. Here, we use a mesh with the same density and final time $t^* = 1$. A timestep $\Delta t_n = 10^{-2}$ is kept constant in this run to highlight differences in the evolution of the variable ε_n, which has an initial value $\varepsilon_0 = 10^{-4}$. These tests are preliminary: In them, the min-Method seems preferable in error behavior but yields smaller values and thus less well-conditioned systems. In the evolution of all four quantities, the GA- and the CLM [13] method exhibit near identical behavior. The min-Method, however, forces ε to be an order of magnitude lower than the values obtained by the other two schemes. This, in turn, forces the divergence to be reduced. Furthermore, both the velocity and pressure errors for the min-Method are smaller than those of the GA- and CLM-methods.

3.3.10 CONCLUSIONS, OPEN PROBLEMS AND FUTURE PROSPECTS

There are many open problems and algorithmic improvements possible. The doubly adaptive algorithm selected smaller values of ε than Δt in our tests with the same tolerance for both. A further synthesis of the methods herein with the modular grad-div algorithm of [38] would eliminate any conditioning issues in the linear system arising. Developing doubly

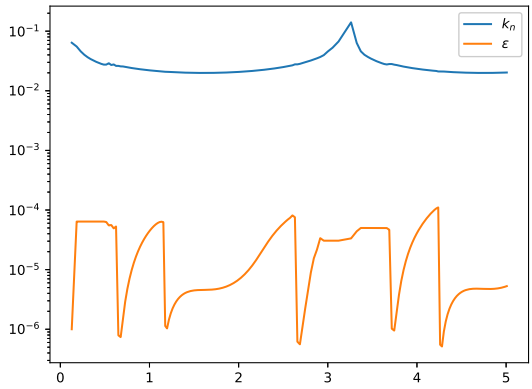

(a) Timestep and ε evolution

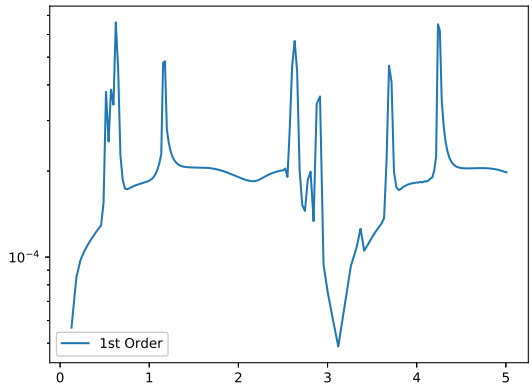

(b) Pressure error evolution

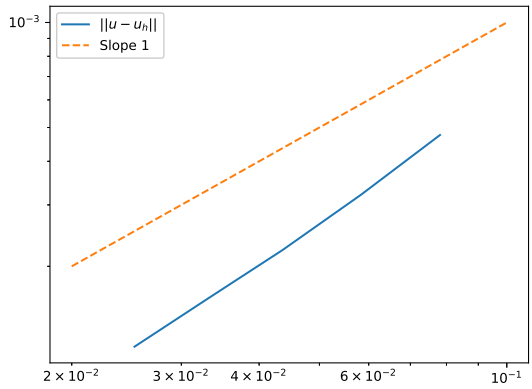

(c) Average timestep vs. velocity error

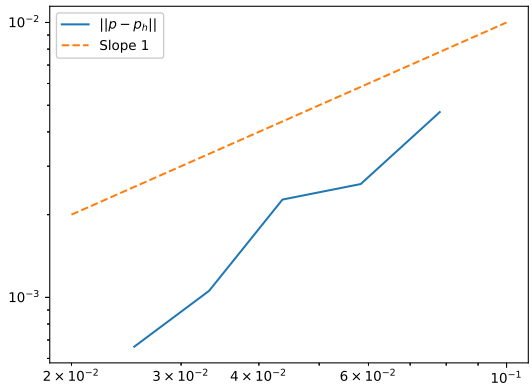

(d) Average timestep vs. pressure error

Figure 3.5: Accuracy and adaptability results for AC methods.

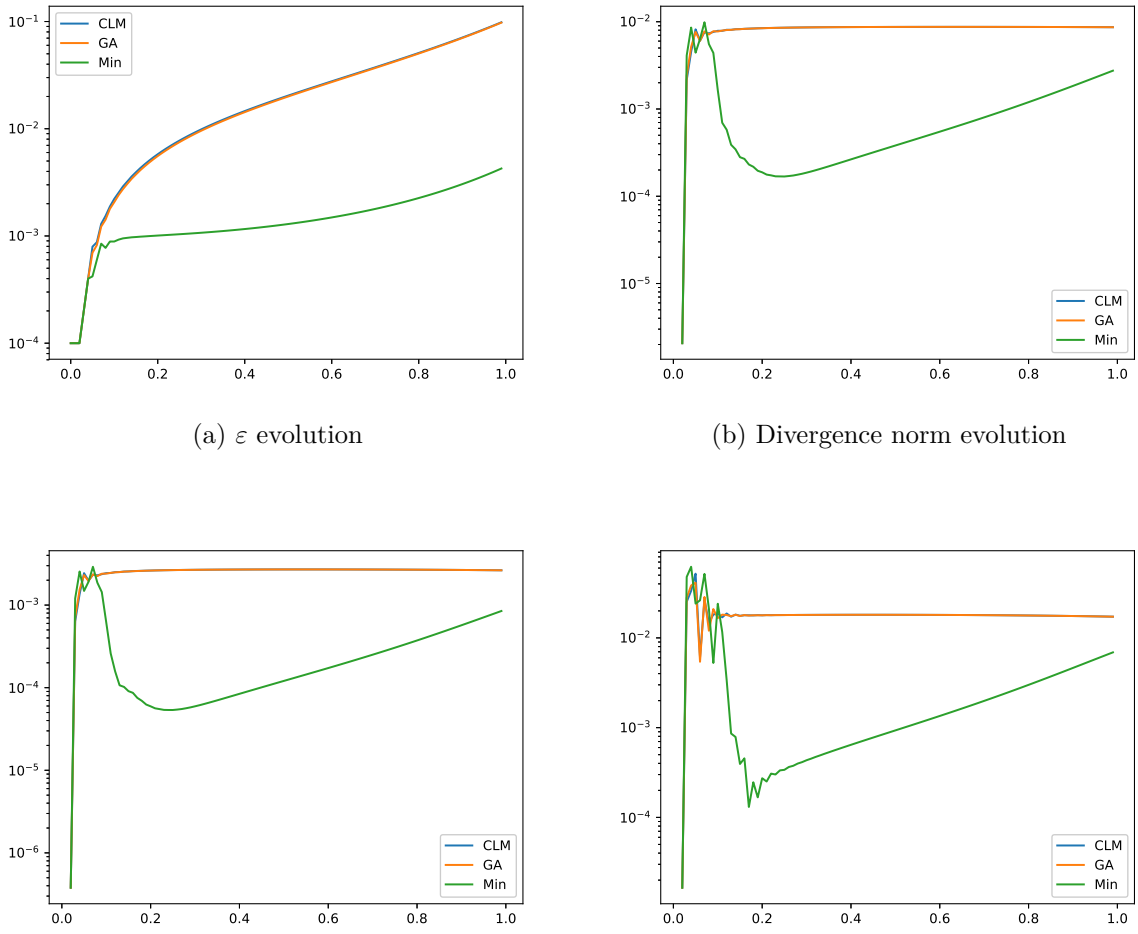

(a) ε evolution

(b) Divergence norm evolution

(c) Velocity error evolution

(d) Pressure error evolution

Figure 3.6: Comparison between GA, Min, and CLM methods.

adaptive methods of order greater than two (with modular grad-div) is an important step to greater time accuracy. We mention in particular the new embedded family of orders 2,3,4 of [27] as a natural extension. The method of Dahlquist, Liniger and Nevanlinna [20] is unexplored for PDEs, but has promise in CFD because it is A-stable for both increasing and decreasing time-steps. Improved error estimators for the second-order method herein would increase reliability. For AC methods, pressure initialization and damping of nonphysical acoustics are important problems where further progress would be useful.

Open problems. The idea of adapting independently Δt and ε is promising but new so there are many open problems. These include:

- Is the ε-adaptation formula $\varepsilon_{new} = \varepsilon_{old}(TOL/\|\nabla \cdot u\|)$ improvable? Perhaps the quotient should be to some fractional power. Perhaps adapting ε should be based of a relative error in $\|\nabla \cdot u\|$, such as $\|\nabla \cdot u\|/\|\nabla u\|$. Analysis of the local (in time) error in $\|\nabla \cdot u\|$ is needed to support an improvement.

- The ε-adaptation strategy seems to need preset limits, $\varepsilon_{\min}, \varepsilon_{\max}$, to enforce $\varepsilon_{\min} \leq \varepsilon \leq \varepsilon_{\max}$. The preset of $\varepsilon_{\min}$ is needed because $\nabla \cdot u = 0$ cannot be enforced pointwise in many finite element spaces. Finding a reasonable strategy for these presets is an open problem. Similarly, it would be useful to develop a coherent strategy for relating the two tolerances rather than simply picking them to be equal (as herein).

- Proving convergence to a weak solution of the incompressible NSE of solutions to the continuum analogue of the min-Method for variable ε is an important open problem. In this analysis it is generally assumed that $\varepsilon(t) \to 0$ in an arbitrary fashion. A more interesting problem is to link $\varepsilon(t)$ and $\|\nabla \cdot u\|$ in the analysis. Similarly, an *á priori* error analysis for variable ε is an open problem and may yield insights on how the variance of $\varepsilon(t)$ should be controlled within an adaptive algorithm. The consistency error of the two methods are $\mathcal{O}(\Delta t + \varepsilon)$ and $\mathcal{O}(\Delta t^2 + \varepsilon)$, respectively. Energy stability has been proven herein for the first order method and for the constant timestep, second order method. Thus, error estimation while technical, should be achievable.

- Comprehensive testing of the variable (first or second) order method is an open problem. VSVO methods are the most effective for systems of ODEs but have little penetration in

CFD. Testing the relative costs and accuracy of VSVO in CFD is an important problem.

3.4 CONCLUSIONS

The approximation of flow problems is made challenging by the coupling of the velocity and pressure variables. For decades, numerical methods have been developed to exploit the saddle-point structure of the NSE. The method of artificial compressibility, developed in the late 1960s, decouples velocity and pressure and suffers no condition number penalty at low-temporal orders. However, these methods as originally constructed are not amenable to time adaptivity. In this chapter, we considered a standard time adaptive AC method and showed its limitations. To overcome these limitations, we constructed a new, unconditionally stable time adaptive AC method and demonstrated its efficacy via numerical tests. Furthermore, we considered its continuum analogue, and showed, under conditions on the transient AC parameter $\varepsilon(t)$, its weak convergence to the NSE.

Next, we observed that the local truncation error of adaptive AC methods allows for the timestep and AC parameter to vary *independently*. Thus, we constructed two new time adaptive AC methods and showed their unconditional stability. To verify the properties of the methods, we compared them, as well as the scheme introduced in Section 3.2, in a suite of numerical tests. In particular, we demonstrated that the methods are stable and that the GA method is time-accurate.

4.0 ENSEMBLE METHODS FOR BOUSSINESQ FLOWS

In Chapter 1, we listed two main challenges that one faces when attempting to approximate flow problems. One challenge was velocity/pressure coupling, addressed in Chapter 3 via artificial compressibility methods and continued in this chapter. The other challenge was the nonlinear convective term, and how its treatment affects solution quality. This treatment becomes much more important when considering *ensemble* simulations, i.e., the running of multiple flow realizations (with different initial conditions, parameters, etc.) to approximate a mean flow. The focus of this chapter is to use a technique from [65] to ensure that all realizations have a *shared* coefficient matrix, reducing the amount of memory needed for each realization. This, coupled with static and adaptive AC methods, yields fast, memory efficient algorithms.

We present an introduction to ensemble schemes in Section 4.1, giving motivation and notation. In Section 4.2, we present artificial compressibility ensemble (ACE) schemes with constant and variable timesteps for use in naturally convected, or Boussinesq, flows. Section 4.2 contains stability analyses for constant and variable timestep ACE schemes, a fully discrete error analysis for the constant stepsize case, and numerical tests. Finally, conclusions are given in Section 4.3.

4.1 INTRODUCTION

Data in physical applications, initial conditions, forcing, parameters, etc. are never known exactly due to fundamental uncertainty in measurement devices. The growth of this uncertainty degrades solution quality, leading to a suboptimal predictability horizon. Ensemble calculations, i.e., the consideration of multiple physical realizations with varying data, extend predictability horizons [133]. The ensemble average is the most likely solution and its variance quantifies uncertainty in the solution. Typically, computing a solution ensemble involves either J sequential, fine mesh runs or J parallel, coarse mesh runs of a given

code (subject to perturbed data). In both situations, high storage costs and long runtimes are barriers to a more accurate ensemble average and an extended predictability horizon, i.e., simulations using more ensemble members. This leads to the fundamental question addressed herein: *Can we increase the number of ensemble members without decreasing mesh density (and vice versa) on a fully utilized computer system?*

Recent breakthroughs in ensemble timestepping algorithms [41, 40, 52, 51, 65, 61, 63, 64, 93, 122] reduce memory requirements and computational costs for ensemble simulations through the following procedure: Decomposition of parameters and/or convective velocity into ensemble mean and fluctuating components is followed by an implicit-explicit (IMEX) time discretization. The resulting linear systems share the same coefficient matrix, dramatically reducing storage costs and, when paired with an efficient iterative block solver, computation time. These works represent a significant advance in the reduction of memory requirements, extending the feasible ensemble size to a new upper limit.

For motivation, we look to the pioneering works of Lorenz. In [87, 88, 86], Lorenz discovered and relayed the fact that physical systems (in his case, atmospheric flow) with slightly perturbed initial conditions with evolve to a point that the solutions obtained appear to be randomly chosen states. Thus, when approximating physical phenomena with any uncertainties present, the approximate solutions have a *predictability horizon* of two weeks. It was then realized that, if meaningful results were to be extracted from numerical methods, inherent uncertainty would have to be addressed. Since initial conditions, parameters, and even physical data all carry uncertainties, the most robust and physically realistic approximations should be in some sense an *average* of realizations, not just a single simulation corresponding to one set of parameters.

Toth and Kalnay [133], among others, proved that this idea was feasible. Now, the idea of *ensemble averaging* forms the basis for numerical weather and climate prediction systems around the world. To wit, suppose that we have J realizations of a physical process, i.e., there exist v_j for $j \in \{1, \ldots, J\}$ satisfying, e.g., the Boussinesq equations (2.7)–(2.9) with different initial conditions, parameters, etc. As was argued, the examination of any single realization is unlikely to yield reliable results due to the predictability horizon. Hence, we proceed in the context of ensemble simulations. We define the *ensemble mean*, or ensemble

average, by

$$\langle v \rangle := \frac{1}{J} \sum_{j=1}^{J} v_j,$$

and the j^{th}-fluctuation about the mean as

$$v_j' := v_j - \langle v \rangle.$$

Below we list some elementary properties of the ensemble mean and fluctuations [61].

Lemma 7. *Let v and w be realizations of a physical process. Then,*

$$\langle v' \rangle = 0,$$
$$\langle (\langle v \rangle, w') \rangle = 0$$

and

$$\langle \langle v \rangle \rangle = \langle v \rangle,$$
$$\langle (\langle v \rangle, w) \rangle = (\langle v \rangle, \langle w \rangle).$$

Proof. The third equality is immediate since $\langle v \rangle$ is independent of j. The first equality comes from the definitions and the third equality, i.e.,

$$\begin{aligned} \langle v' \rangle &= \langle v - \langle v \rangle \rangle \\ &= \langle v \rangle - \langle v \rangle \\ &= 0. \end{aligned}$$

The fourth equality is also immediate by bilinearity of the inner product and the fact that $\langle v \rangle$ is independent of j. Thus, the second equality can be proven by the first equality:

$$\begin{aligned} \langle (\langle v \rangle, w') \rangle &= (\langle v \rangle, \langle w' \rangle) \\ &= 0. \end{aligned}$$

□

Let $\Omega \subset \mathbb{R}^d$ (d=2,3) be a convex polyhedral domain with boundary $\partial\Omega$. We partition the boundary as a union of closed sets with disjoint interior, i.e., $\partial\Omega = \overline{\Gamma_D} \cup \overline{\Gamma_N}$, a Dirichlet part Γ_D of positive measure and a Neumann part Γ_N. Suppose for ensemble members indexed by $j \in \{1, \ldots, J\}$, we have the initial conditions $u(x, 0; \omega_j) = u_j^0$ and $T(x, t; \omega_j) = T_j^0$, as well as f_j a body force and g_j a heat source. Let the velocity $u_j := u(x, t; \omega_j) : \Omega \times (0, t^*] \to \mathbb{R}^d$, pressure $p_j := p(x, t; \omega_j) : \Omega \times (0, t^*] \to \mathbb{R}$, and temperature $T_j := T(x, t; \omega_j) : \Omega \times (0, t^*] \to \mathbb{R}$ satisfy the Boussinesq equations

$$\partial_t u_j + (u_j \cdot \nabla) u_j + \frac{1}{2} (\nabla \cdot u_j) u_j - \mathrm{Pr}\Delta u_j + \nabla p_j = \mathrm{PrRa}\xi T_j + f_j \ \text{ in } \Omega, \tag{4.1}$$

$$\nabla \cdot u_j = 0 \ \text{ in } \Omega, \tag{4.2}$$

$$\partial_t T_j + (u_j \cdot \nabla T_j) + \frac{1}{2} (\nabla \cdot u_j) T_j - \Delta T_j = g_j \ \text{ in } \Omega, \tag{4.3}$$

$$u_j|_{\partial\Omega} = 0, \ T_j|_{\Gamma_D} = 0, \ (n \cdot \nabla T_j)|_{\Gamma_N} = 0. \tag{4.4}$$

Here, we let n be the outward normal on $\partial\Omega$, ξ the unit vector in the direction of gravity, Pr the Prandtl number, and Ra the Rayleigh number. We have also explicitly made the nonlinear term skew-symmetric. Note that the boundary conditions are selected for simplicity; the results presented below extend to inhomogeneous Dirichlet boundary conditions for the velocity and temperature using techniques introduced in [41]. Suppressing the spatial discretization for the moment, we discretize the system (4.1) – (4.4) using linearly-implicit backward Euler (*sans* the temperature term in the momentum equation), i.e.,

$$\frac{u_j^{n+1} - u_j^n}{\Delta t} + (u_j^n \cdot \nabla) u_j^{n+1} + \frac{1}{2} \left(\nabla \cdot u_j^n\right) u_j^{n+1} - \mathrm{Pr}\Delta u_j^{n+1} + \nabla p_j^{n+1} = \mathrm{PrRa}\xi T_j^n + f_j^{n+1},$$

$$\nabla \cdot u_j^{n+1} = 0,$$

$$\frac{T_j^{n+1} - T_j^n}{\Delta t} + (u_j^n \cdot \nabla) T_j^{n+1} + \frac{1}{2} \left(\nabla \cdot u_j^n\right) T_j^{n+1} - \Delta T_j^{n+1} = g_j^{n+1}.$$

Putting all of the data on the right-hand-side, using incompressibility, and factoring yields the linear solves for any j

$$\left[\frac{1}{\Delta t} I + (u_j^n \cdot \nabla) + \frac{1}{2} \left(\nabla \cdot u_j^n\right) - \mathrm{Pr}\Delta\right] u_j^{n+1} = \mathrm{PrRa}\xi T_j^n + f_j^{n+1},$$

$$\left[\frac{1}{\Delta t} I + (u_j^n \cdot \nabla) + \frac{1}{2} \left(\nabla \cdot u_j^n\right) - \Delta\right] T_j^{n+1} = g_j^{n+1}.$$

A cursory glance at the linear systems above shows that they are *dependent* on the realization j. Hence, for each realization, separate linear operators A_j and B_j must be stored to solve

$$A_j u_j^{n+1} = RHS_{u,j},$$
$$B_j T_j^{n+1} = RHS_{T,j}.$$

The need to store these matrices in memory for each realization taxes computational resources and thus reduces the number of realizations that can be considered (limiting the predictability horizon as well). However, note that, e.g.,

$$(u_j^n \cdot \nabla) u_j^{n+1} + \frac{1}{2}\left(\nabla \cdot u_j^n\right) u_j^{n+1} = (\langle u \rangle^n \cdot \nabla) u_j^{n+1} + \frac{1}{2}\left(\nabla \cdot \langle u \rangle^n\right) u_j^{n+1} + (u_j'^n \cdot \nabla) u_j^{n+1} + \frac{1}{2}\left(\nabla \cdot u_j'^n\right) u_j^{n+1}.$$

Here, we have rewritten the lagged component in the nonlinear into a sum of ensemble means and fluctuations. Notice that the dependence on the realization in the lagged terms is only present in the third and fourth terms on the right-hand-side. Lagging these terms fully, we arrive at the scheme

$$\left[\frac{1}{\Delta t} I + (\langle u \rangle^n \cdot \nabla) + \frac{1}{2}\left(\nabla \cdot \langle u \rangle^n\right) - \mathrm{Pr}\Delta\right] u_j^{n+1} = \left[(u_j'^n \cdot \nabla) + \frac{1}{2}\left(\nabla \cdot u_j'^n\right)\right] u_j^n + \mathrm{PrRa}\xi T_j^n + f_j^{n+1},$$
$$\left[\frac{1}{\Delta t} I + (\langle u \rangle^n \cdot \nabla) + \frac{1}{2}\left(\nabla \cdot \langle u \rangle^n\right) - \Delta\right] T_j^{n+1} = \left[(u_j'^n \cdot \nabla) + \frac{1}{2}\left(\nabla \cdot u_j'^n\right)\right] T_j^n + g_j^{n+1}.$$

The matrices on the left-hand-sides are now *independent* of the realization, i.e., the realizations share the same coefficient matrix. This means that only two matrices, instead of $2J$, will have to be loaded and stored in memory, releasing valuable computational resources. Furthermore, the linear systems can be viewed as block systems

$$A[u_1^{n+1} | u_2^{n+1} | \ldots | u_J^{n+1}] = [RHS_{u,1} | RHS_{u,2} | \ldots | RHS_{u,J}],$$
$$B[T_1^{n+1} | T_2^{n+1} | \ldots | T_J^{n+1}] = [RHS_{T,1} | RHS_{T,2} | \ldots | RHS_{T,J}],$$

allowing the use of efficient block iterative solvers such as block LU factorizations [28], block GMRES [59], and block BiCGSTAB [35], among others.

4.2 AC SCHEMES FOR BOUSSINESQ FLOWS

4.2.1 AN AC ENSEMBLE SCHEME FOR CONSTANT TIMESTEPS

The final algorithm presented in Section 4.1 successfully treats the nonlinearity and reduces the amount of memory required for each realization. Herein, we combine this tactic with those delineated in Chapter 3 to increase efficiency and reduce storage requirements and computation time: decoupling velocity, pressure, and temperature solves by artificial compressibility and keeping the coefficient matrix, at each timestep, shared by each ensemble member. Furthermore, we extend our results for variable timesteps. A CFL-type condition is introduced, which causes breakdown near and into turbulent flow regimes. Consequently, the focus of this chapter is on laminar flow. Section 4.2.7 presents numerical tests reinforcing this extension. Let $\langle u\rangle^n := \frac{1}{J}\sum_{j=1}^{J} u(x,t^n;\omega_j)$ and $u_j'^n = u_j^n - \langle u\rangle^n$ be the ensemble average and the j^{th} fluctuation about the mean, respectively. Suppressing the spatial discretization for the moment, we apply an IMEX time discretization to the system (4.1) – (4.4) such that the resulting coefficient matrix is *independent* of the ensemble members. Moreover, we relax mass conservation by adding a discretized version of the artificial compressibility term εp_t. This leads to the artificial compressibility ensemble (ACE) timestepping method:

$$\frac{u_j^{n+1}-u_j^n}{\Delta t} + (\langle u\rangle^n\cdot\nabla)u_j^{n+1} + \frac{1}{2}\left(\nabla\cdot\langle u\rangle^n\right)u_j^{n+1} \tag{4.5}$$
$$+(u_j'^n\cdot\nabla)u_j^n + \frac{1}{2}\left(\nabla\cdot u_j'^n\right)u_j^n - \mathrm{Pr}\Delta u_j^{n+1} + \nabla p_j^{n+1} = \mathrm{PrRa}\xi T_j^n + f_j^{n+1},$$
$$\varepsilon\frac{p_j^{n+1}-p_j^n}{\Delta t} + \nabla\cdot u_j^{n+1} = 0, \tag{4.6}$$
$$\frac{T_j^{n+1}-T_j^n}{\Delta t} + (\langle u\rangle^n\cdot\nabla)T_j^{n+1} + \frac{1}{2}\left(\nabla\cdot\langle u\rangle^n\right)T_j^{n+1} \tag{4.7}$$
$$+(u_j'^n\cdot\nabla)T_j^n + \frac{1}{2}\left(\nabla\cdot u_j'^n\right)T_j^n - \Delta T_j^{n+1} = g_j^{n+1}.$$

The treatment of the nonlinear terms, $(u\cdot\nabla)u + \frac{1}{2}(\nabla\cdot u)\,u$ and $(u\cdot\nabla)T + \frac{1}{2}(\nabla\cdot u)\,T$, leads to a *shared* coefficient matrix, in the above, independent of the ensemble members. The nonlinear term is the *source* of ensemble dependence in the coefficient matrix. In particular,

using (4.6) in (4.5) and rearranging, the following system must be solved:

$$\left(\frac{1}{\Delta t}I + (\langle u\rangle^n \cdot \nabla) + \frac{1}{2}(\nabla \cdot \langle u\rangle^n) I - \mathrm{Pr}\Delta - \frac{\Delta t}{\varepsilon}\nabla\nabla\cdot\right)u_j^{n+1} = RHS_{u,j},$$
$$p_j^{n+1} = \frac{\Delta t}{\varepsilon}\nabla \cdot u_j^{n+1} + p_j^n,$$
$$\left(\frac{1}{\Delta t}I + (\langle u\rangle^n \cdot \nabla) + \frac{1}{2}(\nabla \cdot \langle u\rangle^n) I - \Delta\right)T_j^{n+1} = RHS_{T,j}.$$

It is clear that the velocity, pressure, and temperature solves are fully decoupled. The use of AC changes the saddle-point system with a convection-diffusion problem with grad-div stabilization followed by algebraic pressure update at each timestep, replacing a much larger coupled solve. This decoupling allows the pressure and velocity to be advanced explicitly (and cheaply; our tests indicate a speedup of *3–8* times when compared to a coupled system), and, while not explored herein, allows for the use of non inf-sup stable finite elements. After a finite element spatial discretization, the matrix associated with the nonlinear terms is independent of the ensemble member due to using the ensemble average as the convective velocity.

In Section 4.2.3, we present a fully discrete algorithm based on (4.5) - (4.7) in the context of the finite element method. Stability (Theorem 11) and error analysis (Theorem 12) of the algorithm follow in Section 4.2.4 by using a CFL-type condition. Numerical experiments follow in Section 4.2.7 illustrating first-order convergence, speed advantages, and usefulness of ensembles in the context of naturally convected fluid flow problems. We then present a stability result for the time adaptive ACE scheme.

4.2.2 RELATED WORK

Operator splitting [44, 90, 58], artificial compressibility [16, 25, 48, 103, 110, 112, 127], and projection methods [46, 101], among others, exploit the saddle point structure to decouple the solves for velocity and pressure. Recently, [62] introduced a pressure-correction (a subclass of projection methods) ensemble algorithm for the Boussinesq equations. This approach transforms a coupled Navier-Stokes solve into one velocity solve and a Poisson solve for the pressure, which requires boundary conditions for the pressure. Artificial compressibility decouples the velocity and pressure solves in a similar manner, but requires no

boundary conditions for the pressure and allows for the explicit calculation of the pressure at each timestep. Artificial compressibility methods decrease storage and complexity while increasing speed of computation, can be used to construct schemes of arbitrary temporal order [48], and can even be adapted in time [13, 78, 47].

Artificial (or pseudo-) compressibility methods have been used in a similar manner for the Boussinesq system throughout the literature. The Klemp–Wilhemson time-splitting scheme is used to approximate the compressible Boussinesq equations, where the continuity equation reads $D_t p + c^2 \nabla \cdot u = 0$ for c a wave speed and where $D_t p$ is the material derivative of the pressure [73, 113]. By letting $\varepsilon = \frac{1}{c^2}$, we arrive at $\varepsilon D_t p + \nabla \cdot u = 0$, a pseudo-compressible model explored in [95].

4.2.3 A FULLY DISCRETE ACE SCHEME

For $j \in \{1, \ldots, J\}$, taking inner products and using the definition of the trilinear forms from Chapter 2 yields the corresponding weak form of (4.1) - (4.4):

$$(\partial_t u_j, v) + b_u(u_j, u_j, v) + \mathrm{Pr}(\nabla u_j, \nabla v) - (p_j, \nabla \cdot v) = \mathrm{PrRa}(\xi T_j, v) + (f_j, v) \ \ \forall v \in X,$$
$$(\nabla \cdot u_j, q) = 0 \ \ \forall q \in Q,$$
$$(\partial_t T_j, S) + b_T(u_j, T_j, S) + (\nabla T_j, \nabla S) = (g_j, S) \ \ \forall S \in W_{\Gamma_D}.$$

Denote the J fully discrete solutions by $u^n_{j,h}$, $p^n_{j,h}$, and $T^n_{j,h}$ at time levels $t^n = n\Delta t$, $n \in \{0, 1, \ldots, N\}$, and $t^* = N\Delta t$. For every $n = 0, 1, ..., N-1$, the fully discrete approximation of (4.1) - (4.4) is:

Algorithm 5 (Artificial Compressibility Ensemble Method)**.** *Given $u^n_{j,h} \in X_h$, $p^n_{j,h} \in Q_h$, and $T^n_{j,h} \in W_h$, perform the following steps:*
Step 1: Find $(u^{n+1}_{j,h}, T^{n+1}_{j,h}) \in (X_h, W_h)$ satisfying

$$\frac{1}{\Delta t}(u^{n+1}_{j,h} - u^n_{j,h}, v_h) + b_u(\langle u_h \rangle^n, u^{n+1}_{j,h}, v_h) + b_u(u'^n_{j,h}, u^n_{j,h}, v_h) + Pr(\nabla u^{n+1}_{j,h}, \nabla v_h) \tag{4.8}$$
$$+ \frac{\Delta t}{\varepsilon}(\nabla \cdot u^{n+1}_{j,h}, \nabla \cdot v_h) - (p^n_{j,h}, \nabla \cdot v_h) = PrRa(\xi T^n_{j,h}, v_h) + (f^{n+1}_j, v_h) \ \ \forall v_h \in X_h,$$

$$\frac{1}{\Delta t}(T_{j,h}^{n+1} - T_{j,h}^{n}, S_h) + b_T(\langle u_h \rangle^n, T_{j,h}^{n+1}, S_h) + b_T(u_{j,h}'^n, T_{j,h}^{n}, S_h) \tag{4.9}$$
$$+(\nabla T_{j,h}^{n+1}, \nabla S_h) = (g_j^{n+1}, S_h) \ \ \forall S_h \in W_{\Gamma_1,h}.$$

Step 2: Given $p_{j,h}^n \in Q_h$, find $p_{j,h}^{n+1} \in Q_h$ satisfying

$$p_{j,h}^{n+1} = p_{j,h}^{n} - \frac{\Delta t}{\varepsilon} \nabla \cdot u_{j,h}^{n+1}. \tag{4.10}$$

Remark 12. *This is a consistent first-order approximation provided $\varepsilon = \mathcal{O}(\Delta t^{l+1})$ for $l \geq 0$. However, the condition number of the resulting system grows without bound as $\Delta t \to 0$ when $l \geq 1$.*

4.2.4 NUMERICAL ANALYSIS OF THE ENSEMBLE ALGORITHM

In this section, stability and error results are presented given the timestep condition

$$\frac{C_\dagger \Delta t}{h} \max_{1 \leq j \leq J} \|\nabla u_{j,h}'^n\|^2 \leq 1, \tag{4.11}$$

is satisfied. Here, $C_\dagger \equiv C_\dagger(\Omega, \alpha_{min}, \mathrm{Pr})$.

Remark 13. *For laminar flow, the CFL-type condition (4.11) is less onerous than conditions appearing in typical explicit methods, e.g., conditions containing a $\|\nabla u_{j,h}^n\|$ term, as $\|\nabla u_{j,h}'^n\| \leq \|\nabla u_{j,h}^n\|$.*

For the artificial compressibility parameter, we prescribe the following $\mathcal{O}(\Delta t)$ relationship, for clarity:

$$\varepsilon = \gamma^{-1} \Delta t, \tag{4.12}$$

where $\gamma > 0$ is an arbitrary parameter. Consequently, we have $\frac{\Delta t}{\varepsilon}(\nabla \cdot u_h^{n+1}, \nabla \cdot v_h) = \gamma(\nabla \cdot u_h^{n+1}, \nabla \cdot v_h)$ in equation (4.8). Evidently, the ACE algorithm introduces grad-div stabilization, which is known to have a positive impact on solution quality. Proper selection of the grad-div parameter γ can vary wildly; see e.g. [60] and references therein. Further, modest to large values of γ are known to dramatically slow down iterative solvers. Consequently, appropriate choice of ε will vary with application and should be chosen with care.

The remainder of Section 4.2.4 is as follows. Under condition (4.11), ACE (4.8) - (4.9) is proven to be convergent with first-order accuracy in Theorem 12. Nonlinear, energy stability of the velocity, temperature, and pressure approximations are proven in Theorem 11.

4.2.5 STABILITY ANALYSIS

Theorem 11. *Let $f_j \in L^2(0,t^*;H^{-1}(\Omega)^d)$, $g_j \in L^2(0,t^*;H^{-1}(\Omega))$ with appropriate initial conditions for the velocity, pressure, and temperature. If the scheme (4.8) - (4.9) satisfies condition (4.11), then*

$$\|u_{j,h}^N\|^2 + \|T_{j,h}^N\|^2 + \varepsilon\|p_{j,h}^N\|^2 + \frac{1}{2}\sum_{n=0}^{N-1}\left(\|u_{j,h}^{n+1}-u_{j,h}^n\|^2 + \|T_{j,h}^{n+1}-T_{j,h}^n\|^2 + \varepsilon\|p_{j,h}^{n+1}-p_{j,h}^n\|^2\right)$$
$$+\frac{Pr}{2}|||\nabla u_{j,h}|||_{2,0}^2 + \frac{1}{2}|||\nabla T_{j,h}|||_{2,0}^2 \le \|u_{j,h}^0\|^2 + \|T_{j,h}^0\|^2 + \varepsilon\|p_{j,h}^0\|^2$$
$$+\frac{2}{Pr}|||f_j|||_{2,-1}^2 + 2PrRa^2C_{pf,1}C_T.$$

Proof. We begin by finding bounds for the temperature equation. Taking $S_h = 2\Delta t T_{j,h}^{n+1}$ in (4.9) gives, by skew-symmetry and the polarization identity,

$$\|T_{j,h}^{n+1}\|^2 - \|T_{j,h}^n\|^2 + \|T_{j,h}^{n+1}-T_{j,h}^n\|^2 + 2\Delta t\|\nabla T_{j,h}^{n+1}\|^2$$
$$= 2\Delta t(g_j^{n+1}, T_{j,h}^{n+1}) - 2\Delta t b_T(u_{j,h}'^n, T_{j,h}^n, T_{j,h}^{n+1}).$$

By definition of the dual norm and Young's inequality,

$$2\Delta t(g_j^{n+1}, T_{j,h}^{n+1}) \le \Delta t\|g_j^{n+1}\|_{-1}^2 + \Delta t\|\nabla T_{j,h}^{n+1}\|^2.$$

The bound for the nonlinear term is obtained via skew-symmetry, Lemma 1, the inverse inequality, and the Cauchy-Schwarz-Young inequality:

$$\begin{aligned}
-2\Delta t b_T(u_{j,h}'^n, T_{j,h}^n, T_{j,h}^{n+1}) &= -2\Delta t b_T(u_{j,h}'^n, T_{j,h}^{n+1}, T_{j,h}^{n+1} - T_{j,h}^n) \\
&\le 2\Delta t C_{3,T}\|\nabla u_{j,h}'^n\|\|\nabla T_{j,h}^{n+1}\|\sqrt{\|T_{j,h}^{n+1}-T_{j,h}^n\|\|\nabla(T_{j,h}^{n+1}-T_{j,h}^n)\|} \\
&\le \frac{2\Delta t C_{3,T}\sqrt{C_{\text{inv},2}}}{\sqrt{h}}\|\nabla u_{j,h}'^n\|\|\nabla T_{j,h}^{n+1}\|\|T_{j,h}^{n+1}-T_{j,h}^n\| \\
&\le \frac{2\Delta t^2 C_{3,T}^2 C_{\text{inv},2}}{h}\|\nabla u_{j,h}'^n\|^2\|\nabla T_{j,h}^{n+1}\|^2 + \frac{1}{2}\|T_{j,h}^{n+1}-T_{j,h}^n\|^2.
\end{aligned}$$

Thus,

$$\|T_{j,h}^{n+1}\|^2 - \|T_{j,h}^n\|^2 + \frac{1}{2}\|T_{j,h}^{n+1}-T_{j,h}^n\|^2 \tag{4.13}$$
$$+\Delta t\left(1 - \frac{2\Delta t C_{3,T}^2 C_{\text{inv},2}}{h}\|\nabla u_{j,h}'^n\|^2\right)\|\nabla T_{j,h}^{n+1}\|^2 \le \Delta t\|g_j^{n+1}\|_{-1}^2. \tag{4.14}$$

A telescoping sum, (4.14) implies, after summing from $n = 0$ to $m \leq N-1$, a bound for the temperature of the form $\|T_{j,h}^m\|^2 \leq C_T$ for all $m \in \{1, \ldots, N\}$ provided condition (4.11) is satisfied.

We continue with bounds for the momentum and continuity equations. We will need the following variational form of equation (4.10),

$$\varepsilon(\frac{p_{j,h}^{n+1} - p_{j,h}^n}{\Delta t}, q_h) + (\nabla \cdot u_{j,h}^{n+1}, q_h) = 0 \ \ \forall q_h \in Q_h. \tag{4.15}$$

Use equation (4.10) in equation (4.8) and add equations (4.8) and (4.15). Let $(v_h, q_h) = (2\Delta t u_{j,h}^{n+1}, 2\Delta t p_{j,h}^{n+1}) \in (V_h, Q_h)$ and use the polarization identity. Rearranging and skew-symmetry yields

$$\begin{aligned}\left(\|u_{j,h}^{n+1}\|^2 + \varepsilon\|p_{j,h}^{n+1}\|^2\right) - \left(\|u_{j,h}^{n}\|^2 + \varepsilon\|p_{j,h}^{n}\|^2\right) + \|u_{j,h}^{n+1} - u_{j,h}^{n}\|^2 + \varepsilon\|p_{j,h}^{n+1} - p_{j,h}^{n}\|^2 \qquad (4.16)\\ +2\Delta t \mathrm{Pr}\|\nabla u_{j,h}^{n+1}\|^2 = 2\Delta t \mathrm{PrRa}(\xi T_{j,h}^n, u_{j,h}^{n+1}) + 2\Delta t(f_j^{n+1}, u_{j,h}^{n+1}) - 2\Delta t b_u(u_{j,h}'^n, u_{j,h}^n, u_{j,h}^{n+1})\end{aligned}$$

By the Poincaré-Friedrichs inequality, the Cauchy-Schwarz-Young inequality, and the temperature bound (4.14), we have

$$2\Delta t \mathrm{PrRa}(\xi T_{j,h}^n, u_{j,h}^{n+1}) \leq 2\Delta t \mathrm{PrRa}^2 C_{\mathrm{pf},1}^2 C_T + \frac{\Delta t \mathrm{Pr}}{2}\|\nabla u_{j,h}^{n+1}\|^2.$$

The forcing and nonlinear terms are treated in a similar manner to the temperature case, giving the bounds

$$\begin{aligned}2\Delta t(f_j^{n+1}, u_{j,h}^{n+1}) &\leq \frac{2\Delta t}{\mathrm{Pr}}\|f_{j,h}^{n+1}\|_{-1}^2 + \frac{\Delta t \mathrm{Pr}}{2}\|\nabla u_{j,h}^{n+1}\|^2,\\ -2\Delta t b_u(u_{j,h}'^n, u_{j,h}^n, u_{j,h}^{n+1}) &\leq \frac{2\Delta t^2 C_{3,u}^2 C_{\mathrm{inv},1}}{h}\|\nabla u_{j,h}'^n\|^2\|\nabla u_{j,h}^{n+1}\|^2 + \frac{1}{2}\|u_{j,h}^{n+1} - u_{j,h}^n\|^2.\end{aligned}$$

Adding (4.14) to (4.16) and using the bounds, we arrive at

$$\begin{aligned}\left(\|u_{j,h}^{n+1}\|^2 + \|T_{j,h}^{n+1}\|^2 + \varepsilon\|p_{j,h}^{n+1}\|^2\right) - \left(\|u_{j,h}^{n}\|^2 + \|T_{j,h}^{n}\|^2 + \varepsilon\|p_{j,h}^{n}\|^2\right) + \frac{1}{2}\|u_{j,h}^{n+1} - u_{j,h}^{n}\|^2\\ +\frac{1}{2}\|T_{j,h}^{n+1} - T_{j,h}^{n}\|^2 + \frac{\varepsilon}{2}\|p_{j,h}^{n+1} - p_{j,h}^{n}\|^2 + \frac{1}{2}\|T_{j,h}^{n+1} - T_{j,h}^{n}\|^2\\ +\Delta t\left(\mathrm{Pr} - \frac{2\Delta t C_{3,u}^2 C_{\mathrm{inv},1}}{h}\|\nabla u_{j,h}'^n\|^2\right)\|\nabla u_{j,h}^{n+1}\|^2\\ +\Delta t\left(1 - \frac{2\Delta t C_{3,T}^2 C_{\mathrm{inv},2}}{h}\|\nabla u_{j,h}'^n\|^2\right)\|\nabla T_{j,h}^{n+1}\|^2 \leq \frac{2\Delta t}{\mathrm{Pr}}\|f_j^{n+1}\|_{-1}^2 + 2\Delta t \mathrm{PrRa}^2 C_{\mathrm{pf},1} C_T.\end{aligned}$$

Set now $C_\dagger = \min\{\frac{4C_{3,u}^2 C_{\text{inv},1}}{\text{Pr}}, 4C_{3,T}^2 C_{\text{inv},2}\}$. Then, condition (4.11) is satisfied. Summing from $n = 0$ to $N-1$ gives the bound

$$\|u_{j,h}^N\|^2 + \|T_{j,h}^N\|^2 + \varepsilon\|p_{j,h}^N\|^2 + \frac{1}{2}\sum_{n=0}^{N-1}\Big(\|u_{j,h}^{n+1} - u_{j,h}^n\|^2 + \|T_{j,h}^{n+1} - T_{j,h}^n\|^2 + \varepsilon\|p_{j,h}^{n+1} - p_{j,h}^n\|^2\Big)$$
$$+\frac{\text{Pr}}{2}|||\nabla u_{j,h}|||_{2,0}^2 + \frac{1}{2}|||\nabla T_{j,h}|||_{2,0}^2 \le \|u_{j,h}^0\|^2 + \|T_{j,h}^0\|^2 + \varepsilon\|p_{j,h}^0\|^2$$
$$+\frac{2}{\text{Pr}}|||f_j|||_{2,-1}^2 + 2\text{PrRa}^2 C_{\text{pf},1} C_T,$$

proving nonlinear stability. □

4.2.6 ERROR ANALYSIS

Denote u_j^n, p_j^n, and T_j^n as the true solutions at time $t^n = n\Delta t$. Assume the solutions satisfy the following regularity assumptions:

$$\begin{aligned} &u_j \in L^\infty([0,t^*]; X \cap H^{k+1}(\Omega)),\ T_j \in L^\infty([0,t^*]; W \cap H^{k+1}(\Omega)),\\ &\partial_t u_j, \partial_t T_j \in L^2([0,t^*]; H^{k+1}(\Omega)),\ \partial_{tt} u_j, \partial_{tt} T_j \in L^2([0,t^*]; H^{k+1}(\Omega)),\\ &p_j \in L^2([0,t^*]; Q \cap H^m(\Omega)),\ \partial_t p_j \in L^\infty([0,t^*]; Q(\Omega)). \end{aligned} \tag{4.17}$$

The errors for the solution variables are denoted

$$\begin{aligned} e_{u,j}^n &= (u_j^n - U_j^n) - (u_{j,h}^n - U_j^n) = \eta_j^n - \varphi_{j,h}^n,\\ e_{T,j}^n &= (T_j^n - I_h T_j^n) - (T_{j,h}^n - I_h T_j^n) = \zeta_j^n - \psi_{j,h}^n,\\ e_{p,j}^n &= (p_j^n - P_j^n) - (p_{j,h}^n - P_j^n) = \lambda_j^n - \pi_{j,h}^n. \end{aligned}$$

Definition 2. *(Consistency error). The consistency errors are denoted*

$$\begin{aligned} \varsigma_u(u_j^n; v_h) &= \Big(\frac{u_j^n - u_j^{n-1}}{\Delta t} - \partial_t u_j^n, v_h\Big) - b_u(u_j^n - u^{n-1}, u_j^n, v_h) + PrRa(\xi(T_j^n - T_j^{n-1}), v_h),\\ \varsigma_p(p_j^n; q_h) &= \varepsilon\Big(\frac{1}{\Delta t}\int_{t^{n-1}}^{t^n} \partial_t p_j(s) ds, q_h\Big),\\ \varsigma_T(T_j^n; S_h) &= \Big(\frac{T_j^n - T_j^{n-1}}{\Delta t} - \partial_t T_j^n, S_h\Big) - b_T(u_j^n - u_j^{n-1}, T_j^n, S_h). \end{aligned}$$

Lemma 8. *Provided u_j and T_j satisfy the regularity assumptions 4.17, then there exists a $C > 0$ such that for all $\varepsilon,\ r > 0$*

$$
\begin{aligned}
|\varsigma_u(u_j^n; v_h)| &\leq \frac{CC_{pf,1}^2 C_r \Delta t}{\delta} \|\partial_{tt} u_j\|^2_{L^2(t^{n-1},t^n;L^2(\Omega))} + \frac{C_1^2 C_r \Delta t}{\delta} \|\nabla u_j^n\|^2 \|\nabla\left(\partial_t u_j\right)\|^2_{L^2(t^{n-1},t^n;L^2(\Omega))} \\
&\quad + \frac{C_{pf,1}^2 C_r \Delta t}{\delta} \|\partial_t T_j\|^2_{L^2(t^{n-1},t^n;L^2(\Omega))} + \frac{\delta}{r}\|\nabla v_h\|^2, \\
|\varsigma_T(T_j^n; S_h)| &\leq \frac{CC_{pf,2}^2 C_r \Delta t}{\delta} \|\partial_{tt} T_j\|^2_{L^2(t^{n-1},t^n;L^2(\Omega))} + \frac{C_3^2 C_r \Delta t}{\delta} \|\nabla T_j^n\|^2 \|\nabla\left(\partial_t u_j\right)\|^2_{L^2(t^{n-1},t^n;L^2(\Omega))} \\
&\quad + \frac{\delta}{r}\|\nabla S_h\|^2.
\end{aligned}
$$

Proof. These follow from the Cauchy-Schwarz-Young inequality, Poincaré-Friedrichs inequality, and Taylor's Theorem with integral remainder. □

Theorem 12. *For (u_j, p_j, T_j) satisfying the Boussinesq equations (4.1)–(4.4), suppose that $(u_{j,h}^0, p_{j,h}^0, T_{j,h}^0) \in (X_h, Q_h, W_h)$ are approximations of (u_j^0, p_j^0, T_j^0). Further, suppose that condition (4.11) holds. Then there exists a constant $C > 0$ such that*

$$
\begin{aligned}
&\frac{1}{2}\|e_{T,j}^N\|^2 + \|e_{u,j}^N\|^2 + \varepsilon\|e_{p,j}^N\|^2 + \frac{1}{2}\sum_{n=0}^{N-1}\left\{\|e_{T,j}^{n+1} - e_{T,j}^n\|^2 + \|e_{u,j}^{n+1} - e_{u,j}^n\|^2 + \varepsilon\|e_{p,j}^{n+1} - e_{p,j}^n\|^2\right\} \\
&\qquad + \frac{Pr\Delta t}{4}\|\nabla e_{u,j}^N\|^2 + \frac{1}{4}|||\nabla e_{T,j}|||^2_{2,0} + \frac{Pr}{2}|||\nabla e_{u,j}|||^2_{2,0} \\
&\leq C\exp(C_\star t^*) \inf_{\substack{v_h \in X_h \\ q_h \in Q_h \\ S_h \in \hat{W}_h}} \Big\{\|\partial_t(T_j - S_h)\|^2_{L^2(0,t^*;L^2(\Omega))} + \|\partial_t(u_j - v_h)\|^2_{L^2(0,t^*;L^2(\Omega))} \\
&\qquad + \Delta t^2\|\partial_t(p_j - q_h)\|^2_{L^2(0,t^*;L^2(\Omega))} + h\Delta t\|\nabla(\partial_t(T_j - S_h))\|^2_{L^2(0,t^*;L^2(\Omega))} \\
&\qquad + h\Delta t\|\nabla(\partial_t(u_j - v_h))\|^2_{L^2(0,t^*;L^2(\Omega))} + |||T_j - S_h|||^2_{2,0} \\
&\qquad + |||\nabla(T_j - S_h)|||^2_{2,0} + |||T_j - S_h|||_{2,0}|||\nabla(T_j - S_h)|||_{2,0} + |||u_j - v_h|||_{2,0}|||\nabla(u_j - v_h)|||_{2,0} \\
&\qquad + \Delta t^2 + h\Delta t + 2\|e_{T,j}^0\|^2 + \|e_{u,j}^0\|^2 + \varepsilon\|e_{p,j}^0\|^2 + \frac{Pr\Delta t}{4}\|\nabla e_{u,j}^0\|^2\Big\}
\end{aligned}
$$

Proof. The true solutions to (4.1)–(4.4) satisfy for all $n \in \{0, \ldots, N-1\}$:

$$(\frac{u_j^{n+1} - u_j^n}{\Delta t}, v_h) + b_u(u_j^n, u_j^{n+1}, v_h) + \Pr(\nabla u_j^{n+1}, \nabla v_h) - (p_j^{n+1}, \nabla \cdot v_h) \tag{4.18}$$
$$= \mathrm{PrRa}(\xi T_j^n, v_h) + (f_j^{n+1}, v_h) + \varsigma_u(u_j^{n+1}; v_h) \ \ \forall v_h \in X_h,$$
$$\varepsilon(\frac{p_j^{n+1} - p_j^n}{\Delta t}) + (\nabla \cdot u_j^{n+1}, q_h) = \varsigma_p(p_j^{n+1}; q_h) \ \ \forall q_h \in Q_h, \tag{4.19}$$
$$(\frac{T_j^{n+1} - T_j^n}{\Delta t}, S_h) + b_T(u_j^n, T_j^{n+1}, S_h) + (\nabla T_j^{n+1}, \nabla S_h) \tag{4.20}$$
$$= (g_j^{n+1}, S_h) + \varsigma_T(T_j^{n+1}; S_h) \ \ \forall S_h \in W_{\Gamma_D,h}.$$

Subtract (4.9) from (4.20), then the error equation for temperature is

$$(\frac{e_{T,j}^{n+1} - e_{T,j}^n}{\Delta t}, S_h) + b_T(u_j^n, T_j^{n+1}, S_h) - b_T(\langle u_h \rangle^n, T_{j,h}^{n+1}, S_h) - b_T(u_{j,h}'^n, T_{j,h}^n, S_h) \tag{4.21}$$
$$+(\nabla e_{T,j}^{n+1}, \nabla S_h) = \varsigma_T(\theta_j^{n+1}, S_h) \ \ \forall S_h \in W_{\Gamma_D,h}.$$

Decomposing the error terms and rearranging gives,

$$(\frac{\psi_{j,h}^{n+1} - \psi_{j,h}^n}{\Delta t}, S_h) + (\nabla \psi_{j,h}^{n+1}, \nabla S_h) = (\frac{\zeta_j^{n+1} - \zeta_j^n}{\Delta t}, S_h) + (\nabla \zeta_j^{n+1}, \nabla S_h) + b_T(u_j^n, T_j^{n+1}, S_h)$$
$$-b_T(u_{j,h}^n, T_{j,h}^{n+1}, S_h) + b_T(u_{j,h}'^n, T_{j,h}^{n+1} - T_{j,h}^n, S_h) - \varsigma_T(T_j^{n+1}, S_h) \ \ \forall S_h \in W_{\Gamma_D,h}.$$

Setting $S_h = 2\Delta t \psi_{j,h}^{n+1} \in W_{\Gamma_D,h}$ yields

$$\left\{\|\psi_{j,h}^{n+1}\|^2 - \|\psi_{j,h}^n\|^2 + \|\psi_{j,h}^{n+1} - \psi_{j,h}^n\|^2\right\} + 2\Delta t \|\nabla \psi_{j,h}^{n+1}\|^2 = (\zeta_j^{n+1} - \zeta_j^n, \psi_{j,h}^{n+1})$$
$$+2\Delta t(\nabla \zeta_j^{n+1}, \nabla \psi_{j,h}^{n+1}) + 2\Delta t b_T(u_j^n, T_j^{n+1}, \psi_{j,h}^{n+1}) - 2\Delta t b_T(u_{j,h}^n, T_{j,h}^{n+1}, \psi_{j,h}^{n+1})$$
$$+2\Delta t b_T(u_{j,h}'^n, T_{j,h}^{n+1} - T_{j,h}^n, \psi_{j,h}^{n+1}) - 2\Delta t \varsigma_T(T_j^{n+1}, \psi_{j,h}^{n+1}).$$

Add and subtract $2\Delta t b_T(u_j^n, T_{j,h}^{n+1}, \psi_{j,h}^{n+1})$ and $2\Delta t b_T(u_{j,h}'^n, T_j^{n+1} - T_j^n, \psi_{j,h}^{n+1})$ to the right-hand-side. Rearrange and use skew-symmetry, then

$$\left\{\|\psi_{j,h}^{n+1}\|^2 - \|\psi_{j,h}^n\|^2 + \|\psi_{j,h}^{n+1} - \psi_{j,h}^n\|^2\right\} + 2\Delta t \|\nabla \psi_{j,h}^{n+1}\|^2 = 2(\zeta_j^{n+1} - \zeta_j^n, \psi_{j,h}^{n+1})$$
$$+2\Delta t(\nabla \zeta_j^{n+1}, \nabla \psi_{j,h}^{n+1}) + 2\Delta t b_T(u_j^n, \zeta_j^{n+1}, \psi_{j,h}^{n+1}) + 2\Delta t b_T(\eta_j^n, T_{j,h}^{n+1}, \psi_{j,h}^{n+1}) \tag{4.22}$$
$$-2\Delta t b_T(\phi_{j,h}^n, T_{j,h}^{n+1}, \psi_{j,h}^{n+1}) - 2\Delta t b_T(u_{j,h}'^n, \zeta_j^{n+1} - \zeta_j^n, \psi_{j,h}^{n+1}) - 2\Delta t b_T(u_{j,h}'^n, \psi_{j,h}^n, \psi_{j,h}^{n+1})$$
$$+2\Delta t b_T(u_{j,h}'^n, T_j^{n+1} - T_j^n, \psi_{j,h}^{n+1}) - 2\Delta t \varsigma_T(\theta_j^{n+1}, \psi_{j,h}^{n+1}).$$

Follow analogously for the velocity error equation. Subtract (4.8) from (4.18). Let $v_h = 2\Delta t\phi_{j,h}^{n+1} \in X_h$, add and subtract $b_u(u_j^n, u_{j,h}^{n+1}, \phi_{j,h}^{n+1})$ and $b_u(u_{j,h}'^n, u_j^{n+1} - u_j^n, \phi_{j,h}^{n+1})$, rearrange and use skew-symmetry. Then,

$$\begin{aligned}\Big\{\|\varphi_{j,h}^{n+1}\|^2 - \|\varphi_{j,h}^n\|^2 + \|\varphi_{j,h}^{n+1} - \varphi_{j,h}^n\|^2\Big\} + 2\mathrm{Pr}\Delta t\|\nabla\varphi_{j,h}^{n+1}\|^2 - 2\Delta t(\pi_{j,h}^{n+1}, \nabla\cdot\varphi_{j,h}^{n+1})\\ = 2(\eta_j^{n+1} - \eta_j^n, \varphi_{j,h}^{n+1}) - 2\mathrm{PrRa}\Delta t(\xi\zeta_j^n, \varphi_{j,h}^{n+1}) + 2\mathrm{PrRa}\Delta t(\xi\psi_{j,h}^n, \varphi_{j,h}^{n+1})\\ +2\Delta t b_u(u_j^n, \eta_j^{n+1}, \varphi_{j,h}^{n+1}) + 2\Delta t b_u(\eta_j^n, u_{j,h}^{n+1}, \varphi_{j,h}^{n+1}) - 2\Delta t b_u(\varphi_{j,h}^n, u_{j,h}^{n+1}, \varphi_{j,h}^{n+1})\\ -2\Delta t b_u(u_{j,h}'^n, \eta_j^{n+1} - \eta_j^n, \varphi_{j,h}^{n+1}) - 2\Delta t b(u_{j,h}'^n, \varphi_{j,h}^n, \varphi_{j,h}^{n+1}) + 2\Delta t b_u(u_{j,h}'^n, u_j^{n+1} - u_j^n, \varphi_{j,h}^{n+1})\\ -2\Delta t\varsigma_u(u_j^{n+1}, \varphi_{j,h}^{n+1}).\end{aligned} \tag{4.23}$$

Similarly, for the pressure equation, subtract (4.15) from (4.19). Let $q_h = 2\Delta t\pi_{j,h}^{n+1} \in Q_h$ and rearrange, then

$$\begin{aligned}\varepsilon\Big\{\|\pi_{j,h}^{n+1}\|^2 - \|\pi_{j,h}^n\|^2 + \|\pi_{j,h}^{n+1} - \pi_{j,h}^n\|^2\Big\} + 2\Delta t(\nabla\cdot\varphi_{j,h}^{n+1}, \pi_{j,h}^{n+1})\\ = 2\varepsilon(\lambda_j^{n+1} - \lambda_j^n, \pi_{j,h}^{n+1}) - 2\Delta t\varsigma_p(p_j^{n+1}, \pi_{j,h}^{n+1}).\end{aligned} \tag{4.24}$$

We seek to now estimate all terms on the right-hand-side in such a way that we may subsume the terms involving unknown pieces $\psi_{j,h}^k$, $\varphi_{j,h}^k$, and $\pi_{j,h}^k$ into the left-hand-side. The following estimates are formed using skew-symmetry, Lemma 1, and the Cauchy-Schwarz-Young inequality;

$$\begin{aligned}2\Delta t b_T(u_j^n, \zeta_j^{n+1}, \psi_{j,h}^{n+1}) &\le 2\Delta t C_{3,T}\|\nabla u_j^n\|\|\nabla\psi_{j,h}^{n+1}\|\sqrt{\|\zeta_j^{n+1}\|\|\nabla\zeta_j^{n+1}\|}\\ &\le \frac{4C_r\Delta t C_{3,T}^2}{\delta_4}\|\nabla u_j^n\|^2\|\zeta_j^{n+1}\|\|\nabla\zeta_j^{n+1}\| + \frac{\delta_4\Delta t}{r}\|\nabla\psi_{j,h}^{n+1}\|^2,\\ 2\Delta t b_T(\eta_j^n, T_{j,h}^{n+1}, \psi_{j,h}^{n+1}) &\le \frac{4C_r C_{2,T}^2}{\delta_5}\|\nabla T_{j,h}^{n+1}\|^2\|\eta_j^n\|\|\nabla\eta_j^n\| + \frac{\delta_5}{r}\|\nabla\psi_{j,h}^{n+1}\|^2.\end{aligned} \tag{4.25}$$

Applying Lemma 1, the Cauchy-Schwarz-Young inequality, Taylor's theorem, and condition 4.11 yields,

$$\begin{aligned}
-2\Delta t b_T(u'^n_{j,h}, \zeta_j^{n+1} - \zeta_j^n, \psi_{j,h}^{n+1}) &\leq C_{1,T}\|\nabla u'^n_{j,h}\|\|\nabla\psi_{j,h}^{n+1}\|\|\nabla(\zeta_j^{n+1} - \zeta_j^n)\| \qquad (4.26)\\
&\leq \frac{4C_r C_{1,T}^2\Delta t^2}{\delta_7}\|\nabla u'^n_{j,h}\|^2\|\nabla(\partial_t\zeta_j)\|^2_{L^2(t^n,t^{n+1};L^2(\Omega))}\\
&\quad + \frac{\delta_7\Delta t}{r}\|\nabla\psi_{j,h}^{n+1}\|^2,\\
&\leq \frac{4C_r C_{1,T}^2 h\Delta t}{C_\dagger\delta_7}\|\nabla(\partial_t\zeta_j)\|^2_{L^2(t^n,t^{n+1};L^2(\Omega))} + \frac{\delta_7\Delta t}{r}\|\nabla\psi_{j,h}^{n+1}\|^2,\\
2\Delta t b_T(u'^n_{j,h}, T_j^{n+1} - T_j^n, \psi_{j,h}^{n+1}) &\leq C_{1,T}\|\nabla u'^n_{j,h}\|\|\nabla(T_j^{n+1} - T_j^n)\|\|\nabla\psi_{j,h}^{n+1}\| \qquad (4.27)\\
&\leq \frac{4C_r C_{1,T}^2 h\Delta t}{C_\dagger\delta_9}\|\nabla(\partial_t T_j)\|^2_{L^2(t^n,t^{n+1};L^2(\Omega))} + \frac{\delta_9\Delta t}{r}\|\nabla\psi_{j,h}^{n+1}\|^2.
\end{aligned}$$

Apply the triangle inequality, Lemma 1 and the Cauchy-Schwarz-Young inequality twice. This yields

$$\begin{aligned}
-2\Delta t b_T(\phi_{j,h}^n, T_{j,h}^{n+1}, \psi_{j,h}^{n+1}) &\leq 2C_{2,T}\Delta t\|\nabla T_{j,h}^{n+1}\|\|\nabla\psi_{j,h}^{n+1}\|\sqrt{\|\phi_{j,h}^n\|\|\nabla\phi_{j,h}^n\|} \qquad (4.28)\\
&\leq 2C_{2,T}C_{T,j}\Delta t\|\nabla\psi_{j,h}^{n+1}\|\sqrt{\|\phi_{j,h}^n\|\|\nabla\phi_{j,h}^n\|}\\
&\leq \delta_6\Delta t\|\nabla\psi_{j,h}^{n+1}\|^2 + \frac{C_{2,T}^2C_{T,j}^2\Delta t}{\delta_6}\|\phi_{j,h}^n\|\|\nabla\phi_{j,h}^n\|\\
&\leq \delta_6\Delta t\|\nabla\psi_{j,h}^{n+1}\|^2 + \frac{C_{2,T}^2C_{T,j}^2\Delta t}{2\delta_6\sigma_6}\|\phi_{j,h}^n\|^2 + \frac{C_{2,T}^2C_{T,j}^2\sigma_6\Delta t}{2\delta_6}\|\nabla\phi_{j,h}^n\|^2.
\end{aligned}$$

Use Lemma 1, the inverse inequality, and the Cauchy-Schwarz-Young inequality yielding

$$\begin{aligned}
2\Delta t b_T(u'^n_{j,h}, \psi_{j,h}^n, \psi_{j,h}^{n+1}) &\leq \frac{2C_{3,T}\sqrt{C_{\text{inv},2}}\Delta t}{\sqrt{h}}\|\nabla u'^n_{j,h}\|\|\nabla\psi_{j,h}^{n+1}\|\|\psi_{j,h}^{n+1} - \psi_{j,h}^n\| \qquad (4.29)\\
&\leq \frac{2C_{3,T}^2C_{\text{inv},2}\Delta t^2}{h}\|\nabla u'^n_{j,h}\|^2\|\nabla\psi_{j,h}^{n+1}\|^2 + \frac{1}{2}\|\psi_{j,h}^{n+1} - \psi_{j,h}^n\|^2.
\end{aligned}$$

The Cauchy-Schwarz-Young inequality, Poincaré-Friedrichs inequality and Taylor's theorem yield

$$2(\zeta_j^{n+1} - \zeta_j^n, \psi_{j,h}^{n+1}) \leq \frac{4C_{\text{pf},2}^2C_r}{\delta_1}\|\partial_t\zeta_j\|^2_{L^2(t^n,t^{n+1};L^2(\Omega))} + \frac{\delta_1\Delta t}{r}\|\nabla\psi_{j,h}^{n+1}\|^2. \qquad (4.30)$$

Lastly, use the Cauchy-Schwarz-Young inequality,

$$2\Delta t(\nabla\zeta_j^{n+1}, \nabla\psi_{j,h}^{n+1}) \leq \frac{4C_r\Delta t}{\delta_2}\|\nabla\zeta_j^{n+1}\|^2 + \frac{\delta_2\Delta t}{r}\|\nabla\psi_{j,h}^{n+1}\|^2. \qquad (4.31)$$

Similar estimates follow for the right-hand-side terms in (4.2.6);

$$-2\mathrm{PrRa}\Delta t(\xi\zeta_j^n,\varphi_{j,h}^{n+1}) \leq \frac{4\mathrm{Pr}^2\mathrm{Ra}^2C_{\mathrm{pf},1}^2C_r\Delta t}{\delta_{16}}\|\zeta_j^n\|^2+\frac{\delta_{16}\Delta t}{r}\|\nabla\varphi_{j,h}^{n+1}\|^2, \tag{4.32}$$

$$2\mathrm{PrRa}\Delta t(\xi\psi_{j,h}^n,\varphi_{j,h}^{n+1}) \leq \frac{4\mathrm{Pr}^2\mathrm{Ra}^2C_{\mathrm{pf},1}^2C_r\Delta t}{\delta_{17}}\|\psi_{j,h}^n\|^2+\frac{\delta_{17}\Delta t}{r}\|\nabla\varphi_{j,h}^{n+1}\|^2. \tag{4.33}$$

Next, consider equation (4.24). Add and subtract $2\varepsilon(\lambda_j^{n+1}-\lambda_j^n,\pi_{j,h}^n)$ and $-2\Delta t\varsigma_p(p_j^{n+1},\pi_{j,h}^n)$. Use Taylor's theorem and the Cauchy-Schwarz-Young inequality. This leads to

$$\begin{aligned}2\varepsilon(\lambda_j^{n+1}-\lambda_j^n,\pi_{j,h}^{n+1}) &= 2\varepsilon(\lambda_j^{n+1}-\lambda_j^n,\pi_{j,h}^{n+1}-\pi_{j,h}^n)+2\varepsilon(\lambda_j^{n+1}-\lambda_j^n,\pi_{j,h}^n) \\ &\leq \frac{4\varepsilon C_r\Delta t^2}{\delta_{26}}\|\partial_t\lambda_j\|^2_{L^2(t^n,t^{n+1};L^2(\Omega))}+\frac{\varepsilon\delta_{26}}{r}\|\pi_{j,h}^{n+1}-\pi_{j,h}^n\|^2 \\ &+\frac{4\varepsilon C_r\Delta t}{\delta_{27}}\|\partial_t\lambda_j\|^2_{L^2(t^n,t^{n+1};L^2(\Omega))}+\frac{\varepsilon\delta_{27}\Delta t}{r}\|\pi_{j,h}^n\|^2,\end{aligned} \tag{4.34}$$

$$\begin{aligned}-2\Delta t\varsigma_p(p_j^{n+1},\pi_{j,h}^{n+1}) &\leq \frac{4\varepsilon C_r\Delta t^2}{\delta_{28}}\|\partial_t p_j\|^2_{L^2(t^n,t^{n+1};L^2(\Omega))}+\frac{\varepsilon\delta_{28}}{r}\|\pi_{j,h}^{n+1}-\pi_{j,h}^n\|^2 \\ &+\frac{4\varepsilon C_r\Delta t}{\delta_{29}}\|\partial_t p_j\|^2_{L^\infty(t^n,t^{n+1};L^2(\Omega))}+\frac{\varepsilon\delta_{29}\Delta t}{r}\|\pi_{j,h}^n\|^2.\end{aligned} \tag{4.35}$$

Add equations (4.2.6) - (4.24) together. Apply the above estimates and Lemma 8. Let $r=40$ and choose $\sum_{i\neq6,12}^{14}\delta_i=10$, $\delta_6=\delta_{12}=1/8$, $\sum_{i\neq21}^{25}\delta_i=10$, $\delta_{21}=1/8$, and $\delta_{26}=\delta_{28}=10$. Moreover, let $\sigma_6=\frac{\delta_6}{12C_{3,T}^2C_{T,j}^2}$ and $\sigma_{21}=\frac{\delta_{21}}{12C_2^2C_{u,j}^2}$. Reorganize, use condition (4.11), relation (4.12), and Theorem 11. Take the maximum over all constants associated with $\|\psi_{j,h}^n\|$, $\|\varphi_{j,h}^n\|$, and $\|\pi_{j,h}^n\|$ on the right-hand-side. Lastly, take the maximum over all remaining constants

on the right-hand-side. Then,

$$\Big\{\|\psi_{j,h}^{n+1}\|^2-\|\psi_{j,h}^{n}\|^2\Big\}+\Big\{\|\varphi_{j,h}^{n+1}\|^2-\|\varphi_{j,h}^{n}\|^2\Big\}+\varepsilon\Big\{\|\pi_{j,h}^{n+1}\|^2-\|\pi_{j,h}^{n}\|^2\Big\} \tag{4.36}$$
$$+\frac{1}{2}\Big\{\|\psi_{j,h}^{n+1}-\psi_{j,h}^{n}\|^2+\|\varphi_{j,h}^{n+1}-\varphi_{j,h}^{n}\|^2+\varepsilon\|\pi_{j,h}^{n+1}-\pi_{j,h}^{n}\|^2\Big\}+\frac{\Delta t}{2}\Big\{\|\nabla\psi_{j,h}^{n+1}\|^2+\mathrm{Pr}\|\nabla\varphi_{j,h}^{n+1}\|^2\Big\}$$
$$+\frac{\mathrm{Pr}\Delta t}{4}\Big\{\|\nabla\varphi_{j,h}^{n+1}\|^2-\|\nabla\varphi_{j,h}^{n}\|^2\Big\}\leq C_\star\Delta t\Big\{\|\psi_{j,h}^{n}\|+\|\phi_{j,h}^{n}\|+\varepsilon\|\pi_{j,h}^{n}\|\Big\}$$
$$+C\Delta t\Big\{\frac{1}{\Delta t}\|\partial_t\zeta_j\|^2_{L^2(t^n,t^{n+1};L^2(\Omega))}+\frac{1}{\Delta t}\|\partial_t\eta_j\|^2_{L^2(t^n,t^{n+1};L^2(\Omega))}+\Delta t\|\partial_t\lambda_j\|^2_{L^2(t^n,t^{n+1};L^2(\Omega))}$$
$$+h\|\nabla(\partial_t\zeta_j)\|^2_{L^2(t^n,t^{n+1};L^2(\Omega))}+h\|\nabla(\partial_t\eta_j)\|^2_{L^2(t^n,t^{n+1};L^2(\Omega))}+\|\zeta_j^n\|^2+\|\nabla\zeta_j^{n+1}\|^2$$
$$+\|\zeta_j^{n+1}\|\|\nabla\zeta_j^{n+1}\|+\|\eta_j^n\|\|\nabla\eta_j^n\|+\|\eta_j^{n+1}\|\|\nabla\eta_j^{n+1}\|+\Delta t\|\partial_tT_j\|^2_{L^2(t^n,t^{n+1};L^2(\Omega))}$$
$$+\Delta t^2\|\partial_tp_j\|^2_{L^2(t^n,t^{n+1};L^2(\Omega))}+\Delta t\|\partial_tp_j\|^2_{L^\infty(t^n,t^{n+1};L^2(\Omega))}+\Delta t\|\partial_{tt}T_j\|^2_{L^2(t^n,t^{n+1};L^2(\Omega))}$$
$$+\Delta t\|\partial_{tt}u_j\|^2_{L^2(t^n,t^{n+1};L^2(\Omega))}+(h+\Delta t)\|\nabla(\partial_tT_j)\|^2_{L^2(t^n,t^{n+1};L^2(\Omega))}$$
$$+(h+\Delta t)\|\nabla(\partial_tu_j)\|^2_{L^2(t^n,t^{n+1};L^2(\Omega))}\|\Big\}.$$

Sum from $n=0$ to $n=N-1$, apply Lemmas 3 and 2, take infimums over X_h, Q_h, and $\widehat{W}_h$, and renorm. Then,

$$\|\psi_{j,h}^N\|^2+\|\varphi_{j,h}^N\|^2+\varepsilon\|\pi_{j,h}^N\|^2+\frac{1}{2}\sum_{n=0}^{N-1}\Big\{\|\psi_{j,h}^{n+1}-\psi_{j,h}^{n}\|^2+\|\varphi_{j,h}^{n+1}-\varphi_{j,h}^{n}\|^2+\varepsilon\|\pi_{j,h}^{n+1}-\pi_{j,h}^{n}\|^2\Big\}$$
$$+\frac{\mathrm{Pr}\Delta t}{4}\|\nabla\varphi_{j,h}^N\|^2+\frac{1}{2}|||\nabla\psi_{j,h}|||^2_{2,0}+\frac{\mathrm{Pr}}{2}|||\nabla\varphi_{j,h}|||^2_{2,0}\leq C\exp(C_\star t^*)\inf_{\substack{v_h\in X_h\\ q_h\in Q_h\\ S_h\in\hat{W}_h}}\Big\{\|\partial_t\zeta_j\|^2_{L^2(0,t^*;L^2(\Omega))}$$
$$+\|\partial_t\eta_j\|^2_{L^2(0,t^*;L^2(\Omega))}+\Delta t^2\|\partial_t\lambda_j\|^2_{L^2(0,t^*;L^2(\Omega))}+h\Delta t\|\nabla(\partial_t\zeta_j)\|^2_{L^2(0,t^*;L^2(\Omega))}$$
$$+h\Delta t\|\nabla(\partial_t\eta_j)\|^2_{L^2(0,t^*;L^2(\Omega))}+|||\zeta_j|||^2_{2,0}+|||\nabla\zeta_j|||^2_{2,0}+|||\zeta_j|||_{2,0}|||\nabla\zeta_j|||_{2,0}+|||\eta_j|||_{2,0}|||\nabla\eta_j|||_{2,0}$$
$$+\Delta t^2\|\partial_tT_j\|^2_{L^2(0,t^*;L^2(\Omega))}+\Delta t^2\|\partial_tp_j\|^2_{L^2(0,t^*;L^2(\Omega))}+\Delta t^2\|\partial_tp_j\|^2_{L^\infty(0,t^*;L^2(\Omega))}$$
$$+\Delta t^2\|\partial_{tt}T_j\|^2_{L^2(0,t^*;L^2(\Omega))}+\Delta t^2\|\partial_{tt}u_j\|^2_{L^2(0,t^*;L^2(\Omega))}+(h+\Delta t)\Delta t\|\nabla(\partial_tT_j)\|^2_{L^2(0,t^*;L^2(\Omega))}$$
$$+(h+\Delta t)\Delta t\|\nabla(\partial_tu_j)\|^2_{L^2(0,t^*;L^2(\Omega))}+\|\psi_{j,h}^0\|^2+\|\varphi_{j,h}^0\|^2+\varepsilon\|\pi_{j,h}^0\|^2$$
$$+\frac{\mathrm{Pr}\Delta t}{4}\|\nabla\varphi_{j,h}^0\|^2\Big\}.$$

Assuming $\|\psi_{j,h}^0\|=\|\varphi_{j,h}^0\|=\|\pi_{j,h}^0\|=\|\nabla\phi_{j,h}^0\|=0$, the result follows by the error equations, the triangle inequality, and absorbing constants. □

4.2.7 NUMERICAL EXPERIMENTS

In this section, we illustrate the convergence, speed, stability, and predictability of ACE described by (4.8) - (4.10) using Taylor-Hood (P2-P1-P2) elements to approximate the average velocity, pressure, and temperature. First-order accuracy is observed in Section 4.2.7.1 using homogeneous boundary conditions for the temperature and an analytical solution devised through the method of manufactured solutions. The bred vector algorithm, used to generate ensemble members with maximal separation from the mean flow, is described in Section 4.2.7.3. Sections 4.2.7.2–4.2.7.5 illustrate the stability, speed, and predictability properties of the ACE scheme for inhomogeneous temperature boundary conditions. In particular, the double pane window benchmark [134] is considered for Sections 4.2.7.2 (stability) and 4.2.7.4 (speed and benchmark values). In Section 4.2.7.4, ACE is shown to be 3 to 8 times faster than linearly implicit BDF1 in Section 4.2.7.4. Lastly, in Section 4.2.7.5, we calculate average effective Lyapunov exponents and variance to study the predictability of a Marsigli flow for varying Reynolds numbers. The software platform used for tests in Sections 4.2.7.2 and 4.2.7.4 is FreeFem++ [55], whereas FEniCS [1] is used for Sections 4.2.7.1 and 4.2.7.5.

4.2.7.1 NUMERICAL CONVERGENCE STUDY We now illustrate convergence rates for ACE (4.8) – (4.9). The domain and parameters are $\Omega = (0,1)^2$, $\mathrm{Pr} = 1.0$, and $\mathrm{Ra} = 100$. The unperturbed solution is given by

$$u(x,y,t) = A(t)(x^2(x-1)^2y(y-1)(2y-1), -x(x-1)(2x-1)y^2(y-1)^2)^T, \tag{4.37}$$

$$T(x,y,t) = u_1(x,y,t) + u_2(x,y,t), \tag{4.38}$$

$$p(x,y,t) = A(t)(2x-1)(2y-1), \tag{4.39}$$

with $A(t) = 10\cos(t)$. Perturbed solutions are given by

$$u(x,y,t;\omega_{1,2}) = (1+\delta_{1,2})u(x,y,t),$$
$$T(x,y,t;\omega_{1,2}) = (1+\delta_{1,2})T(x,y,t),$$
$$p(x,y,t;\omega_{1,2}) = (1+\delta_{1,2})p(x,y,t),$$

Table 4.1: Errors and rates for $\langle u \rangle$, $\langle T \rangle$, and $\langle p \rangle$ in corresponding norms.

m	$\|\|\|\langle u_h \rangle^n - u\|\|\|_{\infty,0}$	Rate	$\|\|\|\langle T_h \rangle - T\|\|\|_{\infty,0}$	Rate	$\|\|\|\langle p_h \rangle - p\|\|\|_{\infty,0}$	Rate	$\|\|\|\langle u_h \rangle^n - u\|\|\|_{2,1}$	Rate	$\|\|\|\langle T_h \rangle - T\|\|\|_{2,1}$	Rate	$\|\|\|\langle p_h \rangle - p\|\|\|_{1,0}$	Rate
10	6.70E-3	-	1.32E-5	-	1.17E-1	-	3.18E-2	-	4.05E-4	-	6.06E-2	-
20	3.42E-3	0.97	3.35E-6	1.98	5.71E-2	1.04	1.64E-2	0.95	6.43E-5	2.66	3.07E-2	0.98
30	2.30E-3	0.98	2.11E-6	1.14	3.80E-2	1.01	1.11E-2	0.96	2.58E-5	2.25	2.07E-2	0.97
40	1.73E-3	0.99	1.56E-6	1.04	2.84E-2	1.01	8.38E-3	0.99	1.59E-5	1.69	1.56E-2	0.99
50	1.38E-3	1.00	1.25E-6	1.01	2.27E-2	1.01	6.70E-3	1.00	1.18E-5	1.34	1.25E-2	1.01

where $\delta_1 = 0.001 = -\delta_2$, and satisfy the following relations

$$\begin{aligned}
\langle u \rangle &= 0.5\Big(u(x,y,t;\omega_1) + u(x,y,t;\omega_2)\Big) = u(x,y,t),\\
\langle T \rangle &= 0.5\Big(T(x,y,t;\omega_1) + T(x,y,t;\omega_2)\Big) = T(x,y,t),\\
\langle p \rangle &= 0.5\Big(p(x,y,t;\omega_1) + p(x,y,t;\omega_2)\Big) = p(x,y,t).
\end{aligned}$$

External forces, heat sources, and boundary conditions are adjusted appropriately. The mesh is constructed via Delaunay triangulation generated from m points on each side of the boundary. We calculate errors in the approximations of the average velocity, temperature, and pressure with the $L^\infty(0,t^*;L^2(\Omega))$ norm, as well as the $L^2(0,t^*;H^1(\Omega))$ norm for the velocity and temperature, and the $L^1(0,t^*;L^2(\Omega))$ norm for the pressure. Rates are calculated from the errors at two successive $\Delta t_{1,2}$ via

$$\frac{\log(e_\chi(\Delta t_1)/e_\chi(\Delta t_2))}{\log(\Delta t_1/\Delta t_2)},$$

respectively, with $\chi = u, T, p$. We set $\Delta t = \frac{1}{10m}$ and vary m between 10, 20, 30, 40, and 50. Results are presented in Table 4.1. First-order convergence is observed for each solution variable. The results for velocity and temperature are predicted by our theory; however, pressure is a half-power better than predicted.

4.2.7.2 STABILITY CONDITION Recall that ACE is stable provided condition (4.11) holds:

$$\frac{C_\dagger \Delta t}{h} \max_{1 \le j \le J} \|\nabla u'^n_{j,h}\|^2 \le 1.$$

The stability constant $C_\dagger$ is determined via pre-computations for the double pane window benchmark; it is set to 0.35. Condition (4.11) is checked at each timestep. The timestep is halved and the timestep is repeated if (4.11) violated. The timestep is never increased. The condition is violated three times in Section 4.2.7.4 for $\mathrm{Ra} = 10^6$.

Remark 14. *Although $C_\dagger$ is estimated to be 1, it is set to 0.35. This is done to reduce the timestep when $Ra = 10^6$. At this value of Ra, the stopping condition is not met unless the timestep is reduced. Instead, the solution appears to reach a false quasi-periodic solution. This occurs for linearly implicit BDF1 and variants and may be related to the conditional Lyapunov stability of these methods [121]. This is currently under investigation.*

4.2.7.3 PERTURBATION GENERATION In Section 4.2.7.1, a positive and negative perturbation pair is chosen to manufacture a solution with certain properties. The bred vector (BV) algorithm [133] is used to generate perturbations in Sections 4.2.7.4 and 4.2.7.5. The BV algorithm simulates growth errors due to uncertainty in the initial conditions; this is necessary because *random perturbations are not sufficient* [133]. As a consequence, the nonlinear error growth in the ensemble average is reduced, which is witnessed in Section 4.2.7.5. Our experimental results are drastically different when using BVs compared to random perturbations, consistent with the above.

To begin, an initial random positive and negative perturbation pair is generated, $\pm\varepsilon = \pm(\delta_1, \delta_2, \delta_3, \delta_4)$ with $\delta_i \in (0, 0.01)\ \forall 1 \le i \le 4$. Denoting the control and perturbed numerical approximations χ^n_h and $\chi^n_{p,h}$, respectively, a bred vector $bv(\chi; \delta_i)$ is generated via:

Algorithm 6 (Bred Vectors (BV))**.** *Perform the following steps:*
Step 1: Given χ^0_h and δ_i, put $\chi^0_{p,h} = \chi^0_h + \delta_i$. Select time reinitialization interval $\delta t \ge \Delta t$ and let $t^k = k\delta t$ with $0 \le k \le k^* \le N$.
Step 2: Compute χ^k_h and $\chi^k_{p,h}$. Calculate $bv(\chi^k; \delta_i) = \frac{\delta_i}{\|\chi^k_{p,h} - \chi^k_h\|}(\chi^k_{p,h} - \chi^k_h)$.

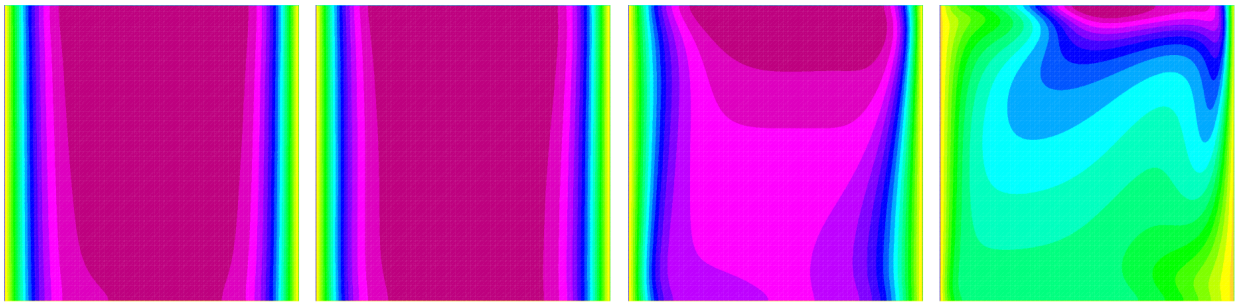

Figure 4.1: BV ($bv(T;+\delta_3)$): Ra $= 10^3, 10^4, 10^5$, and 10^6, left to right.

Step 3: *Put* $\chi^k_{p,h} = \chi^k_h + bv(\chi^k;\delta_i)$.
Step 4: *Repeat from Step 2 with* $k = k+1$.
Step 5: *Put* $bv(\chi;\delta_i) = bv(\chi^{k^*};\delta_i)$.

The bred vector pair generates a pair of initial conditions via $\chi_\pm = \chi^0 + bv(\chi;\pm\delta_i)$. We let $k^* = 5$ and choose $\delta t = \Delta t = 0.001$ for all tests.

4.2.7.4 THE DOUBLE PANE WINDOW PROBLEM This is a classic test problem for natural convection. The problem is the flow of air, Pr $= 0.71$, in a unit square cavity subject to no-slip boundary conditions. The horizontal walls are adiabatic and vertical wall temperature is maintained at constant temperature [134]. We set $\varepsilon = 0.01\Delta t$.

We first validate our code. We set $J = 2$ and vary Ra $\in \{10^3, 10^4, 10^5, 10^6\}$. The finite element mesh is a division of $(0,1)^2$ into 64^2 squares with diagonals connected with a line within each square in the same direction. The initial timestep $\Delta t = 0.001$; it is halved three times for Ra $= 10^6$ to 0.000125. The initial conditions are generated via the BV algorithm,

$$\begin{aligned}
u_\pm(x,y,0) &:= u(x,y,0;\omega_{1,2}) = (u_1^{prev} + bv(u_1;\pm\delta_1), u_2^{prev} + bv(u_2;\pm\delta_2))^T,\\
T_\pm(x,y,0) &:= T(x,y,0;\omega_{1,2}) = T^{prev} + bv(T;\pm\delta_3),\\
p_\pm(x,y,0) &:= p(x,y,0;\omega_{1,2}) = p^{prev} + bv(p;\pm\delta_4),
\end{aligned}$$

where the subscript *prev* denotes the solution from the previous value of Ra; for Ra $= 10^3$, the previous values are all set to 1. The BV, $bv(T;+\delta_3)$, is presented in Figure 4.1. Forcings

are identically zero for $j = 1, 2$. The stopping condition is

$$\max_{0 \le n \le N-1} \Big\{ \frac{\|u_h^{n+1} - u_h^n\|}{\|u_h^{n+1}\|}, \frac{\|T_h^{n+1} - T_h^n\|}{\|T_h^{n+1}\|} \Big\} \le 10^{-5}.$$

The quantities of interest are: $\max_{y \in \Omega_h} u_1(0.5, y, t^*)$, $\max_{x \in \Omega_h} u_2(x, 0.5, t^*)$, the local Nusselt number at vertical walls, and average Nusselt number at the hot wall. The latter two are given by

$$\begin{aligned} Nu_{local} &= \pm \frac{\partial T}{\partial x}, \\ Nu_{avg} &= \int_0^1 Nu_{local} dy, \end{aligned}$$

where $\pm$ corresponds to the cold and hot walls, respectively.

Plots of Nu_{local} at the hot and cold walls are presented in Figure 4.3. Computed values of the remaining quantities are presented, alongside several of those seen in the literature, in Tables 4.2 – 4.4. Figures 4.2a and 4.2b present the velocity streamlines and temperature isotherms for the averages. All results are consistent with benchmark values in the literature [134, 89, 19, 17, 147].

The second test is a timing test comparing ACE vs. linearly implicit BDF1. Standard GMRES is used for the velocity and temperature solves.. We set $J = 1$ and vary $10^3 \le \text{Ra} \le 10^6$. The timestep is chosen to be $\Delta t = 0.001$ for $10^3 \le \text{Ra} \le 10^5$ and $\Delta t = 0.0001$ for $\text{Ra} = 5 \times 10^5$ and 10^6. The initial conditions are prescribed as in the above. Results are presented in Figure 4.4. We see that for $\text{Ra} = 10^3$, both algorithms have increased runtimes relative to all other cases. This is due to the relatively poor choice of initial condition. Moreover, linearly implicit BDF1 suffers from increased runtime with increasing Ra. However, ACE runtimes remain relatively constant. Overall, ACE is 3 to 8 times faster for this test problem.

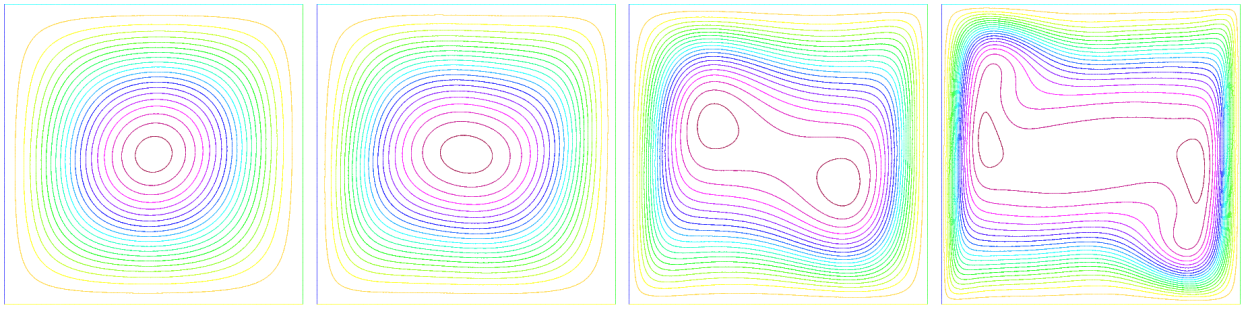

(a) Streamlines: Ra $= 10^3, 10^4, 10^5$, and 10^6, left to right.

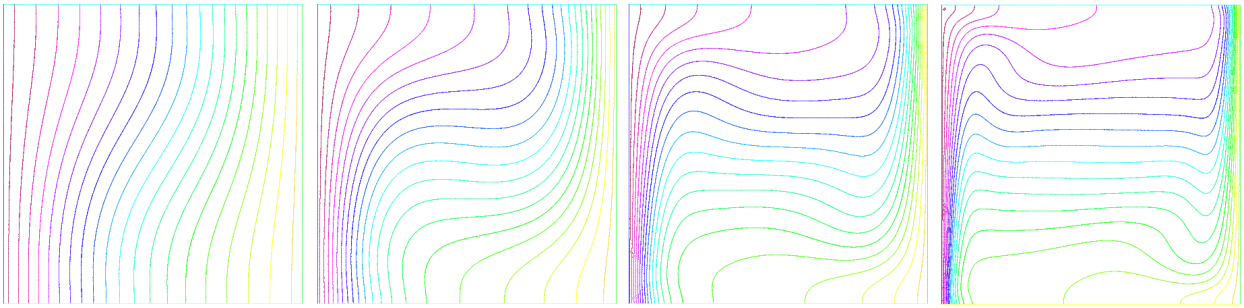

(b) Isotherms: Ra $= 10^3, 10^4, 10^5$, and 10^6, left to right.

Figure 4.2: Streamlines and isotherms for the double pane problem.

Table 4.2: Comparison: maximum u_1 at $x = 0.5$ & mesh size, double pane problem.

Ra	Present study	Ref. [134]	Ref. [89]	Ref. [19]	Ref. [17]	Ref. [147]
10^4	16.16 (64×64)	16.18 (41×41)	16.10 (71×71)	16.10 (101×101)	15.90 (11×11)	16.18 (64×64)
10^5	34.65 (64×64)	34.81 (81×81)	34 (71×71)	34 (101×101)	33.51 (21×21)	34.74 (64×64)
10^6	65.48 (64×64)	65.33 (81×81)	65.40 (71×71)	65.40 (101×101)	65.52 (32×32)	64.81 (64×64)

Table 4.3: Comparison: maximum u_2 at $y = 0.5$ & mesh size, double pane problem.

Ra	Present study	Ref. [134]	Ref. [89]	Ref. [19]	Ref. [17]	Ref. [147]
10^4	19.65 (64×64)	19.51 (41×41)	19.90 (71×71)	19.79 (101×101)	19.91 (11×11)	19.62 (64×64)
10^5	68.88 (64×64)	68.22 (81×81)	70 (71×71)	70.63 (101×101)	70.60 (21×21)	68.48 (64×64)
10^6	218.63 (64×64)	216.75 (81×81)	228 (71×71)	227.11 (101×101)	228.12 (32×32)	220.44 (64×64)

Table 4.4: Comparison: Nu_{avg} on vertical boundary $x = 0$ & mesh size.

Ra	Present study	Ref. [134]	Ref. [89]	Ref. [19]	Ref. [17]	Ref. [147]
10^4	2.24 (64×64)	2.24 (41×41)	2.08 (71×71)	2.25 (101×101)	2.15 (11×11)	2.25 (64×64)
10^5	4.50 (64×64)	4.52 (81×81)	4.30 (71×71)	4.59 (101×101)	4.35 (21×21)	4.53 (64×64)
10^6	8.77 (64×64)	8.92 (81×81)	8.74 (71×71)	8.97 (101×101)	8.83 (32×32)	8.87 (64×64)

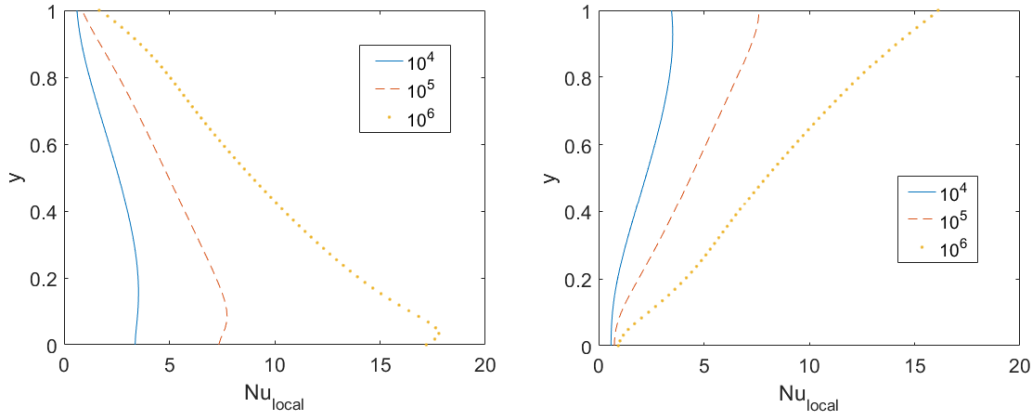

Figure 4.3: Variation of the local Nu at the hot (left) and cold walls (right).

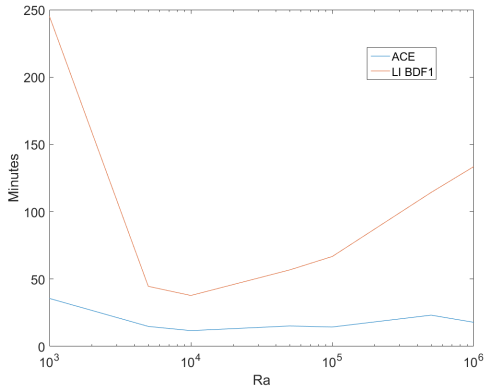

Figure 4.4: Time: ACE vs. linearly implicit BDF1, double pane problem.

4.2.7.5 EXPLORATION OF PREDICTABILITY We now illustrate the usefulness of ensembles regarding the predictability of buoyancy-driven flows. Marsigli flow (or the lock-exchange problem), considered in [85, 6, 105], is generated by the force due to gravity acting on a domain containing fluids of varying density (and hence, by the Boussinesq assumption, temperature). The mixture of the hot and cold fluids exhibits a shear flow resulting in a Kelvin-Helmholtz instability. For this test problem, we rewrite the Boussinesq system as

$$\begin{aligned}
\partial_t u_j + (u_j \cdot \nabla) u_j + \frac{1}{2} (\nabla \cdot u_j) u_j - \frac{1}{\mathrm{Re}} \Delta u_j + \nabla p_j &= \mathrm{Ri} \xi T_j + f_j \\
\nabla \cdot u_j &= 0 \\
\partial_t T_j + (u_j \cdot \nabla) T_j + \frac{1}{2} (\nabla \cdot u_j) T_j - \frac{1}{\mathrm{ReRi}} \Delta T_j &= g_j,
\end{aligned}$$

where Re, Ri are the Reynolds and Richardson numbers, respectively. Let $\Omega = (0, 8) \times (0, 1)$ and $\mathrm{Ri} = 4.0$. Plots of the flow for $\mathrm{Re} = 5000$ at two second intervals (over eight seconds) at a resolution of 2048×256 are given in Figure 4.5. We let the timestep in this simulation be $\Delta t = 0.0005$. Note the similarity of the plots with those in the literature.

We choose a timestep of $\Delta t = 0.005$ and a final time of $t^* = 8$. Correspondingly, we let $\varepsilon = \Delta t$. We assume the flow starts at rest ($u^0 = 0$) and that the velocity is endowed with noslip boundary conditions. To create the shear flow, we define the temperature $T \equiv 1.5$ for $x \leq 4$ and $T \equiv 1.0$ for $x > 4$ at $t = 0$. As the flow is buoyancy-driven, there are no external forces or heat sources. Using the initial condition for the temperature, we also calculate p^0. The test below is run for $\mathrm{Re} = \{1000, 5000, 10000\}$, each on a Delaunay triangulation of Ω with resolution 1024×128. We also generate two ensemble members for each Reynolds number via the BV algorithm. Finally, we utilize the following definitions of energy, variance, and average effective Lyapunov exponent [7]: The energy is given by

$$E := \|T\| + \frac{1}{2} \|u\|^2;$$

the variance of χ is

$$\mathrm{Var}(\chi) := \langle \|\chi\|^2 \rangle - \|\langle \chi \rangle\|^2 = \langle \|\chi'\|^2 \rangle;$$

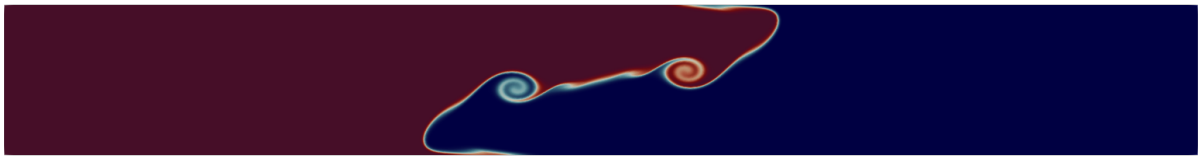

(a) $t = 2$

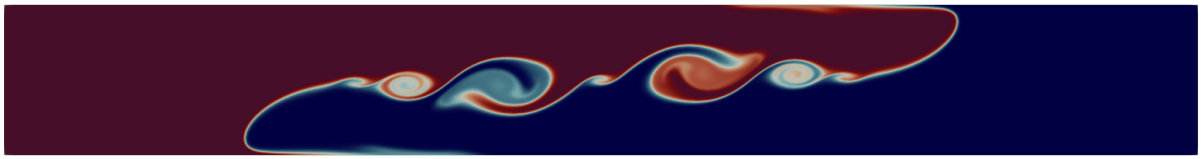

(b) $t = 4$

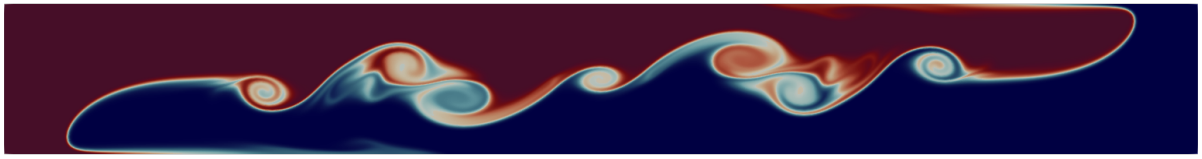

(c) $t = 6$

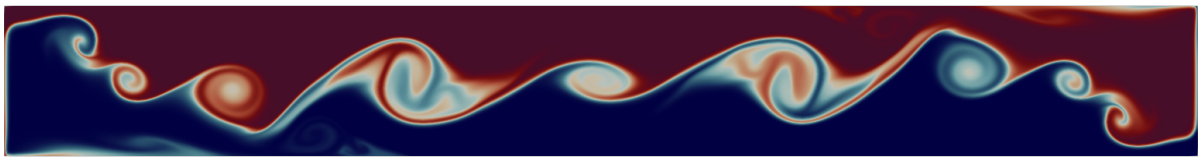

(d) $t = 8$

Figure 4.5: Marsigli flow at Re = 5000.

the relative energy fluctuation is

$$r(t) := \frac{\|\chi_+ - \chi_-\|^2}{\|\chi_+\|\|\chi_-\|},$$

and the average effective Lyapunov exponent over $0 < \tau \leq t^*$ is

$$\gamma_\tau(t) := \frac{1}{2\tau} \log\big(\frac{r(t+\tau)}{r(t)}\big),$$

with $0 < t + \tau \leq t^*$.

Figure 4.6 presents the energy of the approximate solutions with varying Re and the unperturbed solution at the same resolution. Variance is presented in Figure 4.8, and the relative energy fluctuation is given in Figure 4.7. In all cases, the ensemble average and unperturbed energy are in close agreement. Figures 4.8 and 4.7 show that the perturbed velocity and temperature solutions deviate significantly from the unperturbed solution with increasing Re, whereas the pressure solutions seem to be in close agreement. Moreover, the figure indicates that small perturbations in the initial conditions yield unreliable velocity and temperature distributions near the end of the simulation.

The average effective Lyapunov exponents are presented in Figure 4.9. We see that γ_τ is positive for the temperature (indicating finite time flow predictability), whereas the situation complicates for the velocity and pressure. The velocity appears predictable over the first four seconds for all but large enough τ in the simulation. The Lyapunov exponents of the pressure, however, exhibit periodic behavior that indicates predictability for some values of τ and unpredictability for others. For all three solutions, the exponents become increasingly larger (reduced predictability) with increasing Ra. These exponents are in line with the plots for variance, see Figure 4.8.

To see whether the timestep size can improve the fidelity and predictability of the ensemble average, we next present plots of the flow at Re = 5000 in two second intervals for $\Delta t = 0.005$ against $\Delta t = 0.0005$ in Figure 4.10. There are differences in the plots: symmetry of the flow appears to break between $t = 4$ and $t = 6$ for the larger timestep; however, the run with the smaller timestep seems to be in line with the simulation given in Figure 4.5.

Figures 4.11–4.13 show the energy, energy fluctuation, variance, and Lyapunov exponent comparison between the flow run for Re = 5000 and $\Delta t = 0.0005$. The plots are similar to

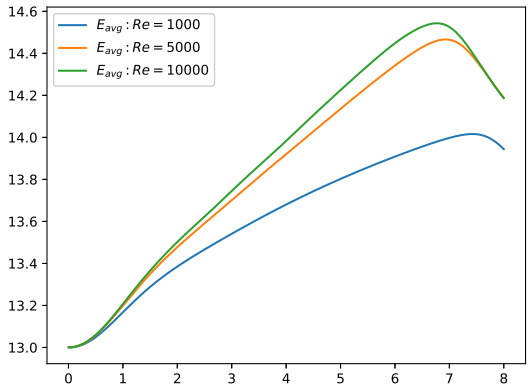

(a) Average energy (2 ensemble members)

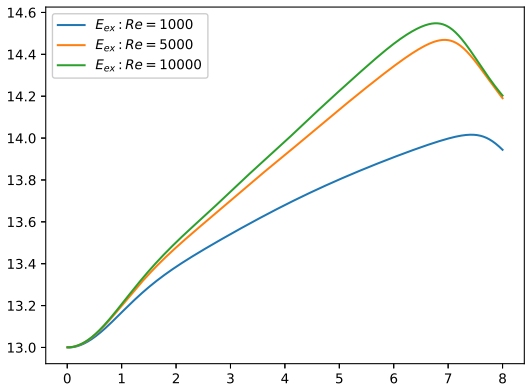

(b) Energy for unperturbed solution

Figure 4.6: Energy in the system for varying Re.

those in Figures 4.6–4.9. Figure 4.11 shows the energy profile of the ensemble average versus the unperturbed solution are almost identical, and the energy fluctuation profiles are very similar to those in Figure 4.7. Figure 4.12 shows variance profiles also similar to those in Figure 4.8; interestingly, the velocity variance appears much more oscillatory in this case. Finally, the average Lyapunov exponent plots are given in Figure 4.13. They appear to be in agreement with the plots in Figure 4.9.

4.2.8 AN AC ENSEMBLE SCHEME FOR VARIABLE TIMESTEPS

In the previous section, we constructed, analyzed, and tested an artificial compressibility ensemble (ACE) scheme for constant timesteps. Now, we extend the analysis for variable timesteps. Let $[0, t^*]$ be a time interval, and consider a partition $0 = t_0 < t_1 < \cdots < t_{N-1} < t_N = t^*$ with n^{th} timestep $\Delta t_n = t_n - t_{n-1}$. Further, consider a transient AC parameter $\varepsilon = \varepsilon(t)$, and let $\varepsilon_n := \varepsilon(t_n)$. We consider an adaptive artificial compressility ensemble method for the Boussinesq equations (4.1)–(4.3), given by

$$\frac{u_j^{n+1} - u_j^n}{\Delta t_{n+1}} + (\langle u \rangle^n \cdot \nabla) u_j^{n+1} + \frac{1}{2} (\nabla \cdot \langle u \rangle^n) u_j^{n+1}$$

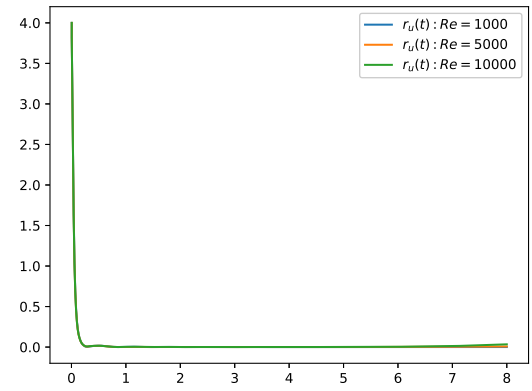

(a) Velocity

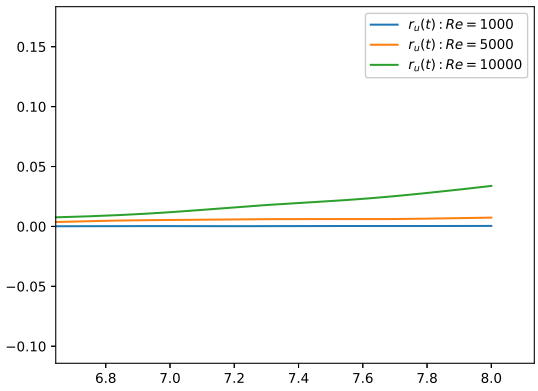

(b) Velocity (near $t = 8$)

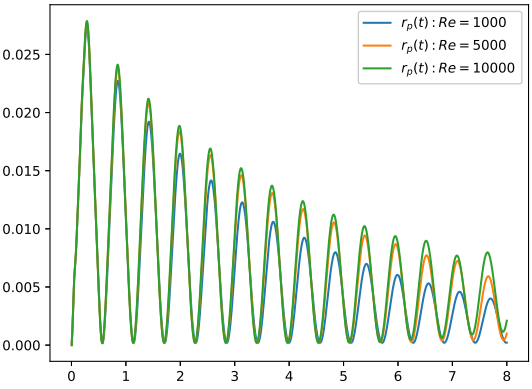

(c) Pressure

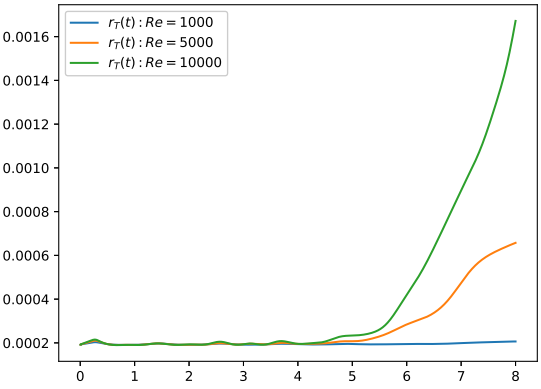

(d) Temperature

Figure 4.7: Energy fluctuation of u, p, and T for varying Re.

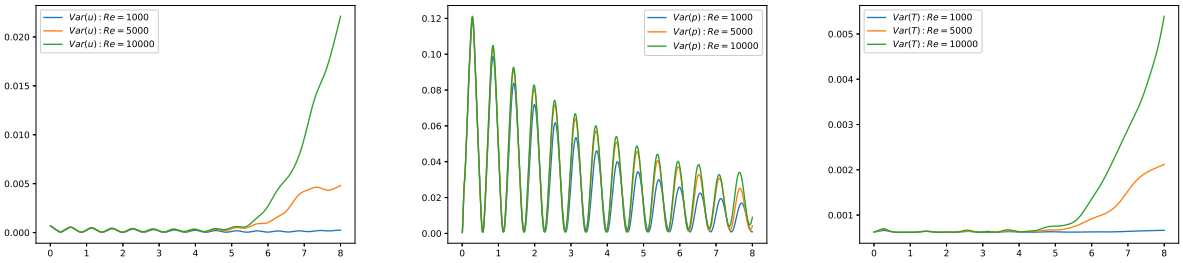

(a) Velocity (b) Pressure (c) Temperature

Figure 4.8: Variance of u, p, and T for varying Re.

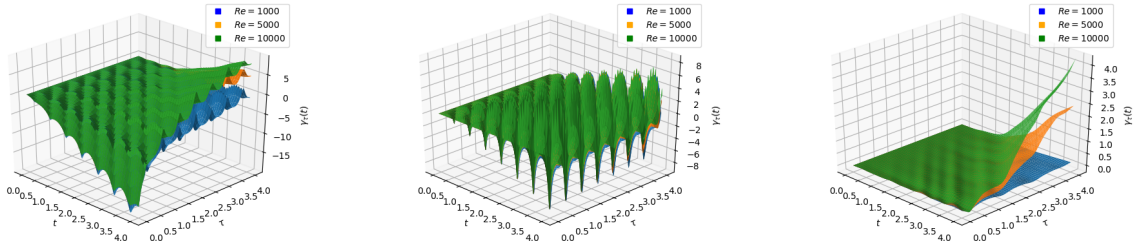

(a) Velocity (b) Pressure (c) Temperature

Figure 4.9: $\gamma_\tau(t)$ of u, p, and T for varying Re.

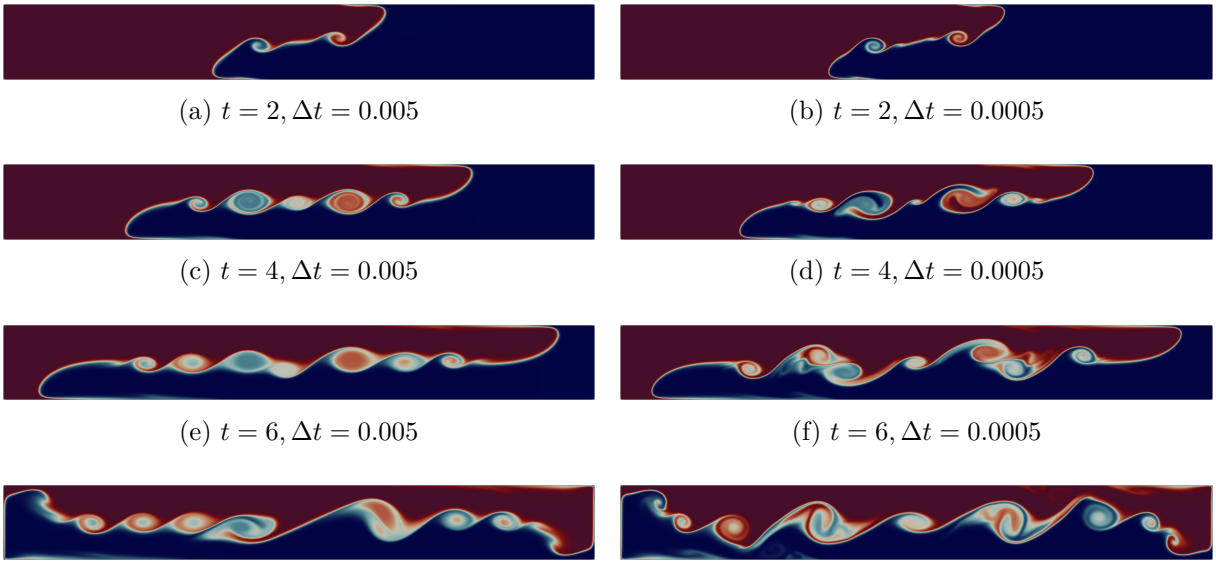

(a) $t = 2, \Delta t = 0.005$ (b) $t = 2, \Delta t = 0.0005$

(c) $t = 4, \Delta t = 0.005$ (d) $t = 4, \Delta t = 0.0005$

(e) $t = 6, \Delta t = 0.005$ (f) $t = 6, \Delta t = 0.0005$

(g) $t = 8, \Delta t = 0.005$ (h) $t = 8, \Delta t = 0.0005$

Figure 4.10: Marsigli flow at $\mathrm{Re} = 5000$ for different Δt.

$$
\begin{aligned}
+(u_j'^n \cdot \nabla)u_j^n + \frac{1}{2}\left(\nabla \cdot u_j'^n\right)u_j^n - \mathrm{Pr}\Delta u_j^{n+1} + \nabla p_j^{n+1} &= \mathrm{PrRa}\xi T_j^n + f_j^{n+1}, \\
\frac{\varepsilon_{n+1}p_j^{n+1} - \widehat{\varepsilon}p_j^n}{\Delta t_{n+1}} + \nabla \cdot u_j^{n+1} &= 0, \\
\frac{T_j^{n+1} - T_j^n}{\Delta t_{n+1}} + (\langle u \rangle^n \cdot \nabla)T_j^{n+1} + \frac{1}{2}\left(\nabla \cdot \langle u \rangle^n\right)T_j^{n+1} & \\
+(u_j'^n \cdot \nabla)T_j^n + \frac{1}{2}\left(\nabla \cdot u_j'^n\right)T_j^n - \Delta T_j^{n+1} &= g_j^{n+1},
\end{aligned}
\tag{4.40}
$$

where $\widehat{\varepsilon} = \sqrt{\varepsilon_{n+1}\varepsilon_n}$ or $\widehat{\varepsilon} = \min\{\varepsilon_{n+1}, \varepsilon_n\}$. We present a stability result for the fully discrete adaptive ACE scheme.

Theorem 13. *Let $f_j \in L^2(0, t^*; H^{-1}(\Omega)^d)$, $g_j \in L^2(0, t^*; H^{-1}(\Omega))$ with appropriate initial conditions for the velocity, pressure, and temperature. If the scheme* (4.40) *satisfies the condition*

$$
\frac{C_\dagger}{h}\max_n \Delta t_n \max_{1 \le j \le J} \|\nabla u_{j,h}'^n\|^2 \le 1, \tag{4.41}
$$

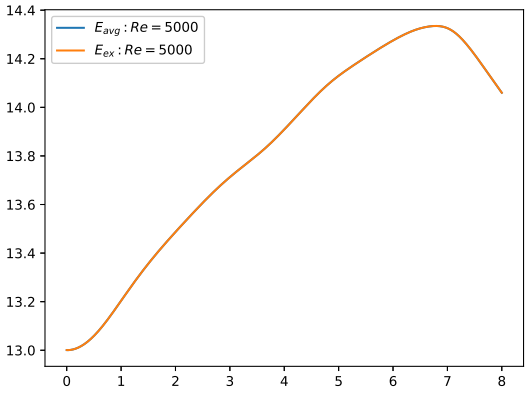

(a) Average energy (2 ensemble members) and exact energy

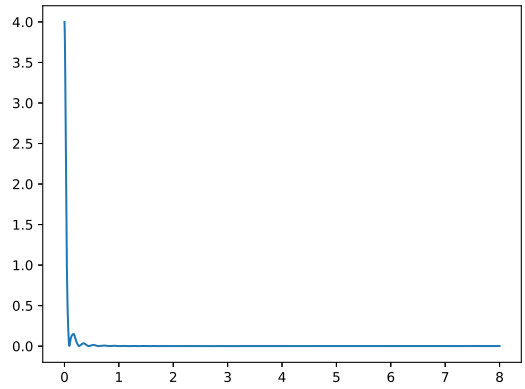

(b) Velocity

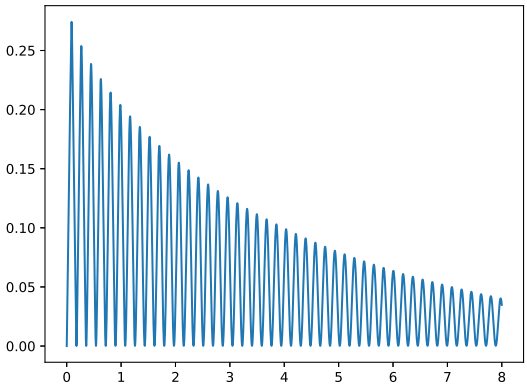

(c) Pressure

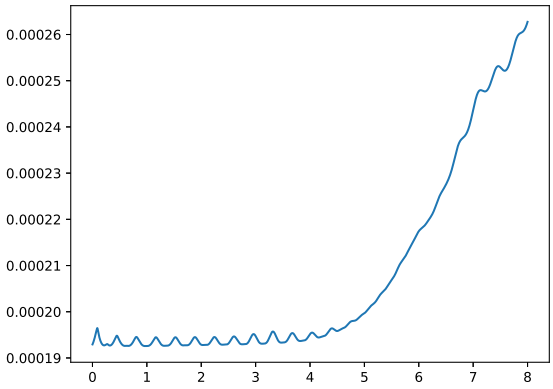

(d) Temperature

Figure 4.11: Energy and fluctuation in the system for $\mathrm{Re} = 5000, \Delta t = 0.0005$.

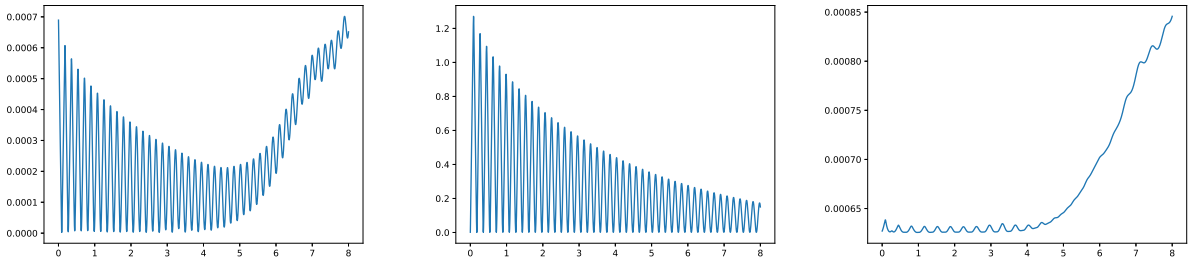

(a) Velocity (b) Pressure (c) Temperature

Figure 4.12: Variance of u, p, and T for $\mathrm{Re} = 5000, \Delta t = 0.0005$.

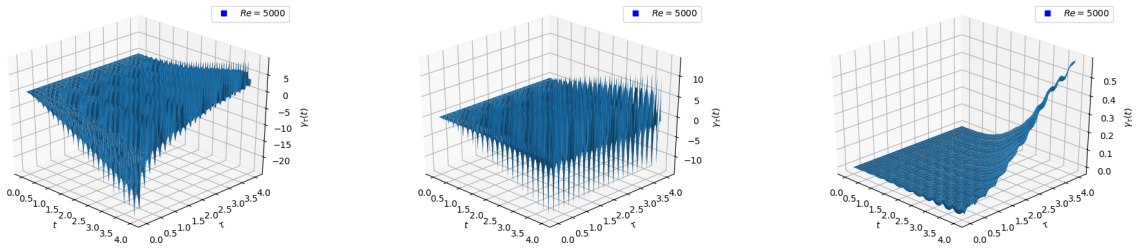

(a) Velocity (b) Pressure (c) Temperature

Figure 4.13: Average effective Lyapunov exponents of u, p, and T for $\mathrm{Re} = 5000, \Delta t = \frac{1}{2000}$.

then the stability bounds for the min-Method

$$\|u_{j,h}^N\|^2 + \|T_{j,h}^N\|^2 + \varepsilon_N\|p_{j,h}^N\|^2 + \frac{1}{2}\sum_{n=0}^{N-1}\Big(\|u_{j,h}^{n+1} - u_{j,h}^n\|^2 + \|T_{j,h}^{n+1} - T_{j,h}^n\|^2$$
$$+ \min\{\varepsilon_{n+1}, \varepsilon_n\}\|p_{j,h}^{n+1} - p_{j,h}^n\|^2 + (\varepsilon_{n+1} - \varepsilon_n)^+\|p_{j,h}^{n+1}\|^2 + (\varepsilon_n - \varepsilon_{n+1})^+\|p_{j,h}^n\|^2\Big)$$
$$+\frac{Pr}{2}|||\nabla u_{j,h}|||_{2,0}^2 + \frac{1}{2}|||\nabla T_{j,h}|||_{2,0}^2 \le \|u_{j,h}^0\|^2 + \|T_{j,h}^0\|^2 + \varepsilon_0\|p_{j,h}^0\|^2$$
$$+\frac{2}{Pr}|||f_j|||_{2,-1}^2 + 2PrRa^2C_{pf,1}C_T$$

and the GA-Method

$$\|u_{j,h}^N\|^2 + \|T_{j,h}^N\|^2 + \varepsilon_N\|p_{j,h}^N\|^2 + \frac{1}{2}\sum_{n=0}^{N-1}\Big(\|u_{j,h}^{n+1} - u_{j,h}^n\|^2 + \|T_{j,h}^{n+1} - T_{j,h}^n\|^2$$
$$+\|\sqrt{\varepsilon_{n+1}}p_{j,h}^{n+1} - \sqrt{\varepsilon_n}p_{j,h}^n\|^2\Big) + \frac{Pr}{2}|||\nabla u_{j,h}|||_{2,0}^2 + \frac{1}{2}|||\nabla T_{j,h}|||_{2,0}^2$$
$$\le \|u_{j,h}^0\|^2 + \|T_{j,h}^0\|^2 + \varepsilon_0\|p_{j,h}^0\|^2 + \frac{2}{Pr}|||f_j|||_{2,-1}^2 + 2PrRa^2C_{pf,1}C_T$$

hold.

Proof. The proof of stability follows in much the same way as the constant timestep case. We take an inner product of the temperature equation with $S_h = 2\Delta t_{n+1}T_{j,h}^{n+1}$ in (4.9) and get

$$\|T_{j,h}^{n+1}\|^2 - \|T_{j,h}^n\|^2 + \|T_{j,h}^{n+1} - T_{j,h}^n\|^2 + 2\Delta t_{n+1}\|\nabla T_{j,h}^{n+1}\|^2$$
$$= 2\Delta t_{n+1}(g_j^{n+1}, T_{j,h}^{n+1}) - 2\Delta t_{n+1}b_T(u_{j,h}'^n, T_{j,h}^n, T_{j,h}^{n+1}).$$

We have, by the definition of the dual norm, Cauchy-Schwarz-Young inequality, and the estimates for the nonlinear term (see Lemma 1 and the inverse inequality)

$$2\Delta t_{n+1}(g_j^{n+1}, T_{j,h}^{n+1}) \le \Delta t_{n+1}\|g_j^{n+1}\|_{-1}^2 + \Delta t_{n+1}\|\nabla T_{j,h}^{n+1}\|^2,$$
$$-2\Delta t_{n+1}b_T(u_{j,h}'^n, T_{j,h}^n, T_{j,h}^{n+1}) = -2\Delta t_{n+1}b_T(u_{j,h}'^n, T_{j,h}^{n+1}, T_{j,h}^{n+1} - T_{j,h}^n)$$
$$\le 2\Delta t_{n+1}C_{3,T}\|\nabla u_{j,h}'^n\|\|\nabla T_{j,h}^{n+1}\|\sqrt{\|T_{j,h}^{n+1} - T_{j,h}^n\|\|\nabla(T_{j,h}^{n+1} - T_{j,h}^n)\|}$$
$$\le \frac{2\Delta t_{n+1}C_{3,T}\sqrt{C_{\text{inv},2}}}{\sqrt{h}}\|\nabla u_{j,h}'^n\|\|\nabla T_{j,h}^{n+1}\|\|T_{j,h}^{n+1} - T_{j,h}^n\|$$
$$\le \frac{2\Delta t_{n+1}^2C_{3,T}^2C_{\text{inv},2}}{h}\|\nabla u_{j,h}'^n\|^2\|\nabla T_{j,h}^{n+1}\|^2 + \frac{1}{2}\|T_{j,h}^{n+1} - T_{j,h}^n\|^2.$$

Therefore, we have the bound

$$\|T_{j,h}^{n+1}\|^2 - \|T_{j,h}^n\|^2 + \frac{1}{2}\|T_{j,h}^{n+1} - T_{j,h}^n\|^2$$
$$+\Delta t_{n+1}\left(1 - \frac{2\Delta t_{n+1}C_{3,T}^2 C_{\text{inv},2}}{h}\|\nabla u_{j,h}'^n\|^2\right)\|\nabla T_{j,h}^{n+1}\|^2 \leq \Delta t\|g_j^{n+1}\|_{-1}^2.$$

We get a bound of the type $\|T_{j,h}^m\|^2 \leq C_T$ after summing from $n = 0$ to $N-1$ and using condition (4.41).

We continue by using the results from Chapter 3: By (3.56) and the estimate for the GA-method, we have

$$(\varepsilon_{n+1}p_{j,h}^{n+1} - \min\{\varepsilon_{n+1}, \varepsilon_n\}p_{j,h}^n, p_{j,h}^{n+1}) =$$
$$= \frac{1}{2}\varepsilon_{n+1}\|p_{j,h}^{n+1}\|^2 - \frac{1}{2}\varepsilon_n\|p_{j,h}^n\|^2 + \frac{1}{2}\min\{\varepsilon_{n+1}, \varepsilon_n\}\|p_{j,h}^{n+1} - p_{j,h}^n\|^2$$
$$+\frac{1}{2}\left(\varepsilon_{n+1} - \varepsilon_n\right)^+\|p_{j,h}^{n+1}\|^2 + \frac{1}{2}\left(\varepsilon_n - \varepsilon_{n+1}\right)^+\|p_{j,h}^n\|^2,$$
$$(\varepsilon_{n+1}p_{j,h}^{n+1} - \sqrt{\varepsilon_{n+1}\varepsilon_n}p_{j,h}^n, p_{j,h}^{n+1})$$
$$= \frac{1}{2}\varepsilon_{n+1}\|p_{j,h}^{n+1}\|^2 - \frac{1}{2}\varepsilon_n\|p_{j,h}^n\|^2 + \frac{1}{2}\|\sqrt{\varepsilon_{n+1}}p_{j,h}^{n+1} - \sqrt{\varepsilon_n}p_{j,h}^n\|^2.$$

Clearly, these telescope and contribute numerical dissipation to the method. Letting (v_h, q_h) $= (2\Delta t_{n+1}u_{j,h}^{n+1}, 2\Delta t_{n+1}p_{j,h}^{n+1}) \in (V_h, Q_h)$ gives, for the min-Method

$$\left(\|u_{j,h}^{n+1}\|^2 + \varepsilon_{n+1}\|p_{j,h}^{n+1}\|^2\right) - \left(\|u_{j,h}^n\|^2 + \varepsilon_n\|p_{j,h}^n\|^2\right) + \|u_{j,h}^{n+1} - u_{j,h}^n\|^2$$
$$+\min\{\varepsilon_{n+1}, \varepsilon_n\}\|p_{j,h}^{n+1} - p_{j,h}^n\|^2 + (\varepsilon_{n+1} - \varepsilon_n)^+\|p_{j,h}^{n+1}\|^2 + (\varepsilon_n - \varepsilon_{n+1})^+\|p_{j,h}^n\|^2$$
$$+2\Delta t_{n+1}\text{Pr}\|\nabla u_{j,h}^{n+1}\|^2 = 2\Delta t_{n+1}\text{PrRa}(\xi T_{j,h}^n, u_{j,h}^{n+1}) + 2\Delta t_{n+1}(f_j^{n+1}, u_{j,h}^{n+1})$$
$$-2\Delta t_{n+1}b_u(u_{j,h}'^n, u_{j,h}^n, u_{j,h}^{n+1}).$$

and, for the GA-Method,

$$\left(\|u_{j,h}^{n+1}\|^2 + \varepsilon_{n+1}\|p_{j,h}^{n+1}\|^2\right) - \left(\|u_{j,h}^n\|^2 + \varepsilon_n\|p_{j,h}^n\|^2\right) + \|u_{j,h}^{n+1} - u_{j,h}^n\|^2$$
$$+\|\sqrt{\varepsilon_{n+1}}p_{j,h}^{n+1} - \sqrt{\varepsilon_n}p_{j,h}^n\|^2 + 2\Delta t_{n+1}\text{Pr}\|\nabla u_{j,h}^{n+1}\|^2 = 2\Delta t_{n+1}\text{PrRa}(\xi T_{j,h}^n, u_{j,h}^{n+1})$$
$$+2\Delta t_{n+1}(f_j^{n+1}, u_{j,h}^{n+1}) - 2\Delta t_{n+1}b_u(u_{j,h}'^n, u_{j,h}^n, u_{j,h}^{n+1}).$$

By the Poincaré-Friedrichs inequality, the Cauchy-Schwarz-Young inequality, and the temperature bound (4.14), we have

$$2\Delta t_{n+1}\mathrm{PrRa}(\xi T_{j,h}^n, u_{j,h}^{n+1}) \leq 2\Delta t_{n+1}\mathrm{PrRa}^2 C_{\mathrm{pf},1}^2 C_T + \frac{\Delta t_{n+1}\mathrm{Pr}}{2}\|\nabla u_{j,h}^{n+1}\|^2.$$

The forcing and nonlinear terms are treated in a similar manner to the temperature case, giving the bounds

$$\begin{aligned}
2\Delta t_{n+1}(f_j^{n+1}, u_{j,h}^{n+1}) &\leq \frac{2\Delta t_{n+1}}{\mathrm{Pr}}\|f_{j,h}^{n+1}\|_{-1}^2 + \frac{\Delta t_{n+1}\mathrm{Pr}}{2}\|\nabla u_{j,h}^{n+1}\|^2, \\
-2\Delta t_{n+1} b_u(u_{j,h}'^n, u_{j,h}^n, u_{j,h}^{n+1}) &\leq \frac{2\Delta t_{n+1}^2 C_{3,u}^2 C_{\mathrm{inv},1}}{h}\|\nabla u_{j,h}'^n\|^2\|\nabla u_{j,h}^{n+1}\|^2 + \frac{1}{2}\|u_{j,h}^{n+1} - u_{j,h}^n\|^2.
\end{aligned}$$

Adding and using the bounds yields, for the min-Method,

$$\begin{aligned}
&\left(\|u_{j,h}^{n+1}\|^2 + \|T_{j,h}^{n+1}\|^2 + \varepsilon_{n+1}\|p_{j,h}^{n+1}\|^2\right) - \left(\|u_{j,h}^n\|^2 + \|T_{j,h}^n\|^2 + \varepsilon_n\|p_{j,h}^n\|^2\right) + \frac{1}{2}\|u_{j,h}^{n+1} - u_{j,h}^n\|^2 \\
&\quad + \frac{1}{2}\|T_{j,h}^{n+1} - T_{j,h}^n\|^2 + \min\{\varepsilon_{n+1}, \varepsilon_n\}\|p_{j,h}^{n+1} - p_{j,h}^n\|^2 + \frac{1}{2}\|T_{j,h}^{n+1} - T_{j,h}^n\|^2 \\
&\quad + (\varepsilon_{n+1} - \varepsilon_n)^+\|p_{j,h}^{n+1}\|^2 + (\varepsilon_n - \varepsilon_{n+1})^+\|p_{j,h}^n\|^2 \\
&\quad + \Delta t_{n+1}\left(\mathrm{Pr} - \frac{2\Delta t_{n+1} C_{3,u}^2 C_{\mathrm{inv},1}}{h}\|\nabla u_{j,h}'^n\|^2\right)\|\nabla u_{j,h}^{n+1}\|^2 \\
&\quad + \Delta t_{n+1}\left(1 - \frac{2\Delta t_{n+1} C_{3,T}^2 C_{\mathrm{inv},2}}{h}\|\nabla u_{j,h}'^n\|^2\right)\|\nabla T_{j,h}^{n+1}\|^2 \\
&\quad \leq \frac{2\Delta t_{n+1}}{\mathrm{Pr}}\|f_j^{n+1}\|_{-1}^2 + 2\Delta t_{n+1}\mathrm{PrRa}^2 C_{\mathrm{pf},1} C_T
\end{aligned}$$

and, for the GA-Method,

$$\begin{aligned}
&\left(\|u_{j,h}^{n+1}\|^2 + \|T_{j,h}^{n+1}\|^2 + \varepsilon_{n+1}\|p_{j,h}^{n+1}\|^2\right) - \left(\|u_{j,h}^n\|^2 + \|T_{j,h}^n\|^2 + \varepsilon_n\|p_{j,h}^n\|^2\right) + \frac{1}{2}\|u_{j,h}^{n+1} - u_{j,h}^n\|^2 \\
&\quad + \frac{1}{2}\|T_{j,h}^{n+1} - T_{j,h}^n\|^2 + \|\sqrt{\varepsilon_{n+1}}p_{j,h}^{n+1} - \sqrt{\varepsilon_n}p_{j,h}^n\|^2 + \frac{1}{2}\|T_{j,h}^{n+1} - T_{j,h}^n\|^2 \\
&\quad + \Delta t_{n+1}\left(\mathrm{Pr} - \frac{2\Delta t_{n+1} C_{3,u}^2 C_{\mathrm{inv},1}}{h}\|\nabla u_{j,h}'^n\|^2\right)\|\nabla u_{j,h}^{n+1}\|^2 \\
&\quad + \Delta t_{n+1}\left(1 - \frac{2\Delta t_{n+1} C_{3,T}^2 C_{\mathrm{inv},2}}{h}\|\nabla u_{j,h}'^n\|^2\right)\|\nabla T_{j,h}^{n+1}\|^2 \\
&\quad \leq \frac{2\Delta t_{n+1}}{\mathrm{Pr}}\|f_j^{n+1}\|_{-1}^2 + 2\Delta t_{n+1}\mathrm{PrRa}^2 C_{\mathrm{pf},1} C_T.
\end{aligned}$$

Set now $C_\dagger = \min\{\frac{4C_{3,u}^2 C_{\text{inv},1}}{\text{Pr}}, 4C_{3,T}^2 C_{\text{inv},2}\}$. Then, condition (4.41) is satisfied. Summing from $n = 0$ to $N-1$ gives the bound

$$\|u_{j,h}^N\|^2 + \|T_{j,h}^N\|^2 + \varepsilon_N\|p_{j,h}^N\|^2 + \frac{1}{2}\sum_{n=0}^{N-1}\Big(\|u_{j,h}^{n+1} - u_{j,h}^n\|^2 + \|T_{j,h}^{n+1} - T_{j,h}^n\|^2$$
$$+ \min\{\varepsilon_{n+1}, \varepsilon_n\}\|p_{j,h}^{n+1} - p_{j,h}^n\|^2 + (\varepsilon_{n+1} - \varepsilon_n)^+\|p_{j,h}^{n+1}\|^2 + (\varepsilon_n - \varepsilon_{n+1})^+\|p_{j,h}^n\|^2\Big)$$
$$+\frac{\text{Pr}}{2}|||\nabla u_{j,h}|||_{2,0}^2 + \frac{1}{2}|||\nabla T_{j,h}|||_{2,0}^2 \le \|u_{j,h}^0\|^2 + \|T_{j,h}^0\|^2 + \varepsilon_0\|p_{j,h}^0\|^2$$
$$+\frac{2}{\text{Pr}}|||f_j|||_{2,-1}^2 + 2\text{PrRa}^2 C_{\text{pf},1}C_T$$

for the min-Method, and

$$\|u_{j,h}^N\|^2 + \|T_{j,h}^N\|^2 + \varepsilon_N\|p_{j,h}^N\|^2 + \frac{1}{2}\sum_{n=0}^{N-1}\Big(\|u_{j,h}^{n+1} - u_{j,h}^n\|^2 + \|T_{j,h}^{n+1} - T_{j,h}^n\|^2$$
$$+\|\sqrt{\varepsilon_{n+1}}p_{j,h}^{n+1} - \sqrt{\varepsilon_n}p_{j,h}^n\|^2\Big) + \frac{\text{Pr}}{2}|||\nabla u_{j,h}|||_{2,0}^2 + \frac{1}{2}|||\nabla T_{j,h}|||_{2,0}^2$$
$$\le \|u_{j,h}^0\|^2 + \|T_{j,h}^0\|^2 + \varepsilon_0\|p_{j,h}^0\|^2 + \frac{2}{\text{Pr}}|||f_j|||_{2,-1}^2 + 2\text{PrRa}^2 C_{\text{pf},1}C_T$$

for the GA-Method. □

4.3 CONCLUSIONS

For physical phenomena with inherent uncertainties, e.g., atmospheric flow, ensemble simulations are essential to glean valuable statistics from the numerical experiments and to extend the predictability horizon. Due to computational constraints, e.g., memory restrictions, the number of realizations that can be considered is limited. Thus, methods that are fast and save memory are essential to extending the predictability horizon. Furthermore, time adaptive algorithms are efficient and easily programmable, making the numerical schemes even faster. In this chapter, we have constructed ensemble schemes that solve all three problems: they are fast, efficient, and save memory.

The methods use a nonlinear splitting technique that results in a shared coefficient matrix for each realization solved, reducing the number of matrices that need to loaded and stored in RAM from J to 1. Furthermore, the fact that the coefficient matrix is shared allows the use

of efficient block solvers. To speed up the computations and circumvent the velocity/pressure coupling, we employ for use in our schemes artificial compressibility. Our numerical tests, summarized in Section 4.2.7, show a speed increase factor of 3–8 times versus a typical coupled numerical method. The constant timestep method is also robust, and can be used for predictability studies (see Section 4.2.7). Finally, we extend our method to the variable timestep case and prove stability of the algorithm.

5.0 ONE-EQUATION URANS MODELS WITH KINEMATIC MIXING LENGTH

5.1 INTRODUCTION

URANS (*unsteady Reynolds averaged Navier-Stokes*) models of turbulence are derived commonly to produce a velocity, $v(x,t) \simeq \overline{u}(x,t)$, that approximates a finite time window average of the Navier-Stokes velocity $u(x,t)$

$$\overline{u}(x,t) = \frac{1}{\tau}\int_{t-\tau}^{t} u(x,t')dt'. \tag{5.1}$$

We note that URANS models are also constructed ad hoc simply by adding $\frac{\partial v}{\partial t}$ to a RANS model without regard to where the term originates. Formulation via averaging over a finite time window is a coherent source for the term. From this connection flows 5 fundamental conditions (listed below) that a coherent URANS model should satisfy and that few do. Herein we delineate these conditions and show that, for the standard 1-equation model, a new kinematic turbulence length scale results in a simpler model satisfying 4 of the 5.

The first condition is a simple observation that the time window τ should influence the model, as $\tau \to 0$ the model should revert to the NSE (Navier-Stokes equations) and as τ increases, more time scales are filtered and thus the eddy viscosity should increase.

Condition 1: *The filter window τ should appear as a model parameter. As $\tau \to 0$ the model reverts to the NSE. As τ increases, the model eddy viscosity $\nu_T(\cdot)$ increases.*

We consider herein 1-equation models of turbulence. These have deficiencies but nevertheless include models considered to have good predictive accuracy and low cost, e.g., Spalart [117] and Figure 2 p.8 in Xiao and Cinnella [144]. The standard 1-equation model (from which all have evolved), introduced by Prandtl [99], is

$$\begin{aligned} v_t + v\cdot\nabla v - \nabla\cdot\left(\left[2\nu + \mu l\sqrt{k}\right]\nabla^s v\right) + \nabla p &= f(x), \\ \nabla\cdot v &= 0, \\ k_t + v\cdot\nabla k - \nabla\cdot\left(\left[\nu + \mu l\sqrt{k}\right]\nabla k\right) + \frac{1}{l}k\sqrt{k} &= \mu l\sqrt{k}|\nabla^s v|^2. \end{aligned} \tag{5.2}$$

Briefly, $p(x,t)$ is a pressure, $f(x)$ is a smooth, divergence free ($\nabla \cdot f = 0$) body force, $\mu \simeq 0.55$ is a calibration parameter, $\nabla^s v = (\nabla v + \nabla^T v)/2$ is the deformation tensor, and $k(x,t)$ is the model approximation to the fluctuations' kinetic energy distribution, $\frac{1}{2}|(u-\overline{u})(x,t)|^2$. Pope [98] calculates the value $\mu = 0.55$ from the ($3d$) law of the wall. An analogy with the kinetic theory of gasses (for which $\nu_T = \frac{1}{3} lU$) yields the value $\mu = \frac{1}{3}\sqrt{2/d}$ which gives $\mu \simeq 0.33$ in 2d and $\mu \simeq 0.27$ in $3d$, Davidson [22] p. 114, eqn. (4.11a). The eddy viscosity coefficient

$$\nu_T(\cdot) = \mu l \sqrt{k}$$

(the Prandtl-Kolmogorov formula) is a dimensionally consistent expression of the observed increase of mixing with turbulence and of the physical idea of Saint-Venant [104] that this mixing increases with "*the intensity of the whirling agitation*," [21], p.235. The k-equation describes the turbulent kinetic energy evolution; see [10] p.99, Section 4.4, [22], [92] p.60, Section 5.3 or [98] p.369, Section 10.3, for a derivation. The model (5.2) holds in a flow domain Ω with initial conditions, $v(x,0)$ and $k(x,0)$, and (here $L-$periodic or no-slip) v, k boundary conditions on the boundary $\partial\Omega$.

The parameter of interest herein is the turbulence length-scale $l = l(x)$, first postulated by Taylor in 1915 [126]. It varies from model to model, flow subregion to subregion (requiring fore knowledge of their locations, [117]) and must be specified by the user; see [140] for many examples of how $l(x)$ is chosen in various subregions. The simplest case is channel flow for which

$$l_0(x) = \min\{0.41y, 0.082\mathrm{Re}^{-1/2}\}$$

where y is the wall normal distance, Wilcox [140] Ch. 3, eqn. (3.99) p.76.

Model solutions are approximations to averages of velocities of the incompressible Navier-Stokes equations. Other fundamental physical properties of NSE solutions (inherited by averages) should also be preserved by the model. These properties include:

Condition 2: *The turbulence length-scale $l(x)$ must $l(x) \to 0$ as $x \to$ walls.*

Condition 2 follows since the eddy viscosity term approximates the Reynolds stresses and

$$\mu l \sqrt{k} \nabla^s v \simeq u'u' \text{ which } \to 0 \text{ at walls like } \mathcal{O}(\textit{wall-distance}^2).$$

Specifications of $l(x)$ violating this are often observed to over-dissipate solutions (in many tests and now with mathematical support [96]).

Condition 3: *(Finite kinetic energy) The model's representation of the total kinetic energy in the fluid must be uniformly bounded in time:*

$$\int_\Omega \frac{1}{2}|v(x,t)|^2 + k(x,t)dx \leq C < \infty \text{ uniformly in time.}$$

The kinetic energy (per unit volume) $\frac{1}{|\Omega|}\int \frac{1}{2}|u|^2 dx$, is distributed between means and fluctuations in the model as

$$\frac{1}{|\Omega|}\int_\Omega \frac{1}{2}|v(x,t)|^2 + k(x,t)dx \simeq \frac{1}{|\Omega|}\int_\Omega \frac{1}{2}|u(x,t)|^2 dx < \infty.$$

This property for the NSE represents the physical fact that bounded energy input does not grow to unbounded energy solutions.

Condition 4: *(Time-averaged statistical equilibrium) The time average of the model's total energy dissipation rate, $\varepsilon_{\text{model}}$ (5.4) below, should be at most the time average energy input rate:*

$$\limsup_{t^*\to\infty} \frac{1}{t^*}\int_0^{t^*} \varepsilon_{\text{model}}(t)dt \leq C\frac{U^3}{L}, \text{ uniformly in Re.}$$

The most common failure model for turbulence models is over-dissipation. Condition 4 expresses aggregate non-over-dissipation. The energy dissipation rate is a fundamental statistic of turbulence, e.g., [98, 135]. This balance is observed in physical experiments [42, 135] and has been proven for the NSE, [31, 29, 30].

The fifth condition is that the model allows an intermittent flow of energy from fluctuations back to means. This energy flow is important, e.g. [118, 137], less well understood and not addressed herein; for background see [64].

Condition 5: *The model allows flow of energy from fluctuations back to means without negative eddy viscosities. This energy flow has space time average zero.*

To develop Conditions 3 and 4, multiple the v-equation (5.2) by v and integrate over Ω. Add to this the k-equation integrated over Ω. After standard manipulations and cancellations of terms there follows the model's global energy balance

$$\frac{d}{dt}\int_\Omega \frac{1}{2}|v(x,t)|^2 + k(x,t)dx + \int_\Omega 2\nu|\nabla^s v(x,t)|^2 + \frac{1}{l(x)}k^{3/2}(x,t)dx \qquad (5.3)$$
$$= \int_\Omega f(x)\cdot v(x,t)dx.$$

Thus, for the 1-equation model we have (per unit volume)

$$\text{Kinetic energy} = \frac{1}{|\Omega|}\int_\Omega \frac{1}{2}|v(x,t)|^2 + k(x,t)dx,$$
$$\text{Dissipation rate } \varepsilon_{\text{model}}(t) = \frac{1}{|\Omega|}\int_\Omega 2\nu|\nabla^s v(x,t)|^2 + \frac{1}{l(x)}k^{3/2}(x,t)dx \qquad (5.4)$$

The standard 1*-equation model has difficulties with all 5 conditions.* Conditions 1 and 5 are clearly violated. The second, $l(x) \to 0$ *at walls*, is not easily enforced for complex boundaries; it is further complicated in current models, e.g., Spalart [117], Wilcox [140], by requiring user input of (unknown) subregion locations where different formulas for $l(x)$ are used. Conditions 3 and 4 also seem to be unknown for the standard model; they do not follow from standard differential inequalities due to the mismatch of the powers of k in the energy term and the dissipation term.

The correction herein is a kinematic $l(x,t)$. We prove herein that a *kinematic* turbulence length-scale enforces Conditions 1, 2, 3 and 4 as well as simplifying the model. This can also be argued to be a *dynamic* choice since the estimate of $|u'|$ in $l(x,t)$ is calculated from an (approximate) causal law. In its origin, the turbulence length-scale (then called a *mixing length*) was an analog to the mean free pass in the kinetic theory of gases. It represented the distance two fluctuating structures must traverse to interact. Prandtl [100] in 1926 also mentioned a second possibility: "*...the distance traversed by a mass of this type before it becomes blended in with neighboring masses...*".

The idea expressed by Prandtl above is ambiguous but can be interpreted as suggesting $l = |u'(x,t)|\tau$, i.e., the *distance a fluctuating eddy travels in one time unit.* This choice means

to select a turbulence time scale τ (e.g., from (5.1)) and, as $|u'| \simeq \sqrt{2}k(x,t)^{1/2}$, define $l(x,t)$ *kinematically* by

$$l(x,t) = \sqrt{2}k(x,t)^{1/2}\tau. \tag{5.5}$$

The k-equation and a weak maximum principle imply $k(x,t) \geq 0$, following [143], [81]. Thus, $k^{1/2}$ is well defined. With this choice the *time window* τ enters into the model. To our knowledge, (5.5) is little developed. Recently in [66] the idea of $l = |u'|\tau$ has been shown to have positive features in ensemble simulations. With (5.5), the model (5.2) is modified to

$$\begin{aligned} v_t + v\cdot\nabla v - \nabla\cdot\left(\left[2\nu + \sqrt{2}\mu k\tau\right]\nabla^s v\right) + \nabla p &= f(x), \\ \nabla\cdot v &= 0, \\ k_t + v\cdot\nabla k - \nabla\cdot\left(\left[\nu + \sqrt{2}\mu k\tau\right]\nabla k\right) + \frac{\sqrt{2}}{2}\tau^{-1}k &= \sqrt{2}\mu k\tau|\nabla^s v|^2. \end{aligned} \tag{5.6}$$

Let L, U denote large length and velocity scales, equation (5.9), $\mathrm{Re} = LU/\nu$ the usual Reynolds number, and let $T^* = L/U$ denote the large scale turnover time. The main result herein is that with the kinematic length scale selection (5.5) Conditions 1–4 are now satisfied.

Theorem 14. *Let μ, τ be positive and Ω a bounded regular domain. Let*

$$l(x,t) = \sqrt{2}k(x,t)^{1/2}\tau.$$

Then, Condition 1 holds.

Suppose the boundary conditions are noslip ($v = 0, k = 0$ on $\partial\Omega$). Then, Condition 2 is satisfied. At walls

$$l(x) \to 0 \text{ as } x \to walls.$$

Suppose the model's energy inequality, equation (5.11) below, holds. If the boundary conditions are either noslip or periodic with zero mean for v and periodic for k, (5.8) below, Condition 3 also holds:

$$\int_\Omega \frac{1}{2}|v(x,t)|^2 + k(x,t)dx \leq C < \infty \text{ uniformly in time.}$$

The model's energy dissipation rate is

$$\varepsilon_{model}(t) = \frac{1}{|\Omega|}\int_\Omega 2\nu|\nabla^s v(x,t)|^2 + \frac{\sqrt{2}}{2}\tau^{-1}k(x,t)dx.$$

Time averages of the model's energy dissipation rate are finite:

$$\limsup_{t^*\to\infty} \frac{1}{t^*}\int_0^{t^*} \varepsilon_{model}(t)dt < \infty.$$

Suppose the boundary conditions are either periodic with zero mean for v and periodic for k, (5.8) below, or noslip ($v = 0, k = 0$ on the boundary) and the body force satisfies $f(x) = 0$ on the boundary. If the selected time averaging window satisfies

$$\frac{\tau}{T^*} \le \frac{1}{\sqrt{\mu}} \quad (\simeq 1.35 \text{ for } \mu = 0.55)$$

then Condition 4 holds uniformly in the Reynolds number

$$\limsup_{t^*\to\infty} \frac{1}{t^*}\int_0^{t^*} \varepsilon_{model}(t)dt \le 4\left(1 + Re^{-1}\right)\frac{U^3}{L}.$$

Proof. The proof that Condition 4 holds will be presented in Section 5.3. The remainder is proven as follows. Condition 1 is obvious. Since $l(x,t) = \sqrt{2}k(x,t)^{1/2}\tau$ and $k(x,t)$ vanishes at walls it follows that so does $l(x,t)$ so Condition 2 holds.

In the energy inequality (5.11), $l(x,t) = \sqrt{2}k(x,t)^{1/2}\tau$ yields

$$\frac{d}{dt}\int_\Omega \frac{1}{2}|v(x,t)|^2 + k(x,t)dx + \int_\Omega 2\nu|\nabla^s v(x,t)|^2 + \frac{\sqrt{2}}{2}\tau^{-1}k(x,t)dx \le \int_\Omega f(x)\cdot v(x,t)dx. \tag{5.7}$$

By Korn's inequality and the Poincaré-Friedrichs inequality

$$\alpha\int_\Omega \frac{1}{2}|v(x,t)|^2 + k(x,t)dx \le \int_\Omega 2\nu|\nabla^s v(x,t)|^2 + \frac{\sqrt{2}}{2}\tau^{-1}k(x,t)dx,$$
$$\text{where } \alpha = \alpha(C_{PF},\nu,\tau) > 0.$$

Let $y(t) = \int \frac{1}{2}|v(x,t)|^2 + k(x,t)dx$. Thus, $y(t)$ satisfies

$$y'(t) + \alpha y(t) \le \int_\Omega f(x)\cdot v(x,t)dx \le \frac{\alpha}{2}y(t) + C(\alpha)\int_\Omega |f|^2 dx.$$

An integrating factor then implies

$$y(t) \le e^{-\frac{\alpha}{2}t}y(0) + \left(C(\alpha)\int_\Omega |f|^2 dx\right)\int_0^t e^{-\frac{\alpha}{2}(t-s)}ds$$

which is uniformly bounded in time, verifying Condition 3.

For the last claim, time average the energy balance (5.7). The result can be compressed to read

$$\frac{y(t^*)-y(0)}{t^*}+\frac{1}{t^*}\int_0^{t^*}\varepsilon_{\text{model}}(t)dt=\frac{1}{t^*}\int_0^{t^*}\left(\int_\Omega f(x)\cdot v(x,t)dx\right)dt$$

The first term on the left hand side is $\mathcal{O}(\frac{1}{t^*})$ since $y(t)$ is uniformly bounded. The RHS is also uniformly in t^* bounded (again since $y(t)$ is uniformly bounded). Thus so is $\frac{1}{t^*}\int_0^{t^*}\varepsilon_{\text{model}}(t)dt$. □

The estimate $\varepsilon \simeq U^3/L$ in Theorem 14 is consistent as $\text{Re}\to\infty$ with both phenomenology, [98], and the rate proven for the Navier-Stokes equations in [139, 29, 31]. Building on this work, the proof consists of estimating 4 key terms. The first 3 are a close parallel to the NSE analysis in these papers and the fourth is model specific.

The main contribution herein is then recognition that several flaws of the model (5.2) originate in the turbulence length-scale specification. These are corrected by the kinematic choice (5.5) rather than by calibrating l with increased complexity. The second main contribution is the proof in Section 5.3 that the kinematic choice does not over dissipate, i.e., Condition 4 holds.

Model existence is an open problem. The proof of Theorem 14 requires assuming weak solutions of the model exist and satisfy an energy inequality (i.e., (5.3) with $=$ replaced by $\leq$), $k(x,t)\geq 0$ and that in the model's weak formulation the test function may be chosen to be the (smooth) body force $f(x)$. Such a theory for the standard model (with static $l=l(x)$) has been developed over 20+ years of difficult progress from intense effort including [80], with positivity of k established in [81], see also [143], existence of suitable weak solutions in [8], culminating in Chapter 8 of [10] and [9] including an energy inequality (with equality an open problem) and uniqueness under restrictive conditions. Conditions 3 and 4 are open problems for the standard model. Based on this work we conjecture that an existence theory, while not the topic of this chapter, may be possible for the (related) 1-equation model with kinematic length scale (5.6).

5.2 PRELIMINARIES AND NOTATION

This section will develop Condition 4, that after time averaging $\varepsilon_{\text{model}} \simeq U^3/L$, and present notation and preliminaries needed for the proof in Section 5.3. We impose periodic boundary conditions on $k(x,t)$ and periodic with zero mean boundary conditions on v, p, v_0, f. Periodicity and zero mean denote respectively

$$\textit{Periodic}\colon\ \phi(x + L_\Omega e_j, t) = \phi(x,t) \text{ and } \textit{Zero mean}\colon \int_\Omega \phi dx = 0\,. \tag{5.8}$$

The proof when the boundary conditions are noslip, $v = 0, k = 0$ on $\partial\Omega$, and $f(x) = 0$ on $\partial\Omega$ will be omitted. It is exactly the same as in the periodic case.

The long time average of a function $\phi(t)$ is

$$\begin{aligned} \langle\phi\rangle &= \lim\sup_{t^*\to\infty} \frac{1}{t^*}\int_0^{t^*} \phi(t)dt \text{ and satisfies} \\ \langle\phi\psi\rangle &\le \left\langle|\phi|^2\right\rangle^{1/2}\left\langle|\psi|^2\right\rangle^{1/2} \text{ and } \langle\langle\phi\rangle\rangle = \langle\phi\rangle\,. \end{aligned}$$

Define the global velocity scale U, the body force scale F and large length scale L by

$$\left.\begin{aligned} F &= \left(\tfrac{1}{|\Omega|}\textstyle\int_\Omega |f(x)|^2 dx\right)^{1/2}, \\ L &= \min\left[L_\Omega, \tfrac{F}{\sup_{x\in\Omega}|\nabla^s f(x)|}, \tfrac{F}{\left(\frac{1}{|\Omega|}\int_\Omega |\nabla^s f(x)|^2 dx\right)^{1/2}}\right] \\ U &= \left(\limsup_{t^*\to\infty} \tfrac{1}{t^*}\textstyle\int_0^{t^*} \tfrac{1}{|\Omega|}\int_\Omega |v(x,t)|^2 dx dt\right)^{1/2}. \end{aligned}\right\} \tag{5.9}$$

L has units of length and satisfies

$$||\nabla^s f||_\infty \le \frac{F}{L} \text{ and } \frac{1}{|\Omega|}||\nabla^s f||^2 \le \frac{F^2}{L^2}\,. \tag{5.10}$$

We assume that weak solutions of the system satisfy the following energy inequality.

$$\frac{d}{dt}\left(\frac{1}{2}||v||^2 + \int_\Omega k dx\right) + 2\nu||\nabla^s v||^2 + \frac{\sqrt{2}}{2\tau}\int_\Omega k dx \le (f, v). \tag{5.11}$$

This is unproven for the new model but consistent with what is known for the standard model, e.g., [10]. We assume the following energy equality for the separate k-equation.

$$\frac{d}{dt}\int_\Omega k dx + \frac{\sqrt{2}}{2\tau}\int_\Omega k dx = \int_\Omega \sqrt{2}\mu k\tau |\nabla^s v|^2 dx. \tag{5.12}$$

This follows from the definition of a distributional solution by taking the test function to be $\phi(x) \equiv 1$.

5.3 PROOF THAT CONDITION 4 HOLDS

This section presents a proof that Condition 4 holds for the model (5.6). The first steps of the proof parallel the estimates in the NSE case in, e.g., [31, 29]. With the above compressed notation, the assumed model energy inequality, motivated by (5.11), can be written

$$\frac{d}{dt}\left(\frac{1}{2|\Omega|}||v||^2+\frac{1}{|\Omega|}\int_\Omega k dx\right)+\frac{1}{|\Omega|}\int_\Omega 2\nu|\nabla^s v|^2+\frac{\sqrt{2}}{2\tau}k dx\le\frac{1}{|\Omega|}(f,v(t)).$$

In the introduction the following uniform in t^* bounds were proven

$$\left.\begin{array}{c}\frac{1}{2}||v(t^*)||^2+\int_\Omega k(t^*)dx\le C<\infty\ ,\\ \frac{1}{t^*}\int_0^{t^*}\int_\Omega\left(2\nu|\nabla^s v|^2+\frac{\sqrt{2}}{2\tau}k\right)dxdt\le C<\infty.\end{array}\right\}\tag{5.13}$$

Time averaging over $0<t<t^*$ gives

$$\frac{1}{t^*}\left(\frac{1}{2}||v(t^*)||^2+\int_\Omega k(x,t^*)dx-\frac{1}{2}||v(0)||^2-\int_\Omega k(x,0)dx\right)+$$
$$+\frac{1}{t^*}\int_0^{t^*}\int_\Omega\left(2\nu|\nabla^s v|^2+\frac{\sqrt{2}}{2\tau}k\right)dxdt=\frac{1}{t^*}\int_0^{t^*}(f,v(t))dt.$$

In view of the *á priori* bounds (5.13) and the Cauchy-Schwarz inequality, this implies

$$\mathcal{O}\left(\frac{1}{t^*}\right)+\frac{1}{t^*}\int_0^{t^*}\varepsilon_{\text{model}}(t)dt\le F\left(\frac{1}{t^*}\int_0^{t^*}\frac{1}{|\Omega|}||v||^2dt\right)^{\frac{1}{2}}.\tag{5.14}$$

To bound F in terms of flow quantities, take the $L^2(\Omega)$ inner product of (5.6) with $f(x)$, integrate by parts (i.e., select the test function to be $f(x)$ in the variational formulation) and average over $[0,t^*]$. This gives

$$F^2=\frac{1}{t^*}\frac{1}{|\Omega|}(v(t^*)-v_0,f)-\frac{1}{t^*}\int_0^{t^*}\frac{1}{|\Omega|}(vv,\nabla^s f)dt+\tag{5.15}$$
$$+\frac{1}{t^*}\int_0^{t^*}\frac{1}{|\Omega|}\int_\Omega 2\nu\nabla^s v:\nabla^s f+\sqrt{2}\mu k\tau\nabla^s v:\nabla^s f dxdt.$$

The **first term** on the RHS is $\mathcal{O}(1/t^*)$ as above. The **second term** is bounded by the Cauchy-Schwarz inequality and (5.10). For any $0<\beta<1$

$$\textbf{Second: }\left|\frac{1}{t^*}\int_0^{t^*}\frac{1}{|\Omega|}(vv,\nabla^s f)dt\right|\le\frac{1}{t^*}\int_0^{t^*}||\nabla^s f(\cdot)||_\infty\frac{1}{|\Omega|}||vv||^2dt$$
$$\le||\nabla^s f(\cdot)||_\infty\frac{1}{t^*}\int_0^{t^*}\frac{1}{|\Omega|}||v(\cdot,t)||^2dt\le\frac{F}{L}\frac{1}{t^*}\int_0^{t^*}\frac{1}{|\Omega|}||v(\cdot,t)||^2dt.$$

The **third term** is bounded by analogous steps to the second term. For any $0 < \beta < 1$

$$\begin{aligned}
&\textbf{Third: } \frac{1}{t^*}\int_0^{t^*}\frac{1}{|\Omega|}\int_\Omega 2\nu\nabla^s v(x,t) : \nabla^s f(x)dxdt \\
&\leq \left(\frac{1}{t^*}\int_0^{t^*}\frac{4\nu^2}{|\Omega|}||\nabla^s v||^2 dt\right)^{\frac{1}{2}}\left(\frac{1}{t^*}\int_0^{t^*}\frac{1}{|\Omega|}||\nabla^s f||^2 dt\right)^{\frac{1}{2}} \\
&\leq \left(\frac{1}{t^*}\int_0^{t^*}\frac{2\nu}{|\Omega|}||\nabla^s v||^2 dt\right)^{\frac{1}{2}}\frac{\sqrt{2\nu}F}{L} \leq \frac{\beta F}{2U}\frac{1}{t^*}\int_0^{t^*}\frac{2\nu}{|\Omega|}||\nabla^s v||^2 dt + \frac{1}{\beta}\frac{\nu U F}{L^2}.
\end{aligned}$$

The **fourth term** is model specific. Its estimation begins by successive applications of the space then time Cauchy-Schwarz inequality as follows

$$\begin{aligned}
&\textbf{Fourth: } \left|\frac{1}{t^*}\int_0^{t^*}\frac{1}{|\Omega|}\int_\Omega \sqrt{2}\mu k\tau\nabla^s v(x,t) : \nabla^s f(x)dxdt\right| \\
&\leq \frac{1}{t^*}\int_0^{t^*}\frac{1}{|\Omega|}\int_\Omega \left(\sqrt{\sqrt{2}\mu k\tau}\right)\left(\sqrt{\sqrt{2}\mu k\tau}|\nabla^s v|\right)|\nabla^s f|dxdt \\
&\leq ||\nabla^s f||_\infty \frac{1}{t^*}\int_0^{t^*}\left(\frac{1}{|\Omega|}\int_\Omega \sqrt{2}\mu k\tau dx\right)^{\frac{1}{2}}\left(\frac{1}{|\Omega|}\int_\Omega \sqrt{2}\mu k\tau|\nabla^s v|^2 dx\right)^{\frac{1}{2}} dxdt \\
&\leq \frac{F}{L}\left(\frac{U}{Ft^*}\int_0^{t^*}\frac{1}{|\Omega|}\int_\Omega \sqrt{2}\mu k\tau dxdt\right)^{\frac{1}{2}}\left(\frac{F}{Ut^*}\int_0^{t^*}\frac{1}{|\Omega|}\int_\Omega \sqrt{2}\mu k\tau|\nabla^s v|^2 dxdt\right)^{\frac{1}{2}}.
\end{aligned}$$

The arithmetic-geometric mean inequality then implies

$$\begin{aligned}
&\textbf{Fourth: } \left|\frac{1}{t^*}\int_0^{t^*}\frac{1}{|\Omega|}\int_\Omega \sqrt{2}\mu k\tau\nabla^s v(x,t) : \nabla^s f(x)dxdt\right| \\
&\leq \frac{\beta}{2}\frac{F}{Ut^*}\int_0^{t^*}\frac{1}{|\Omega|}\int_\Omega \sqrt{2}\mu k\tau|\nabla^s v|^2 dxdt + \frac{U}{2\beta F}\frac{F^2}{L^2}\frac{1}{t^*}\int_0^{t^*}\frac{1}{|\Omega|}\int_\Omega \sqrt{2}\mu k\tau dxdt \\
&\leq \frac{\beta}{2}\frac{F}{Ut^*}\int_0^{t^*}\frac{1}{|\Omega|}\int_\Omega \sqrt{2}\mu k\tau|\nabla^s v|^2 dxdt + \frac{1}{2\beta}\frac{UF}{L^2t^*}\int_0^{t^*}\frac{1}{|\Omega|}\int_\Omega \sqrt{2}\mu k\tau dxdt.
\end{aligned}$$

Using these four estimates in the bound for F^2 yields

$$\begin{aligned}
F^2 \leq\ &\mathcal{O}\left(\frac{1}{t^*}\right) + \frac{F}{L}\frac{1}{t^*}\int_0^{t^*}\frac{1}{|\Omega|}||v||^2 dt + \frac{1}{2\beta}\frac{UF}{L^2}\frac{1}{t^*}\int_0^{t^*}\frac{1}{|\Omega|}\int_\Omega \sqrt{2}\mu k\tau dxdt \\
&+ \frac{1}{\beta}\frac{\nu U F}{L^2} + \frac{\beta F}{2U}\frac{1}{t^*}\int_0^{t^*}\frac{1}{|\Omega|}\int_\Omega \left[2\nu + \sqrt{2}\mu k\tau\right]|\nabla^s v|^2 dxdt.
\end{aligned}$$

Thus, we have an estimate for $F\left(\frac{1}{t^*}\int_0^{t^*}\frac{1}{|\Omega|}||v||^2dt\right)^{\frac{1}{2}}$:

$$F\left(\frac{1}{t^*}\int_0^{t^*}\frac{1}{|\Omega|}||v||^2dt\right)^{\frac{1}{2}} \leq \mathcal{O}\left(\frac{1}{t^*}\right)+\frac{1}{L}\left(\frac{1}{t^*}\int_0^{t^*}\frac{1}{|\Omega|}||v||^2dt\right)^{\frac{3}{2}}+$$
$$+\frac{\beta}{2}\frac{\left(\frac{1}{t^*}\int_0^{t^*}\frac{1}{|\Omega|}||v||^2dt\right)^{\frac{1}{2}}}{U}\frac{1}{t^*}\int_0^{t^*}\frac{1}{|\Omega|}\int_\Omega\left[2\nu+\sqrt{2}\mu k\tau\right]|\nabla^s v|^2dxdt+$$
$$+\frac{1}{2\beta}\left(\frac{1}{t^*}\int_0^{t^*}\frac{1}{|\Omega|}||v||^2dt\right)^{\frac{1}{2}}\frac{2\nu U}{L^2}+$$
$$+\frac{1}{2\beta}\left(\frac{1}{t^*}\int_0^{t^*}\frac{1}{|\Omega|}||v||^2dt\right)^{\frac{1}{2}}\frac{U}{L^2}\frac{1}{t^*}\int_0^{t^*}\frac{1}{|\Omega|}\int_\Omega\sqrt{2}\mu k\tau dxdt.$$

Inserting this on the RHS of (5.14) yields

$$\frac{1}{t^*}\int_0^{t^*}\varepsilon_{\text{model}}dt \leq \mathcal{O}\left(\frac{1}{t^*}\right)+\frac{1}{L}\left(\frac{1}{t^*}\int_0^{t^*}\frac{1}{|\Omega|}||v||^2dt\right)^{\frac{3}{2}}+ \tag{5.16}$$
$$+\frac{\beta}{2}\frac{\left(\frac{1}{t^*}\int_0^{t^*}\frac{1}{|\Omega|}||v||^2dt\right)^{\frac{1}{2}}}{U}\frac{1}{t^*}\int_0^{t^*}\frac{1}{|\Omega|}\int_\Omega\left[2\nu+\sqrt{2}\mu k\tau\right]|\nabla^s v|^2dxdt+$$
$$+\frac{1}{2\beta}\left(\frac{1}{t^*}\int_0^{t^*}\frac{1}{|\Omega|}||v||^2dt\right)^{\frac{1}{2}}U\frac{2\nu}{L^2}+$$
$$+\frac{1}{2\beta}\left(\frac{1}{t^*}\int_0^{t^*}\frac{1}{|\Omega|}||v||^2dt\right)^{\frac{1}{2}}\frac{U}{L^2}\left(\frac{1}{t^*}\int_0^{t^*}\frac{1}{|\Omega|}\int_\Omega\sqrt{2}\mu k\tau dxdt\right).$$

We prove in the next lemma an estimate for the last, model specific, term $\int\sqrt{2}\mu k\tau dx$ on the RHS. This estimate has the interpretation that, on time average, the decay (relaxation) rate of $k(x,t)$ balances the transfer rate of kinetic energy from means to fluctuations.

Lemma 9. *For weak solutions of the k-equation we have*

$$\left\langle\frac{1}{|\Omega|}\int_\Omega\sqrt{2}\mu k(x,t)\tau dx\right\rangle = 2\mu\tau^2\left\langle\frac{1}{|\Omega|}\int_\Omega\sqrt{2}\mu k\tau|\nabla^s v|^2dx\right\rangle.$$

Proof. Integrating the k-equation (i.e., choosing $\phi(x)\equiv 1$ in the equation's distributional formulation) yields

$$\frac{d}{dt}\frac{1}{|\Omega|}\int_\Omega kdx+\frac{\sqrt{2}}{2\tau}\frac{1}{|\Omega|}\int_\Omega kdx=\frac{1}{|\Omega|}\int_\Omega\sqrt{2}\mu k\tau|\nabla^s v|^2dx.$$

From Theorem 14, $\int k dx$ (and thus its time averages) is uniformly bounded in time. Thus, we can time average the above. This gives

$$\mathcal{O}\left(\frac{1}{t^*}\right) + \frac{\sqrt{2}}{2\tau}\frac{1}{t^*}\int_0^{t^*}\frac{1}{|\Omega|}\int_\Omega k dx dt = \frac{1}{t^*}\int_0^{t^*}\frac{1}{|\Omega|}\int_\Omega \sqrt{2}\mu k\tau |\nabla^s v|^2 dx dt,$$

and thus

$$\left\langle \frac{1}{|\Omega|}\int_\Omega \sqrt{2}\mu k(x,t)\tau dx \right\rangle = 2\mu\tau^2 \left\langle \frac{1}{|\Omega|}\int_\Omega \sqrt{2}\mu k\tau |\nabla^s v|^2 dx \right\rangle,$$

proving the lemma. □

To continue the proof of Theorem 14, this lemma is now used to replace terms on the RHS of (5.16) involving $\sqrt{2}\mu k\tau|\nabla^s v|^2$ by terms with $\sqrt{2}\mu k(x,t)\tau$. Let $t^* \to \infty$ in (5.16), recalling the definition of $\varepsilon_{\text{model}}$ and inserting the above relation for the last term yields

$$\begin{aligned}\left\langle \frac{1}{|\Omega|}\int_\Omega \left[2\nu|\nabla^s v(x,t)|^2 + \frac{\sqrt{2}}{2}\tau^{-1}k(x,t)\right] dx \right\rangle &\le \frac{U^3}{L} \\ +\frac{\beta}{2}\left\langle \frac{1}{|\Omega|}\int_\Omega 2\nu|\nabla^s v|^2 + \frac{1}{2\mu\tau^2}\sqrt{2}\mu k(x,t)\tau dx \right\rangle &+ \\ +\frac{1}{\beta}U^2\frac{\nu}{L^2} + \frac{1}{2\beta}\frac{U^2}{L^2}\left\langle \frac{1}{|\Omega|}\int_\Omega \sqrt{2}\mu k(x,t)\tau dx \right\rangle &.\end{aligned} \tag{5.17}$$

Collecting terms gives

$$\begin{aligned}\left\langle \frac{1}{|\Omega|}\int_\Omega \left[2\nu|\nabla^s v(x,t)|^2 + \frac{\sqrt{2}}{2}\tau^{-1}k(x,t)\right] dx \right\rangle &\le \frac{1}{L}U^3 + \frac{1}{\beta}U^2\frac{\nu}{L^2} \\ +\frac{\beta}{2}\left\langle \frac{1}{|\Omega|}\int_\Omega 2\nu|\nabla^s v|^2 + \left(\frac{1}{2\mu\tau^2} + \frac{1}{2\beta}\frac{U^2}{L^2}\right)\sqrt{2}\mu k(x,t)\tau dx \right\rangle &.\end{aligned} \tag{5.18}$$

The multiplier of $\sqrt{2}\mu k(x,t)\tau$ simplifies to

$$\frac{\beta}{2}\left(\frac{1}{2\mu\tau^2} + \frac{1}{2\beta}\frac{U^2}{L^2}\right)\sqrt{2}\mu\tau = \frac{\sqrt{2}}{2}\tau^{-1}\left[\frac{\beta}{2} + \frac{1}{2}\mu\frac{U^2}{L^2}\tau^2\right].$$

Thus, rearrange the above inequality to read

$$\begin{aligned}\left\langle \frac{1}{|\Omega|}\int_\Omega \left[\left(1-\frac{\beta}{2}\right)\nu|\nabla^s v|^2 + \left(1 - \left\{\frac{\beta}{2} + \frac{\mu}{2}\frac{U^2}{L^2}\tau^2\right\}\right)\frac{\sqrt{2}}{2}\tau^{-1}k\right] dx \right\rangle \\ \le \frac{U^3}{L} + \frac{1}{\beta}U^2\frac{\nu}{L^2} = \left(1 + \frac{1}{\beta}\mathrm{Re}^{-1}\right)\frac{U^3}{L}.\end{aligned}$$

Pick (without optimizing) $\beta = 1$. This yields

$$\left\langle \frac{1}{|\Omega|}\int_\Omega \left[\nu|\nabla^s v(x,t)|^2 + \frac{\sqrt{2}}{2}\tau^{-1}k(x,t)\right]dx\right\rangle$$
$$\leq \frac{2}{\min\{1, 1-\mu\frac{U^2}{L^2}\tau^2\}}\left\{\frac{U^3}{L} + \mathrm{Re}^{-1}\frac{U^3}{L}\right\}.$$

We clearly desire

$$1 - \mu\frac{U^2}{L^2}\tau^2 = 1 - \mu\left(\frac{\tau}{T^*}\right)^2 \geq \frac{1}{2}.$$

This holds if the time cutoff τ is chosen with respect to the global turnover time $T^* = L/U$ so that

$$\frac{\tau}{T^*} \leq \sqrt{\frac{1}{\mu}} \simeq 1.35, \text{ for } \mu = 0.55.$$

Then we have, as claimed,

$$\left\langle \frac{1}{|\Omega|}\int_\Omega \left[\nu|\nabla^s v|^2 + \frac{\sqrt{2}}{2}\tau^{-1}k\right]dx\right\rangle \leq 4\left(1+\mathrm{Re}^{-1}\right)\frac{U^3}{L}.$$

5.4 NUMERICAL ILLUSTRATIONS IN 2D AND 3D

This section shows that the static and kinematic turbulence length scales produces flows with different statistics. We use the simplest reasonable choices

$$l_0(x) = \min\{0.41y, 0.41\cdot 0.2\mathrm{Re}^{-1/2}\} \text{ and } l_K(x,t) = \sqrt{2}k(x,t)^{1/2}\tau.$$

All numerical experiments were performed using the package FEniCS [1]. We consider several normalized, space-averaged statistics. Recall that the *turbulence intensity* is $I = \langle||u'||^2\rangle / \langle||\overline{u}||^2\rangle$. An approximation to the (time) evolution of this is calculable from the model

$$I_{\text{model}}(t) := \frac{\frac{2}{|\Omega|}\int_\Omega k(x,t)dx}{\frac{1}{|\Omega|}\int_\Omega |v(x,t)|^2 dx}.$$

Next we consider the effective viscosity coefficient for the two methods. The *effective viscosity* is a useful statistic to quantify the aggregate, space averaged effect of fluctuating eddy viscosity terms. It is

$$\nu_{\text{effective}}(t) := \frac{\frac{1}{|\Omega|}\int_\Omega \left[\nu + \mu l\sqrt{k}\right] |\nabla^s v|^2 dx}{\frac{1}{|\Omega|}\int_\Omega |\nabla^s v|^2 dx}.$$

We also consider the related statistic of the *viscosity ratio of turbulent viscosity to molecular viscosity*

$$VR(t) := \frac{\frac{1}{|\Omega|}\int_\Omega \mu l\sqrt{k}|\nabla^s v|^2 dx}{\frac{1}{|\Omega|}\int_\Omega 2\nu|\nabla^s v|^2 dx}.$$

We also calculate the evolution of the *Taylor microscale* of each model's solution:

$$\lambda_{\text{Taylor}}(t) := \left(\frac{\int_\Omega |\nabla^s v|^2 dt}{\int_\Omega |v|^2 dt}\right)^{-1/2}.$$

The time evolution of the *scaled averaged turbulence length scale* and turbulent viscosity are also of interest:

$$\frac{avg(l)}{L} := \frac{1}{L}\left(\frac{1}{|\Omega|}\int_\Omega l(x,t)^2 dx\right)^{1/2}$$
$$\frac{avg(\nu_T)}{LU} := \frac{1}{LU}\frac{1}{|\Omega|}\int_\Omega \mu l(x,t)\sqrt{k(x,t)}dx.$$

5.4.1 TEST 1: FLOW BETWEEN 2D OFFSET CIRCLES

For the first test, we consider a two-dimensional rotational flow obstructed by a circular obstacle with no-slip boundary conditions. Let $\Omega_1 \subset \mathbb{R}^2$, where

$$\Omega_1 = \{(x,y) \in \mathbb{R}^2 : x^2 + y^2 < 1\} \setminus \{(x,y) \in \mathbb{R}^2 : (x-.5)^2 + y^2 \leq .01\}.$$

The domain Ω_1 is discretized via a Delaunay triangulation with a maximal mesh width of .01; a plot is given below. From the plot in Figure 1 of the model's Taylor microscale this mesh fully resolves the model solution.

We start the test at rest, i.e., $v_0 = (0,0)^T$, and let the fluid have kinematic viscosity $\nu = 0.0001$. We take the final time $t^* = 10$ and averaging window $\tau = 1$. Rather than give an interpretation of the time average for $0 \leq t < 1$ we harvest flow statistics for $t \geq 1$

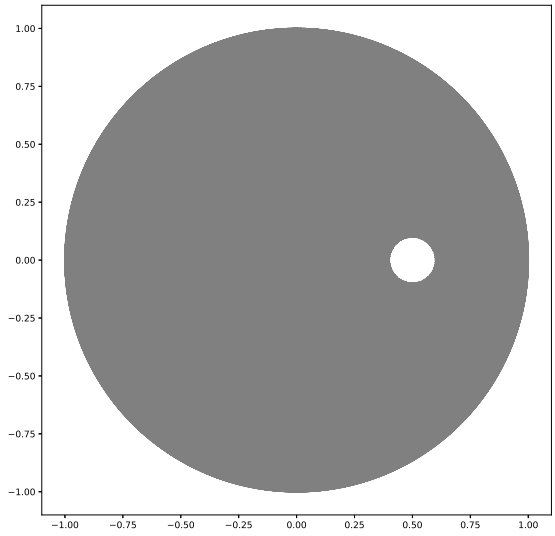

(a) Ω

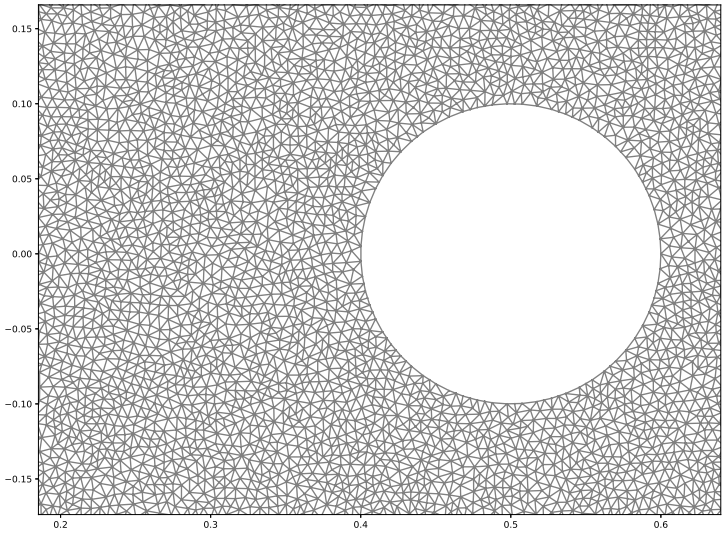

(b) Ω near the obstacle

Figure 5.1: Discretization of Ω.

after a cold start and ramping up the body force with a multiplier $\min\{t, 1\}$. To generate counter-clockwise motion we impose the body force

$$f(x, y; t) = \min\{t, 1\}(-4y(1 - x^2 - y^2), 4x(1 - x^2 - y^2))^T.$$

Initial Conditions. An initial condition for the velocity, $v(x, 0)$, and for the TKE $k(x, 0)$ must be specified. For some flows, standard choices are known. For example, for turbulent flow in a square duct, a choice is

$$k(x, 0) = 1.5|u_0(x)|^2 I^2 \text{ where}$$
$$I = \text{turbulent intensity} \simeq 0.16\text{Re}^{-1/8} .$$

We use a different and systematic approach to the initial condition $k(x, 0)$ as follows. From $l(x, t) = \sqrt{2}k^{1/2}\tau$ we set at $t = 0$, $l = l_0(x)$ and solve for $k(x, 0)$. This yields the initial condition

$$k(x, 0) = \frac{1}{2\tau^2} l_0^2(x) \text{ where } l_0(x) = \min\{0.41y, 0.082\text{Re}^{-1/2}\}.$$

This choice means that $l_0(x) = l_K(x, 0)$.

To compare the models, we plot the temporal evolution of the above statistics. For both models, we let $\mu = 0.55$ and timestep $\Delta t = .01$. To let the flow develop, we first activate both models when $t = 1$. In the test, the model's estimate of the turbulent intensity for both is similar, as shown in Figure 5.2a. In [66] the turbulent intensity was estimated by an ensemble simulation. For ensemble averaging I was significantly larger than calculated here by time averaging and with the 1-equation model. Either intensities by time and ensemble averaging do not coincide or I_{model} is not an accurate turbulent intensity. Figure 5.2b shows that the effective viscosity for the kinematic length scale is significantly smaller than for the standard model. This is consistent with Figure 5.2c, 5.2e and 5.2f. In Figure 5.2d the Taylor microscale is larger than expected, possibly due to numerical dissipation in the linearly-implicit time discretization used.

The statistics considered reveal differences in the two models. Figure 5.2b shows that the kinematic model has an effective viscosity that decays to $\nu_{\text{effective}} = 0.0001$ more rapidly than does the static model. More evidence of this fact is given in Figure 5.2c, which shows

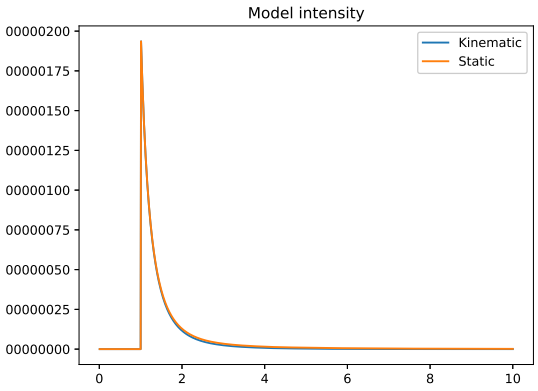

(a) Model intensity I_{model}

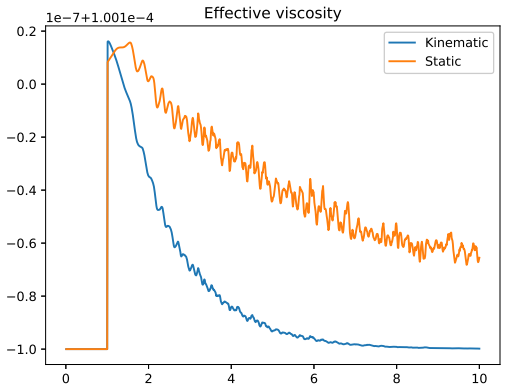

(b) Effective viscosity $\nu_{\text{effective}}$

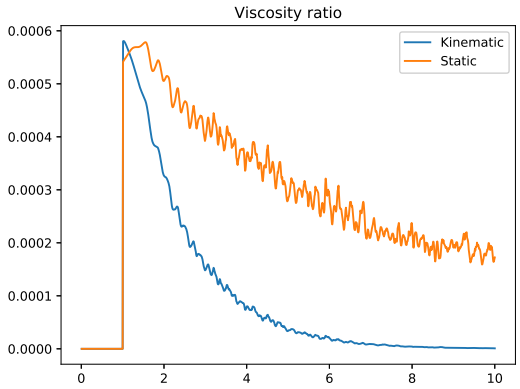

(c) Viscosity ratio VR_1

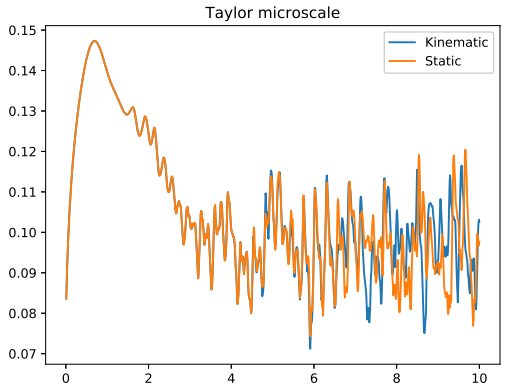

(d) Taylor microscale λ_{Taylor}

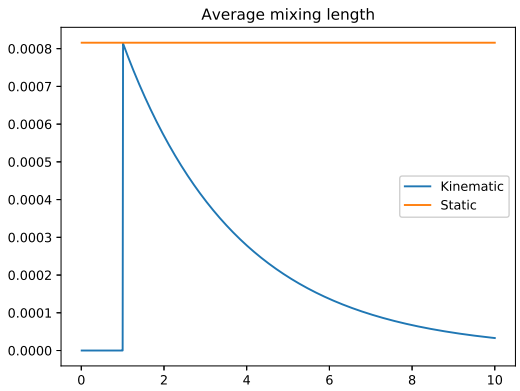

(e) $avg(l)/L$

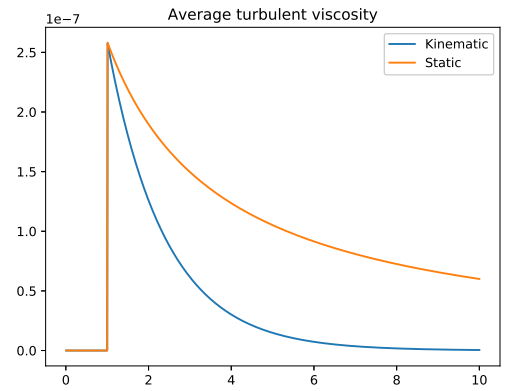

(f) $avg(\nu_T)/UL$

Figure 5.2: 2d flow statistics for both models.

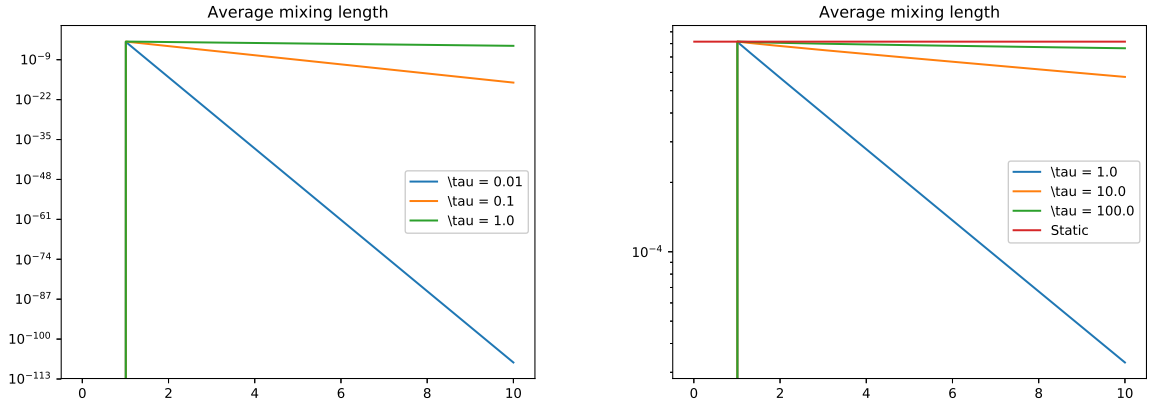

(a) $avg(l)/L$ for $\tau = .01, .1, 1$.

(b) $avg(l)/L$ for $\tau = 1, 10, 100$ and the static model.

Figure 5.3: Average mixing length comparison.

the turbulent-to-molecular viscosity ratio. The comparison of the evolution of the Taylor microscale, given in Figure 5.2d, shows similar profiles until $t \approx 5$. Figure 5.2e, which compares the evolution of the average mixing length, shows that the kinematic mixing length model decreases the turbulence length scale over the course of the simulation. Finally, Figure 5.2f shows that the average turbulent viscosity for the kinematic model is consistently smaller than that of the static model. Statistical comparisons of both of these models with different parameters (in particular, the turbulent time scale τ) are also of interest. Below, we give semilog (in the vertical axis) plots of the average mixing length with different values of τ.

Figure 5.3 shows that decreasing values of τ lead to a vanishing average mixing length, whereas increasing τ yields average mixing lengths that appear to converge to the static mixing length.

Next, we give plots of the velocity magnitude and squared vorticity for the kinematic model at $t = 1, 5$, and 10.

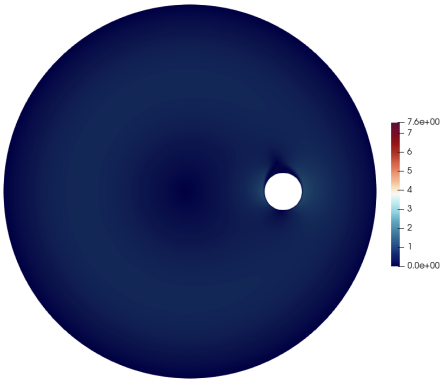

(a) Velocity ($t = 1$)

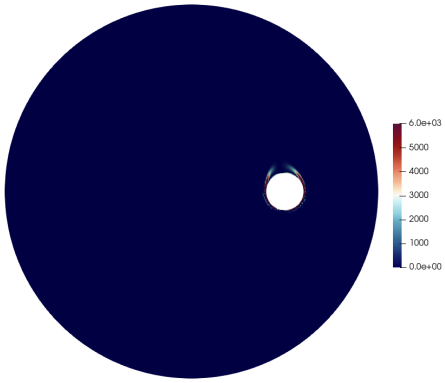

(b) Squared vorticity ($t = 1$)

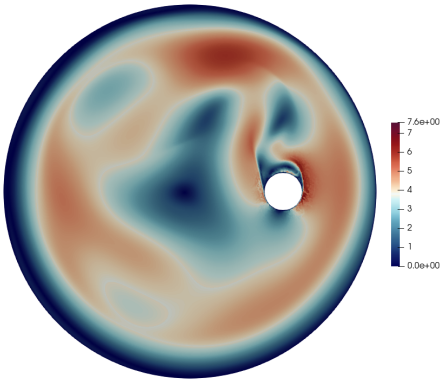

(c) Velocity ($t = 5$)

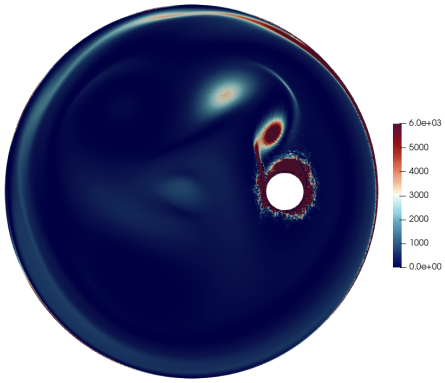

(d) Squared vorticity ($t = 5$)

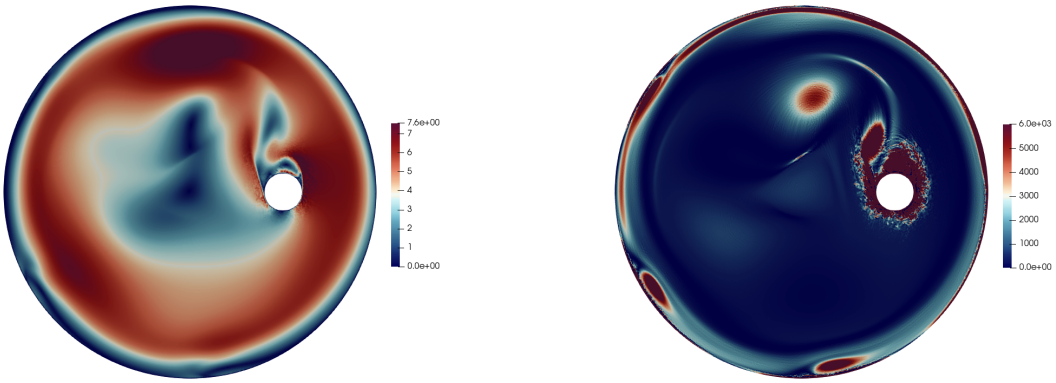

(e) Velocity ($t = 10$)

(f) Squared vorticity ($t = 10$)

Figure 5.4: Kinematic mixing length model velocity and vorticity.

5.4.2 TEST 2: FLOW BETWEEN 3D OFFSET CYLINDERS

The second test is a 3d analogue of the first. It shows similar differences in the two models. Taking Ω_1 to be the domain given in the first test, we define $\Omega = \Omega_1 \times (0, 1)$, a cylinder of radius and height one with a cylindrical obstacle removed. The domain Ω was discretized with Delaunay tetrahedrons with a maximal mesh width of approximately 0.1. As before, we start the flow from rest ($v_0 = (0, 0, 0)^T$) and let the kinematic viscosity $\nu = 0.0001$. The flow evolves via the body force

$$f(x, y, z; t) = \min\{t, 1\}(-4y(1 - x^2 - y^2), 4x(1 - x^2 - y^2), 0)^T,$$

and is observed over the time interval $(0, 10]$, with $\Delta t = .05$ and the initial conditions for k being set in the same way as the first test. Below, we present the evolution of the statistics introduced above.

The statistics shown in Figure 5.5 exhibit similar differences between the 2 models as in the 2d case, Figs. 5.5a–5.5c, 5.5e–5.5f. As before, the evolution of the Taylor microscale in Figure 5.5d is similar in both models, with slight differences appearing as the flow evolves.

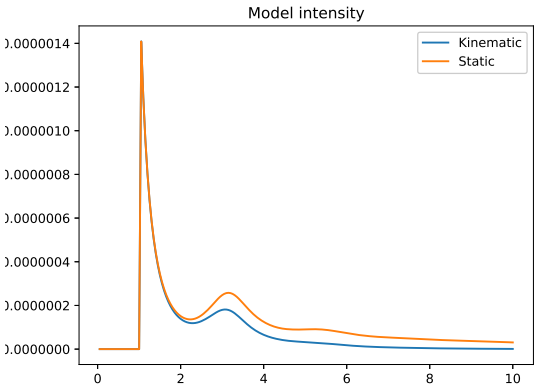

(a) Model intensity I_{model}

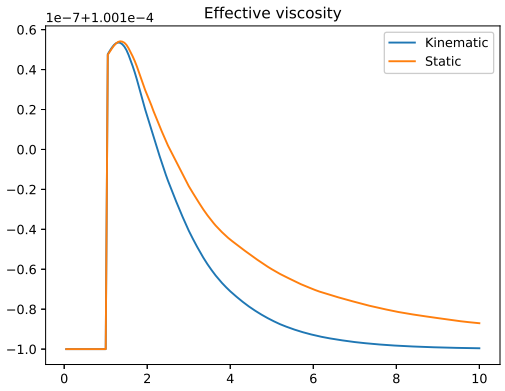

(b) Effective viscosity $\nu_{\text{effective}}$

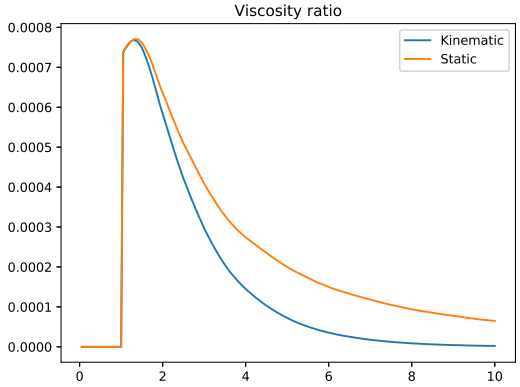

(c) Viscosity ratio VR_1

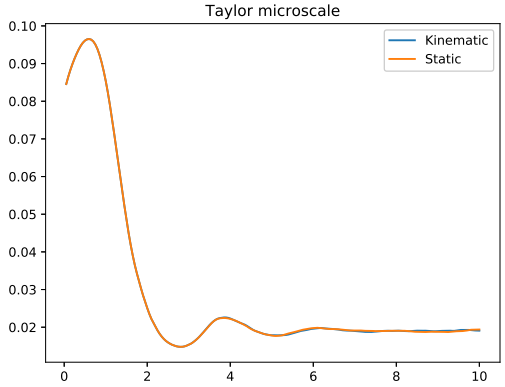

(d) Taylor microscale λ_{Taylor}

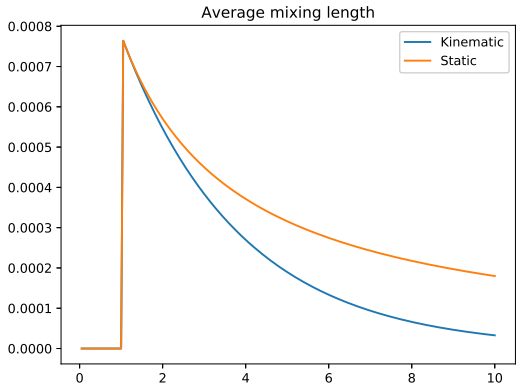

(e) $avg(l)/L$

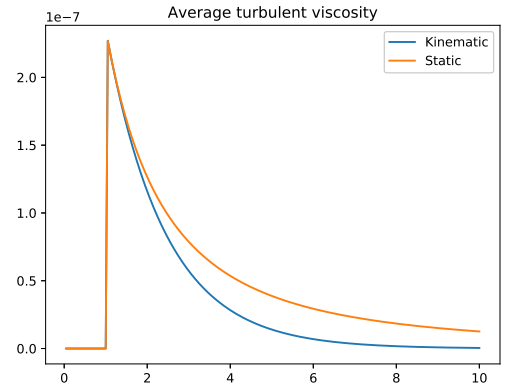

(f) $avg(\nu_T)/UL$

Figure 5.5: Flow statistics for the 3d offset cylinder problem.

Here the Taylor microscale is much smaller for the 3d test than the previous 2d test (even though the mesh is coarser).

To conclude, we present streamline plots of the offset cylinder simulation as viewed from above. In the figures, color signifies the magnitude of velocity. At $t = 1$, the flow appears laminar, and over the course of the simulation becomes turbulent, as evidenced by the plots at $t = 5, 10$. This behavior can be seen in Figure 5.7, which views the domain from the positive y direction and considers a slice at $z = .1$.

5.5 CONCLUSIONS

Predictive simulation of turbulent flows using a URANS model requires some prior knowledge of the flow to calibrate the model and side conditions. Our intuition is that *the better the model represents flow physics the less complex this calibration will be.* To this end we have suggested a simple modification of the standard 1-equation model that analysis shows better represents flow physics.

In turbulence, it is of course easier to list open problems than known facts. However, there are a few within current technique for the modified model herein.

- Extension of estimates of $\langle \varepsilon_{\text{model}} \rangle$ to turbulent shear flows is open and would give insight into near wall behavior. Various methods for reducing the turbulent viscosity locally in regions of persistent, coherent structures have been proposed, e.g., [138], [79] . Sharpening the (global) analysis of $\langle \varepsilon_{\text{model}} \rangle$ for these (local) schemes would be a significant breakthrough.
- Extension of an existence theory to the modified model is another important open problem. Our intuition is that existence will hold but there may always occur hidden difficulties.
- The estimate in Theorem 14 requires an upper limit on the time average's window of $\tau/T^* \leq \mu^{-1/2}$. We do not know if a restriction of this type can be removed through sharper analysis or if there exists a fundamental barrier on the time average's window. Connected with this question, the behavior of the model as $\tau \to \infty$ is an open problem.

- Eddy viscosity models do not permit transfer of energy from fluctuations back to means. Recently in [64] an idea for correcting these features of eddy viscosity models was developed. Extension to the present context would be a significant step forward in model accuracy.
- Various averages of the classic turbulence length scale with the kinematic one proposed herein are possible, such as the geometric average

$$l_\theta(x,t) = l_0^\theta(x) l_K^{1-\theta}(x,t).$$

  It is possible that such a weighted combination will perform better than either alone. For example, for decaying turbulence when $v = 0, \nabla v = 0$ the $k-$equation reduces to

$$k_t + \frac{1}{l_\theta} k\sqrt{k} = 0.$$

  Decaying turbulence experiments in 1966 of Compte-Bellot-Corsin, e.g., p.56-57 in [92], suggest polynomial decay as $k(t) = k(0)\,(1+\lambda t)^{-1.3}$. Neither mixing length formula replicates this decay. But choosing $\theta = \frac{2}{1.3} \simeq 1.54$ yields polynomial decay with exponent -1.3. The effect of this data-fitting on the predictive power of the model and on the Conditions 1-4 are an open problem.
- Our intuition is that for many tests numerical dissipation is greater than model dissipation (and acts on different features and scales of those features). Thus the analysis of numerical dissipation including time discretizations is an important open problems.
- Comparative tests on problems known to be challenging for RANS and URANS models is an important assessment step.

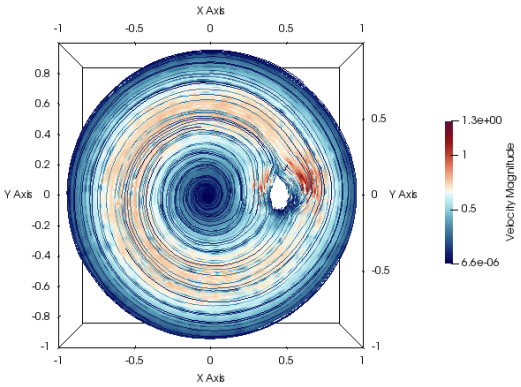

(a) $t = 1$

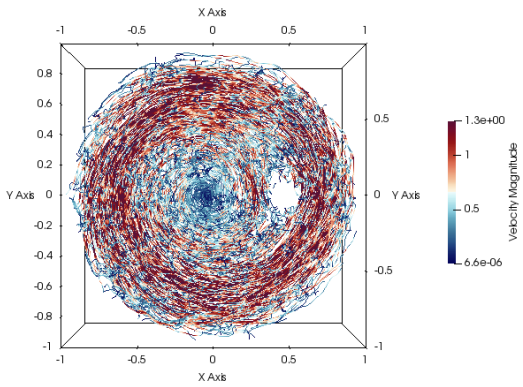

(b) $t = 5$

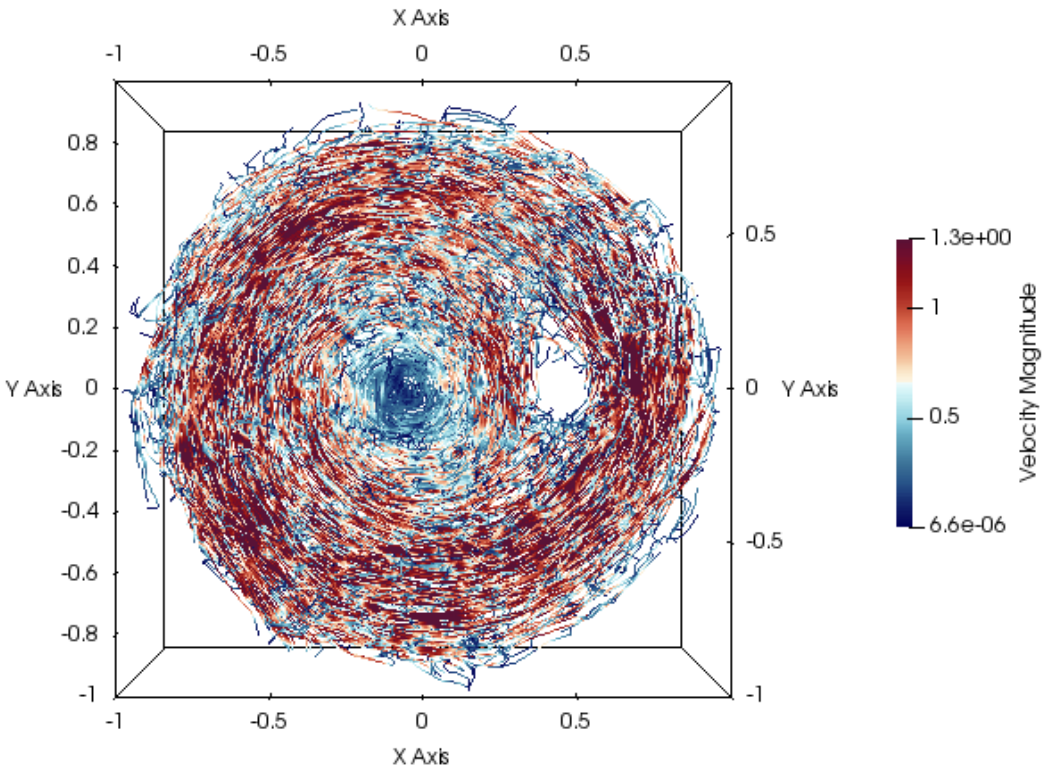

(c) $t = 10$

Figure 5.6: Streamlines for the 3d offset cylinder problem.

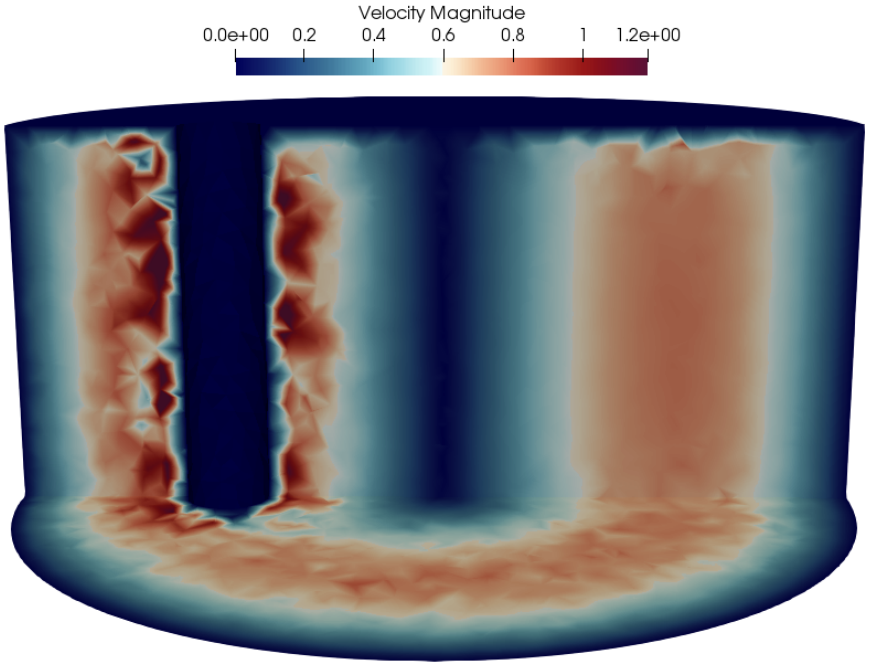

(a) $t = 1$

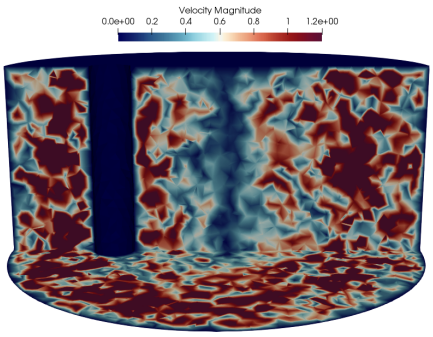

(b) $t = 5$

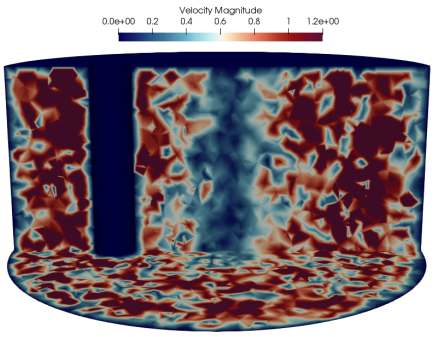

(c) $t = 10$

Figure 5.7: Velocity magnitude for the 3d offset cylinder problem.

6.0 CONCLUSIONS AND OPEN PROBLEMS

With the rapid warming of the planet comes the need for time-accurate simulations of fluid flow. Accurate approximations are essential to the forecasting of weather systems across the planet. Due to uncertainties in initial conditions, data, etc., ensemble simulations are used to glean statistics and better approximate the chaotic nature of the atmosphere. However, these simulations are computationally intensive, limiting the length of the predictability horizon. Thus, fast, efficient numerical methods are of the utmost importance, as they allow for the use of more realizations in ensemble schemes, lengthening the predictability horizon. Inherent also in fluid problems is the coupling of velocity and pressure. Artificial compressibility methods exploit this structure, yielding robust numerical schemes that are time-accurate and fast at low-temporal orders. However, they prove resistant to timestepping schemes using a variable timestep.

The main focus of this dissertation is the construction, analysis, and validation of fast, efficient, adaptive ensemble methods for the NSE and Boussinesq equations. In Chapter 2, we recognize the difficulties in adapting AC methods in time. To overcome these challenges, we construct an adaptive AC method for the NSE based on a new slightly compressible continuum model. We show the method is unconditionally, nonlinearly, longtime stable, and validate the model via numerical experiments. Chapter 2 also analyzes the new continuum model: We show, under some conditions on the evolution of the AC parameter ε, that the new model converges weakly to the incompressible NSE. Following on the theme of adaptive AC methods, we develop, analyze, and test two new adaptive AC methods at the end of Chapter 2.

Chapter 3 is concerned with the development of AC ensemble methods for the Boussinesq equations. In this chapter, we show stability and error results for the fully-discrete ACE scheme. We follow up on the analysis with a suite of numerical tests, culminating in a predictability study of the lock-exchange problem, otherwise known as Marsigli flow. Finally, we show the stability of a new adaptive ACE algorithm based on the work presented in Chapter 2. Error analyses and numerical tests for the novel adaptive artificial compressibility

ensemble scheme are an open problem.

In Chapter 4, we present work on a novel one-equation model that utilizes a kinematic mixing length. We present five conditions that URANS models should satisfy, and argue that the original model of Prandtl can be vastly improved. The new model, based on specifying a mixing length that is a function of the time-averaged kinetic energy, satisfies four of the five conditions. Chapter 4 presents a proof that these conditions are met, and the model is numerically validated and compared with the original via tests in two and three dimensions.

There is much work to be done on the development of adaptive AC methods, and AC methods in general. The original adaptive method, which is only proven stable under a stringent condition, has proven itself in numerical tests. We conjecture that an ease on the stringent condition is possible, which would make adaptive AC methods much more efficient.

Another open problem comes from the decoupled form of AC methods. Since a grad-div term appears in the momentum equation, an application of a modular grad-div method could make AC methods more robust, especially at higher orders. There are many ways to formulate a modular grad-div AC method, with advantages and disadvantages in each formulation. Analysis and numerical tests are needed for these methods, and we believe they are attainable. Another application, which needs numerical tests and analysis, is the application of modular grad-div to improve mass conservation in AC methods.

Ensemble methods have seen an enormous development in the past five years. Due to their importance, that development will continue into the future. An interesting extension of this work will be to extend the stability and error analyses to the stochastic case, as well as validate the schemes with numerical tests. Another application will be to extend these ensemble methods to other equation sets; in particular, the hydrostatic primitive equations. We conjecture this is possible, at least for vertically structured meshes.

Finally, much work remains on the one-equation model presented in Chapter 4. At the end of the chapter, we presented a list of open problems and refer the reader there.

7.0 BIBLIOGRAPHY

[1] M. S. Alnæs et al., *The FEniCS Project Version 1.5*, Archive of Numerical Software 3.100 (2015), DOI: 10.11588/ans.2015.100.20553.

[2] P. R. Amestoy et al., *A fully asynchronous multifrontal solver using distributed dynamic scheduling*, SIAM J. Matrix Anal. Appl. 23.1 (2001), pp. 15–41, ISSN: 0895-4798, DOI: 10.1137/S0895479899358194, URL: https://doi-org.pitt.idm.oclc.org/10.1137/S0895479899358194.

[3] R. Asselin, *Frequency filter for time integrations*, Mon. Wea. Rev. 100 (1972), pp. 487–490.

[4] J.-P. Aubin, *Un théorème de compacité*, C. R. Acad. Sci. Paris 256 (1963), pp. 5042–5044, ISSN: 0001-4036.

[5] G. Baker, *Galerkin approximations for the Navier-Stokes equations*, Harvard University (1976).

[6] M. A. Belenli, S. Kaya, and L. G. Rebholz, *An explicitly decoupled variational multiscale method for incompressible, non-isothermal flows*, Comput. Methods Appl. Math. 15.1 (2015), pp. 1–20, ISSN: 1609-4840, DOI: 10.1515/cmam-2014-0026, URL: https://doi.org/10.1515/cmam-2014-0026.

[7] G. Boffetta et al., *Predictability in two-dimensional decaying turbulence*, Physics of Fluids 9.3 (1997), pp. 724–734.

[8] M. Bulíček, R. Lewandowski, and J. Málek, *On evolutionary Navier-Stokes-Fourier type systems in three spatial dimensions*, Comment. Math. Univ. Carolin. 52.1 (2011), pp. 89–114, ISSN: 0010-2628.

[9] M. Bulíček and J. Málek, *Large data analysis for Kolmogorov's two-equation model of turbulence*, Nonlinear Anal. Real World Appl. 50 (2019), pp. 104–143, ISSN: 1468-1218, DOI: 10.1016/j.nonrwa.2019.04.008, URL: https://doi-org.pitt.idm.oclc.org/10.1016/j.nonrwa.2019.04.008.

[10] T. Chacón Rebollo and R. Lewandowski, *Mathematical and numerical foundations of turbulence models and applications*, Modeling and Simulation in Science, Engineering and Technology, Birkhäuser/Springer, New York, 2014, pp. xviii+517, isbn: 978-1-4939-0454-9; 978-1-4939-0455-6, doi: 10.1007/978-1-4939-0455-6, url: https://doi-org.pitt.idm.oclc.org/10.1007/978-1-4939-0455-6.

[11] S. Chandrasekhar, *Hydrodynamic and hydromagnetic stability*, Courier Corporation, 2013.

[12] S. Charnyi et al., *On conservation laws of Navier-Stokes Galerkin discretizations*, J. Comput. Phys. 337 (2017), pp. 289–308, issn: 0021-9991, doi: 10.1016/j.jcp.2017.02.039, url: https://doi.org/10.1016/j.jcp.2017.02.039.

[13] R. M. Chen, W. Layton, and M. McLaughlin, *Analysis of variable-step/non-autonomous artificial compression methods*, Journal of Mathematical Fluid Mechanics 21.2 (2019), p. 30.

[14] A. J. Chorin, *Numerical solution of the Navier-Stokes equations*, Math. Comp. 22 (1968), pp. 745–762, issn: 0025-5718, doi: 10.2307/2004575, url: https://doi.org/10.2307/2004575.

[15] A. J. Chorin, *On the convergence of discrete approximations to the Navier-Stokes equations*, Math. Comp. 23 (1969), pp. 341–353, issn: 0025-5718, doi: 10.2307/2004428, url: https://doi-org.pitt.idm.oclc.org/10.2307/2004428.

[16] A. J. Chorin, *The numerical solution of the Navier-Stokes equations for an incompressible fluid*, Bulletin of the American Mathematical Society 73.6 (1967), pp. 928–931.

[17] A. Çıbık and S. Kaya, *A projection-based stabilized finite element method for steady-state natural convection problem*, Journal of Mathematical Analysis and Applications 381.2 (2011), pp. 469–484.

[18] J. M. Connors, J. S. Howell, and W. J. Layton, *Decoupled time stepping methods for fluid-fluid interaction*, SIAM J. Numer. Anal. 50.3 (2012), pp. 1297–1319, issn: 0036-1429, doi: 10.1137/090773362, url: https://doi-org.pitt.idm.oclc.org/10.1137/090773362.

[19] G. W. D.C. Wan BSV Patnaik, *A new benchmark quality solution for the buoyancy-driven cavity by discrete singular convolution*, Numerical Heat Transfer: Part B: Fundamentals 40.3 (2001), pp. 199–228.

[20] G. G. Dahlquist, W. Liniger, and O. Nevanlinna, *Stability of two-step methods for variable integration steps*, SIAM J. Numer. Anal. 20.5 (1983), pp. 1071–1085, issn: 0036-1429, doi: 10.1137/0720076, url: https://doi-org.pitt.idm.oclc.org/10.1137/0720076.

[21] O. Darrigol, *Worlds of flow*, A history of hydrodynamics from the Bernoullis to Prandtl, Oxford University Press, New York, 2005, pp. xiv+356, isbn: 0-19-856843-6.

[22] P. A. Davidson, *Turbulence: an introduction for scientists and engineers*, Oxford University Press, 2015.

[23] T. A. Davis, *Direct methods for sparse linear systems*, vol. 2, Fundamentals of Algorithms, Society for Industrial and Applied Mathematics (SIAM), Philadelphia, PA, 2006, pp. xii+217, isbn: 978-0-898716-13-9; 0-89871-613-6, doi: 10.1137/1.9780898718881, url: https://doi-org.pitt.idm.oclc.org/10.1137/1.9780898718881.

[24] V. DeCaria, W. Layton, and H. Zhao, *Analysis of a low complexity, time-accurate discretization of the Navier-Stokes equations*, Preprint arXiv:1810.06705 (2018).

[25] V. DeCaria, W. Layton, and M. McLaughlin, *A conservative, second order, unconditionally stable artificial compression method*, Comput. Methods Appl. Mech. Engrg. 325 (2017), pp. 733–747, issn: 0045-7825, doi: 10.1016/j.cma.2017.07.033, url: https://doi-org.pitt.idm.oclc.org/10.1016/j.cma.2017.07.033.

[26] V. DeCaria, W. Layton, and M. McLaughlin, *An analysis of the Robert–Asselin time filter for the correction of nonphysical acoustics in an artificial compression method*, Numerical Methods for Partial Differential Equations ().

[27] V. DeCaria et al., *A new embedded variable stepsize, variable order family of low computational complexity*, arXiv preprint arXiv:1810.06670 (2018).

[28] J. W. Demmel, N. J. Higham, and R. S. Schreiber, *Stability of block LU factorization*, Numerical linear algebra with applications 2.2 (1995), pp. 173–190.

[29] C. R. Doering and C. Foias, *Energy dissipation in body-forced turbulence*, J. Fluid Mech. 467 (2002), pp. 289–306, ISSN: 0022-1120, DOI: 10.1017/S0022112002001386, URL: https://doi-org.pitt.idm.oclc.org/10.1017/S0022112002001386.

[30] C. R. Doering and J. D. Gibbon, *Applied analysis of the Navier-Stokes equations*, Cambridge Texts in Applied Mathematics, Cambridge University Press, Cambridge, 1995, pp. xiv+217, ISBN: 0-521-44557-4; 0-521-44568-X, DOI: 10.1017/CBO9780511608803, URL: https://doi-org.pitt.idm.oclc.org/10.1017/CBO9780511608803.

[31] C. R. Doering and P. Constantin, *Energy dissipation in shear driven turbulence*, Physical review letters 69.11 (1992), p. 1648.

[32] D. Donatelli and P. Marcati, *A dispersive approach to the artificial compressibility approximations of the Navier-Stokes equations in 3D*, J. Hyperbolic Differ. Equ. 3.3 (2006), pp. 575–588, ISSN: 0219-8916, DOI: 10.1142/S0219891606000914, URL: https://doi-org.pitt.idm.oclc.org/10.1142/S0219891606000914.

[33] D. Donatelli and P. Marcati, *Leray weak solutions of the incompressible Navier Stokes system on exterior domains via the artificial compressibility method*, Indiana Univ. Math. J. 59.5 (2010), pp. 1831–1852, ISSN: 0022-2518, DOI: 10.1512/iumj.2010.59.3936, URL: https://doi-org.pitt.idm.oclc.org/10.1512/iumj.2010.59.3936.

[34] C. Egbers and G. Pfister, *Physics of rotating fluids: selected topics of the 11th international Couette-Taylor workshop held at Bremen, Germany, 20–23 July 1999*, vol. 549, Springer, 2008.

[35] A. El Guennouni, K. Jbilou, and H. Sadok, *A block version of BiCGSTAB for linear systems with multiple right-hand sides*, Electronic Transactions on Numerical Analysis 16.129-142 (2003), p. 2.

[36] A. Ern and J.-L. Guermond, *Theory and practice of finite elements*, vol. 159, Springer Science & Business Media, 2013.

[37] L. C. Evans, *Partial differential equations*, 2nd, vol. 19, Graduate Studies in Mathematics, American Mathematical Society, Providence, RI, 2010, pp. xxii+749, ISBN: 978-0-8218-4974-3, DOI: 10.1090/gsm/019, URL: https://doi.org/10.1090/gsm/019.

[38] J. A. Fiordilino, W. Layton, and Y. Rong, *An efficient and modular grad-div stabilization*, Comput. Methods Appl. Mech. Engrg. 335 (2018), pp. 327–346, ISSN: 0045-7825, DOI: 10.1016/j.cma.2018.02.023, URL: https://doi-org.pitt.idm.oclc.org/10.1016/j.cma.2018.02.023.

[39] J. Fiordilino, *Ensemble time-stepping algorithms for natural convection*, Sept. 2018, URL: http://d-scholarship.pitt.edu/34680/.

[40] J. A. Fiordilino, *A second order ensemble timestepping algorithm for natural convection*, SIAM Journal on Numerical Analysis 56.2 (2018), pp. 816–837.

[41] J. A. Fiordilino and S. Khankan, *Ensemble timestepping algorithms for natural convection*, Int. J. Numer. Anal. Model. 15.4-5 (2018), pp. 524–551.

[42] U. Frisch, *Turbulence*, The legacy of A. N. Kolmogorov, Cambridge University Press, Cambridge, 1995, pp. xiv+296, ISBN: 0-521-45103-5.

[43] J. Ginibre and G. Velo, *Generalized Strichartz inequalities for the wave equation*, J. Funct. Anal. 133.1 (1995), pp. 50–68, ISSN: 0022-1236, DOI: 10.1006/jfan.1995.1119, URL: https://doi-org.pitt.idm.oclc.org/10.1006/jfan.1995.1119.

[44] R. Glowinski and P. Le Tallec, *Augmented Lagrangian and operator-splitting methods in nonlinear mechanics*, vol. 9, SIAM, 1989.

[45] P. Gresho and R. Sani, *Incompressible flow and the finite element method. Volume 2*, Wiley, 2000.

[46] J. L. Guermond, P. Minev, and J. Shen, *An overview of projection methods for incompressible flows*, Comput. Methods Appl. Mech. Engrg. 195.44-47 (2006), pp. 6011–6045, ISSN: 0045-7825, DOI: 10.1016/j.cma.2005.10.010, URL: http://dx.doi.org.pitt.idm.oclc.org/10.1016/j.cma.2005.10.010.

[47] J.-L. Guermond and P. Minev, *High-Order Adaptive Time Stepping for the Incompressible Navier–Stokes Equations*, SIAM Journal on Scientific Computing 41.2 (2019), A770–A788.

[48] J.-L. Guermond and P. Minev, *High-Order Time Stepping for the Incompressible Navier-Stokes Equations*, SIAM Journal on Scientific Computing 37.6 (2015), A2656–A2681.

[49] J.-L. Guermond and P. D. Minev, *High-order time stepping for the Navier–Stokes equations with minimal computational complexity*, Journal of Computational and Applied Mathematics 310 (2017), pp. 92–103.

[50] M. D. Gunzburger, *Finite element methods for viscous incompressible flows*, Computer Science and Scientific Computing, A guide to theory, practice, and algorithms, Academic Press, Inc., Boston, MA, 1989, pp. xviii+269, isbn: 0-12-307350-2.

[51] M. Gunzburger, N. Jiang, and Z. Wang, *A second-order time-stepping scheme for simulating ensembles of parameterized flow problems*, Computational Methods in Applied Mathematics 19.3 (2019), pp. 681–701.

[52] M. Gunzburger, N. Jiang, and Z. Wang, *An efficient algorithm for simulating ensembles of parameterized flow problems*, IMA Journal of Numerical Analysis 39.3 (2018), pp. 1180–1205.

[53] A. Guzel and W. Layton, *Time filters increase accuracy of the fully implicit method*, BIT 58.2 (2018), pp. 301–315, issn: 0006-3835, doi: 10.1007/s10543-018-0695-z, url: https://doi-org.pitt.idm.oclc.org/10.1007/s10543-018-0695-z.

[54] A. Hay et al., *hp-adaptive time integration based on the BDF for viscous flows*, J. Comput. Phys. 291 (2015), pp. 151–176, issn: 0021-9991, doi: 10.1016/j.jcp.2015.03.022, url: https://doi-org.pitt.idm.oclc.org/10.1016/j.jcp.2015.03.022.

[55] F. Hecht, *New development in Freefem++*, J. Numer. Math. 20.3-4 (2012), pp. 251–265, issn: 1570-2820.

[56] J. G. Heywood and R. Rannacher, *Finite-element approximation of the nonstationary Navier-Stokes problem. part IV: error analysis for second-order time discretization*, SIAM Journal on Numerical Analysis 27.2 (1990), pp. 353–384.

[57] J. Hoffman and C. Johnson, *Computational turbulent incompressible flow*, vol. 4, Applied Mathematics: Body and Soul, Springer, Berlin, 2007, pp. xx+397, ISBN: 978-3-540-46531-7; 3-540-46531-6, DOI: 10.1007/978-3-540-46533-1, URL: https://doi-org.pitt.idm.oclc.org/10.1007/978-3-540-46533-1.

[58] N. N. Janenko, *The method of fractional steps*, Springer, 1971.

[59] K. Jbilou, A. Messaoudi, and H. Sadok, *Global FOM and GMRES algorithms for matrix equations*, Applied Numerical Mathematics 31.1 (1999), pp. 49–63.

[60] E. W. Jenkins et al., *On the parameter choice in grad-div stabilization for the Stokes equations*, Advances in Computational Mathematics 40.2 (2014), pp. 491–516.

[61] N. Jiang, *A higher order ensemble simulation algorithm for fluid flows*, J. Sci. Comput. 64.1 (2015), pp. 264–288, ISSN: 0885-7474, DOI: 10.1007/s10915-014-9932-z, URL: http://dx.doi.org.pitt.idm.oclc.org/10.1007/s10915-014-9932-z.

[62] N. Jiang, *A Pressure-Correction Ensemble Scheme for Computing Evolutionary Boussinesq Equations*, Journal of Scientific Computing (2019), pp. 1–36.

[63] N. Jiang, S. Kaya, and W. Layton, *Analysis of model variance for ensemble based turbulence modeling*, Computational Methods in Applied Mathematics 15.2 (2015), pp. 173–188.

[64] N. Jiang and W. Layton, *Algorithms and models for turbulence not at statistical equilibrium*, Computers & Mathematics with Applications 71.11 (2016), pp. 2352–2372.

[65] N. Jiang and W. Layton, *An algorithm for fast calculation of flow ensembles*, Int. J. Uncertain. Quantif. 4.4 (2014), pp. 273–301, ISSN: 2152-5080, DOI: 10.1615/Int.J.UncertaintyQuantification.2014007691, URL: http://dx.doi.org.pitt.idm.oclc.org/10.1615/Int.J.UncertaintyQuantification.2014007691.

[66] N. Jiang and W. Layton, *Numerical analysis of two ensemble eddy viscosity numerical regularizations of fluid motion*, Numerical Methods for Partial Differential Equations 31.3 (2015), pp. 630–651.

[67] V. John, *Finite element methods for incompressible flow problems*, Springer, 2016.

[68] H. Johnston and J.-G. Liu, *Accurate, stable and efficient Navier-Stokes solvers based on explicit treatment of the pressure term*, J. Comput. Phys. 199.1 (2004), pp. 221–259, ISSN: 0021-9991, DOI: 10.1016/j.jcp.2004.02.009, URL: https://doi.org/10.1016/j.jcp.2004.02.009.

[69] J. van Kan, *A second-order accurate pressure-correction scheme for viscous incompressible flow*, SIAM J. Sci. Statist. Comput. 7.3 (1986), pp. 870–891, ISSN: 0196-5204, DOI: 10.1137/0907059, URL: https://doi.org/10.1137/0907059.

[70] D. A. Kay et al., *Adaptive time-stepping for incompressible flow. II. Navier-Stokes equations*, SIAM J. Sci. Comput. 32.1 (2010), pp. 111–128, ISSN: 1064-8275, DOI: 10.1137/080728032, URL: https://doi-org.pitt.idm.oclc.org/10.1137/080728032.

[71] M. Keel and T. Tao, *Endpoint Strichartz estimates*, Amer. J. Math. 120.5 (1998), pp. 955–980, ISSN: 0002-9327, URL: http://muse.jhu.edu.pitt.idm.oclc.org/journals/american_journal_of_mathematics/v120/120.5keel.pdf.

[72] S. Klainerman and M. Machedon, *Space-time estimates for null forms and the local existence theorem*, Comm. Pure Appl. Math. 46.9 (1993), pp. 1221–1268, ISSN: 0010-3640, DOI: 10.1002/cpa.3160460902, URL: https://doi-org.pitt.idm.oclc.org/10.1002/cpa.3160460902.

[73] J. B. Klemp and R. B. Wilhelmson, *The simulation of three-dimensional convective storm dynamics*, Journal of the Atmospheric Sciences 35.6 (1978), pp. 1070–1096.

[74] G. M. Kobel'kov, *Symmetric approximations of the Navier-Stokes equations*, Matematicheskii Sbornik 193.7 (2002), p. 1027.

[75] W. Layton, *Introduction to the numerical analysis of incompressible viscous flows*, vol. 6, Siam, 2008.

[76] W. J. Layton, *An energy analysis of degenerate hyperbolic partial differential equations*, Apl. Mat. 29.5 (1984), pp. 351–366, ISSN: 0373-6725.

[77] W. Layton, Y. Li, and C. Trenchea, *Recent developments in IMEX methods with time filters for systems of evolution equations*, J. Comput. Appl. Math. 299

(2016), pp. 50–67, ISSN: 0377-0427, DOI: 10.1016/j.cam.2015.09.038, URL: https://doi-org.pitt.idm.oclc.org/10.1016/j.cam.2015.09.038.

[78] W. Layton and M. McLaughlin, *Doubly-Adaptive Artificial Compression Methods for Incompressible Flow*, Journal of Numerical Mathematics (2019).

[79] W. Layton, L. G. Rebholz, and C. Trenchea, *Modular nonlinear filter stabilization of methods for higher Reynolds numbers flow*, J. Math. Fluid Mech. 14.2 (2012), pp. 325–354, ISSN: 1422-6928, DOI: 10.1007/s00021-011-0072-z, URL: https://doi-org.pitt.idm.oclc.org/10.1007/s00021-011-0072-z.

[80] R. Lewandowski, *The mathematical analysis of the coupling of a turbulent kinetic energy equation to the Navier-Stokes equation with an eddy viscosity*, Nonlinear Anal. 28.2 (1997), pp. 393–417, ISSN: 0362-546X, DOI: 10.1016/0362-546X(95)00149-P, URL: https://doi-org.pitt.idm.oclc.org/10.1016/0362-546X(95)00149-P.

[81] R. Lewandowski and B. Mohammadi, *Existence and positivity results for the ϕ-θ and a modified k-ϵ two-equation turbulence models*, Math. Models Methods Appl. Sci. 3.2 (1993), pp. 195–215, ISSN: 0218-2025, DOI: 10.1142/S0218202593000114, URL: https://doi-org.pitt.idm.oclc.org/10.1142/S0218202593000114.

[82] J.-L. Lions, *Quelques méthodes de résolution des problèmes aux limites non linéaires*, Dunod; Gauthier-Villars, Paris, 1969, pp. xx+554.

[83] J.-L. Lions, *Sur l'existence de solutions des équations de Navier-Stokes*, C. R. Acad. Sci. Paris 248 (1959), pp. 2847–2849, ISSN: 0001-4036.

[84] P.-L. Lions, *Mathematical Topics in Fluid Mechanics: Volume 2: Compressible Models*, vol. 2, Oxford University Press on Demand, 1996.

[85] J.-G. Liu, C. Wang, and H. Johnston, *A fourth order scheme for incompressible Boussinesq equations*, J. Sci. Comput. 18.2 (2003), pp. 253–285, ISSN: 0885-7474, DOI: 10.1023/A:1021168924020, URL: https://doi.org/10.1023/A:1021168924020.

[86] E. N. Lorenz, *A study of the predictability of a 28-variable atmospheric model*, Tellus 17.3 (1965), pp. 321–333.

[87] E. N. Lorenz, *Deterministic nonperiodic flow*, Journal of the atmospheric sciences 20.2 (1963), pp. 130–141.

[88] E. N. Lorenz, *Section of planetary sciences: The predictability of hydrodynamic flow*, Transactions of the New York Academy of Sciences 25.4 Series II (1963), pp. 409–432.

[89] M. Manzari, *An explicit finite element algorithm for convection heat transfer problems*, International Journal of Numerical Methods for Heat & Fluid Flow 9.8 (1999), pp. 860–877.

[90] N. Massarotti, P. Nithiarasu, and O. Zienkiewicz, *Characteristic-based-split (CBS) algorithm for incompressible flow problems with heat transfer*, International Journal of Numerical Methods for Heat & Fluid Flow 8.8 (1998), pp. 969–990.

[91] G. Mockenhaupt, A. Seeger, and C. D. Sogge, *Local smoothing of Fourier integral operators and Carleson-Sjölin estimates*, J. Amer. Math. Soc. 6.1 (1993), pp. 65–130, ISSN: 0894-0347, DOI: 10.2307/2152795, URL: https://doi-org.pitt.idm.oclc.org/10.2307/2152795.

[92] B. Mohammadi and O. Pironneau, *Analysis of the k-epsilon turbulence model*, RAM: Research in Applied Mathematics, Masson, Paris; John Wiley & Sons, Ltd., Chichester, 1994, pp. xiv+196, ISBN: 2-225-84391-0.

[93] M. Mohebujjaman and L. G. Rebholz, *An efficient algorithm for computation of MHD flow ensembles*, Computational Methods in Applied Mathematics 17.1 (2017), pp. 121–137.

[94] T. Ohwada and P. Asinari, *Artificial compressibility method revisited: asymptotic numerical method for incompressible Navier-Stokes equations*, Journal of Computational Physics 229.5 (2010), pp. 1698–1723.

[95] A. Oskolkov, *A small-parameter quasi-linear parabolic system approximating the Navier-Stokes system*, Journal of Mathematical Sciences 1.4 (1973), pp. 452–470.

[96] A. Pakzad, *Damping functions correct over-dissipation of the Smagorinsky model*, Math. Methods Appl. Sci. 40.16 (2017), pp. 5933–5945, ISSN: 0170-4214, DOI: 10.1002/mma.4444, URL: https://doi-org.pitt.idm.oclc.org/10.1002/mma.4444.

[97] R. L. Panton, *Incompressible flow*, A Wiley-Interscience Publication, John Wiley & Sons, Inc., New York, 1984, pp. xv+780, ISBN: 0-471-89765-5.

[98] S. B. Pope, *Turbulent flows*, Cambridge University Press, Cambridge, 2000, ISBN: 0-521-59886-9, DOI: 10.1017/CBO9780511840531, URL: https://doi-org.pitt.idm.oclc.org/10.1017/CBO9780511840531.

[99] L. Prandtl and K. Wieghardt, *Über ein neues Formelsystem für die ausgebildete Turbulenz*, Nachr. Akad. Wiss. Göttingen. Math.-Phys. Kl. Math.-Phys.-Chem. Abt. 1945 (1945), pp. 6–19, ISSN: 0369-3163.

[100] L. Prandtl, *On fully developed turbulence*, in: *Proceedings of the 2nd International Congress of Applied Mechanics, Zurich*, 1926, pp. 62–74.

[101] A. Prohl, *Projection and quasi-compressibility methods for solving the incompressible Navier-Stokes equations*, Springer, 1997.

[102] A. Robert, *The integration of a spectral model of the atmosphere by the implicit method*, in: *Proc. WMO/IUGG Symposium on NWP, Tokyo, Japan Meteorological Agency*, vol. 7, 1969, pp. 19–24.

[103] Y. Rong, W. Layton, and H. Zhao, *Numerical analysis of an artificial compression method for magnetohydrodynamic flows at low magnetic Reynolds numbers*, Journal of Scientific Computing 76.3 (2018), pp. 1458–1483.

[104] B. de Saint-Venant, *Note á joindre au mémoire sur la dynamique des fluides*, Comptes rendus 17 (1843), pp. 1240–1244.

[105] O. San and J. Borggaard, *Principal interval decomposition framework for POD reduced-order modeling of convective Boussinesq flows*, Internat. J. Numer. Methods Fluids 78.1 (2015), pp. 37–62, ISSN: 0271-2091, DOI: 10.1002/fld.4006, URL: https://doi.org/10.1002/fld.4006.

[106] J. Shen, *A remark on the projection-3 method*, Internat. J. Numer. Methods Fluids 16.3 (1993), pp. 249–253, ISSN: 0271-2091, DOI: 10.1002/fld.1650160308, URL: https://doi-org.pitt.idm.oclc.org/10.1002/fld.1650160308.

[107] J. Shen, *On a new pseudocompressibility method for the incompressible Navier-Stokes equations*, Appl. Numer. Math. 21.1 (1996), pp. 71–90, ISSN: 0168-9274, DOI:

10.1016/0168-9274(95)00132-8, URL: http://dx.doi.org.pitt.idm.oclc.org/10.1016/0168-9274(95)00132-8.

[108] J. Shen, *On error estimates of projection methods for Navier-Stokes equations: first-order schemes*, SIAM Journal on Numerical Analysis 29.1 (1992), pp. 57–77.

[109] J. Shen, *On error estimates of some higher order projection and penalty-projection methods for Navier-Stokes equations*, Numerische Mathematik 62.1 (1992), pp. 49–73.

[110] J. Shen, *On error estimates of the penalty method for unsteady Navier-Stokes equations*, SIAM J. Numer. Anal. 32.2 (1995), pp. 386–403, ISSN: 0036-1429, DOI: 10.1137/0732016, URL: http://dx.doi.org.pitt.idm.oclc.org/10.1137/0732016.

[111] J. Shen, *On error estimates of the projection methods for the Navier-Stokes equations: second-order schemes*, Math. Comp. 65.215 (1996), pp. 1039–1065, ISSN: 0025-5718, DOI: 10.1090/S0025-5718-96-00750-8, URL: https://doi-org.pitt.idm.oclc.org/10.1090/S0025-5718-96-00750-8.

[112] J. Shen, *Pseudo-compressibility methods for the unsteady incompressible Navier-Stokes equations*, in: *Proceedings of the 1994 Beijing symposium on nonlinear evolution equations and infinite dynamical systems*, 1997, pp. 68–78.

[113] W. C. Skamarock and J. B. Klemp, *Efficiency and accuracy of the Klemp-Wilhelmson time-splitting technique*, Monthly Weather Review 122.11 (1994), 2623–2630.

[114] H. F. Smith, *A parametrix construction for wave equations with $C^{1,1}$ coefficients*, Ann. Inst. Fourier (Grenoble) 48.3 (1998), pp. 797–835, ISSN: 0373-0956, URL: http://www.numdam.org/item?id=AIF_1998__48_3_797_0.

[115] G. Söderlind, I. Fekete, and I. Faragó, *On the zero-stability of multistep methods on smooth nonuniform grids*, BIT 58.4 (2018), pp. 1125–1143, ISSN: 0006-3835, DOI: 10.1007/s10543-018-0716-y, URL: https://doi-org.pitt.idm.oclc.org/10.1007/s10543-018-0716-y.

[116] C. D. Sogge, *Lectures on nonlinear wave equations*, Monographs in Analysis, II, International Press, Boston, MA, 1995, pp. vi+159, ISBN: 1-57146-032-2.

[117] P. R. Spalart, *Philosophies and fallacies in turbulence modeling*, Progress in Aerospace Sciences 74 (2015), pp. 1–15.

[118] V. Starr, *Physics of negative viscosity phenomena*, Earth and Planetary Science Series 256 (1966).

[119] E. M. Stein, *Harmonic analysis: real-variable methods, orthogonality, and oscillatory integrals*, vol. 43, Princeton Mathematical Series, With the assistance of Timothy S. Murphy, Monographs in Harmonic Analysis, III, Princeton University Press, Princeton, NJ, 1993, pp. xiv+695, ISBN: 0-691-03216-5.

[120] R. S. Strichartz, *Restrictions of Fourier transforms to quadratic surfaces and decay of solutions of wave equations*, Duke Math. J. 44.3 (1977), pp. 705–714, ISSN: 0012-7094, URL: http://projecteuclid.org.pitt.idm.oclc.org/euclid.dmj/1077312392.

[121] M. Sussman, *A stability example*, tech. rep., University of Pittsburgh, 2010.

[122] A. Takhirov, M. Neda, and J. Waters, *Time relaxation algorithm for flow ensembles*, Numerical Methods for Partial Differential Equations 32.3 (2016), pp. 757–777.

[123] D. Tataru, *Strichartz estimates for operators with nonsmooth coefficients and the nonlinear wave equation*, Amer. J. Math. 122.2 (2000), pp. 349–376, ISSN: 0002-9327, URL: http://muse.jhu.edu.pitt.idm.oclc.org/journals/american_journal_of_mathematics/v122/122.2tataru.pdf.

[124] D. Tataru, *Strichartz estimates for second order hyperbolic operators with nonsmooth coefficients. II*, Amer. J. Math. 123.3 (2001), pp. 385–423, ISSN: 0002-9327, URL: http://muse.jhu.edu.pitt.idm.oclc.org/journals/american_journal_of_mathematics/v123/123.3tataru.pdf.

[125] D. Tataru, *Strichartz estimates for second order hyperbolic operators with nonsmooth coefficients. III*, J. Amer. Math. Soc. 15.2 (2002), pp. 419–442, ISSN: 0894-0347, DOI: 10.1090/S0894-0347-01-00375-7, URL: https://doi-org.pitt.idm.oclc.org/10.1090/S0894-0347-01-00375-7.

[126] G. I. Taylor, *I. Eddy motion in the atmosphere*, Philosophical Transactions of the Royal Society of London. Series A, Containing Papers of a Mathematical or Physical Character 215.523-537 (1915), pp. 1–26.

[127] R. Témam, *Sur l'approximation de la solution des équations de Navier-Stokes par la méthode des pas fractionnaires. I*, Arch. Rational Mech. Anal. 32 (1969), pp. 135–153, issn: 0003-9527, doi: 10.1007/BF00247678, url: http://dx.doi.org.pitt.idm.oclc.org/10.1007/BF00247678.

[128] R. Témam, *Sur l'approximation de la solution des équations de Navier-Stokes par la méthode des pas fractionnaires. II*, Arch. Rational Mech. Anal. 33 (1969), pp. 377–385, issn: 0003-9527, doi: 10.1007/BF00247696, url: https://doi-org.pitt.idm.oclc.org/10.1007/BF00247696.

[129] R. Temam, *Navier-Stokes equations and nonlinear functional analysis*, vol. 41, CBMS-NSF Regional Conference Series in Applied Mathematics, Society for Industrial and Applied Mathematics (SIAM), Philadelphia, PA, 1983, pp. xii+122, isbn: 0-89871-183-5.

[130] R. Temam, *Navier-Stokes equations: theory and numerical analysis*, vol. 343, American Mathematical Soc., 2001.

[131] R. Temam, *Une méthode d'approximation de la solution des équations de Navier-Stokes*, Bull. Soc. Math. France 96 (1968), pp. 115–152, issn: 0037-9484, url: http://www.numdam.org/item?id=BSMF_1968__96__115_0.

[132] C. Temperton and A. Staniforth, *An efficient two-time-level semi-Lagrangian semi-implicit integration scheme*, Quarterly Journal of the Royal Meteorological Society 113.477 (1987), pp. 1025–1039.

[133] Z. Toth and E. Kalnay, *Ensemble forecasting at NMC: The generation of perturbations*, Bulletin of the american meteorological society 74.12 (1993), pp. 2317–2330.

[134] G. de Vahl Davis, *Natural convection of air in a square cavity: a bench mark numerical solution*, International Journal for numerical methods in fluids 3.3 (1983), pp. 249–264.

[135] J. C. Vassilicos, *Dissipation in turbulent flows*, in: *Annual review of fluid mechanics. Vol. 47*, vol. 47, Annu. Rev. Fluid Mech. Annual Reviews, Palo Alto, CA, 2015, pp. 95–114.

[136] A. Veneziani and U. Villa, *ALADINS: an ALgebraic splitting time ADaptive solver for the Incompressible Navier-Stokes equations*, J. Comput. Phys. 238 (2013), pp. 359–375, ISSN: 0021-9991, DOI: 10.1016/j.jcp.2012.11.049, URL: https://doi-org.pitt.idm.oclc.org/10.1016/j.jcp.2012.11.049.

[137] M. Vergassola, S. Gama, and U. Frisch, *Proving the existence of negative isotropic eddy viscosity.* In: *Solar and Planetary Dynamos*, 1993, pp. 321–327.

[138] A. Vreman, *An eddy-viscosity subgrid-scale model for turbulent shear flow: Algebraic theory and applications*, Physics of fluids 16.10 (2004), pp. 3670–3681.

[139] X. Wang, *Time averaged energy dissipation rate for shear driven flows in* $\mathbb{R}^n$, Physica D: Nonlinear Phenomena 99.4 (1997), pp. 555–563.

[140] D. C. Wilcox, *Turbulence modeling for CFD. La Canada, CA: DCW Industries*, Inc, November (2006).

[141] P. D. Williams, *A Proposed Modification to the Robert-Asselin Time Filter*, Monthly Weather Review 137.8 (2009), pp. 2538–2546, DOI: 10.1175/2009MWR2724.1, eprint: http://dx.doi.org/10.1175/2009MWR2724.1, URL: http://dx.doi.org/10.1175/2009MWR2724.1.

[142] P. D. Williams, *The RAW Filter: An Improvement to the Robert-Asselin Filter in Semi-Implicit Integrations*, Monthly Weather Review 139.6 (2011), pp. 1996–2007, DOI: 10.1175/2010MWR3601.1, eprint: https://doi.org/10.1175/2010MWR3601.1, URL: https://doi.org/10.1175/2010MWR3601.1.

[143] Z.-N. Wu and S. Fu, *Positivity of k-epsilon turbulence models for incompressible flow*, Math. Models Methods Appl. Sci. 12.3 (2002), pp. 393–406, ISSN: 0218-2025, DOI: 10.1142/S0218202502001702, URL: https://doi-org.pitt.idm.oclc.org/10.1142/S0218202502001702.

[144] H. Xiao and P. Cinnella, *Quantification of model uncertainty in RANS simulations: A review*, Progress in Aerospace Sciences (2019).

[145] L. Yang, S. Badia, and R. Codina, *A pseudo-compressible variational multiscale solver for turbulent incompressible flows*, Comput. Mech. 58.6 (2016), pp. 1051–1069, issn: 0178-7675, doi: 10.1007/s00466-016-1332-9, url: https://doi-org.pitt.idm.oclc.org/10.1007/s00466-016-1332-9.

[146] R. K. Zeytounian, *Topics in hyposonic flow theory*, vol. 672, Lecture Notes in Physics, Reprint of the 2006 edition, Springer-Verlag, Berlin, 2010, pp. xvi+284, isbn: 978-3-642-06495-1.

[147] Y. Zhang and Y. Hou, *The Crank-Nicolson extrapolation stabilized finite element method for natural convection problem*, Mathematical Problems in Engineering 2014 (2014).